# Modeling

# Non-Linear Dynamic Phenomena in Biochemical Networks

Berichterstatter:   Prof. Dr. Ulrich Faigle
                       Prof. Dr. Dietmar Schomburg

Tag der mündlichen Prüfung: 26. Oktober 2007

# Deutsche Zusammenfassung

Durch die Entwicklung von Hochdurchsatztechniken hat sich der Fokus biologischer Forschung in den letzten Jahrzehnten von der Untersuchung einzelner Zellkomponenten zu einen systemorientierten Ansatz hin verschoben, der versucht, Wechselwirkungen zwischen diesen Komponenten zu erfassen. Diese Zielsetzung erfordert Modellierungsansätze und Analysemethoden zur Beschreibung solcher regulatorischer Netzwerke.

In dieser Arbeit werden Mechanismen untersucht, die mit qualitativen dynamischen Verhaltensweisen in Zusammenhang stehen. Hierzu verwenden wir ein Differenzialgleichungsmodell, das auf chemischen Bindungsreaktionen basiert, und schätzen Parameter aus Zeitreihenkonzentrationsdaten. Im ersten Teil zeigen wir Anwendungen auf regulatorische Subsysteme mit qualitativ unterschiedlichem Verhalten: Die Antwort des *Mycobacterium tuberculosis* auf Beschädigung der DNA wird durch Relaxation des Systems zu seinem Fixpunkt nach Störung beschrieben. Die spezifische Regulierung von Genen in *Escherichia coli* durch das globale Regulatorprotein H-NS wird durch das Zusammenwirken mehrerer Rückkopplungsmechanismen erklärt. Um das für das Lernen biologischer Netzwerke aus experimentellen Daten typische Problem des "Overfitting" zu vermeiden, stellen wir einen Bayes'schen Ansatz vor, der zusätzliches Wissen über das System in Form von Wahrscheinlichkeitsverteilungen einbindet. Dieser wird auf simulierten Daten und auf einem Datensatz des *Saccharomyces cerevisiae* Zellzyklus getestet.

Motiviert durch eine Analyse des gelernten Hefezellzyklusmodells beschäftigt sich der zweite Teil mit der Robustheit periodischen Verhaltens in regulatorischen Netzwerken. Das vorgestellte Modell gehört zu einer Differenzialgleichungsklasse, deren Lösung im allgemeinen zu einem Gleichgewicht konvergiert. Periodisches Verhalten ist nicht robust gegenüber Parameteränderungen. Wir erklären dieses Phänomen mit einer Bifurkationsanalyse und einer Analyse der Stabilität von Fixpunkten. Es wird gezeigt, dass große Zeitskalenunterschiede und Zeitverzögerungen periodisches Verhalten stabilisieren können und somit eine wichtige Rolle in biologischen Oszillatoren spielen.

# Abstract

Facilitated by the development of high-throughput techniques, the focus of biological research has changed in the last decades from the investigation of single cell components to a system-level approach, which aims at an understanding of interactions between these cell components. This objective requires modeling and analysis methods for these regulatory networks.

In this thesis, we investigate mechanisms causing qualitative dynamic behaviors of regulatory subsystems. For this purpose, we introduce a differential equation model based on underlying molecular binding reactions, whose parameters are estimated using time series concentration data. In the first part, the model is applied to subsystems with qualitatively different dynamic behaviors: The response of the *Mycobacterium tuberculosis* to DNA damages is described as the relaxation of a system to its steady state after external perturbation. Specific repression of genes in *Escherichia coli* by the global regulator protein H-NS is explained by the interrelation of feedback mechanisms. In order to prevent overfitting, a typical problem in network inference from experimental data, we introduce an approach based on Bayesian statistics, which includes prior knowledge about the system in terms of prior probability distributions. This approach is applied to simulated data and to the regulatory network of the *Saccharomyces cerevisiae* cell cycle.

Motivated by results on the yeast cell cycle, the second part of this thesis investigates the robustness of periodic behavior in regulatory networks. The model presented belongs to a class of differential equations whose solutions tend to converge to a steady state. Accordingly, periodic behavior is not robust with respect to parameter variations. We explain this phenomenon by applying a bifurcation analysis and investigating the stability of steady states. It is shown that large time scale differences and an inclusion of time-delays can stabilize sustained oscillations, and we postulate that they are important to maintain oscillations in biological systems.

# Danksagung

Meine Promotion war eine sehr schöne und auch lehrreiche Zeit. Hierzu haben viele Menschen wesentlich beigetragen, bei denen ich mich an dieser Stelle bedanken möchte. Allen voran danke ich Prof. Dr. Ulrich Faigle und Prof. Dr. Rainer Schrader, die es mir ermöglicht haben, am Zentrum für Angewandte Informatik meine Arbeit anzufertigen, und bei vielen Fragestellungen hilfreich zur Seite gestanden haben. Bei Prof. Dr. Ulrich Faigle als Betreuer dieser Arbeit bedanke ich mich außerdem für viele Anregungen und das entgegengebrachte Vertrauen, das mir ein sehr selbständiges Arbeiten erlaubt hat. Herrn Prof. Dr. Dietmar Schomburg danke ich für das kontinuierliche Interesse an meiner Arbeit sowie für die Übernahme des Koreferates.

Frau Prof. Dr. Karin Schnetz, Herr Dr. Christian Forst und Herr Prof. Dr. Andreas Burkovski haben mir als Kooperationspartner in vielerlei Hinsicht geholfen biologische Zusammenhänge zu verstehen. Ihr Zutun war ein wesentlicher Beitrag zum Gelingen dieser Arbeit, und ich bedanke mich bei allen dafür.

**Ein herzliches Dankeschön insbesondere auch an:**

- Jutta Gebert für die sehr gute Zusammenarbeit über die gesamte Zeit am ZAIK und viele interessante Gespräche über Wissenschaft und anderes.

- Lars Kaderali für die sehr gute Zusammenarbeit und für zahlreiche Diskussionen, aus denen ich viel gelernt habe.

- Ralf Müller für moralischen Beistand in so mancher "Krisensituation" sowie für das gründliche Korrekturlesen und die vielen Anregungen zu meiner Arbeit.

- Martin Lätsch für die stets gute Versorgung mit Schoki und Knusperflocken, viele gemeinsame Konzertbesuche und andere schöne Unternehmungen hier in Köln.

- Gerhard-Wilhelm Weber für seine stete Hilfsbereitschaft und viele interessante Gespräche.

- Meine Korrekturleser Ralf Müller, Jutta Gebert, Lars Kaderali, Daniel Weiss, Alexander Schönhuth und Isabelle Czerny für viele konstruktive Verbesserungsvorschläge.

- Meine Familie, die mich mein ganzes Leben lang in allem unterstützt und mir in manchen schwierigen Lebenslagen Mut und Selbstbewußtsein gegeben hat.

# Contents

# Foreword

The ultimate goal in systems biology is the *in silico* reconstruction of biological systems, enabling the simulation of, for example, metabolic pathways, regulatory networks or whole cells. In silico means that the behavior of a system is analyzed by computer simulations. Thus, in silico cellular models allow to carry out experiments entirely on a computer. This can revolutionize the drug discovery field since it lowers the risk and financial burden of clinical trials [7, 16]. Potential drugs are traditionally found by testing chemical substrates on animals, frequently with a trial and error method. Understanding regulation mechanisms of metabolic or signaling pathways related to diseases can highly facilitate the discovery of new drug targets [7]. Drugs are designed to bind specifically to these biological targets and thus to affect their activity. Thereby, regulatory pathways involving the target are inhibited or promoted. Besides drug design, systems biology approaches are also applied in plant breeding or in the industrial production of amino acids. Objectives are the determination of genetic markers which enhance a desired performance feature of a plant, such as resistance against vermins, or an increase in the productivity of amino acids required for animal feed, food and pharmaceutical products [93].

In silico models require a detailed understanding of regulation processes at the molecular level. This can only be achieved by interdisciplinary cooperations between biologists, mathematicians and computer scientists. The basis for such an understanding is provided by recent advances in experimental techniques. These commence the -omics area, which comprises genomics, transcriptomics, proteomics and metabolomics. Modern DNA sequencing methods analyze large DNA sequences within a reasonable time. They provide the basis to find sequences encoding genes, and thus to determine the potential components of these regulatory networks. The genomes of prokaryotes such as *Escherichia coli* and *Mycobacterium tuberculosis* have already been sequenced in the 90ies. The yeast genome was the first completely sequenced eukaryotic genome in 1996. Today, six years after the completion of the human genome project in 2001 [112, 202], the sequences of many genomes such as that of chimpanzees, sea urchins, honey bees and bovines are known and stored in databases. High-throughput techniques allow to measure concentrations of all gene products of a cell simultaneously. The transcriptome can be measured with DNA-microarrays and provides information about the activity of genes. High-throughput techniques for proteins and metabolites are gradually becoming feasible [73]. A lot of different databases have been created in the last decades to store the large amounts of data produced with

1

these techniques. Sequence information is stored in the sequence database GenBank[1], the protein database PDB[2] contains information about proteins, and BRENDA[3] lists information about enzymes and metabolic pathways, to mention only a few of them. Defining standard formats, which allow a rapid extraction of information from these databases, is still in progress.

Using these data to build models which can predict the global behavior of a biological system poses a great challenge for the future. Many *top down* approaches have been developed for this task in the last years. These approaches start with very general and abstract models to describe interaction processes between components of the system. Subsystems are defined afterwards in greater detail. This is contrary to conventional *bottom up* approaches, which start with a detailed description of subsystems and extend these successively to obtain a comprehensive model of the system. In top down approaches, high-throughput measurements, usually microarray measurements, are used to fit the models to the observed behavior, and to infer interactions between cell components. Fitting is formulated as an optimization problem. Typically, the datasets are *sparse*, meaning that many components are measured under only few conditions. This leads to ill-posed optimization problems. Various *regularization methods* have been proposed to prevent overfitting in this setting. However, results are often not satisfactory, and many false positive interactions are predicted. Consequently, questions such as "how does a bacterium respond to a new medium?" or "how does a mutation of a gene affect the phenotype of a cell?" can frequently not be answered yet. One of the main reasons for this is the simplicity of model classes used in these top down approaches, which allow to recognize at most rough structures of the interaction networks. Thus, in order to obtain reliable predictions, these models have to be complemented with specific biological knowledge. Furthermore, certain dynamic behaviors can only be explained by quantitative models that are based on underlying reaction kinetics. Usually, the behavior of a regulatory network is determined by the interplay of various regulation mechanisms acting at the transcriptional and post-transcriptional level.

In this thesis, we use a differential equation model based on Michaelis Menten kinetics to describe the dynamic behavior of biochemical networks. Applications to three regulatory subsystems are shown: the response of the DNA repair mechanism of the *Macobacterium tuberculosis* to DNA damages, the specific repression of genes by the protein H-NS in *Escherichia coli* and regulation mechanisms in the *Saccharomyces cerevisiae* cell cycle. An analysis of results of the inferred cell cycle network leads to the second, more theoretical part of this thesis, the investigation of mechanisms related to the robustness of periodic behavior in regulatory networks. The contents of this thesis are outlined in more detail in the following section.

---

[1]GenBank: (http://www.ncbi.nlm.nih.gov/Genbank)
[2]PDB: (http://pdb.org)
[3]BRENDA: (http://www.brenda.uni-koeln.de)

# Structure of the thesis

An introduction to regulation processes in the cell is given in **Chapter 1**. Here, we will also present different modeling approaches for these processes and discuss methods to estimate the corresponding model parameters from experimental data. This chapter intends to give an insight into the variety of currently used model classes and approaches to fit these models to experimental data. Much of the contents presented is taken from [7, 92, 104].

**Chapter 2** focuses on modeling gene regulatory networks with ordinary differential equations. Terms and theorems from the theory of dynamical systems, which will be used throughout this thesis, are introduced in this chapter. Most of the definitions listed can be found in [147].

We derive a model based on chemical reaction kinetics. Regulation processes are described as reversible chemical reactions in this model, leading to sigmoidal dependences between activities of regulators and the effect on the regulated components. This model was inspired by the work of Yagil and Yagil [213] and Jacob and Monod [101]. It provided the basis to develop a piecewise linear differential equation model, which was done in collaboration with my colleague Jutta Gebert and was published in [77].

Our non-linear model is compared with the frequently used class of linear models. The latter have some advantages concerning the estimation of parameters, since there exist various regression methods for linear objective functions. However, they cannot capture complex dynamic behavior such as stable oscillations, multi-stationarity, switch-like behavior or hysteresis, which are essential to model biological phenomena.

In collaboration with biological experts, we applied the model to three regulatory subsystems. The aim was to build models that reflect the biological knowledge about the systems at hand, and to answer specific questions, which were developed with our cooperation partners. All models demonstrate that by the inclusion of biological knowledge one can obtain quantitative statements about the systems in spite of a very limited number of data points available.

Two of these models are presented in this thesis. The third one can be found in [74, 75, 76]. This model describes the dynamic response of *Corynebacterium glutamicum* to varying external nitrogen concentrations and has been built in cooperation with Prof. Dr. Andreas Burkovski (Institute of Biology, University Erlangen-Nürnberg).

The dynamic response of *M. tuberculosis* to a treatment with DNA damaging drugs is modeled in **Chapter 3**. This work was a collaboration with Dr. Christian Forst (Bioscience Division, Los Alamos National Laboratories). If a bacterium's DNA is damaged to a certain extent, it reacts by increasing the production rate of so-called SOS proteins. These proteins are required to repair the damages and make sure that cell division is temporarily suspended. Some regulation mechanisms of this repair system are known from studies in the model organism *E. coli*, but in general little is known yet about which genes are involved and how they interact. We present a statistical analysis, which uses correlations between gene expression patterns and interaction data, in order to find potential

candidate genes. A subsequent parameter estimation and simulation indicates that the gene *Rv2719c* might play an important role in this repair system. This result was published in [155]. Independently, our hypothesis was experimentally confirmed by Chauhan *et al.* [28] and Brooks *et al.* [20] in the meantime.

**Chapter 4** presents a model that seeks to explain the highly specific silencing of a group of commonly regulated genes in *E. coli*. These genes encode proteins which are involved in the uptake and fermentation of aryl-$\beta$-glucosidic sugars. In wild type strains, expression of these genes is highly repressed through binding of a global regulatory protein, H-NS, to specific binding sites at the DNA, whereas this repression is relieved in *hns* mutants lacking the protein H-NS. Together with Prof. Dr. Karin Schnetz (Institute of Genetics, University of Cologne), we built a model for this repression, and estimated parameters using concentration measurements in wild types and *hns* mutants. According to our model, the specific repression is explained by the interplay of two positive feedback loops in the corresponding interaction graph. A publication of results is under way [154].

Together with Dr. Lars Kaderali (Viroquant Research Group Modeling, University of Heidelberg), we developed a new top down approach to estimate parameters of the differential equation model from time series concentration data. This approach is presented in **Chapter 5**. We apply a Bayesian learning approach, in which a restriction of the parameter space is achieved by specifying a priori probability distributions over network parameters. These distributions reflect our expectation of outcome and thus provide a framework to include biological knowledge into the estimation process. We evaluate our approach on simulated data and on a publicly available microarray dataset on the yeast cell cycle. Results on simulated data show that the Bayesian approach presented can improve parameter estimation compared to a maximum likelihood estimation, in particular, when only a few noisy time points are available. This is the typical case in microarray studies. Accordingly, we concluded that the presented approach provides an appropriate framework to analyze microarray data. An analysis of regulations in the yeast cell cycle shows that our method is able to reveal several main regulations between gene products. The method and results are published in [156].

Simulations using the inferred model parameters indicate that capturing the periodic behavior of cell cycle genes is much more difficult than just inferring interactions between genes. Hence, the focus of Chapters 6, 7 and 8 is on the problem to infer an oscillating differential equation model for regulatory networks. We will make use of the theory of dynamical systems in these chapters, and they are of more theoretical nature than the previous Chapters 3 and 4.

**Chapter 6** starts with some theoretical aspects of our differential equation model, which affect the inferred model for the yeast cell cycle. With a few exceptions, the model belongs to the class of differential equation systems which have Jacobian matrices with constant signs. Such systems have been shown to tend to converge to unique steady states

[96]. Feedback mechanisms are a necessary condition for more complex dynamic behavior such as oscillations and multi-stationarity [84, 169, 191]. We use these results to extend our model. A core network for the yeast cell cycle is presented which is able to show periodic behavior. Oscillations in this core model occur within a certain parameter range bounded by saddle-node and Hopf bifurcations. The model shows some characteristics that are typical for many differential equation models used to describe oscillating behavior. We will discuss these in this chapter as well. Parameters for this core network are obtained from experimental data using a maximum likelihood estimation.

In **Chapter 7**, the Bayesian approach is used to extend the inferred core model by further components and regulations. We are able to infer an oscillating network for the yeast cell cycle from experimental data. Simulations using the inferred model are in good accordance with experimental data. These results have been published in [157].

However, this extension also indicates that the oscillations obtained with the core model are structurally not stable. The qualitative behavior of the system is very sensitive to parameter changes, and periodic behavior is thus difficult to learn. Results on simulated data give an impression of the size of the dataset required to capture the periodic behavior with the presented core model. A subsequent bifurcation analysis of the core network supports our observation that the oscillations are not robust.

The results from the analysis in Chapter 7 are in contrast to oscillating biological systems. Most of them seem to be structurally extremely stable and function in a wide range of parameters or under considerable stochastic influences and varying external conditions [8, 203]. **Chapter 8** addresses this contradiction and investigates some theoretical aspects of modeling structurally stable oscillations with differential equations. In order to capture structurally stable periodic behavior, the core network has to be modified. We show that the structural stability of oscillations can be increased by an increase of time scale differences for the two variables or by an inclusion of time-delays. These results might hint that time delays, for example caused by transport and diffusion processes or by the duration of gene expression, are important to maintain robustness of the cell cycle. Moreover, since statements are based on rather general properties of the core model, they hold as well for similar models used to describe other oscillating regulatory networks. This chapter concludes with an extension of principles to a system of more than just two components.

In the end of each Chapter, we summarize results and discuss specific, mainly technical improvements and extensions. The thesis concludes with an overall more general summary of the main results and perspectives for future work in **Chapter 9**.

# Chapter 1

# Introduction

This chapter introduces regulation processes in gene expression and gives an overview of frequently used approaches to infer such regulatory interactions. Section 1.1 provides a description of gene expression regulation at different levels. Much of the information given here can be found in [2, 12, 41, 42]. Different modeling and inference approaches of these regulation processes from experimental data are discussed in Section 1.2. This section loosely follows [104]. Good reviews about modeling gene networks and network reconstruction from experimental data are for example [7, 15, 48, 92, 99, 181, 209].

## 1.1 Biological background

### 1.1.1 Gene expression

*Proteins* are key elements in the organization of different processes within a cell. Proteins are macromolecules consisting of long folded chains of amino acids. They carry out various functions essential for the survival of the cell: They participate in transport processes such as oxygen transport in the blood, regulate the ion concentration in the cell as ion channels, and thus influence the activity of nerves and muscles, catalyze chemical reactions as enzymes, transmit external signals, or act as antibodies in the immune system. Deoxyribonucleic acid (DNA) encodes the entirety of proteins a cell can produce. DNA is a sequence of four different nucleotides. Genes are segments of this sequence which encode proteins. The order of nucleotides in a gene contains the information to produce a functional protein.

The process of protein production is called *gene expression*. It is a two-step procedure. During *transcription*, the nucleotide sequence of a gene is transcribed into an intermediate product called messengerRNA or short *mRNA*. This mRNA serves as a template to produce a protein in a second step, the *translation*. The expression rate of a gene and hence the synthesis rate of the corresponding protein is highly regulated at different levels and can vary in a wide range. This enables the cell to flexibly adapt to external conditions such as nutrition supply, salinity and temperature. Moreover, regulation of gene expression allows

cells to respond to perturbations, such as heat shock or treatment by various drugs, and to maintain basic metabolic processes necessary for survival. A snapshot of gene product (mRNA or protein) concentrations is a *gene expression pattern*. The expression pattern of a cell is determined by the tissue and can be influenced by external conditions. We refer to a typical mRNA expression pattern for an organism or a tissue as *transcriptome*. The transcriptome of stem cells gives insights into the process how cells differentiate [132, 159]. Furthermore, it is known that the concentration of some genes is up- or down-regulated in cancer cells ([103] and references therein). These genes are said to be *differentially expressed*. A protein concentration pattern is called *proteome*.

Organisms are distinguished according to their cell types: A *prokaryote* is an organism consisting of one or more prokaryotic cells. These are cells lacking a cell nucleus. Most prokaryotes are bacteria. Contrary, cells of an *eukaryote* contain a nucleus. Animals and plants belong to this class. Prokaryotic and eukaryotic cells differ in many aspects, including, for example, their structure, size, and consistence of the cell membrane. Eukaryotic cells are larger and have a complex cell structure divided into different cell compartments. Protein concentrations can vary in a wide range within an eukaryotic cell. Hence diffusion and transport processes might affect regulatory mechanisms in eukaryotic cells [142, 177], whereas their influence is less important in prokaryotes. Both organisms also differ in their genome and the regulation of gene expression. Nearly the whole genome of a prokaryotic cell encodes proteins or exhibits a control function. In contrast, over 90% of the human genome, for example, consists of non-coding regions, whose function is not yet completely identified.

## 1.1.2  Regulation of gene expression

### Regulation of transcription

In the following, we describe regulation mechanisms of gene expression. Here, we focus on transcriptional regulation, which is probably the most important mechanism in prokaryotes [208]. It affects directly the concentrations of mRNAs, which are measured in microarray experiments. Mostly, transcription regulation happens at the transcription initiation. Transcription initiation is triggered by an enzyme called *RNA polymerase* (RNAP), which binds to the *promoter*, a regulatory region upstream of a gene's coding region. The affinity of the RNAP to the promoter is affected by binding of proteins to specific binding sites at the DNA [168], frequently located within the promoter region. Proteins which bind to the DNA and influence transcription are called *transcription factors*. In prokaryotes, 2-3%, and in eukaryotes, 6-7% of all genes encode DNA binding proteins [197]. They can either positively or negatively influence gene expression. Different transcription factor distributions within cells have been shown to determine cell differentiation, development and evolution [150, 159, 168].

A lot of efforts have been made in order to understand binding mechanisms of transcription factors and how they can efficiently search for specific binding sites. Generally, transcription factors interact unspecifically with nucleotides of the DNA and are assumed

to be weakly bound to the DNA most of the time [78, 178, 206]. This unspecific binding is caused by displacements of ions from DNA phosphate groups by positively charged protein side chains [206]. This results in an electrostatic force. Models give evidence that a transcription factor searches for its specific binding site mainly by moving along the DNA and jumping from one DNA site to another [78]. If a specific binding site is recognized, the transcription factor presumably undergoes a conformational change, which allows for additional hydrogen bonds further stabilizing the complex [206]. The stability of the complex depends on the sequence of nucleotides [197, 206]. A transcription factor favors binding to short specific sequences of 6-20 nucleotides [56].

Besides the promoter there exist further regulatory regions on the DNA called *enhancers* or *silencers*. All these regions direct the expression level of a gene in concert. Models which capture regulation of transcription initiation by binding of proteins to the DNA are called *gene regulatory networks*.

In prokaryotes, genes which encode proteins involved in the same metabolic processes are frequently organized in *operons*. Genes in an operon are located side by side on the DNA. They are commonly regulated by the same promoter and are even sometimes transcribed into a single mRNA. Their expression patterns are thus highly correlated. An example is the *lac* operon in *E. coli*. It consists of three genes responsible for the transport and metabolism of lactose. The expression of these genes depends among other factors on the availability of glucose and lactose in the bacterium's environment. In Chapter 4, we investigate the *E. coli bgl* operon. Genes in this operon are needed for the uptake and fermentation of aryl-$\beta$-glucosidic sugars.

Transcription factors also sometimes affect the process of RNA production, the *transcription elongation*, by inducing conformational changes of the DNA. An example for such a regulation is also given in Chapter 4.

Transcription factors do not always act independently, but can influence each other. Some transcription factors even become active only in a complex. Frequently appearing complexes are *homo-dimers* consisting of two equal proteins, *hetero-dimers* consisting of two different proteins, and *tetramers* which contain four subunits [3, 168, 181]. Mutual enhancement is also due to electrostatic attraction between a transcription factor bound to the DNA and an unbound one. If several transcription factors compete for the same binding site or if their corresponding binding sites overlap, they inhibit each other.

**Post-transcriptional regulation**

Regulation of gene expression also happens after mRNA production. We refer to this as *post-transcriptional* regulation. An example is a protein that changes the secondary structure of an mRNA molecule, thereby stabilizing it or marking it for degradation. Analogously, regulation of the protein concentration after translation is called *post-translational* modification. This level of regulation includes among others complex formations or chemical modifications, which cause a conformational change and thereby activate or inhibit a protein. Many transcription factors taking part in signal transduction pathways are chemically activated by an external signal. Examples are the activation of the protein RecA

in *M. tuberculosis* in case of a DNA damage described in Chapter 3, or the modification of the protein GlnK in *C. glutamicum* to respond to nitrogen starvation in the environment [24, 25, 186]. Chemical modifications happen at a much faster time scale than gene expression [3] and thus enable the organism to respond quickly to environmental changes.

Models which include not only the regulation of transcription initiation, but also post-transcriptional or post-translational regulation mechanisms, are denoted *biochemical networks*. Thus, a biochemical network is a generic term for a gene regulatory network.

Regulation mechanisms in eukaryotes are more complex than in prokaryotes. Post-transcriptional regulations are more important here and cannot always be neglected. For example, the proteins are often regulated by *phosphorylation*. This is a reversible chemical modification of a protein, which affects the proteins activity by inducing conformational changes, which alter binding properties or subcellular locations. Phosphorylation or dephosphorylation is often done by macromolecules called *kinases* or *phosphatases*. A single kinase is able to activate many proteins, and thus they can quickly amplify an external signal. Phosphorylation plays a role in all *signal transduction pathways*. A famous example is the phosphorylation of the tumor suppressor protein p53 when the cell is damaged. In its active state, p53 stimulates transcription of genes that suppress the cell cycle. Activity control of proteins by phosphorylation also plays a crucial role in the regulation of the cell cycle.

In eucaryotes, genes are usually not organized in operons, but regulated separately. Moreover, a process called *alternative splicing* enables eukaryotes to produce different proteins from the same mRNA and hence additionally affects protein concentrations after transcription.

## 1.2   Modeling cells as systems

In a systems biology approach, cells or cellular subsystems such as gene regulatory networks are understood as *systems S* consisting of $n$ different interacting molecular components. $S$ is assumed to be fully characterized by a *state* $x = (x_1, \ldots, x_n)$, whose components correspond to states $x_i \in \Omega_i$ of each component of $S$. In the following, we refer to these states $x_i$ as *variables* of $S$. The *state space* $\Omega = (\Omega_1, \ldots, \Omega_n)$ describes the set of possible states. An *observation* $\tilde{x} = (\tilde{x}_1, \ldots, \tilde{x}_n)$ is an element of $\Omega$.

In deterministic models, the behavior of the system is assumed to be characterized by a function $f : \Omega \times T \to \Omega$, which assigns each tuple $(x, t) \in \Omega \times T$ an element in the state space $\Omega$. The set $T$ can generally be associated with any conditions influencing the system.

In autonomous dynamic models, the states $x$ depend on time, $x = x(t)$, and the set $T$ describes a set of different time points. In time-discrete models, $T = \{t_0, \ldots, t_N\}$ contains a set of discrete time points, in time-continuous models, $T$ is usually chosen to be the set of real numbers, $T = \mathbb{R}$. The function $f$ can be specified to be

$$f : \Omega \times T \to \Omega, \quad x(t) = f(t, x(t_0)). \tag{1.1}$$

Thus, we assume a functional relation between the state $x(t)$ of the system at time $t$ and the state $x(t_0)$ of the system at a previous time point $t_0$.

In *stochastic models* with discrete state space, states $x$ of the system are described by *probability distributions $p$*,

$$p : \Omega \times T \to [0,1], \quad p(\tilde{x}, \tilde{t}) = \Pr(x_1 = \tilde{x}_1, \ldots, x_n = \tilde{x}_n, t = \tilde{t}). \tag{1.2}$$

In case of continuous state spaces, states are described by *probability density functions* $p : \Omega \times T \to \mathbb{R}_{0,+}$ with $\int_\Omega \int_T p(x,t) dt dx = 1$.

## 1.2.1 Network inference

**Formulation as an optimization problem**

We are given a state space $\Omega$, a set $T$ of conditions and a model set $\mathcal{F}$ of functions $f : \Omega \times T \to \Omega$. Moreover, a set $\tilde{x}(t')$ of states has been observed for different conditions $t' \in T' \subseteq T$. The number of elements in the set $T'$ is assumed to be finite, $T' = \{t_0, \ldots, t_d\}$. All $d$ observations are collected in a dataset $\mathcal{D} = \{\tilde{x}(t_0), \ldots, \tilde{x}(t_d)\}$. The network inference problem aims to select a function $\hat{f} \in \mathcal{F}$ that best fits the dataset $\mathcal{D}$. Fitness is described by a real valued function $F : \mathcal{F} \times \mathcal{D} \to \mathbb{R}$, frequently denoted *error function*, and the network inference problem is formulated as an *optimization problem*

$$\hat{f} = arg \min_{f \in \mathcal{F}} F(f, \mathcal{D}). \tag{1.3}$$

The functions $f \in \mathcal{F}$ might be given in parameterized form. Hence, each model is characterized by a parameter vector $\omega$.

A common choice for the objective function of a deterministic model is the sum of squared errors (MSE) between measurements and model predictions, which is minimized with respect to $\omega$, to obtain an estimator $\hat{\omega}_{MSE}$:

$$\hat{\omega}_{MSE} := arg \min_{\omega} \left( F_{MSE}(\omega, \mathcal{D}) := \sum_{i=1}^{n} \sum_{z=1}^{d} \| x_i(t_z, \omega) - \tilde{x}_i(t_z) \|^2 \right) \tag{1.4}$$

In stochastic model approaches, such as *Bayesian networks*, the traditional estimator is the *maximum likelihood estimator*. Here, the data are interpreted as samples drawn from an underlying distribution. The best model parameter $\hat{\omega}_{MLE}$ is assumed to be the one which maximizes the probability $p(\mathcal{D}|\omega)$ to obtain the observed dataset $\mathcal{D}$ given a parameter vector $\omega$. This objective function is denoted *likelihood function $\mathcal{L}_\mathcal{D}(\omega)$*:

$$\hat{\omega}_{MLE} := arg \max_{\omega} p(\mathcal{D}|\omega) = arg \max_{\omega} \mathcal{L}_\mathcal{D}(\omega) \tag{1.5}$$

Maximum likelihood estimation will be used in Chapter 5.

**Regularization**

In the following, we concentrate on modeling gene regulatory networks by systems. Here, the variables $x_i$ describe concentrations of gene products, that are mRNAs or proteins, and the dataset $\mathcal{D}$ contains microarray gene expression measurements. Typically, the dataset $\mathcal{D}$ is *sparse*. That means, the number $n$ of network components is large, often mRNA concentrations of several hundreds or thousands of genes have been measured, whereas the number $d$ of different conditions/time points is small at the same time. Thus $\omega$ has many components, and we have to fit a high-dimensional function to only a few data points. The corresponding optimization problems are ill-posed, and $\omega$ may be adjusted to specific random features of $\mathcal{D}$, which are not necessarily related to the problem [163]. Accordingly, the model $\hat{\omega}$ fits the dataset $\mathcal{D}$ used for learning very well in this case, but shows bad performance on new datasets. *Regularization* methods have been developed to face this problem. Well-known regularization methods for stochastic models are the *Akaike information criterion* (AIC) and the *Bayesian information criterion* (BIC). They are used in case that the model set $\mathcal{F}$ contains models $\omega^k$ that differ in their numbers $k \in \mathbb{N}$ of parameters. Both, AIC and BIC, include the negative logarithm of the likelihood function $\mathcal{L}_{\mathcal{D}}(\omega)$ and a term which penalizes models having a large number of parameters. They are used as objective functions to be minimized with respect to model parameters:

$$\hat{\omega}^k_{AIC} \quad := \quad arg \min_{\omega^k} \left[ F_{AIC}(\omega^k) := -2 \ln \mathcal{L}_{\mathcal{D}}(\omega) + 2k \right] \tag{1.6}$$

$$\hat{\omega}^k_{BIC} \quad := \quad arg \min_{\omega^k} \left[ F_{BIC}(\omega^k) := -2 \ln \mathcal{L}_{\mathcal{D}}(\omega) + k \ln d \right] \tag{1.7}$$

Both, $\hat{\omega}^k_{AIC}$ and $\hat{\omega}^k_{BIC}$ have been used to infer cell cycle networks in yeast [31, 136]. More biologically motivated approaches restrict the parameter space by including biological knowledge into the optimization process. This can be obtained by introducing constraints to the optimization problem such as, for example, upper bounds for single parameters. Alternatively, similar to the AIC and the BIC, penalty terms that favor networks with only few edges are added to the likelihood function (see for instance [114, 184, 200]). An example for the latter regularization approach is presented in Chapter 5.

## 1.2.2   Boolean networks

*Boolean networks* are deterministic dynamic models. The state space consists of binary vectors of length $n$, $\Omega = \mathbb{F}_2^n$. Boolean functions

$$f : \Omega \times T \to \Omega, \quad x(t_{k+1}) = f(x(t_k)), \quad x(t_k) \in \mathbb{F}_2^n, k \in \mathbb{N} \tag{1.8}$$

are used to update the state of the system at each time point.

Kauffman [106] first introduced Boolean networks to model gene regulation in 1969. Since that time, these models have frequently been used to describe the dynamic of gene regulatory networks [1, 16, 116, 118, 176, 189]. Boolean networks can show a rich variety of dynamic behaviors such as convergence to a stable steady state, multi-stationarity, oscillations, switch-like behavior or hysteresis [192, 193].

The simplicity of a Boolean description makes Boolean networks useful to analyze large networks containing several hundreds or thousands of genes. This is a clear advantage compared to more complex models. Moreover, Boolean functions include mutual influences of different regulators, whereas in most other models different regulators are assumed to act independently in order to keep the model tractable. However, a description of expression values as binary variables and synchronous updates are of course very strict assumptions, which are not biologically reasonable. Thus Boolean networks allow at most for qualitative statements.

When learning a Boolean network from experimental time series data, the data have to be binarized in a preprocessing step. Thereby, much of the information contained in the data is lost [114]. Often the results depend considerably on the threshold values used. Moreover, it has been shown that the qualitative dynamic behavior of Boolean networks and corresponding differential equations are not always consistent [79, 181]. Steady states of Boolean networks correspond to steady states of an equivalent differential equation model, but the reverse does not necessarily hold [79]. On the other hand, limit cycles in the Boolean model do not always occur as limit cycles in the continuous model. This also restricts the utility of Boolean networks, even if the focus is on the qualitative dynamic behavior.

Finally, Boolean networks belong to the class of deterministic models. Hence they cannot capture the stochastic nature of gene expression and do not account for noise in the measurements.

Several extensions of Boolean networks have been proposed in order to overcome some of the limitations mentioned [114, 140, 185, 192, 193]. The most prominent among these are *probabilistic Boolean networks* [174, 175]. In these networks, a set of Boolean functions is randomly chosen for the transition $x(t) \mapsto x(t + 1)$ in each time step according to a probability distribution over a set of possible functions. This extension was developed to account for stochastic fluctuations in the regulation processes.

## 1.2.3 Bayesian networks

A *Bayesian network* is a stochastic system with a set $V = \{x_1, \ldots, x_n\}$ of $n$ variables and a state space $\Omega$ that is assumed to be discrete for our purposes here. Bayesian networks are static models, and we assume the set $T$ to be empty in the following. The *joint probability distribution* $p : \Omega \to [0, 1]$ consists of a set of *local conditional probability distributions* $p(x_i|par(x_i))$ combined with a set of *conditional independence assertions* that allow the construction of a global probability distribution from the local distributions:

$$p(\tilde{x}_1, \ldots, \tilde{x}_n) = \prod_{i=1}^{n} p(\tilde{x}_i|p\tilde{a}r(x_i)). \tag{1.9}$$

The set $par(x_i) \subseteq V \setminus \{x_i\}$ is called the *parent set* of $x_i$, and $p(\tilde{x}_i|p\tilde{a}r(x_i)) = \{\tilde{x}_j|x_j \in par(x_i)\}$. The independence assertions state that a variable $x_j$ which is a successor of a variable $x_i$ cannot at the same time be a predecessor of $x_i$. Otherwise, Table 1.1 illustrates

Table 1.1: System of two variables $x_1$ and $x_2$. If $x_1 \in par(x_2)$ and vice versa, equation (1.9) for the joint distribution $p(\tilde{x}_1, \tilde{x}_2)$ is not properly be defined.

| $\tilde{x}_1$ | $\tilde{x}_2$ | $p(\tilde{x}_1\|\tilde{x}_2)$ | $p(\tilde{x}_2\|\tilde{x}_1)$ |
|---|---|---|---|
| 0 | 0 | 0 | 1 |
| 1 | 0 | 1 | 0 |
| 0 | 1 | 1 | 0 |
| 1 | 1 | 0 | 1 |

that the joint probability distribution cannot be properly defined. Here, we consider two variables $x_1$ and $x_2$ with $par(x_1) = \{x_2\}$ and $par(x_2) = \{x_1\}$. The state space is chosen to be $\mathbb{F}_2^2$, and the local distributions are listed in the table. Although these conditional distributions are well-defined, using equation (1.9) to calculate the joint distribution $p(\tilde{x}_1, \tilde{x}_2)$ for this system would lead to $p(\tilde{x}_1, \tilde{x}_2) = 0$ for all observations $\tilde{x}_1, \tilde{x}_2 \in \mathbb{F}_2$. This example demonstrates that the Bayesian network must have variables $x_i$ with empty parent sets. The local probability distributions for these variables are said to be *unconditional*.

A Bayesian network can graphically be represented as a *directed acyclic graph* (DAG) $G(V, E)$ with nodes corresponding to system variables. There is an edge $e_{j \to i}$ in this DAG, if $x_j$ is a parent of $x_i$, $x_j \in par(x_i)$. Equation (1.9) is based on *Bayes' formula*: $p(A, B) = p(B|A)p(A) = p(A|B)p(B)$.

Murphy and Mian [133] were among the first who modeled gene interactions with a Bayesian network. Bayesian networks are still frequently used to reconstruct interactions between genes from expression data [13, 22, 70, 90, 100, 146]. Learning a Bayesian network from experimental data corresponds to estimating the joint probability distribution $p(x_1, \ldots, x_n)$, which defines the structure of the DAG. It is usually not possible to infer a unique DAG. While arcs describe conditional dependencies, a DAG can also be considered to represent conditional independencies, which are defined by the term *d-separation*:

**Definition 1.2.1** [d-separation [144]] Two variables $x_i$ and $x_j$ of a Bayesian network are *d-separated* by a given set $S \subseteq V \setminus \{x_i, x_j\}$ if and only if $x_i$ and $x_j$ are conditionally independent given values of the variables in $S$.

D-separation includes not only direct dependencies, but describes also indirect ones, which are for example represented by a directed path between two variables in the DAG containing at least one intermediate variable. According to Definition 1.2.1, the variables $x_1$ and $x_3$ are d-separated by variable $x_2$ in all three DAGs $x_1 \to x_2 \to x_3$, $x_1 \leftarrow x_2 \leftarrow x_3$ and $x_1 \leftarrow x_2 \to x_3$. Thus, $x_1$ and $x_3$ are conditionally independent given the value of $x_2$.

Two DAGs are said to be equivalent if they represent the same independence structure. The best we can hope to learn from data is a Bayesian network which is in the same equivalence class as the real network [145].

Similar to network inference approaches based on correlations between variables, it is not always possible to get information about the direction of an edge.

Compared to deterministic models, Bayesian networks consider stochastic effects and can thus account for stochastic fluctuations in regulation processes and noisy measure-

ments, which are presumably related to different phenotypes [129]. However, they have two main drawbacks, which make them inappropriate for our purposes: First, they are static models and do not incorporate evolution over time. Second, the underlying interaction graph has to be acyclic in order to obtain a well-defined joint probability distribution. This is a major limitation, since circuits in the interaction graph are necessary to model complex phenomena such as oscillations, multi-stationarity and hysteresis [92, 99, 163, 181, 192, 193].

To overcome both limitations, several authors have suggested to use *dynamic Bayesian networks* [71, 100, 132, 133, 145, 216]. In these networks, the local probabilities depend on time.

## 1.2.4 Differential equations

The state space of *ordinary differential equations* (ODEs) is the set $\mathbb{R}^n$. ODEs offer a deterministic time and state continuous description of a system. The evolution of the state of a system is specified by a function

$$\Phi : \mathbb{R}^n \times \mathbb{R} \to \mathbb{R}^n, \quad x(t) = \Phi(x(t_0), t), \tag{1.10}$$

which is assumed to be the solution of an *initial value problem*

$$\dot{x}(t) = f(x(t)), \quad x(t_0) = x_0 \tag{1.11}$$

with given state $x_0 \in \mathbb{R}^n$ at a time $t_0$ and a continuously differentiable function $f \in \mathcal{C}^1(\mathbb{R}^n \to \mathbb{R}^n)$.

ODEs have been established in recent years to model the dynamic behavior of gene regulatory networks quantitatively. Several parameterizations of the function $f(x(t))$ have been suggested. Chen *et al.* [34] first proposed a linear ODE model to reconstruct interactions between genes from expression data. The behavior of linear models is discussed in Chapter 2. We will also present a non-linear approach, which is based on *chemical reaction kinetics*. A further popular model class for gene regulatory networks are *synergistic systems*, shortly denoted *S-systems* [204]. In these models, regulatory influences are described by power law functions:

$$\dot{x}_i(t) = \alpha_i \prod_{j=1}^{n} x_j(t)^{g_{ij}} - \beta_i \prod_{j=1}^{n} x_j(t)^{h_{ij}} \tag{1.12}$$

The *kinetic orders* $g_{ij}$ and $h_{ij}$ and the *rate constants* $\alpha_i$ and $\beta_i$ have to be estimated in these models. The first term in equation (1.12) describes the effect of positive regulators, the second one refers to inhibitors. S-systems can capture many relevant types of biological dynamics [107]. Steady states of these systems can be calculated analytically, making these models attractive for network inference [37, 107, 204].

Minimization of the objective function $F_{MSE}(\omega, \mathcal{D})$ in the optimization problem (1.4) requires a solution of the system of differential equations. For most models, this cannot be

done analytically, but the system has to be integrated numerically. When problem (1.4) is solved heuristically, numerical integration has to be carried out several times and is often the most time consuming part of the parameter estimation procedure [205]. Hence, it can be useful to define an objective function that contains directly the time derivatives instead of concentrations, for example

$$F^*(\omega, \mathcal{D}) := \sum_{i=1}^{n} \sum_{t=1}^{T} \parallel \dot{x}_i(\omega, t) - \dot{\tilde{x}}_i(t) \parallel^2 . \qquad (1.13)$$

Here, $\dot{\tilde{x}}_i(t)$ denotes the time derivative of variable $x_i$ at time $t$, which has to be estimated using the dataset $\mathcal{D}$. $T$ corresponds to the number of observed time points. We will use this modified objective function in Chapter 3.

In contrast to Boolean networks, ODE models provide a quantitative description of a system's dynamic behavior. The consequence is that network inference from microarray data can only be done for regulatory subnetworks of at most a few tens of components, assuming that these subnetworks are relatively independent from the rest of the network. In comparison to Boolean and Bayesian networks, differential equation models lead to a better understanding of underlying mechanisms causing certain kinds of dynamic behaviors. One reason for this is that ODE models are built on chemical reaction mechanisms. Thus, model parameters correspond directly to reaction rates, binding affinities or degradation rates. This is helpful for both, a reasonable restriction of the parameter space and the interpretation of inference results. This interpretation is a great advantage of ODE models, as will be demonstrated in various examples in this thesis. We will also exploit the well-established theory of differential equations in order to analyze the dynamic behavior of our models. This leads to interesting questions and conclusions about the robustness of qualitative dynamic behaviors.

Finally, extensions of ordinary differential equation models include *stochastic kinetic approaches*, *partial differential equations* and *delay differential equations* [104]. In stochastic kinetic approaches, concentrations are discrete and change according to some probability distribution. They have been developed to explain the observed variety in experiments, in particular, in case that the number of molecules is small [48, 92, 125, 181]. Partial differential equations include derivatives with respect to time and space. They are used to account for spatial inhomogeneities within a cell and to model diffusion processes [48]. In delay differential equations, the temporal change of a variable $x_i$ at time $t$, $\dot{x}_i(t)$, is a function of the states of the system at some previous time points $x(t-\tau)$. Such time delays might be important if the system includes processes at different time scales, or if reactions are delayed by transport processes [26, 165]. All these approaches require information that is not included in microarray studies. Hence they do not belong to frequently used model classes for network inference from microarray data. However, all of these extensions can alter the qualitative dynamic behavior of a system compared to corresponding ODE systems. We will see in Chapter 8 that an inclusion of a time-delay $\tau$ into a differential

equation model can increase the robustness of sustained oscillations.

# Chapter 2

# Modeling Regulatory Networks with Differential Equations

In this chapter, we use *dynamical systems*, which can be described by ordinary differential equations (ODEs), to model regulatory networks. This is a rather technical chapter, because we define a lot of terms which will be used throughout this thesis. We start explaining the relation between a system of first order ordinary differential equations and dynamical systems in Section 2.1. A parameterization for an additive ODE model for gene regulatory networks is specified. Section 2.2 focuses on linear additive models. The main statement of this section is that the qualitative behavior of linear systems $\dot{x} = Ax + b$ can be classified in terms of the eigenvalues of the matrix $A$. Table 2.1 illustrates this classification for a two-dimensional system and thus represents this main statement. Section 2.3 introduces a non-linear differential equation model for gene regulatory networks based on chemical reaction kinetics, which is used in all subsequent chapters. In the beginning of this section, we discuss the analysis of limit sets of non-linear systems. We explain how the stability of an equilibrium point can be determined, and we connect periodic behavior of dynamical systems to stable periodic orbits. We will need these concepts in Chapters 6, 7 and 8, where mechanisms causing periodic behavior in chemical reaction systems are discussed.

## 2.1 Introduction: Dynamical systems

We assume that the temporal behavior of a state $x(t)$ of a system that is used to model a regulatory network is given as a function $\Phi(x(0), t)$ of the initial state $x(0)$ and the time $t$. Moreover, we assume that $x(t)$ satisfies an initial value problem of the form

$$\dot{x}(t) = f(x(t)), \quad x \in E, \, x(0) = x_0, \tag{2.1}$$

where $E$ is an open subset of $\mathbb{R}^n$ and the function $f \in \mathcal{C}^1(E \to \mathbb{R}^n)$ is a *continuously differentiable function*. That is, all partial derivatives of $f$ with respect to $x_j$, $\partial f_i / \partial x_j$, $i, j = 1, \ldots, n$, exist and are continuous. This guarantees the existence of a unique solution $x(t)$ in a time interval $[-a, a]$, given an initial state $x(0)$.

19

**Theorem 2.1.1 (Fundamental Existence-Uniqueness Theorem [147])** *Let $E$ be an open subset of $\mathbb{R}^n$ containing $x_0$ and assume that $f \in \mathcal{C}^1(E)$. Then there exists an $a > 0$ such that the initial value problem*

$$\dot{x}(t) = f(x(t))$$

*with initial value $x(0) = x_0$ has a unique solution $x(t)$ on the time interval $[-a, a]$.*

Subsequently, we will abbreviate the vector $x(t)$ with $x$ and keep in mind that it is in fact a function of time $t$.

With our assumptions, the solution of system (2.1) is related to a dynamical system, which provides a functional description of the solution of the system. Therefore, we first give a formal definition of a dynamical system and reveal the connection to system (2.1) afterwards.

**Definition 2.1.2** [Dynamical System [147]] A *dynamical system* on $E$ is a $\mathcal{C}^1$-map

$$\Phi : \mathbb{R} \times E \to E, \tag{2.2}$$

where $E$ is an open subset of $\mathbb{R}^n$, and if $\Phi_t(x) := \Phi(t, x)$ then $\Phi_t$ satisfies

1. $\Phi_0(x) = x$ for all $x \in E$ and

2. $\Phi_t \circ \Phi_s(x) = \Phi_{t+s}(x)$ for all $s, t \in \mathbb{R}$ and $x \in E$.

For fixed $x_0 \in E$, $\Phi(t, x_0)$ corresponds to the solution of the initial value problem in Theorem 2.1.1. The first property in Definition 2.1.2 assures that the initial condition $x(0) = x_0$ is fulfilled. The second one states that the evolution of the system is uniquely determined for every $t' \in \mathbb{R}$ if the state $x$ of the system at any time $t$ is known. This means that solution curves in the state space cannot intersect, since otherwise the time evolution of the system would not be unique at the intersection point. More precisely, we state the following relation between a dynamical system and an initial value problem:

When $\Phi(t, x)$ is a dynamical system defined on $E \subseteq \mathbb{R}^n$, then

$$f(x) = \frac{d}{dt}\Phi(t, x)\Big|_{t=0} \tag{2.3}$$

defines a $\mathcal{C}^1$-*vector field* on $E$, and for each $x_0 \in E$, $\Phi(t, x_0)$ solves the initial value problem (2.1). Furthermore, a solution of the initial value problem (2.1) exists for every $t \in \mathbb{R}$, meaning that for each $x_0 \in E$, the maximal interval of existence of $\Phi(t, x_0)$ is the time interval $I(x_0) = (-\infty, \infty)$. Thus, each dynamical system is related to a $\mathcal{C}^1$-vector field $f$, and the dynamical system describes the solution set of the differential equation defined by this vector field. Conversely, given a differential equation $\dot{x} = f(x)$, $x \in E$ with $f \in \mathcal{C}^1(E)$ and $E$ an open subset of $\mathbb{R}^n$, the solution $\Phi(t, x_0)$ of the initial value problem (2.1) with $x_0 \in E$ will be a dynamical system on $E$ if and only if for all $x_0 \in E$, the maximal interval of existence $I(x_0)$ of $\Phi(t, x_0)$ is $(-\infty, \infty)$. In this case, we say that $\Phi(t, x_0)$ is the dynamical system on $E$ defined by the differential equation $\dot{x} = f(x)$ [147]. $\Phi(t, x_0)$ can also be regarded as the motion of the set $E$ through the state space. It is therefore also called *flow* of the differential equation:

**Definition 2.1.3** [Flow [147]] Let $E$ be an open subset of $\mathbb{R}^n$ and let $f \in \mathcal{C}^1(E)$. Let $\Phi(t, x_0)$ with $x_0 \in E$ be the solution of the initial value problem (2.1) defined on its maximal interval of existence $I(x_0)$. Then for $t \in I(x_0)$, the mapping $\Phi_t : E \to E$ defined by

$$\Phi_t(x_0) := \Phi(t, x_0) \tag{2.4}$$

is called the *flow of the differential equation* $\dot{x} = f(x)$; $\Phi_t$ is also referred to as the *flow of the vector field f(x)*.

In subsequent chapters, we will often consider only the time dependence of $\Phi(t, x_0)$ for a *fixed* initial concentration vector $x_0$, which is given by the experimental time series. We will therefore use the short hand notation $x$, which corresponds to $\Phi(t, x_0)$ for this fixed $x_0$ and $t \in I(x_0)$. The mapping $\Phi(\cdot, x_0) : I(x_0) \to E$ defines a *solution curve* or *trajectory* $\Gamma(x_0)$ of the system $\dot{x} = f(x)$ through the point $x_0$:

$$\Gamma(x_0) := \{x \in E | x = \Phi(t, x_0), t \in \mathbb{R}\}. \tag{2.5}$$

The *positive half-trajectory* $\Gamma^+(x_0)$ is the solution curve for positive time $t \geq 0$ that starts in $x_0$:

$$\Gamma^+(x_0) := \{x \in E | x = \Phi(t, x_0), t \geq 0\}. \tag{2.6}$$

## 2.1.1 Differential equation models for gene regulatory networks

In gene regulatory networks, the components of the vector $x$ correspond to concentrations of network components. In this thesis, we use the term 'network component' as a general term for all components whose dynamic behavior is described by differential equations.

One usually assumes a linear dependence between mRNA and protein concentrations in order to infer model parameters from microarray data. Thus the experimentally available mRNA concentrations are assumed to be a measure for the actual regulators, which are proteins. In other words, the main regulations, which determine the behavior of the system, are assumed to take place at the transcriptional level. All post-transcriptional regulations are neglected. Consequently, we interpret the networks inferred from microarray data as projections of the whole regulatory networks onto the space of transcriptional regulations.

Let's go back to equation (2.1). Although this approach looks rather general, it presumes a functional relation between the temporal change $\dot{x}$ of concentrations at time $t$ and the concentration vector $x$. This means that the temporal change of $x$ is uniquely determined by $x$ itself at any given time point $t \in \mathbb{R}$. Thus, there is already a strong assumption behind the general modeling approach (2.1), which is also made in most approaches that aim at learning gene regulatory networks from time series concentration data. In Section 2.3, we will see that this assumption implies a *quasi-steady state approximation* for the differential equations which will be derived here.

When describing gene regulatory networks with differential equations, a frequently used form for the vector field $f$ is (see for example [210])

$$\dot{x}_i = s_i - \gamma_i x_i + g_i(x) =: f_i(x) \quad i = 1, \ldots, n, \tag{2.7}$$

where $s_i \in \mathbb{R}_{0,+}$ is a *basal synthesis rate* and $\gamma_i x_i$ a first order degradation term with *degradation rate* $\gamma_i \in \mathbb{R}_+$. The function $g_i(x)$ accounts for influences of regulators acting on component $i$. The index $i$ runs over all $n$ network components. The terms $s_i$ and $\gamma_i$ determine the dynamic behavior of $x_i$ in case that there are no regulators, that is $g_i(x) \equiv 0$. In this case, component $i$ exponentially approaches a constant value $x_{i,s}$, which is given by the ratio of synthesis and degradation rates,

$$x_{i,s} = \frac{s_i}{\gamma_i}, \quad i = 1, \ldots, n. \tag{2.8}$$

When extracting cell components like mRNA or proteins from the cell, they usually degrade after some time. In model (2.7), this is described by the degradation term:

$$\dot{x}_i = -\gamma_i x_i \quad \Rightarrow \quad x = e^{-\gamma_i t} x_0, \tag{2.9}$$

where $x_0$ is the amount right after extraction. Here, we define the *half life* $T_{i,1/2}$ of component $i$ as the time after which half of the initial amount $x_0$ still exists,

$$x_i = e^{-\gamma_i T_{i,1/2}} x_{i,0} \overset{!}{=} \frac{x_{i,0}}{2}. \tag{2.10}$$

Degradation rate $\gamma_i$ and half life $T_{i,1/2}$ are thereby connected via

$$T_{i,1/2} = \frac{\ln 2}{\gamma_i}. \tag{2.11}$$

The half life of proteins or mRNAs is sometimes experimentally accessible and can thus directly be included into our model according to equation (2.11).

**Additive models**

Coupling of the differential equations is expressed by the function $g_i(x)$, which depends on concentrations of all regulators acting on component $i$. Most models of the form (2.7) are *additive models* [34, 53, 201]. In these models, different regulators are supposed to act independently, and the total effect on $x_i$ is the sum of single influences,

$$g_i(x) = \sum_{j=1}^{n} r_{ij}(x_j). \tag{2.12}$$

Here, the *regulation function* $r_{ij}$ describes the change of concentration of component $i$ under the influence of regulator $j$. The assumption of additivity of single influences is a simple way to choose a parameterization of the function $g_i$. It is, however, a rigorous

restriction for the model. We have seen in Section 1.1 that different regulators can in fact influence one another, for example by competing for the same binding site or by forming complexes. Certainly, these effects cannot always be neglected. On the other hand, for interaction networks of moderate and large size, for which the structure of the network is not yet known, it is often the only way to keep quantitative models of the form (2.7) tractable. Without this assumption, the regulation functions would be multi-dimensional. They would depend on several input concentrations, since effects of different regulators could not be regarded separately. This means, one would have to specify how to describe interactions between regulators, and it is not always clear how to do this in a general way without adapting the model to specific systems. In Chapter 6, we will overcome this strict limitation, when we consider a regulatory core network of the yeast cell cycle, and explicitly model interactions between several regulators. In this context, we will also see that these interactions can be important for the qualitative dynamic behavior of the model. However, such a detailed modeling is only possible because the cell cycle mechanisms are well-known, and we include a lot of biological knowledge into our model. In the present chapter, we will focus on additive regulation functions.

Equation (2.12) decouples the total influence of all regulators acting on $i$ into one-dimensional regulation functions, and this entails a great advantage for the network inference problem: The form of a single regulation function is accessible through experiments and has been in the focus of theoretical and experimental studies already several years ago [101, 213].

In the following sections, we will consider two additive model classes: simple *linear models* are highlighted in Section 2.2, and Section 2.3 focuses on more advanced non-linear equations with *sigmoidal regulation functions*. A parameterization of the latter class is derived from chemical reaction kinetics. Concepts from an analysis of the former linear models can partially also be used for the analysis of non-linear systems.

Before we go into detail with specific models, we make a further general assumption, which has, in contrast to the additivity assumption, a comprehensive biological justification. A regulator $j$ is supposed to have either an activating or an inhibiting effect on the regulated component. This 'OR' is an exclusive 'OR', such that the regulation function $r_{ij}(x_j)$ is either monotonically increasing, namely if $j$ activates $i$, or, if $j$ is inhibiting, $r_{ij}(x_j)$ monotonically decreases.

Our model can now be written as

$$\dot{x}_i = s_i - \gamma_i x_i + \sum_{i=1}^{n} r_{ij}(x_j) \quad s_i \in \mathbb{R}_{0,+}, \gamma_i \in \mathbb{R}_+ \tag{2.13}$$

with monotone functions $r_{ij} : \mathbb{R} \to \mathbb{R}$. This so defined *general additive model* for gene regulatory networks can graphically be represent as a directed graph $G(V, E)$ with a set of nodes $V = \{v_1, \ldots, v_n\}$ and a set of edges $E \subset V \times V$, where $e_{ij} := (i, j) \in E \Leftrightarrow$ j regulates i. Nodes correspond to network components, and a directed edge from $j$ to $i$ indicates that $j$ is a regulator of $i$. Furthermore, we have a labeling $c : E \to \{+, -\}$ of the edges, where
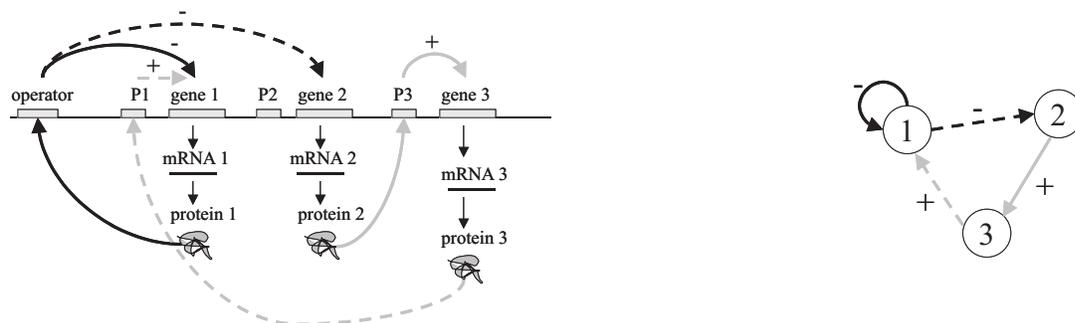
Figure 2.1: An example for a gene regulatory network with three components. **Left:** Protein 1 inhibits expression of genes 1 and 2 by binding to an operator site. Protein 2 binds to the promoter of protein 3 and activates expression of gene 3, and protein 3 in turn activates gene 1 by the same mechanism. **Right:** Interaction graph of the sample network. Here, mRNA and the corresponding protein are represented by one common node, and regulations of gene expression are represented as directed sign-labeled edges.

$c(e_{ij}) =' +'$ if $j$ activates $i$ and $c(e_{ij}) =' -'$ in case of an inhibition. This so defined *interaction graph* encodes qualitative information about the regulation functions $r_{ij}(x_j)$, that is, the structure of the coupling between network components or the topology of the graph $G(V, E)$, respectively. It does not provide any information about quantitative values and synthesis or degradation rates. The interaction graph can also contain circuits of length one in case that a cell component regulates its own expression. This is called *auto-regulation.*

A small sample gene regulatory network with three components is shown in Figure 2.1. Three genes are expressed and act as transcription factors. Protein 1 binds to an operator which inhibits expression of the two genes 1 and 2. Protein 2 binds to the promoter of gene 3 and has an activating effect on the expression of gene 3. The same holds for protein 3, which binds to promoter 1 and thus promotes transcription of gene 1. The corresponding interaction graph is shown on the right hand side of Figure 2.1. Here, assuming a linear relation between the concentrations of mRNA and protein, both are represented as one single component. According to this, an influence on an expression rate by binding of a protein to a promoter region of a gene is represented by an edge between the two corresponding nodes. Hence, the influence of protein 2 on protein 3, which is represented by two solid grey lines in the figure on the left hand side, has been shrunken to one single line from node 2 to node 3 in the gene regulatory network on the right hand side.

## 2.2   Linear models

In this section, we examine linear regulation functions of the form

$$r_{ij}(x_j) = k_{ij}x_j \quad k_{ij} \in \mathbb{R}, \tag{2.14}$$

and work out general properties of the resulting differential equation (2.13), which can be written as a simple linear system. We will consider the solutions of these systems, and thereby introduce basic terms of dynamical systems, which will be needed in subsequent chapters. Moreover, we will investigate the *stability* of fixed points of linear systems, since results can be transferred to analyze the stability of fixed points of non-linear systems as well. This is assured by the *Hartman-Grobman Theorem* [147], which states that near an hyperbolic equilibrium point $x_s$, a non-linear system has the same qualitative structure as the linear system that is obtained by a linearization about $x_s$.

For our purposes, it is sufficient to illustrate the dynamic behavior of linear differential equations for *planar systems*. In $\mathbb{R}^2$, eigenvalues can be calculated analytically, and trajectories can graphically be represented in a two-dimensional coordinate system. Basic concepts concerning the stability of fixed points can, at least theoretically, easily be extended to higher dimensions.

Inserting equation (2.14) into (2.13), $\dot{x}_i$ becomes a linear function of $x_j$ with slope $k_{ij}$, which will subsequently be denoted *regulation strength*. Accordingly, the whole system can be written as a system of coupled linear differential equations:

$$
\dot{x} = \underbrace{\begin{pmatrix} s_1 \\ s_2 \\ \vdots \\ s_n \end{pmatrix}}_{s} + \left[ \underbrace{\begin{pmatrix} k_{11} & k_{12} & \ldots & k_{1n} \\ k_{21} & k_{22} & \ldots & k_{2n} \\ \vdots & \ddots & & \vdots \\ k_{n1} & \ldots & \ldots & k_{nn} \end{pmatrix}}_{K} - \underbrace{\begin{pmatrix} \gamma_1 & 0 & \ldots & 0 \\ 0 & \gamma_2 & 0 & \ldots \\ \vdots & \ddots & & \vdots \\ 0 & \ldots & \ldots & \gamma_n \end{pmatrix}}_{G} \right] x \tag{2.15}
$$

Summarizing the matrices $K$ and $G$ into one single matrix $A := K - G$, system (2.15) can shortly be written as

$$
\dot{x} = Ax + s, \quad s \in \mathbb{R}^n_{0,+}, A \in \mathbb{R}^{n \times n}. \tag{2.16}
$$

It can easily be seen by setting $\dot{x} = 0$ that $x_s = -A^{-1}s$ is the only point where the vector field $f(x)$ vanishes. This holds in the generic case when the matrix $A$ is invertible, what is assumed here. Such a point $x_s$ is called *equilibrium point*. Formally, it is defined as

**Definition 2.2.1** [Equilibrium point [147]] A point $x_s \in \mathbb{R}^n$ is called an *equilibrium point* of a system $\dot{x} = f(x)$ if $f(x_s) = 0$. An equilibrium point $x_s$ is called a *hyperbolic equilibrium point* if none of the eigenvalues of the Jacobian matrix $J_f(x_s)$ has zero real part. The linear system $\dot{x} = J_f(x_s)x$ is called the *linearization* of (2.1) at $x_s$.

If $x_s$ is an equilibrium point of $\dot{x} = f(x)$ and $\Phi_t$ is the flow of the system, then $\Phi_t(x_s) = x_s$ for all $t \in \mathbb{R}$. We call $x_s$ also a *fixed point* of the flow $\Phi_t$ or a *steady state*. Fixed points are important for the long term behavior of a dynamical system. A fixed point $x_s$ is *stable* if trajectories near $x_s$ stay in a neighborhood of $x_s$ for positive time $t$. More formally, we refer to the following definition:

**Definition 2.2.2** [Stability of an equilibrium point [147]] Let $\Phi_t(x)$ denote the flow of the differential equation $\dot{x} = f(x)$ defined for all $t \in \mathbb{R}$. An equilibrium point $x_s$ of this system
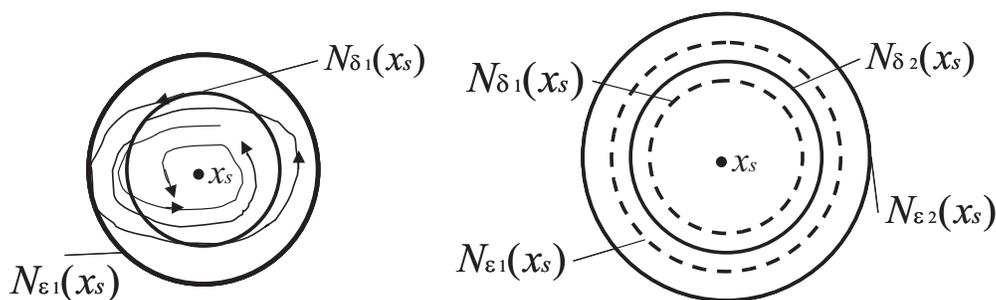
Figure 2.2: Stability of a fixed point in the state space. **Left:** The fixed point $x_s$ of a system $\dot{x} = f(x)$ is stable if for all $\epsilon_1 > 0$ there is a $\delta_1 > 0$, such that every trajectory starting in the neighborhood $N_{\delta_1}(x_s)$ never leaves $N_{\epsilon_1}(x_s)$. **Right:** The neighborhood $N_\delta(x_s)$ depends on the neighborhood $N_\epsilon(x_s)$.

is *stable* if for all $\epsilon > 0$ there exists a $\delta > 0$ such that for all $x \in N_\delta(x_s)$ and all $t \geq 0$ we have

$$\Phi_t(x) \in N_\epsilon(x_s). \tag{2.17}$$

The equilibrium point $x_s$ is *unstable* if it is not stable. And $x_s$ is *asymptotically stable* if there exists a neighborhood $N_\delta(x_s)$ of $x_s$ such that the system approaches $x_s$ for all $x_0 \in N_\delta(x_s)$:

**Definition 2.2.3** [Asymptotic stability of an equilibrium point [147]] An equilibrium point $x_s$ of a system $\dot{x} = f(x)$ is *asymptotically stable* if there exists a $\delta > 0$ such that for all $x \in N_\delta(x_s)$ we have

$$\lim_{t \to \infty} \Phi_t(x) = x_s. \tag{2.18}$$

An asymptotically stable equilibrium point is stable. Figure 2.2 illustrates that the stability of a fixed point is a property which refers to the state space. Figure 2.3 shows an asymptotically stable fixed point $x_s$. Every initial point $x_0$ in the neighborhood $N_\delta(x_s)$ approaches $x_s$ as $t \to \infty$. In contrast to Figure 2.2, there is a time $T^* \geq 0$ such that the flow $\Phi_t(x)$ even stays within $N_\delta(x_s)$ for $t > T^*$.

An investigation of equilibrium points and their stability is essential to analyze the global dynamic behavior of a dynamical system. Linear systems are particularly easy to analyze, since they can be solved analytically with classical methods[1](see for example [85, 147]). The solution $x$ of system (2.16) is the sum of the general solution for the corresponding homogeneous equation

$$\dot{x}_h = A x_h \tag{2.19}$$

and a special solution for the inhomogeneous equation (2.16).

---

[1]You can write down an analytic expression for the flow $\Phi_t(x_0)$ in terms of eigenvalues and eigenvectors of the matrix $A$. In $n > 3$ dimensions, eigenvalues usually have to be determined numerically.
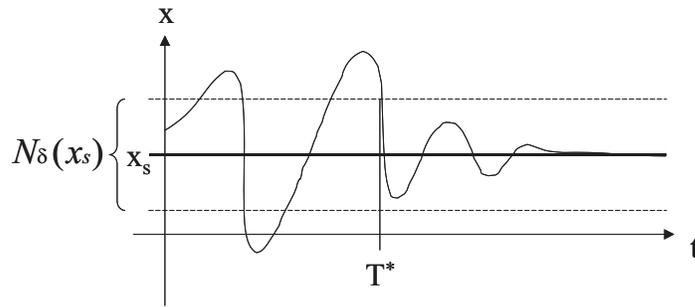
Figure 2.3: Asymptotic stability of a fixed point. The fixed point $x_s$ is asymptotically stable if there exists a neighborhood $N_\delta(x_s)$ such that every trajectory starting in $N_\delta(x_s)$ eventually approaches $x_s$ as $t \to \infty$.

## 2.2.1 Homogeneous system

According to the Fundamental Theorem for linear systems, for any initial concentration vector $x_0$, the solution of (2.19) is given by

$$x_h = e^{At}x_0, \tag{2.20}$$

where the linear operator $e^{At}$ is defined by its *Taylor series*

$$e^{At} := \sum_{k=0}^{\infty} \frac{(At)^k}{k!}. \tag{2.21}$$

In [147] it is shown that this operator is well-defined, and it can be computed in terms of the eigenvalues and eigenvectors of $A$. The idea is to decouple the equations by a transformation, such that $A$ has Jordan canonical form. The qualitative behavior of the system is solely determined by the eigenvalues and eigenvectors of $A$.

For planar systems, any matrix $A$ can be transformed into one of the following matrices [147]:

$$B = \begin{bmatrix} \lambda_1 & 0 \\ 0 & \lambda_2 \end{bmatrix}, \quad B = \begin{bmatrix} \lambda & 1 \\ 0 & \lambda \end{bmatrix} \quad \text{or} \quad B = \begin{bmatrix} b & -a \\ a & b \end{bmatrix} \tag{2.22}$$

with $\lambda_1, \lambda_2, \lambda \in \mathbb{R}$ being eigenvalues of the matrix $A$ and $a, b \in \mathbb{R}$. $B$ is determined by a linear transformation with an invertible matrix $T^* \in \mathbb{R}^{2\times 2}$:

$$B = (T^*)^{-1}AT^*. \tag{2.23}$$

The matrix $T^* \in \mathbb{R}^{2\times 2}$ contains two linearly independent eigenvectors of $A$ in the first case and one eigenvector and the first generalized eigenvector in the second case. In the third case, matrix $A$ has two complex conjugate eigenvalues $\lambda$ and $\bar{\lambda}$ and eigenvectors $v$ and $\bar{v}$. The transformation matrix $T^*$ contains the linear combinations $\frac{1}{2}(v + \bar{v})$ and $\frac{1}{2i}(v - \bar{v})$, which have real entries. For more details see [147]. The solution of the transformed system

$$\dot{y}_h = By_h \quad \text{with } \dot{y}_h = (T^*)^{-1}\dot{x}_h, \, y_h = (T^*)^{-1}x_h \tag{2.24}$$

is given by

$$y_h = e^{Bt} y_0. \tag{2.25}$$

Inserting (2.22) into (2.21), the matrix $e^{Bt}$ is specified to have one of the following forms:

$$\begin{bmatrix} e^{\lambda_1 t} & 0 \\ 0 & e^{\lambda_2 t} \end{bmatrix}, \quad e^{\lambda t} \begin{bmatrix} 1 & t \\ 0 & 1 \end{bmatrix} \quad \text{or} \quad e^{bt} \begin{bmatrix} \cos(at) & -\sin(at) \\ \sin(at) & \cos(at) \end{bmatrix}, \tag{2.26}$$

respectively. In the first case, the components of $y_h$ decrease or increase exponentially, depending on the signs of $\lambda_1$ and $\lambda_2$:

$$y_{1,h}(t) = e^{\lambda_1 t} y_1(0) \tag{2.27}$$
$$y_{2,h}(t) = e^{\lambda_2 t} y_2(0) \tag{2.28}$$

In the second case, a linear term is added to the exponential function in the first component,

$$y_{1,h}(t) = e^{\lambda t}(y_1(0) + ty_2(0)) \tag{2.29}$$
$$y_{2,h}(t) = e^{\lambda t} y_2(0). \tag{2.30}$$

The third case describes an exponentially damped oscillation in case of $\lambda < 0$ and oscillations with exponentially increasing amplitude for $\lambda > 0$:

$$y_{1,h}(t) = e^{bt}[\cos(at)y_1(0) - \sin(at)y_2(0)] \tag{2.31}$$
$$y_{2,h}(t) = e^{bt}[\sin(at)y_1(0) + \cos(at)y_2(0)] \tag{2.32}$$

Table 2.1 shows the various *phase portraits* that result from these solutions. The phase portrait of a system of differential equations is the set of all solution curves of the system in the state space. Note that the only equilibrium point of a homogeneous linear system is the origin. Solutions of the original system (2.19) are obtained by a linear transformation of coordinates, and thus its phase portrait is linearly equivalent to one of the phase portraits shown in Table 2.1. If the matrix $A$ has real eigenvalues, the origin can either be a *stable* or an *unstable node* or a *saddle* with a stable and an unstable manifold, which are spanned by the eigenvectors that correspond to the negative and positive eigenvalues, respectively. In case of two conjugate complex eigenvalues, the origin is a *focus* or a *center*. Trajectories spiral towards a stable focus if the real parts of the eigenvalues are negative, and the system shows damped oscillations. In case of positive real parts, the system oscillates with exponentially increasing amplitude. If $A$ has purely imaginary eigenvalues, the origin is a center. In this special case, according to Definition 2.2.2, the origin is stable, but not asymptotically stable. In all other cases, the origin is either asymptotically stable or unstable. In the special case that matrix $A$ has an eigenvalue $\lambda = 0$, the origin is a *degenerate equilibrium point*.

The classification of solutions of two-dimensional linear systems in terms of eigenvalues and eigenvectors of the matrix $A$ can offhand be extended to $n \geq 3$ dimensions. To do so, we have to calculate eigenvalues of an $n \times n$-matrix, that is, search for the zeros of

$$\text{eigenvalues of } A = \begin{pmatrix} a_{11} & a_{12} \\ a_{21} & a_{22} \end{pmatrix}$$

| | real eigenvalues | | | | | | | complex eigenvalues | | |
|---|---|---|---|---|---|---|---|---|---|---|
| eigenvalues | $\lambda_1 \neq \lambda_2$ | | | $\lambda_1 = \lambda_2 = \lambda$ | | | | $\lambda_{1,2} = \lambda \pm ib$ | | |
| eigenvectors | $v_1 \neq v_2 \in \mathbb{R}^2$ | | | $v_1 \neq v_2 \in \mathbb{R}^2$ | | $v_1 \in \mathbb{R}^2$ | | $v_1, \bar{v}_1 \in \mathbb{C}^2$ | | |
| matrix B | $\begin{pmatrix} \lambda_1 & 0 \\ 0 & \lambda_2 \end{pmatrix}$ | | | $\begin{pmatrix} \lambda & 0 \\ 0 & \lambda \end{pmatrix}$ | | $\begin{pmatrix} \lambda & 1 \\ 0 & \lambda \end{pmatrix}$ | | $\begin{pmatrix} \lambda & -b \\ b & \lambda \end{pmatrix}$ | | |
| matrix $e^B$ | $\begin{pmatrix} e^{\lambda_1 t} & 0 \\ 0 & e^{\lambda_2 t} \end{pmatrix}$ | | | $e^{\lambda t}\begin{pmatrix} 1 & 0 \\ 0 & 1 \end{pmatrix}$ | | $e^{\lambda t}\begin{pmatrix} 1 & t \\ 0 & 1 \end{pmatrix}$ | | $e^{\lambda t}\begin{pmatrix} \cos(bt) & -\sin(bt) \\ \sin(bt) & \cos(bt) \end{pmatrix}$ | | |
| sign $\sigma(\lambda)$ | $\lambda_{1,2} < 0$ | $\lambda_{1,2} > 0$ | $\lambda_1 > 0,$ $\lambda_2 < 0$ | $\lambda < 0$ | $\lambda > 0$ | $\lambda < 0$ | $\lambda > 0$ | $\lambda < 0$ | $\lambda > 0$ | $\lambda = 0$ |
| fixed point | stable node | unstable node | saddle | stable node | unstable node | stable node | unstable node | stable focus | unstable focus | center |
| phase portrait |  |  |  |  |  |  |  |  |  |  |
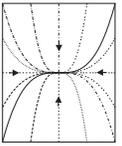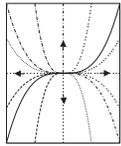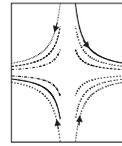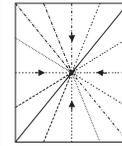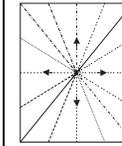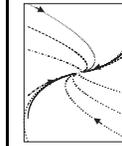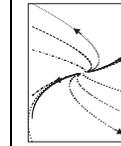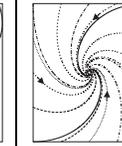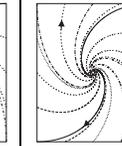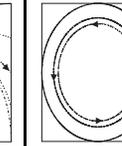
Table 2.1: Eigenvalues and singularities of two-dimensional linear systems $\dot{x} = Ax$. Axes in the phase portraits correspond to eigenvectors of the matrix $A$.
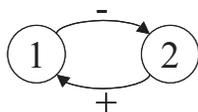
Figure 2.4: A gene regulatory network of two components

a polynomial of degree $n$. For $n \geq 4$, this can usually only be done numerically. Hence linear systems can only partly be solved analytically. For planar systems, it was possible to distinguish between three different forms of the transformed matrix $B$. For higher dimensional systems, we have to generalize this and consider a *Jordan canonical form* of the matrix $A$ (see [147]).

## 2.2.2   Inhomogeneous system

A special solution of the inhomogeneous linear system (2.16) is given by

$$x_{inh} = T \left( J^{-1}(e^{Jt} - I_n) \right) s, \tag{2.33}$$

with the matrix $T$ containing the Jordan basis of $A$ and $I_n$ denoting the $n \times n$-unit matrix. Matrix $J$ is the Jordan canonical form of the matrix $A$ in system (2.16).

The general solution of system (2.16) is the sum of the solution of the homogeneous system and a special solution of the inhomogeneous system:

$$x = x_h + x_{inh} \tag{2.34}$$

**Example 2.2.4** [Analyzing the phase portrait of a linear system] We present an example for a classification of the phase portrait of a two-component system using Table 2.1. Component $x_1$ regulates $x_2$ negatively with regulation strength $k_{21} = -1$. Component $x_2$ in turn is an activator of $x_1$ with strength $k_{12} = 2$. The gene regulatory network is shown in Figure 2.4. Degradation and synthesis rates are set to $s_i = \gamma_i = 1$ for both components. The corresponding system of differential equations reads

$$\dot{x} = \underbrace{\begin{pmatrix} -1 & 2 \\ -1 & -1 \end{pmatrix}}_{A} x + \underbrace{\begin{pmatrix} 1 \\ 1 \end{pmatrix}}_{s}. \tag{2.35}$$

The fixed point of system (2.35) is given by $x_s = -A^{-1}s = (1,0)$. Matrix $A$ has two complex conjugate eigenvalues $\lambda_{1,2} = -1 \pm i\sqrt{2}$ with negative real parts. Hence, according to Table 2.1, $x_s$ is specified as a stable focus. The corresponding phase portrait is shown in Figure 2.5.
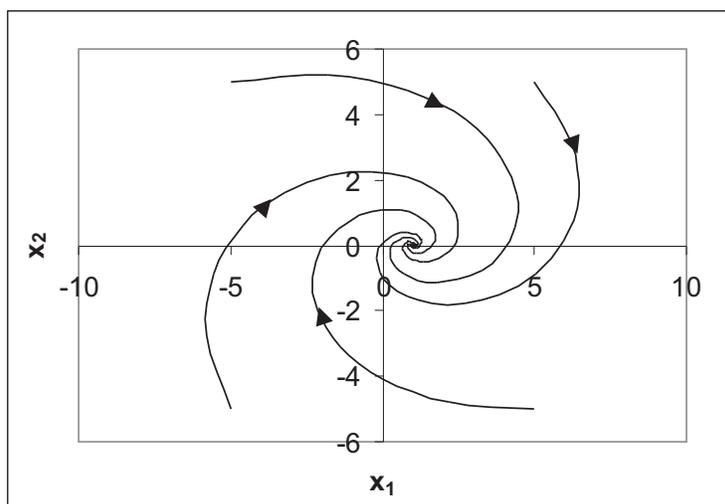
Figure 2.5: Phase portrait of system (2.35). The fixed point $x_s = (1,0)^T$ is a stable focus.

## 2.2.3 Linear models and gene regulation

To our knowledge, Chen and Church first proposed to model gene regulation with linear differential equations of the form

$$\dot{x} = Ax, \quad x \in \mathbb{R}^n,\, A \in \mathbb{R}^{n \times n} \tag{2.36}$$

in 1999 [34]. D'Haeseler *et al.* [53], van Someren *et al.* [201] and Wu *et al.* [211] used a discretized linear model to infer the structure of regulatory networks. In spite of the limited dynamics linear models can show, they are still frequently used to infer regulations among cell components (see for example [39, 87, 88, 110, 162, 198, 200, 211, 215]). In most of these and related works, a main goal was the inference of the structure of the interaction graph rather than capturing the dynamic behavior. Gustafsson *et al.* [87] argue that regulation functions can often be quite accurately approximated by their linearization about a specific working point. Thus, a linear model could provide a good starting point for further considerations. Sanguinetti *et al.* [164], who also used linear models to infer gene regulations, summarizes benefits and drawbacks of linear models for gene regulatory networks as follows:

> Perhaps the most glaring assumption we make is that an additive linear model is appropriate to describe a complex biological process, such as transcription. While this is clearly not the case, a linear model should still capture the most prominent features of the system. Although nonlinear models do obtain better results [...], their computational complexity rules out inference on a genome-wide scale, thus providing a serious limit to their usefulness in exploratory studies.

Linear models have several advantages concerning the parameter estimation from experimental data [87]. The number of parameters is usually smaller than for more compli-

cated models. Moreover, they are analytically solvable, and the minimization of the sum of squared errors between measurements and model predictions is an optimization problem with a quadratic objective function. However, linear models cannot capture a lot of dynamic behaviors observed in regulatory networks such as periodic behavior, multi-stationarity and hysteresis. Examples for the occurrence of these behaviors in biological systems are given in the end of this chapter and throughout the thesis. We have seen that linear models have only one single isolated equilibrium point which can be stable or unstable. When it is stable, it is globally stable, and the system eventually converges to this equilibrium point from all initial conditions. Furthermore, a linear system is unstable in the sense that it does not exclude unbounded solutions. An example to demonstrate this is a single component that promotes its own expression with regulation strength $k$:

$$\dot{x} = s - \gamma x + kx = s + (k - \gamma)x \tag{2.37}$$

The solution for given $x_0$ is

$$x = e^{(k-\gamma)t}x_0 + \frac{s}{k - \gamma}\left(e^{(k-\gamma)t} - 1\right). \tag{2.38}$$

Here, $x$ grows exponentially when $k > \gamma$, that is, the auto-regulation is stronger than the degradation.

Trajectories of linear systems that start with positive initial values, $x_0 \in \mathbb{R}_+^n$, do not always stay positive. This means, $\mathbb{R}_+^n$ is not an *invariant set*, and thus one can also get solutions with negative components. A state space of a biologically plausible model for gene regulatory networks should be restricted to $\mathbb{R}_+^n$, and the model should assure, at least for the range of interest, that trajectories never leave this region. This can only be achieved for linear models if all regulations are activating, and this is definitely not a realistic constraint.

## 2.3 Nonlinear models based on chemical reaction kinetics

In this section, we derive a biologically motivated model for the regulation functions $r_{ij}(x_j)$ in equation (2.13). For this purpose, we consider the binding of a transcription factor to a specific binding site in the promoter region of the regulated gene as a reversible chemical reaction in equilibrium. This leads to a parameterization of $r_{ij}(x_j)$ with a *sigmoidal function*. Boundedness and monotonicity of each regulation imply that the model is stable in the sense that the solutions are bounded as well. Moreover, the constraints which assure that the positive orthant $\mathbb{R}_+^n$ is an invariant set are less restrictive than for linear models. Complex dynamic behaviors such as sustained oscillations, hysteresis or multi-stationarity are non-linear phenomena and can thus only be captured with non-linear equations. In Chapter 6, we will actually show that systems of differential equations of the form (2.13) with monotone regulation functions mostly cause the system to converge towards a stable

fixed point. This raises the interesting question about mechanisms leading to more complex dynamic behaviors, which will also be taken up in this thesis for oscillating behavior.

We start this section by taking up some concepts and definitions of differential equations, which have already been introduced in the last section. These will be generalized and extended for non-linear systems. In Subsection 2.3.2, we use chemical reaction kinetics to derive parameterizations for the regulation functions. Properties of the resulting model will be discussed, and biological examples for certain dynamic behaviors will be given.

## 2.3.1 Analyzing non-linear models

Let us again consider a dynamical system $\Phi(t, x)$ defined by

$$\dot{x} = f(x), \quad x \in E \tag{2.39}$$

with an open subset $E \in \mathbb{R}^n$ and a vector field $f \in \mathcal{C}^1(E)$. In general, such a system is analytically not tractable. An analysis usually starts locally around limit sets, which determine the long-term behavior of the system.

### Stability of hyperbolic fixed points

The Hartman-Grobman Theorem and the Stable Manifold Theorem state that the local behavior around a hyperbolic fixed point $x_s$ is topologically equivalent to the corresponding linearized system

$$\dot{x} = J_f(x_s)(x - x_s). \tag{2.40}$$

Throughout this section, we assume that the equilibrium point $x_s$ under consideration has been translated to the origin.

**Theorem 2.3.1 (Hartman-Grobman Theorem [147])** *Let $E$ be an open subset of $\mathbb{R}^n$ containing the origin, let $f \in \mathcal{C}^1(E)$, and let $\Phi_t$ be the flow of the non-linear system (2.39). Suppose that $f(0) = 0$ and that the matrix $A = J_f(0)$ has no eigenvalue with zero real part. Then there exists a homeomorphism $H$ of an open set $U$ containing the origin onto an open subset $V$ containing the origin such that for each $x_0 \in U$, there is an open interval $I_0 \subset \mathbb{R}$ containing zero such that for all $x_0 \in U$ and $t \in I_0$*

$$H \circ \Phi_t(x_0) = e^{At} H(x_0); \tag{2.41}$$

*that is, $H$ maps trajectories of (2.39) near the origin onto trajectories of (2.40) near the origin and preserves the parameterization.*

The Hartman-Grobman Theorem is an important result in the local qualitative theory of ordinary differential equations. It provides a simple way to examine the stability of equilibrium points. According to this theorem, a given equilibrium point $x_s$ is stable if all eigenvalues of the Jacobian matrix $J_f(x_s)$ have negative real parts. It is a saddle point if there are eigenvalues with both positive and negative real parts, and it is unstable in case

that at least one eigenvalue has a positive real part. We will make use of this theorem in Chapters 6, 7 and 8.

In this context, the *Routh-Hurwitz method* is very useful, in particular, for high-dimensional systems. It provides a method to determine the number of roots of a polynomial that have positive real parts using only the coefficients in the polynomial [38, 135].

A hyperbolic fixed point is either asymptotically stable or unstable. In case that the Jacobian has an eigenvalue $\lambda$ with $\Re(\lambda) = 0$, the fixed point is non-hyperbolic, and the Hartman-Grobman Theorem cannot be used to analyze its stability. We will see in Chapter 7 that non-hyperbolic equilibrium points are particularly interesting in bifurcation theory, where the qualitative dynamic behavior of the system is considered subject to varying model parameters.

The Stable Manifold Theorem further details the connection between the original system (2.39) and the linearized system (2.40):

**Theorem 2.3.2 (Stable Manifold Theorem [147])** *Let $E$ be an open subset of $\mathbb{R}^n$ containing the origin, let $f \in \mathcal{C}^1(E)$, and let $\Phi_t$ be the flow of the non-linear system (2.39). Suppose that $f(0) = 0$ and that $J_f(0)$ has $k$ eigenvalues with negative real part and $n - k$ eigenvalues with positive real part. Then there exists a $k$-dimensional differentiable manifold $S$ tangent to the stable subspace $E^S$ of the linear system (2.40) at $0$ such that for all $t \geq 0$, $\Phi_t(S) \subset S$ and for all $x_0 \in S$,*

$$\lim_{t \to \infty} \Phi_t(x_0) = 0; \tag{2.42}$$

*and there exists an $n - k$ dimensional differentiable manifold $U$ tangent to the unstable subspace $E^U$ of (2.40) at $0$ such that for all $t \leq 0$, $\Phi_t(U) \subset U$ and for all $x_0 \in U$,*

$$\lim_{t \to -\infty} \Phi_t(x_0) = 0. \tag{2.43}$$

For an example, we go back to Table 2.1. In case that the origin is a stable equilibrium point, the stable subspace is the whole $\mathbb{R}^2$. The saddle point in this classification scheme has a one-dimensional stable subspace , the x-axis, and a one-dimensional unstable subspace, the y-axis. A non-linear two-dimensional system with $f(0) = 0$ and a Jacobian matrix $J_f(0)$ with two real eigenvalues of opposite sign has, according to Theorem 2.3.2, a one-dimensional stable manifold, which is tangent to the x-axis at $x_s$, and a one-dimensional unstable manifold tangent to the y-axis.

A stability analysis of an equilibrium point $x_s$ by linearizing about $x_s$ and calculating the eigenvalues of the corresponding Jacobian matrix $J_f(x_s)$ does not provide any information about the neighborhood in which the system is topologically equivalent to the linearized system. It should also be mentioned that a stability analysis of a non-hyperbolic equilibrium point is more involved. It can sometimes be done via searching for a *Liapunov*

*function* for the system [122]. Here, it is also possible to draw conclusions about the neighborhood $U$ in Theorem 2.3.1. We will give an example for a Liapunov function in Chapter 8.

### Limit sets and their stability

So far, we have only considered fixed points of a dynamical system and the local behavior in a neighborhood of these points. However, the long term behavior of a dynamical system can also be determined by other attracting sets, and thus we generalize the definition of an asymptotically stable equilibrium point $x_s$. Remember that if the point $x_s$ is asymptotically stable, every trajectory that contains a point $x_0$ near $x_s$ converges to $x_s$ for $t \to \infty$. More generally, if there exists a sequence $t_n$ of successive time points for which the system approaches a certain point $p$ in the state space, then $p$ is called a *limit point*. We distinguish between $\omega$- and $\alpha$-limit points:

**Definition 2.3.3** [Limit point of a trajectory [147]] A point $p \in E$ is an $\omega$-*limit point* of the trajectory $\Phi(\cdot, x)$ of system (2.39) if there is a sequence $t_n \to \infty$ such that

$$\lim_{n \to \infty} \Phi(t_n, x) = p. \tag{2.44}$$

Similarly, if there is a sequence $t_n \to -\infty$ such that

$$\lim_{n \to \infty} \Phi(t_n, x) = q, \tag{2.45}$$

with $q \in E$, then $q$ is called an $\alpha$-*limit point* of the trajectory $\Phi(\cdot, x)$ of (2.39). The entire set of all $\omega$- and $\alpha$-limit points of a trajectory $\Phi(\cdot, x) = \Gamma(x)$ is called the $\omega$-*limit set* $\omega(\Gamma(x))$ and the $\alpha$-*limit set* $\alpha(\Gamma(x))$, respectively. The union of both sets, $\omega(\Gamma(x)) \cup \alpha(\Gamma(x))$, is the *limit set* of $\Gamma(x)$.

In Table 2.1, for example, a stable node is an $\omega$-limit point of all trajectories $\Gamma(x)$, $x \in \mathbb{R}^2$. Similarly, an unstable node is an $\alpha$-limit point of $\Phi(t, x)$ for all $x \in \mathbb{R}^2$. The saddle in this scheme is an $\omega$-limit point of $\Gamma(x)$ for all $x$ lying on the stable manifold, here the $x_1$-axis, and it is at the same time an $\alpha$-limit point for all vectors $x$ on the unstable manifold, the $x_2$-axis.

For our work, periodic behavior of a dynamical system is of particular importance. Oscillating behavior of components of $x$ corresponds to closed curves in the state space:

**Definition 2.3.4** [Periodic Orbit [147]] A *cycle* or *periodic orbit* of (2.39) is any closed solution curve $\Gamma^\circ$ of system (2.39) in the state space which is not an equilibrium point of (2.39).

Thus, starting with an initial state $x_0 \in \Gamma^\circ$, the system eventually returns to $x_0$ after some time $T$, called the *oscillation period*:

$$T := \min_{t \in \mathbb{R}_+} \{t | \Phi(t, x_0) = x_0, \ x_0 \in \Gamma^\circ\} \tag{2.46}$$

In this connection, we also define the *oscillation amplitude* $a_i$ for each variable $x_i$, $i = 1, \ldots, n$ as the difference between the minimum and the maximum value of $x_i$ on the periodic orbit $\Gamma^\circ$:

$$x_i^{min}(\Gamma^\circ) \quad := \quad \min_{x_i \in \Gamma^\circ} x_i \tag{2.47}$$

$$x_i^{max}(\Gamma^\circ) \quad := \quad \max_{x_i \in \Gamma^\circ} x_i \tag{2.48}$$

$$a_i(\Gamma^\circ) \quad := \quad d(x_i^{max}(\Gamma^\circ), x_i^{min}(\Gamma^\circ)) \tag{2.49}$$

Similar to the stability of an equilibrium point, we can define the stability of a *periodic orbit* $\Gamma^\circ$. $\Gamma^\circ$ is said to be stable if trajectories through points near $\Gamma^\circ$ stay in a neighborhood of $\Gamma^\circ$ for $t > 0$:

**Definition 2.3.5** [Stability of a periodic orbit [147]] A periodic orbit $\Gamma^\circ$ is called *stable* if for each $\epsilon > 0$ there is a neighborhood $U$ of $\Gamma^\circ$ such that for all $x \in U$ and $t \geq 0$, $d(\Phi(t, x), \Gamma^\circ) < \epsilon$. If a periodic orbit is not stable, it is *unstable*. $\Gamma^\circ$ is *asymptotically stable* if for all $x$ in a neighborhood $U$ of $\Gamma^\circ$

$$\lim_{t \to \infty} d(\Phi(t, x), \Gamma^\circ) = 0. \tag{2.50}$$

An asymptotically stable periodic orbit is the $\omega$-limit set of all trajectories $\Phi(\cdot, x_0)$ with $x_0$ in the neighborhood $U$ specified in Definition 2.3.5.

Note that linear systems cannot have asymptotically stable periodic orbits. Stable fixed points or stable periodic orbits are sets the system eventually evolves to. Such sets are called *attractors* of a dynamical system. We will not give a formal definition here and refer to [85] or [147]. Besides fixed points and periodic orbits, an attractor can also be a manifold or a strange attractor. Attractors are *invariant sets* under the vector field $f$. This means that for an attractor $A$ and an $x \in A$, $\Phi(t, x) \in A$ for all $t \in \mathbb{R}_+$. The set of all points $x$ for which $\Phi(x, t)$ approaches $A$ as $t \to \infty$ build the *basin of attraction* of $A$. For linear systems, the basin of attraction of a stable node is the whole state space.

In the following subsection, we turn back to our model (2.13) for gene regulatory networks.

## 2.3.2   Sigmoidal regulation function

We recall our general additive model (2.13), where the temporal change of concentration of network component $i$ is described by a basal synthesis rate $s_i$, a first-order degradation term $-\gamma_i x_i$, and the sum of all influences of regulators acting on $i$:

$$\dot{x}_i = s_i - \gamma_i x_i + \sum_{j=1}^n r_{ij}(x_j), \quad i = 1, \ldots, n. \tag{2.51}$$

Considering the binding of a transcription factor to a specific binding site at the DNA a *reversible chemical reaction in equilibrium*, we will derive a non-linear parameterization of the regulation functions $r_{ij}(x_j)$. Therefore, we will exploit the *theory of Michaelis and Menten*, which actually describes the kinetics of enzymes and substrates [68]. The result is a hyperbolic regulation function, which equals the well-known Michaelis-Menten equation (see for example [196]). Taking cooperative effects between single transcription factors into account, the function becomes sigmoidal. In this form it is also known as *Hill equation*.

In Chapter 1, we saw that transcription was initiated when the RNA polymerase binds to the promoter region of a gene. Binding of transcription factors to specific binding sites can influence the affinity of this binding reaction. In the following, we examine the effect of transcription factors on the transcription of the regulated gene.

### 2.3.3   Reactions on different time scales

A transcription factor $TF$ can bind to a specific DNA binding site $BS$ and form a stable complex $C$. This is assumed to be a reversible reaction with *rate constants* $k_1$ and $k_{-1}$:

$$TF + BS \underset{k_{-1}}{\overset{k}{\rightleftharpoons}} C \tag{2.52}$$
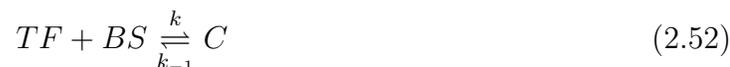
The rate constants are measures for the probabilities that the corresponding reaction takes place in the next time unit, normalized to the density of the reactants. Thus $k_1$ and $k_{-1}$ do not depend on the total concentrations of reactants and products and are constant with respect to these parameters. Actually, they can vary with external conditions such as temperature and binding energy [149], which is frequently described by the *Arrhenius equation* (Appendix A).

In a gene regulatory network, we consider reaction processes on two *different time scales*: The *fast time scale* is defined by the binding reaction (2.52), which reaches an equilibrium state within a few seconds [3, 168]. On this time scale, the total concentration of transcription factors, which changes on the *slow time scale* of minutes or hours [3], is assumed to be constant. Contrary, if we are interested in the evolution of the system on the slow time scale, we can reduce the number of variables by a *quasi-steady state approximation* (QSSA), assuming that the fast reactions are in a slowly changing equilibrium state. The slow time scale is the important scale to infer gene regulatory networks from microarray data. In the following, we describe reactions on the fast time scale. Then we formulate our final model by applying a QSSA for this fast time scale.

**The fast time scale**

Given all concentrations of reactants and products, the change in concentration of all particles involved in reaction (2.52) can be written as a system of differential equations,

$$
\begin{aligned}
\frac{d}{dt}[TF](t) &= -k_1[TF](t)[BS](t) + k_{-1}[C](t) \\
\frac{d}{dt}[BS](t) &= -k_1[TF](t)[BS](t) + k_{-1}[C](t) \\
\frac{d}{dt}[C](t) &= k_1[TF](t)[BS](t) - k_{-1}[C](t),
\end{aligned}
\tag{2.53}
$$

where $[X](t)$ denotes the concentration of component $X$ at time $t$. Here, the underlying assumption is that the reactions proceed quickly, and intermediate products do not occur. Furthermore, the probability that a transcription factor and a binding site 'collide' is assumed to be proportional to the product of their concentrations. Inserting

$$
\begin{aligned}
[BS](t) &= [BS](0) + [TF](t) - [TF](0) & \tag{2.54} \\
[C](t) &= [C](0) + [TF](0) - [TF](t) & \tag{2.55}
\end{aligned}
$$

into the first equation of (2.53) leads to a quadratic differential equation for $[TF]$:

$$
\begin{aligned}
\frac{d}{dt}[TF](t) = &-k_1[TF](t)\left([BS](0) + [TF](t) - [TF](0)\right) \\
&+ k_{-1}\left([C](0) + [TF](0) - [TF](t)\right)
\end{aligned}
\tag{2.56}
$$

Equation (2.56) can be solved analytically by separating the variables (see [19]). The solution describes on the fast time scale how binding of a transcription factor to its binding site reaches an equilibrium state.

**The slow time scale - Quasi-steady state approximation**

However, we are not interested in the general solution of equation (2.56), since we want to describe the system on the slow time scale. We consider the binding reaction (2.52) in a *chemical equilibrium*, in which the average concentrations of reactants and products do not change over time. Such an equilibrium exists for an arbitrary reversible chemical reaction described by the same kind of kinetics as above, and it converges to a globally stable steady state of the corresponding differential equation system. In a chemical equilibrium, the number of complexes that are formed per unit time equals on average the number of complexes that dissociate, and there is no net reaction.

  The equilibrium assumption or QSSA can be justified from a biological and a mathematical point of view:

  1. The reaction is still in equilibrium even if variables, which might have an influence on the equilibrium of the system, change on a very slow time scale. This could be, for

example, a slightly varying temperature, which affects the reaction rate constants, or a change in the protein concentrations over time. A reaction on the fast time scale has always time to adapt to slow changes and hence converges rapidly to its slowly changing steady state. The QSSA can reduce the dimension of the problem by eliminating variables [68, 203]. We will see further examples in Chapter 6, where we model mechanisms of the yeast cell cycle including reactions on different time scales, and in Chapter 8, where a time-scale parameter is explicitly included into the model. When analyzing the dynamic behavior of gene regulatory networks, we are interested in the evolution of the system on the time scale of changes in protein and mRNA concentrations. These are minutes or hours, whereas binding of a transcription factor to its binding site often reaches an equilibrium state within a few seconds [3, 168].

2. Mathematically, a description of the system under consideration without the QSSA would be much more complex. A lot of specific knowledge about single reaction rates or measurements on both, the slow and the fast time scale, are needed to estimate all model parameters. The QSSA in turn only requires ratios of rate constants, as we will see in the following. Usually, time series measurements of mRNA concentrations are collected at the slow time scale and thus do not allow for such a detailed description. The QSSA is necessary to obtain a functional relation between the change of concentrations, $\dot{x}$, and the concentration vector $x$, as it is postulated in our general model (2.1). It is the basis to justify a description of gene regulatory networks with ordinary differential equations.

To consider the regulatory system on the slow time scale, we go back to system (2.53) and set the derivatives with respect to time to zero. This leads to the steady state concentrations $[X]_s$ of the reaction system (2.53):

$$
\begin{aligned}
0 &= -k_1[TF]_s[BS]_s + k_{-1}[C]_s \\
0 &= -k_1[TF]_s[BS]_s + k_{-1}[C]_s \\
0 &= k_1[TF]_s[BS]_s - k_{-1}[C]_s
\end{aligned}
$$

These equations give rise to define the *equilibrium constant* of the chemical reaction as the ratio of product and reactant concentrations:

$$
K := \frac{k_1}{k_{-1}} = \frac{[C]_s}{[TF]_s[BS]_s} \tag{2.57}
$$

According to equation (2.57), the ratio of products and reactants in chemical equilibrium is determined by the ratio of $k_1$ and $k_{-1}$, and knowledge about the values of both variables separately is not required. $K$ determines the direction of the net reaction for given initial concentrations: For $[C]_0/([TF]_0[BS]_0) < K$ the system favors the right hand side of reaction (2.52), and the concentration of the complex $C$ increases until it has reached its steady state concentration $[C]_s$ and *vice versa*. A constant $K \gg 1$ means that the equilibrium is 'on the right hand side'. Roughly speaking, the number of products far

exceeds the number of reactants in this case. Note that the equilibrium constant, simi-
lar to the reaction constants, actually depends on temperature, as described in Appendix A.

Rewriting (2.57) and substituting the complex concentration by the difference of the
total concentration of binding sites, $[BS]_t$, and that of free binding sites, $[C]_s = [BS]_t - [BS]_s$, leads to

$$1 - \frac{[BS]_s}{[BS]_t} =: \frac{[BS]_b}{[BS]_t} = \frac{[TF]_s}{[TF]_s + K^{-1}}. \tag{2.58}$$

The fraction $[BS]_b$ of occupied binding sites increases hyperbolically with the transcription
factor concentration.

At first glance, the notation $[BS]$ can be misleading, because we usually refer to only
one or two specific binding sites for a transcription factor within a promoter region of a
gene. But this is not a problem for our formalism. For one single binding site, the left
hand side of equation (2.58) can be interpreted as the probability of this site to be bound
by a transcription factor [168]. Therefore, if the number of unbound transcription factors
far exceeds the number of bound ones, $[TF]_s \approx [TF]_t$, the probability $P_c$ of the binding
site to be bound can be written in terms of $[TF]_t$:

$$P_c([TF]_t) = \frac{[TF]_t}{[TF]_t + K^{-1}} \tag{2.59}$$

This is a reasonable approximation, since the number of specific binding sites for a tran-
scription factor is usually much smaller than the number of transcription factors. This
probability is proportional to the change in concentration of the regulated network com-
ponent $i$, provided that mRNA half life and translation rates are constant, leading to the
following parameterization for the regulation function $r_{ij}(x_j)$:

$$r_{ij}(x_j) = k_{ij}\frac{x_j}{x_j + \theta_{ij}} \tag{2.60}$$

Function (2.60) is a hyperbolically increasing function in case that the regulation strength
is positive, $k_{ij} > 0$, and it is decreasing for negative strengths, $k_{ij} < 0$. The *threshold value*
$\theta_{ij}$ is related to the reaction constant $K$ (see equation (2.59)). If the concentration of the
regulator $j$ equals $\theta_{ij}$, the regulation reaches half of its maximal strength. Contrary to the
linear regulation functions introduced in Section 2.2, function (2.60) is bounded by 0 and
$k_{ij}$. The regulation strength $k_{ij}$ is the expression rate that is reached if the binding site is
bound by a transcription factor all the time, that is, $P_c = 1$.

The concept of chemical equilibrium of reversible reactions can be generalized to arbi-
trary reactions of the form

$$\sum_{i=1}^{m} \nu_i X_i \stackrel{K}{\rightleftharpoons} \sum_{j=1}^{n} \mu_j Y_j \tag{2.61}$$
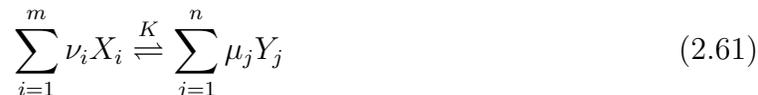
Here too, the reaction constant $K$ is given by the ratio of products and reactants. This can easily be seen by writing down the corresponding differential equations and setting the time derivatives to zero. The *stoichiometric coefficients* $\nu_i$ and $\mu_j$ appear as exponents:

$$K = \frac{\prod_{j=1}^{m} [Y_j]^{\mu_j}}{\prod_{i=1}^{n} [X_i]^{\nu_i}} \tag{2.62}$$

Relation (2.62) is also known as *law of mass action*.

## 2.3.4 Cooperative regulation - Hill equation

So far, we treated every transcription factor independently. This is not always realistic, since many transcription factors actually appear as protein complexes. Complex formation of identical proteins can be included into our model by assuming that the binding reaction happens with $n$ transcription factors. The corresponding chemical reaction then reads:

$$nTF + BS \underset{k_{-1}}{\overset{k}{\rightleftharpoons}} C \tag{2.63}$$

Here, the stoichiometric coefficient for the transcription factors is $n$, that for the binding sites and the complexes is 1, and, according to the law of mass action (2.62):

$$K = \frac{[C]_s}{[TF]_s^n [BS]_s}. \tag{2.64}$$

With the same substitutions and transformations as above, we arrive at a regulation function of the form

$$r_{ij}(x_j) = k_{ij} \frac{x_j^{m_{ij}}}{x_j^{m_{ij}} + \theta_{ij}^{m_{ij}}}, \tag{2.65}$$

also known as *Hill equation* [3]. Here, the exponent $m_{ij}$ equals the number of transcription factors, n, in reaction (2.63). In the literature, it is frequently denoted by *Hill-coefficient*.

The Hill-coefficient does not need to be an integer. The Hill function also provides a phenomenological description of interactions between transcription factors in general. For instance, binding of a transcription factor can sometimes be facilitated if another transcription factor has already bound to the DNA. This is expressed by a Hill-coefficient $m_{ij} > 1$, and the two transcription factors are said to act *in cooperation*. In case that binding is prevented by another transcription factor, the proteins interact competitively and $0 < m_{ij} < 1$.

Figure 2.6 illustrates equation (2.65) with different Hill-coefficients for an activating regulation. The regulation function is sigmoidally dependent on the regulator concentration $x_j$ and converges to its maximum value $k_{ij}$ as $x_j \to \infty$. At the threshold $\theta_{ij}$, the influence reaches half of its maximal strength for all curves. The slope of the curve is determined by the Hill-coefficient. A coefficient $m_{ij} = 1$ corresponds to the case of independent transcription factors (equation (2.60)), and the corresponding regulation function increases
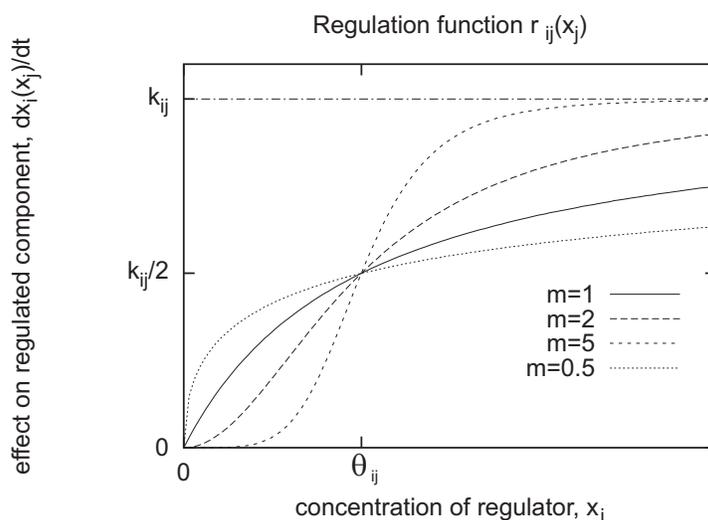
Figure 2.6: Sigmoidal regulation function according to equation (2.65).

hyperbolically. For competitive interactions between transcription factors, indicated by $m_{ij} = 0.5$ in the figure, the influence exceeds the independent case for low regulator concentrations $x_j < \theta_{ij}$ and falls below the independent curve for $x_j > \theta_{ij}$. This is reversed in case of a cooperative interaction.

## 2.3.5   Piecewise linear models

Several modifications of equation (2.65) have been proposed. The most prominent among these are probably the *piecewise linear differential equations* (PLDE), which have been investigated by Mestl *et al.* [131] and de Jong and coworkers [49, 50, 51]. Here, the sigmoidal regulation (2.65) is replaced by a *step function*, which is zero for regulator concentrations below a threshold value $\theta \geq 0$ and $k_{ij}$ for concentrations greater than $\theta$. This description leads to a partition of the state space into cuboids, whose boundaries are given by the threshold values. Within such a cuboid, the system of differential equations is linear and thus analytically solvable. Moreover, the matrix in equation (2.16) is a diagonal matrix, and hence the equations are already decoupled. However, PLDEs of this form can cause difficulties at the thresholds. These can contain artificial steady states or limit cycles. An analysis of the dynamic behavior of PLDEs can thus be far more complicated than for simple linear equations. We proposed a piecewise linear model with *logoid regulation functions* in [75, 77]. A logoid regulation function $r_{ij}(x_j)$ is zero for regulator concentrations $x_j$ below a threshold value $\theta_{1,ij}$, increases or decreases linearly between the first threshold $\theta_{1,ij}$ and a second threshold $\theta_{2,ij} > \theta_{1,ij}$ and equals a constant value $k_{ij}$ for $x_j > \theta_{2,ij}$. Unlike step functions, logoid regulation functions are continuous. This prohibits non-transparent threshold hyper-planes, but requires a diagonalization of the equations in order to solve the system. A detailed analysis of differential equations with logoid regulation functions can be found in [74].

### 2.3.6   Properties of the derived model

Inserting the sigmoidal regulation function into our system (2.51), we arrive at the following model for gene regulatory networks, upon which our work is build:

$$\dot{x}_i = s_i - \gamma_i x_i + \sum_{j=1}^{n} k_{ij} \frac{x_j^{m_{ij}}}{x_j^{m_{ij}} + \theta_{ij}^{m_{ij}}}, \quad x_i \in \mathbb{R} \quad i = 1, \ldots, n \tag{2.66}$$

with parameters $\gamma_i, m_{ij}, \theta_{ij} \in \mathbb{R}_+$, $s_i \in \mathbb{R}_{0,+}$ and $k_{ij} \in \mathbb{R}$. Here, we point out some basic properties of system (2.66) and show the main differences to linear models. First of all, boundedness of the regulation functions $r_{ij}(x_j)$ is sufficient to stabilize our model in the sense that there exists a bounded *trapping region* in the state space, which eventually attracts every trajectory. Every single regulation function $r_{ij}(x_j)$ is bounded by 0 and the regulation strength $k_{ij}$. Thus the sum over all regulation functions in system (2.66) is bounded above by the sum of positive regulation strengths, and bounded below by the sum of negative strengths. It is easy to show that

$$\dot{x}_i \leq 0 \quad \text{for } x_i \geq \frac{1}{\gamma_i} \left( s_i + \sum_{k_{ij} \in \mathbb{R}_+} k_{ij} \right) =: x_i^{max},$$

$$\text{and} \quad \dot{x}_i \geq 0 \quad \text{for } x_i \leq \frac{1}{\gamma_i} \left( s_i + \sum_{-k_{ij} \in \mathbb{R}_+} k_{ij} \right) =: x_i^{min}. \tag{2.67}$$

Hence the cuboid which is bounded by $x_i^{min}$ and $x_i^{max}$, $i = 1, \ldots, n$, is a trapping region for system (2.66). Every trajectory eventually reaches this region and never leaves it any more. The trapping region is an *invariant set* of the system. This is a biologically plausible property on the one hand, and it facilitates the analysis of the system's global behavior on the other hand, since we can concentrate our analysis of the long-term behavior on the trapping region.

According to (2.67), the condition

$$s_i > \sum_{-k_{ij} \in \mathbb{R}_+} k_{ij}, \tag{2.68}$$

which means that the basal synthesis rate $s_i$ compensates for all negative regulations, is sufficient for $\mathbb{R}_+^n$ to be an invariant set. With this condition, system (2.66) is a positive system (definition according to [52]). This condition is less restrictive than for linear regulation functions, where we have to exclude all negative regulations in order to get a positive system.

Our model is able to capture complex dynamic behaviors. Multiple steady states, for example, can already be achieved by a single component $x$ that positively regulates itself.
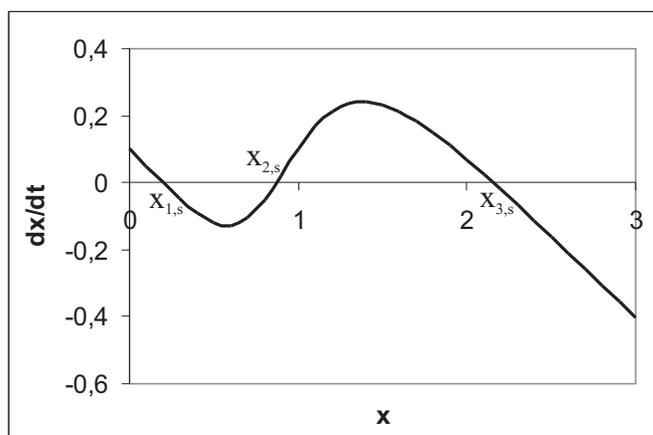
Figure 2.7: Vector field $f(x)$ of system (2.69), which has two stable steady states $x_{1,s}$ and $x_{3,s}$ and an unstable steady state $x_{2,s}$.

This phenomenon is denoted *multi-stationarity*. It is related to cell differentiation and memory [191, 193].

**Example 2.3.6** [Multi-stationarity] We consider the system

$$\dot{x} = f(x) = 0.1 - 0.5x + \frac{x^5}{x^5 + 1}. \tag{2.69}$$

As can be seen in Figure 2.7, this system has three steady states $x_{1,s} \approx 0.2$, $x_{2,s} \approx 0.9$ and $x_{3,s} \approx 2.2$. The states $x_{1,s}$ and $x_{3,s}$ are stable, $x_{2,s}$ is unstable. The system converges to one of the two stable states, depending on the initial concentration $x_0$: For $x_0 > x_{2,s}$ it converges to the upper equilibrium $x_{3,s}$, whereas for $x_0 < x_{2,s}$, the system tends to the lower stable fixed point $x_{1,s}$. Thus, the system can also switch between these two stable steady states when it is disturbed. This so-called *switch-like behavior* is observed, for instance, in in the switch between a lysogenic and lytic state in viruses [92].

We come back to this example in the next chapter, in which we model a regulatory subsystem in *E. coli*. Here too, a positive auto-regulation causes the system to show a phenomenon called *hysteresis*, which is related to multi-stationarity.

We do not get the advantages of non-linear models for free. First of all, we have seen that non-linear models are not analytically solvable any more. We have to apply numerical methods in order to simulate the behavior of the system. A detailed analysis of auto-regulating components shows that a large Hill-coefficient is required to obtain multi-stationarity. However, sigmoidal regulation functions with large Hill-coefficients are very steep about their threshold value $\theta$. This means that we have to deal with *stiff differential equations*, which are described in more detail in Chapter 8.

## 2.4 Summary

In this chapter, we described modeling of the dynamic behavior of gene regulatory networks by ordinary first order differential equations. The basis for this description is the assumption that transcription factor concentrations uniquely determine the regulatory processes. For the sake of simplicity and generality, we concentrated on *additive models*. In these models, regulatory effects caused by different transcription factors are assumed to be independent. As a consequence, the total effect on the regulated component equals the sum of single effects. Two important classes of additive models were introduced: Simple linear models are favorable concerning parameter estimation from experimental data, in particular if the number of network components is large. Thus they are frequently used for this purpose. However, we have seen that they are not always appropriate to capture the dynamic behavior of biological networks. Phenomena such as multi-stationarity, switch-like behavior or sustained oscillations, which are observed in biological systems [36], cannot be modeled with linear differential equations.

Nevertheless, the theory about the stability of solutions of linear models can also be used for non-linear models. This is ensured by the Hartman-Grobman Theorem. In Section 2.3.2, we derived a parameterization for a non-linear additive model. Regulation of gene expression through binding of a transcription factor to the DNA was described as a reversible chemical reaction in equilibrium. This approach is based on a *quasi-steady state approximation*. This approximation does not only reduce the number of variables in the model, but is also necessary to preserve the functional relation between $\dot{x}$ and $x$. A monotone and bounded regulation function was derived, which offers a more realistic description of gene regulatory networks than linear models. Trajectories eventually reach a trapping region, such that concentrations are bounded in this non-linear model.

Generally, non-linear terms in the system of differential equations are needed to capture complex dynamic behavior. The inference of parameters of these non-linear models from experimental data can be more complicated than for linear models. Apart from the regulation strengths $k_{ij}$, which appear as linear parameters in the model, the regulation functions also contain two non-linear parameters $m_{ij}$ and $\theta_{ij}$.

In the following chapters, we will use the non-linear additive model (2.66) to infer regulatory networks from experimental data. The model is used to explain the observed dynamic behavior quantitatively and qualitatively. The model in Chapter 3 shows the response of the system to a temporary external perturbation, which could also, at least qualitatively, be described by simple linear systems, whereas our non-linear model is required to explain the dynamic behavior of regulatory subsystems in *E. coli* and in *S. cerevisiae*. In Chapter 4, we will introduce a model which explains an experimentally observed threshold phenomenon by a switch of the system between different stable steady states. This is an example for multi-stationarity. The focus of the remaining Chapters 6, 7 and 8 is to explain mechanisms causing sustained oscillations, which are related to an asymptotically stable periodic orbit.

# Chapter 3

# Modeling the SOS Repair System in
# *Mycobacterium tuberculosis*

The focus of the following study is on modeling the *SOS repair system* in *Mycobacterium tuberculosis (Mtb)*. *Mtb* is the causative agent of tuberculosis, an airborne infection with a world-wide incidence rate of more than three million cases a year [62]. The genome of the bacterium was completely sequenced in 1998 [40], providing the basis for a comprehensive understanding of the pathogenity of *Mtb*. However, little is known yet about specific regulatory mechanisms in this bacterium in comparison to other bacteria such as, for example, *E. coli* or *C. glutamicum*. The whole genome of *Mtb* is estimated to contain approximately 4000 genes, but only about 350 of them have so far been identified [127] (data from 2005). The reason for this lack of knowledge is that *Mtb* is a very slowly growing bacterium. It only divides every 22-24 hours [153]. This is about 70 times slower than the cell cycle of *E. coli*. Thus, the duration of experiments is also much longer. *Mtb* has some characteristic features that make this bacterium resistant to several drugs. It has a very robust cell wall, and it is able to shift between two physiologically distinct growth states: an active state, in which the cells grow and divide, and a dormant non-replicative state [62, 214]. This dormant state enables the bacterium to survive in a host cell for a long time and to become active only when the immune system is weakened. The DNA repair system of *Mtb* is essential for its survival in hostile environments, for example induced by anti-microbial drugs. An understanding of regulatory mechanisms in the SOS repair system at the molecular level may also contribute to the fight against various drug-resistant strains, which have emerged in the last years [127].

The SOS repair system is a mechanism of bacteria to respond to damages in the DNA that are, for example, caused by pathogenesis radiation or drugs. Double strand breaks frequently serve as a stimulating signal for the response of the organism, resulting in an up-regulation of genes involved in DNA repair and a disruption of the cell division process. A well-conserved *SOS core system* containing the regulatory genes *recA* and *lexA* exists in several bacteria, including *E. coli* and *Mtb* [158]. The regulatory mechanisms in this core system are well-known due to extensive studies in *E. coli* (see for example [207])

and can be transfered to the Mycobacterium as well [47, 158]. Aside from the *recA-lexA* mechanism, experiments give evidence for an alternative DNA repair system in *Mtb*, which is independent of *recA* and *lexA* [20, 47, 158]. So far, little is known about the genes involved in this alternative mechanism. Related to this lack of knowledge, the aim of our modeling is two-fold:

1. Finding genes potentially participating in this alternative regulatory mechanism and which are somehow related to the core mechanism. For this purpose, we use an algorithm developed by Cabusora *et al.* [27], which uses multiple data sources, and analyze the output of this algorithm statistically.

2. Building a model that explains the dynamic response of the system to DNA damages. The model should include known regulations among the well-known *recA-lexA* core mechanism and hypothetical regulations between potential candidate genes representing the alternative mechanism.

For our analysis, we use gene expression data of the whole *Mtb* genome. The interaction graph considered here represents a biochemical rather than a gene regulatory network. Some of the edges stand for transcriptional regulations, and others represent regulations affecting the activity of proteins. Therefore, some of the nodes in this network correspond to proteins, and the corresponding variables in the system describe their activities. For these nodes, the assumption of a linear relation between concentrations of mRNA and proteins does not hold. We incorporate this into the model by explicitly including biological knowledge about the regulation mechanisms.

This chapter is structured as follows: A *core model* representing the *recA-lexA* core mechanism is introduced in Section 3.1. This model is extended by further components representing the alternative mechanism in Section 3.2. Section 3.3 presents simulations with the extended model. Parameters are estimated using gene expression time series data. Finally, results are discussed in Section 3.4.

## 3.1   Core model

### 3.1.1   Interaction graph

The main components of the *recA-lexA* core system are the proteins RecA and LexA. Together, they regulate about 35-40 genes in *Mtb*. LexA is a repressor protein that binds to specific binding sites on the DNA, called *SOS boxes*. It represses the transcription of the so-called *SOS genes*. These are genes containing an SOS box in their promoter region. When the DNA is damaged, the protein RecA binds to single-stranded DNA and causes the auto-catalytic cleavage of LexA. Thereby, LexA is prevented from binding to the SOS boxes, and consequently, expression of the SOS genes increases. An SOS gene is said to be *up-regulated* or *induced* by DNA-damage. SOS boxes are also found in the promoter

regions of *lexA* and *recA*. This enables the bacterium to rapidly react to damages of the DNA. Rand *et al.* [158] conducted experiments with wild types and *recA* mutants ($\Delta recA$) lacking the protein RecA. They identified genes which are DNA-damage-inducible even in *recA* mutants. Thus, these SOS genes are assumed to be regulated by an alternative mechanism independent of RecA and LexA, and the SOS genes can be categorized into three groups:

- **Group 1:** Genes that are solely regulated by RecA and LexA. They have an SOS box in their promoter region and, in case of a DNA damage, are not up-regulated in *recA* mutants.

- **Group 2:** Genes that are solely regulated by the alternative mechanism and are independent of RecA and LexA. These genes lack an SOS box in their promoter region. When the DNA is damaged, they are up-regulated to the same extend in wild types and *recA* mutants.

- **Group 3:** Genes which are regulated by both mechanisms. After DNA damage, genes belonging to this group are fully induced in wild types, but only partially in *recA* mutants.

We include the gene *linB* as a representative of group 1 into our model [158]. The gene *ruvC* represents the genes in group 3, which are regulated by both mechanisms [158]. Group two is disregarded, since genes in this group are not related to the *lexA-recA* system.

Figure 3.1 shows the interaction graph of the *recA-lexA core network* model. The active protein LexA, denoted by LexASOS, is bound to SOS boxes and thereby represses transcription of the SOS genes *ruvC, linB, recA* and *lexA*. This is indicated by negatively labeled edges from LexASOS to these genes. The SOS response is activated if single stranded DNA, emerging from breaks of double strands, functions as a signal, which activates the protein RecA. Accordingly, RecA stimulates the auto-catalytic cleavage of the active protein LexASOS. Thus, RecA negatively regulates LexASOS. The amount of LexASOS also depends on the total amount of LexA, which will be approximated by its mRNA concentration in our model. In Figure 3.1, this dependence is indicated by a positive regulation from LexA to LexASOS.

Both proteins, RecA and LexA, are regulated at the transcriptional and post-transcriptional level. Even so, we use one single variable RecA for the total amount of the protein RecA, given by the corresponding amount of mRNA, and the fraction of active protein. This simplification does not affect the dynamic of the network considerably. The same procedure is not convenient for the protein LexA. Here, a distinction of the fraction of active protein LexA, LexASOS, and the total amount of the protein is necessary to capture the dynamic behavior of the system.

## 3.1.2 Parameter estimation

In order to model the dynamic response of this network to DNA damage, we estimate parameters using a gene expression dataset accessible through the Gene Expression Omnibus
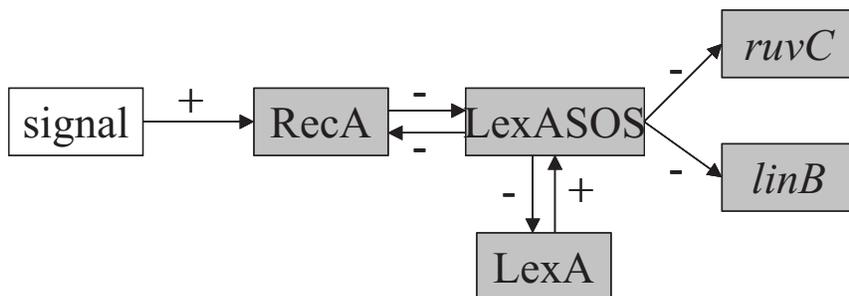
Figure 3.1: Core network of the *Mtb* SOS repair system.  A DNA-damage signal activates RecA to stimulate the auto-catalytic cleavage of the repressor LexASOS. Consequently, LexASOS becomes inactive and the SOS genes (*ruvC, linB, recA* and *lexA*) are up-regulated.  LexA denotes the total amount of the protein LexA, that is, the sum of active protein LexASOS and inactive protein.

Table 3.1: SOS response of core network genes to a treatment with 0.2 $\mu$g/ml mitomycin C. Shown are normalized ratios of expression values of treated cells and control cells.

| gene/time [h] | 0.5 | 1.25 | 1.5 | 2 | 4 | 6 | 8 | 12 |
|---|---|---|---|---|---|---|---|---|
| *recA* | 0.73 | 1.0 | 0.94 | 2.96 | 3.62 | 11.26 | 9.12 | 10.29 |
| *lexA* | - | 1.54 | - | - | 1.04 | 3.84 | 5.03 | 3.52 |
| *ruvC* | 0.84 | 0.56 | 0.84 | 1.53 | 1.17 | 1.69 | 1.89 | 2.44 |
| *linB* | 0.83 | 0.97 | 0.98 | 1.41 | 1.57 | 11.54 | 4.76 | 3.53 |

at NCBI (GEO;http://www.ncbi.nlm.nih.gov/-geo) with GEO platform accession number GPL1396.  Additional information about background intensities has been made available by Helena Boshoff (National Institute of Allergy and Infectious Diseases in Rockville, USA). Details can also be found in [17].

This dataset contains gene expression values of about 4000 *Mtb* genes and includes 16 experiments that show the response of *Mtb* cells to an exposure to *mitomycin C*, an antibiotic drug causing damages to the DNA. These 16 measurements are used in our study.  Gene expression was measured at 0.5, 1.25, 1.5, 2, 4, 6, 8 and 12 hours after treatment. The raw dataset, which includes measurements of treated cells and untreated control cells as well as background intensities for both, were preprocessed using BRB ArrayTools.  This is an open access package for the visualization and statistical analysis of DNA microarray gene expression data developed by Dr. Richard Simon and Amy Peng Lam (http://linus.ncbi.nih.gov/BRB-ArrayTools.html).  We used no filters and normalized the data by subtracting the median log-ratio of treated and control cells for each array, such that the median of the log-ratios of the normalized array is zero.  Expression values of genes in the core network are listed in Table 3.1.  Means were used for all time points which have been measured several times.  We build our model according to the non-linear

additive model derived in Chapter 2:

$$\dot{x}_i = s_i - \gamma_i x_i + \sum_{j=1}^{n} k_{ij} \frac{x_j^{m_{ij}}}{x_j^{m_{ij}} + \theta_{ij}^{m_{ij}}} \quad i = 1, \ldots, n, \tag{3.1}$$

with parameters $s_i, \gamma_i, m_{ij}, \theta_{ij} \in \mathbb{R}_+$ and $k_{ij} \in \mathbb{R}$. In order to be able to estimate parameters with only 8 time points, we replace the sigmoidal regulation functions by Boolean functions:

$$k_{ij} \frac{x_j^{m_{ij}}}{x_j^{m_{ij}} + \theta_{ij}^{m_{ij}}} \approx \begin{cases} 0 & x_j \le \theta_{ij} \\ k_{ij} & x_j > \theta_{ij} \end{cases} =: k_{ij} b_{\theta_{ij}}(x_j) \tag{3.2}$$

Inserting these Boolean functions into (3.1), the threshold values $\theta_{ij}$ partition the state space into cuboids. Within each of these cuboids, the corresponding system of differential equations becomes linear. Moreover, the differential equations are not coupled any more, since for fixed threshold $\theta_{ij}$ the regulation function $b_{\theta_{ij}}$ is constant and does not depend on the concentration $x_j$ of the regulator.

Including the information provided by the interaction graph in Figure 3.1, our model is written as

$$\begin{align} \text{RecA}: \quad \dot{x}_1(t) &= s_1 - \gamma_1 x_1(t) + k_{1,5} b_{\theta_{1,5}}(x_5) + as(t) \tag{3.3} \\ \text{LexA}: \quad \dot{x}_2(t) &= s_2 - \gamma_2 x_2(t) + k_{2,5} b_{\theta_{2,5}}(x_5) \tag{3.4} \\ \text{ruvC}: \quad \dot{x}_3(t) &= s_3 - \gamma_3 x_3(t) + k_{3,5} b_{\theta_{3,5}}(x_5) \tag{3.5} \\ \text{linB}: \quad \dot{x}_4(t) &= s_4 - \gamma_4 x_4(t) + k_{4,5} b_{\theta_{4,5}}(x_5) \tag{3.6} \end{align}$$

with synthesis and degradation rates $s_i, \gamma_i \in \mathbb{R}_+$, regulation strengths $k_{ij} \in \mathbb{R}_-$ and a parameter $a \in \mathbb{R}_+$ for the strength of the signal. The signal $s(t)$ is assumed to increase linearly until $t = 6h$ and is set to zero afterwards. The index 5 refers to the active fraction of the protein LexA, LexASOS. The influence of this variable has to be set manually. We couple its concentration to the course of expression values and the signal: The data show that *Mtb* responds to the treatment only after 2-4 hours. Thus we assume that LexA becomes inactive four hours after treatment and resumes its function as a repressor four hours later, when the DNA-damage signal has disappeared. The corresponding system is described by

**For** $0h \le t \le 4h$ **or** $t > 8h$ :

$$\begin{align} \text{RecA}: \quad \dot{x}_1(t) &= s_1 - \gamma_1 x_1(t) + as(t) \tag{3.7} \\ \text{LexA}: \quad \dot{x}_2(t) &= s_2 - \gamma_2 x_2(t) \tag{3.8} \\ \text{ruvC}: \quad \dot{x}_3(t) &= s_3 - \gamma_3 x_3(t) \tag{3.9} \\ \text{linB}: \quad \dot{x}_4(t) &= s_4 - \gamma_4 x_4(t) \tag{3.10} \end{align}$$

**For** $4h < t \leq 8h$ :

$$
\begin{aligned}
\text{RecA}: \quad \dot{x}_1(t) &= s_1 - \gamma_1 x_1(t) + k_{1,5} + as(t) & (3.11) \\
\text{LexA}: \quad \dot{x}_2(t) &= s_2 - \gamma_2 x_2(t) + k_{2,5} & (3.12) \\
ruvC: \quad \dot{x}_3(t) &= s_3 - \gamma_3 x_3(t) + k_{3,5} & (3.13) \\
linB: \quad \dot{x}_4(t) &= s_4 - \gamma_4 x_4(t) + k_{4,5} & (3.14)
\end{aligned}
$$

with a signal

$$
s(t) = \begin{cases} t & t \leq 6h \\ 0 & t > 6h \end{cases} \tag{3.15}
$$

Parameters $\omega$ of the model are estimated by minimizing the sum of squared errors between time derivatives $\hat{x}_i(t)$, estimated from the data, and the corresponding time derivatives $\dot{x}_i(t, \omega)$, predicted by the model, with respect to $\omega$. Here, $\omega$ is defined by

$$
\omega := (a, s_1, s_2, s_3, s_4, \gamma_1, \gamma_2, \gamma_3, \gamma_4, -k_{1,5}, -k_{2,5}, -k_{3,5}, -k_{4,5}). \tag{3.16}
$$

The resulting optimization problem is

$$
\min_{\omega} \sum_{z=1}^{8} \sum_{i=1}^{4} \| \dot{x}_i(t_z, \omega) - \hat{x}_i(t_z) \|^2 \quad \text{subject to } \omega \in \mathbb{R}_+^{13}. \tag{3.17}
$$

Time derivatives $\hat{x}_i(t)$ are estimated by polynomial interpolation. We approximate the derivative of $x_i(t)$ by the derivative of the polynomial $p(t)$ of degree two, fitted to expression values of three consecutive time points $x_i(t-1), x_i(t)$ and $x_i(t+1)$. This leads to

$$
\begin{aligned}
\hat{x}_i(t) = \quad & \frac{x_i(t_{k-1})}{(t_{k-1}-t_k)(t_{k-1}-t_{k+1})}(t_k - t_{k+1}) \\
&+ \frac{x_i(t_k)}{(t_k-t_{k-1})(t_k-t_{k+1})}(2t_k - t_{k-1} - t_{k+1}) \\
&+ \frac{x_i(t_{k+1})}{(t_{k+1}-t_{k-1})(t_{k+1}-t_k)}(t_k - t_{k-1}).
\end{aligned} \tag{3.18}
$$

The optimization problem (3.17) is under-determined, and we further restrict the parameter space by fixing the degradation rates to $\gamma_i = 0.1h^{-1}$, $i = 1, \ldots, 4$. These values are chosen to be approximately of the same order of magnitude as the expression values of the involved genes. A comparison of results using several other values for these rates shows that results depend only weakly on these parameters. In addition, we expect the ratio of concentrations of treated cells and control cells to converge to 1 for $t \to \infty$, assuming that the treated cells have successfully repaired all DNA damages after a while. This expectation can be formulated as a constraint for the synthesis rates $s_i$. The steady states $x_{i,s}$ for untreated cells are obtained by setting the left hand sides of equations (3.11), (3.12), (3.13) and (3.14) to zero and resolving each for $x_{i,s}$. The steady states are given by the ratios of production rates $s_i + k_{i,5}$ and degradation rates $\gamma_i$,

$$
x_{i,s} = \frac{s_i + k_{i,5}}{\gamma_i} \overset{!}{=} 1 \quad i = 1, \ldots 4. \tag{3.19}
$$

Table 3.2: Estimated parameter values for the *recA-lexA* core network.

| model parameter | $a$ | $s_1$ | $s_2$ | $s_3$ | $s_4$ | $\gamma_1$ | $\gamma_2$ |
|---|---|---|---|---|---|---|---|
| estimated value $[h^{-1}]$ | 0.55 | 0.10 | 1.00 | 0.27 | 0.92 | 0.10 | 0.10 |
| model parameter | $\gamma_3$ | $\gamma_4$ | $-k_{1,5}$ | $-k_{2,5}$ | $-k_{3,5}$ | $-k_{4,5}$ | |
| estimated value $[h^{-1}]$ | 0.10 | 0.10 | 0.00 | 0.90 | 0.17 | 0.82 | |

Hence the synthesis rates $s_i$ are given by the difference of the degradation rates $\gamma_i$ and the regulation strengths $k_{i,5}$, $s_i = \gamma_i - k_{i,5}$.

To solve the optimization problem with respect to all constraints, we use the Generalized Reduced Gradient (GRG2) algorithm, a nonlinear optimization code which is implemented in Excel. This algorithm was developed by Lasdon and Waren [113] and exhibits a local search. It has been shown to solve constrained non-linear optimization problems robustly and efficiently. In this implementation, derivatives with respect to model parameters are numerically calculated by slightly varying each parameter and calculating finite differences in the objective function. Estimated parameter values are listed in Table 3.2. The regulation of RecA by LexASOS has not been identified, $-k_{1,5} = 0$, inhibition of LexA and *linB* by LexASOS, described by the regulation strengths $k_{2,5}$ and $k_{4,5}$, respectively, are of the same order of magnitude. Compared to these two regulation strengths, expression of the gene *ruvC* depends only moderately on LexASOS, indicated by a value $-k_{3,5}$ that is smaller than $-k_{2,5}$ and $-k_{4,5}$.

### 3.1.3 Simulation

We use an Euler integration, which approximates the time derivatives in the differential equations with a difference quotient, and a time step $\Delta t = 0.5h$, to simulate courses of all four network components. The results along with experimental data are shown in Figure 3.2. Expression of RecA increases immediately after treatment due to coupling to the signal $s(t)$ and reaches its maximum of approximately ten-fold expression after six hours. Then the concentration falls back and converges slowly to its steady state. A comparison with the experimental data indicates that the fast increase in the first six hours after treatment is captured by the inferred model, whereas after six hours, the experimental RecA concentration seems to remain higher as predicted by the model. The genes *lexA*, *ruvC* and *linB* are up-regulated only four hours after treatment, when the protein LexA becomes inactive. They reach their maxima eight hours after drug treatment and decrease thereafter due to anew inhibition through LexA. Maximal expression levels of both *lexA* and *linB* correspond to an approximately four-fold increase, whereas *ruvC* increases only marginally. Comparing model predictions with experimental data and interpreting the high concentration of *linB* at $t = 6h$ as an outlier, the qualitative courses of LexA and *linB* are satisfactorily captured, albeit the simulated courses slightly underestimate the corresponding experimental data. Similar to RecA, the response of the gene *ruvC* is predicted to abate 8 hours after treatment, whereas experimental values indicate that the concentration
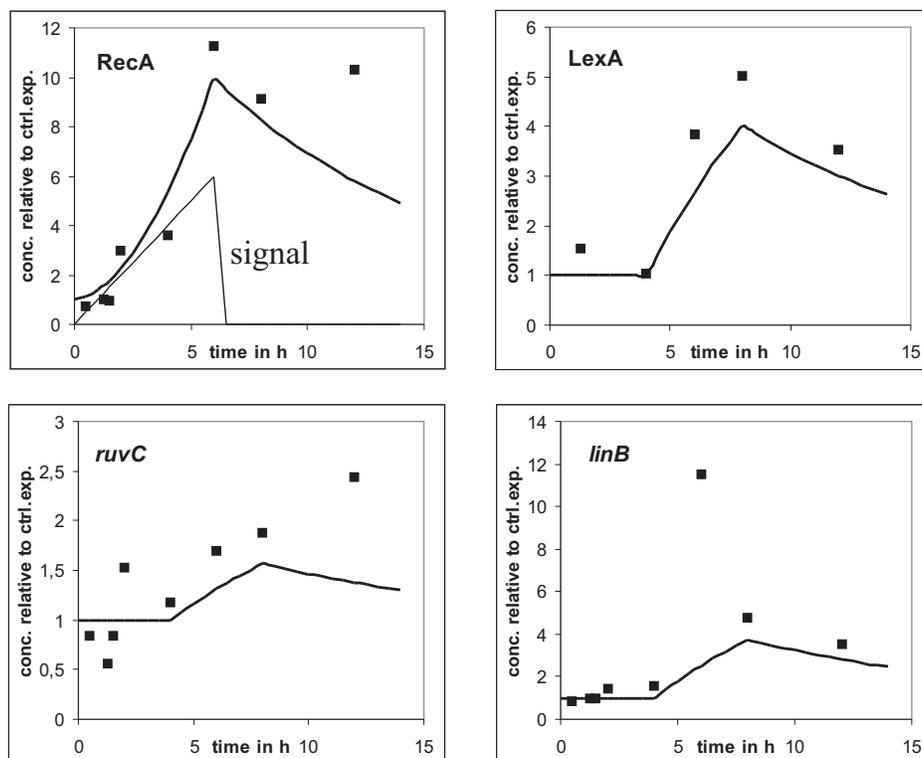
Figure 3.2: Dynamic response of the inferred SOS repair core network (*lines*) along with experimental data (*rectangles*). Initial concentrations were set to $x_i(0) = 1$, $i = 1, \ldots, 4$.

still increases after 12 hours.

## 3.2    Searching for candidate genes

In this Section, we address the question how the SOS repair core network should be extended by other genes, which potentially play a role in the DNA repair system and are related to the core network. For this purpose, we use an algorithm developed by Cabusora *et al.* [27]. Input of this algorithm is a set of *seed genes*, a table of interaction information about *Mtb* genes provided by Dr. Christian Forst, and gene expression data.

We use the genes *recA, lexA, ruvC* and *linB* as seed genes. In the first step, the table of interaction information is used to construct an interaction graph. Edges in this graph correspond to various interactions between *Mtb* genes listed in the table, for example protein-protein interactions, metabolic reactions or collective transcriptional regulations (for more details see [27, 127]). This graph contains about 1000 *Mtb* genes and about 70.000 interactions. In a subsequent step, a subgraph is created by calculating the $k$-shortest paths between every pair of seed genes. The method used for this setting is motivated and explained in Jiménez and Marzal [102] and Hershberger *et al.* [94]. The distance $d_{ij}$ between two nodes $v_i$ and $v_j$ is determined by the correlation coefficient $\tau_{ij}$ of

their expression values,

$$d_{ij} = \Phi^{-1}(1 - |\tau_{ij}|), \tag{3.20}$$

where $\Phi^{-1}$ is the inverse of the cumulative normal distribution. The user has to specify a cutoff value $l$ for the path length, motivated by the assumption that short paths are preferred by the cell, and fix the number $k$ of shortest paths. We apply the *Kendall correlation coefficient*

$$\tau_{ij} = \frac{P - I}{\sqrt{\left(\frac{n(n-1)}{2} - T_i\right)\left(\frac{n(n-1)}{2} - T_j\right)}}. \tag{3.21}$$

Here, each pair of expression values for gene $i$ and times $t$ and $\tilde{t}$, $(x_i(t), x_i(\tilde{t}))$, is compared with the corresponding pair of expression values of gene $j$, $(x_j(t), x_j(\tilde{t}))$. A *proversion* is a homogeneous change in both variables, that is $x_i(t) < x_i(\tilde{t})$ and $x_j(t) < x_j(\tilde{t})$ or $x_i(t) > x_i(\tilde{t})$ and $x_j(t) > x_j(\tilde{t})$. $P$ is the number of proversions in equation (3.21). If both variables change in opposite directions, this is called an *inversion*. $I$ denotes the total number of inversions. $T_i$ and $T_j$ are the numbers of *bindings*, that is, the number of pairs $(x_i(t), x_i(\tilde{t}))$ with $x_i(t) = x_i(\tilde{t})$ or $x_j(t) = x_j(\tilde{t})$, respectively. In comparison to the frequently used Pearson correlation coefficient, the Kendall correlation coefficient can discover general monotonous relations between two variables, not only linear ones. Moreover, it is less sensitive to outliers. Both properties make it appropriate to analyze gene expression data. First, the relations are expected to be non-linear, and second, these data are usually quite noisy.

The output of the algorithm is an undirected subgraph containing the seed genes and candidate genes along the $k$-shortest paths between two seed genes. Figure 3.3 shows the output for the SOS repair system with seed genes *recA, lexA, ruvC* and *linB* and parameters $k = 4$ and $l = 10$. Edges are labeled with the Kendall correlation coefficients. All seed genes, which are marked in grey, are connected with one another in Figure 3.3. Particularly high correlations can be found between *recA*, *linB* and *ruvC*, which are commonly regulated by LexA and RecA. Thus the output of the algorithm reflects the structure of the core network. The set of candidate genes consists of the genes *infB, dnaE2* and *Rv2719c*. These candidate genes are assumed to be potentially involved in the SOS repair system, and we will further analyze their expression patterns statistically.

We introduce a method which assigns significance levels to correlation coefficients shown in the subgraph in Figure 3.3. These levels are used to decide whether an edge is statistically significant and should be included into the *extended network model*. Therefore, we calculate correlation coefficients of the seed genes to all remaining measured genes in the organism. The set of these correlation coefficients is assumed to represent the real distribution $\mathcal{D}$ of correlations within the whole gene regulatory network of *Mtb* during SOS response. The whole dataset contains about 4000 genes. Thus, the representation of $\mathcal{D}$ is build on approximately $4 \cdot 4000$ correlation coefficients. Figure 3.4 shows the observed frequencies of these coefficients. We apply a two-tailed test. Therefore, we define two subsets $S^{min}$ and
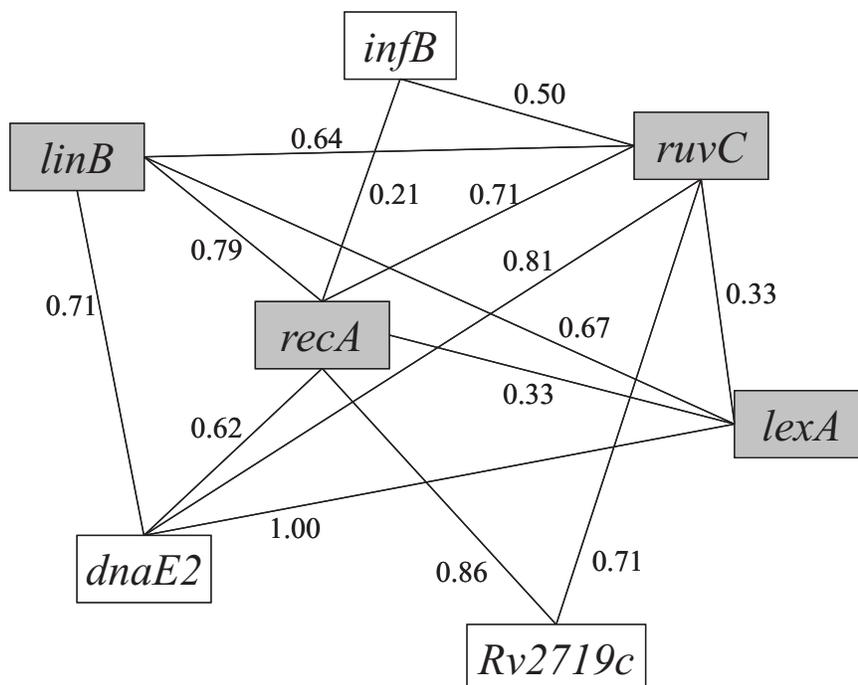
Figure 3.3: Output of the algorithm developed by Cabusora *et al.* [27]. The seed genes *recA, lexA, ruvC* and *linB* are marked in grey. Shown are the 4-shortest paths with maximal path length $l = 10$. Edges are labeled with Kendall correlation coefficients.
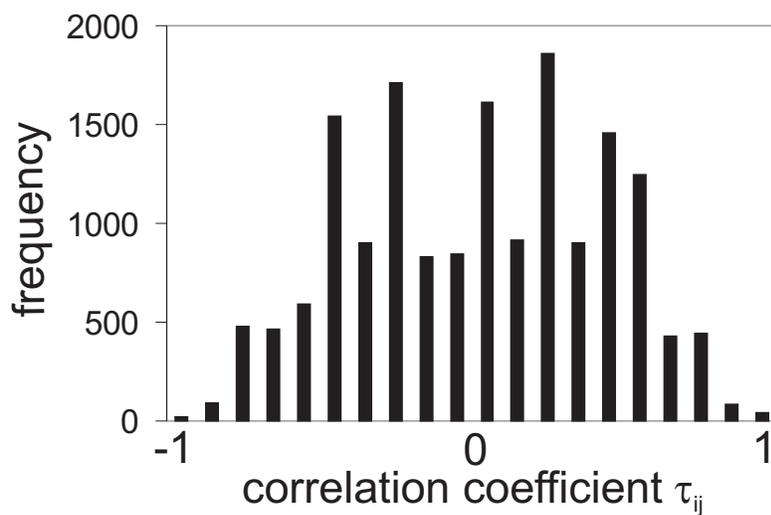


Figure 3.4: Frequencies of Kendall correlation coefficients. Included are correlations of the seed genes to all other genes in *Mtb*.

Table 3.3: Kendall correlation coefficients for each pair of genes in the subgraph (Figure 3.3). Significant values according to a significance level $\alpha = 5\%$ are marked in bold.

| genes | lexA | recA | ruvC | linB | infB | dnaE2 | Rv2719c |
|---|---|---|---|---|---|---|---|
| lexA | 1.00 | 0.33 | 0.33 | 0.67 | -0.67 | **1.00** | 0.00 |
| recA | | 1.00 | **0.71** | **0.79** | 0.21 | 0.62 | **0.86** |
| ruvC | | | 1.00 | 0.64 | 0.50 | **0.81** | **0.71** |
| linB | | | | 1.00 | 0.29 | **0.71** | **0.79** |
| infB | | | | | 1.00 | 0.62 | 0.36 |
| dnaE2 | | | | | | 1.00 | 0.52 |
| Rv2719c | | | | | | | 1.00 |

$S^{max}$ according to a cutoff value $\alpha$ for the significance levels: The subset $S^{min}$ contains $\alpha\%$ of all coefficients $\tau_{ij}$ with the smallest values and $S^{max}$ contains the same fraction with the largest values. The maximum of $S^{min}$, $\tau_{min}$, and the minimum of $S^{max}$, $\tau_{max}$, define cutoff values for the significance of an edge $e_{ij}$:

$$e_{ij} \text{ is significant} :\Leftrightarrow (\tau_{ij} \leq \tau_{min} \text{ or } \tau_{ij} \geq \tau_{max}) \tag{3.22}$$

The significance level $\alpha$ determines the sparseness of the network and is set to $\alpha = 0.05$. The corresponding thresholds for correlation coefficients are $\tau_{min} = -0.71$ and $\tau_{max} = 0.71$. Significant correlations in the subgraph according to our analysis are marked in bold in Figure 3.5. According to Table 3.3 and Figure 3.5, we exclude the gene *infB* from our extended model, because it shows no significant correlations to other genes in the network. The gene *dnaE2* has an SOS box and is not induced in *recA* mutants [158]. It belongs to the first group of genes, which are solely regulated by *recA* and *lexA*. Therefore, it is assumed to give no information about the unknown mechanism. Moreover, its maximum expression ratio is only about two, a value which often marks a significance limit for biologists, and it is thus excluded as well. The gene *Rv2719c* shows a 12-fold up-regulation, and its expression values correlate significantly with these of the genes *recA* and *ruvC* (see Figure 3.5). Thus we conclude that the gene *Rv2719c* might play an important role in the SOS repair system and has to be included into the model. This result is in accordance with the analysis of SOS genes described by Dullaghan *et al.* [61], who also suggested *Rv2719c* to take part in the DNA repair mechanism.

## 3.3 Extended model

### 3.3.1 Comparison with the core model

We extend our core model by the gene *Rv2719c* in the following way: *Rv2719c* has been shown to have an SOS box in its promoter region [61]. It is thus controlled by LexA-SOS, indicated by a negative regulation in the interaction graph in Figure 3.6. We make the strong assumption that *Rv2719c* represents the alternative mechanism. As we do not
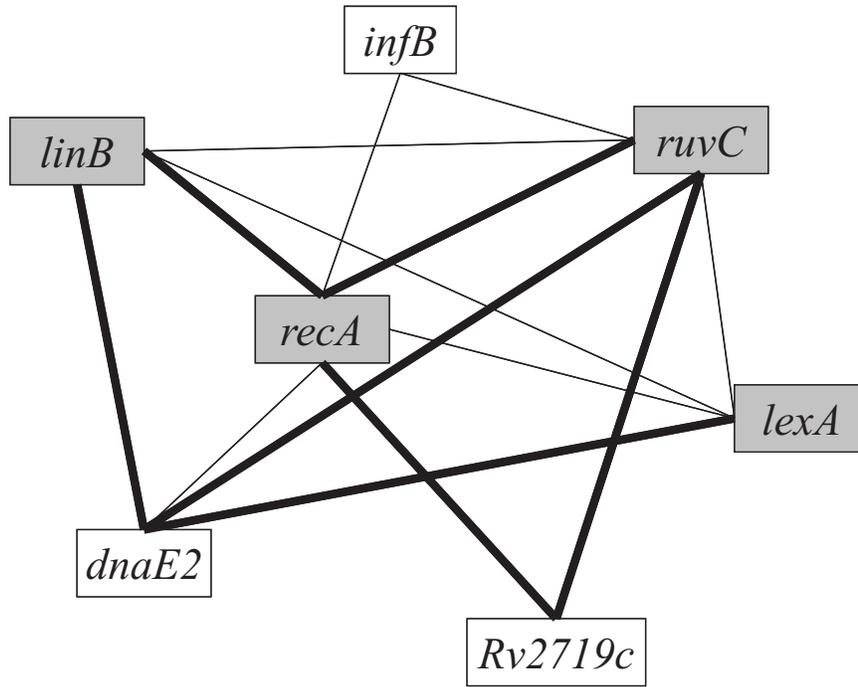
Figure 3.5: Significant correlations (*bold lines*) in the subgraph shown in Figure 3.3.

Table 3.4: Expression values of the gene *Rv2719c*

| time in h | 0.5 | 1.25 | 1 | 2 | 4 | 6 | 8 | 12 |
|---|---|---|---|---|---|---|---|---|
| *Rv2719c* | 0.85 | 1.39 | 0.87 | 1.84 | 2.4 | 8.78 | 6.09 | 12.73 |

know anything about regulation mechanisms acting on *Rv2719c*, we include it as an external variable into the model and use directly the experimental expression values for the parameter estimation. These are shown in Table 3.4. The genes *recA* and *ruvC* belong to the third group of genes, which are regulated by RecA and LexA and by the alternative mechanism [158]. Thus we propose a positive regulation from *Rv2719c* onto both genes. These regulations have already been found to be significant in Figure 3.5. In contrast, neither *lexA* nor *linB* are up-regulated in *recA* mutant strains [158]. Hence they are assumed to be regulated solely by RecA and LexA and are independent of *Rv2719c*, a result, which is also reflected by our analysis shown in Figure 3.5. The system of differential equations which describes the dynamic behavior of the network is modified accordingly:

$$\text{RecA}: \quad \dot{x}_1(t) = \quad s_1 - \gamma_1 x_1(t) + k_{1,5}b_{\theta_{1,5}}(x_5) + as(t)$$
$$+\mathbf{k_{1,6}b_{\theta_{1,6}}(x_6)} \tag{3.23}$$

$$\text{LexA}: \quad \dot{x}_2(t) = \quad s_2 - \gamma_2 x_2(t) + k_{2,5}b_{\theta_{2,5}}(x_5) \tag{3.24}$$

$$\text{ruvC}: \quad \dot{x}_3(t) = \quad s_3 - \gamma_3 x_3(t) + k_{3,5}b_{\theta_{3,5}}(x_5)$$
$$+\mathbf{k_{3,6}b_{\theta_{3,6}}(x_6)} \tag{3.25}$$

$$\text{linB}: \quad \dot{x}_4(t) = \quad s_4 - \gamma_4 x_4(t) + k_{4,5}b_{\theta_{4,5}}(x_5) \tag{3.26}$$
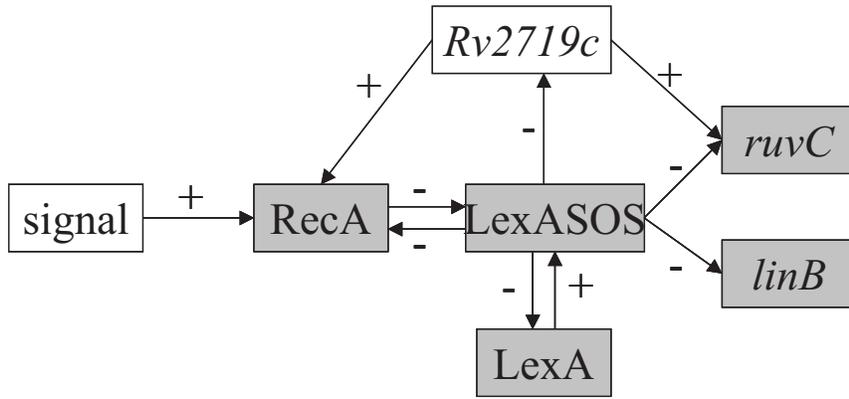
Figure 3.6: Extended network of the *Mtb* SOS repair system. The gene *Rv2719c* was added and assumed to regulate *recA* and *ruvC*. *Rv2719c* is itself regulated by LexASOS.

Table 3.5: Estimated parameter values for the extended network.

| model parameter | $a$ | $s_1$ | $s_2$ | $s_3$ | $s_4$ | $\gamma_1$ | $\gamma_2$ | $\gamma_3$ |
|---|---|---|---|---|---|---|---|---|
| estimated value $[h^{-1}]$ | 0.51 | 0.10 | 1.00 | 0.11 | 0.92 | 0.10 | 0.10 | 0.10 |
| model parameter | $\gamma_4$ | $-k_{1,5}$ | $-k_{2,5}$ | $-k_{3,5}$ | $-k_{4,5}$ | $k_{1,6}$ | $k_{3,6}$ | |
| estimated value $[h^{-1}]$ | 0.10 | 0.00 | 0.90 | 0.01 | 0.82 | 0.46 | 0.23 | |

Here, the new terms are marked in bold. The regulation strengths $k_{1,6}$ and $k_{3,6} \in \mathbb{R}_+$ account for the influence of *Rv2719c* (variable $x_6$) on *recA* and *ruvC*, respectively. The thresholds $\theta_{1,6}$ and $\theta_{3,6}$ are set to be reached after six hours, when gene *Rv2719c* first shows a significant, 8-fold, up-regulation (see Table 3.4).

Optimization of model parameters yields the values shown in Table 3.5. In comparison to the parameters of the core network (Table 3.2), the signal strength $a$ has slightly decreased. The new gene *Rv2719c* has a considerable influence on RecA. The gene *ruvC* is also mainly regulated by *Rv2719c* in the extended model, whereas regulation by LexASOS is predicted to be very weak. Parameters referring to RecA and *linB* are the same as in the core model, since the corresponding equations have not been changed in the new model.

A simulation with the corresponding parameters is shown in Figure 3.7. Up to six hours after treatment, all courses are very similar to the courses of the core network in Figure 3.2. Thereafter, the expression values of *recA* and *ruvC* are higher than in the core network due to the positive influence of *Rv2719c* on both genes. Moreover, *ruvC* has not yet reached its maximum within 14 hours. Courses of both genes in the extended network indicate that the response persists for a longer time than in the core network. This seems to be in better accordance with the experimental data. Thus, these results suggest again that the gene *Rv2719c* may play an important role in the SOS response of *Mtb*.
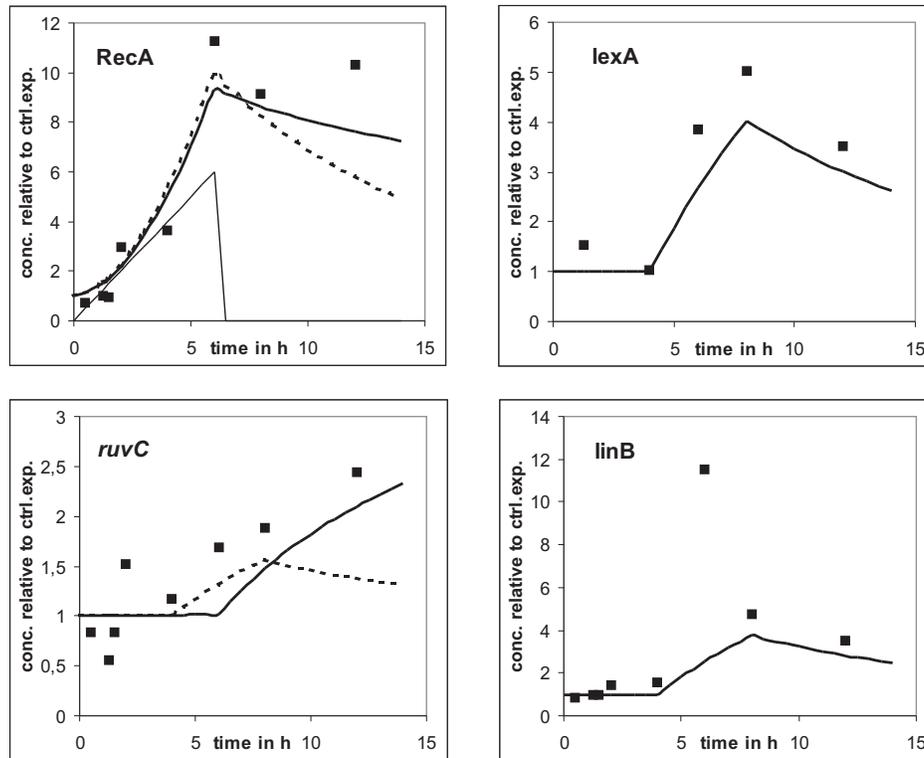
Figure 3.7: Simulated courses of the extended network model including the gene *Rv2719c*. Continuous lines correspond to predictions with the extended model, dashed lines refer to the core model. Both models differ for RecA and *ruvC*. Experimental data are plotted as rectangles.

## 3.4 Discussion and concluding remarks

We have introduced a quantitative model for the response of *Mtb* to DNA damage. Parameters were estimated using gene expression measurements after treatment of the bacterium with the DNA-damaging agent mitomycin C. We built a core model, which represents a core mechanism of the SOS repair system found as well in many other bacteria. This model includes the two main regulatory proteins RecA and LexA and the genes *ruvC* and *linB*, which are both regulated by RecA and LexA. Regulation mechanisms of this core system are well-known due to extensive studies in *E.coli*, and results of these studies can be transfered to *Mtb*. However, in recent years the existence of an alternative mechanism in *Mtb*, which is independent of RecA and LexA, has been suggested. Brooks *et al.* [21] conducted experiments which show the existence of genes that are up-regulated although they lack an SOS box in their promoter region. They concluded that these genes are regulated by an alternative mechanism. Rand *et al.* [158] confirmed this result by an analysis of microarray measurements in wild types and *recA* mutants. They concluded that most of the inducible DNA repair genes in *Mtb* are regulated independently of RecA, emphasizing the importance of this alternative mechanism in *Mtb*.

We focused our modeling on this alternative mechanism. The main regulators of this mechanism are not yet known. Thus, in order to find potential candidate genes that have to be included into the model of the SOS repair system, we applied an algorithm developed by Cabusora *et al.* [27]. This algorithm starts with a set of seed genes belonging to a special regulatory subsystem. For our purpose we used components of the *recA-lexA* mechanism. Interaction information of *Mtb* genes and gene expression measurements were used to determine an interaction graph which includes the seed genes as well as some other genes, whose expression values are highly correlated with these seed genes. The output of this algorithm was further investigated using a statistical analysis of correlation coefficients in the network.

We found the gene *Rv2719c* to be significantly correlated with some of the seed genes. Moreover, this gene is strongly up-regulated in cells treated with DNA-damaging agents. We suggested that *Rv2719c* might play an important role in the DNA repair system of *Mtb*. This result is in accordance with results in Dullaghan *et al.* [61]. They conducted experiments with mutations in the SOS boxes of genes, which prevent binding of LexA, and predicted the gene *Rv2719c* to be involved in the DNA repair mechanism. We extended the core model for *Rv2719c*, using biological knowledge to define a plausible network structure in advance. Estimation of parameters and a comparison of simulations with experimental data supported the assumption that *Rv2719c* is important in the SOS response of *Mtb*.

The set of parameters estimated for the extended model can be used to predict the maximal expression levels of the genes *recA* and *ruvC* in wild types and in *recA* mutants which lack the functional protein RecA. These levels correspond to the fixed points of the differential equations, which are given by the ratios of production rates and degradation rates (compare equation (3.19)). We compare the results with experiments shown in Rand *et al.* [158]. In this study, expression values of *Mtb* genes were measured 24 hours after a treatment of the cells with mitomycin C (0.2$\mu$g/ml). Results are shown in Table 3.6.

Table 3.6: Maximal concentrations relative to control experiments of the genes *recA* and *ruvC* in wild types and *recA* mutant strains ($\Delta recA$) are compared with microarray measurements shown in Rand *et al.* [158].

|  | *recA* | *ruvC* |
| --- | --- | --- |
| wild type, model | $(s_1 + k_{1,6})/\gamma_1 = 5.6$ | $(s_3 + k_{3,6})/\gamma_3 = 3.4$ |
| wild type, Rand *et al.* | $11.4 \pm 3.4$ | $5.3 \pm 0.8$ |
| $\Delta recA$, model | $(s_1 + k_{1,5} + k_{1,6})/\gamma_1 = 5.6$ | $(s_3 + k_{3,5} + k_{3,6})/\gamma_3 = 3.3$ |
| $\Delta recA$, Rand *et al.* | $4.4 \pm 0.9$ | $2.1 \pm 0.3$ |

For both genes, the maximal expression levels in the wild types are lower in our model compared to the experimental values in Rand *et al.* [158]. Conversely, for the *recA* mutant the values predicted by the model are both larger than the experimental values. This might indicate that the regulation of *recA* and *ruvC* by RecA and LexA is actually stronger than predicted by the model. The model compensates this with a too strong regulation of both genes by *Rv2719c*. Further experiments could help to clarify this contradiction. For example, a comparison of the dynamic response in wild types and *recA* mutants to a treatment with mitomycin C could be used to estimate the relative influences of RecA and the alternative mechanism on the expression of *recA* and *ruvC*.

Finally, two recent publications help to clarify the function and regulation of *Rv2719c*. Both appeared in 2006, after we had published our results about the SOS repair system. Brooks *et al.* [20] confirm the presence of inducible promoters independent of LexA and RecA, in particular, the promoters of *recA* and *Rv2719c*. Moreover, they show experimental evidence that *Rv2719c* is up-regulated to the same extend in wild types and *recA* mutants, although its promoter region contains an SOS box. Chauhan *et al.* [28] supposed *Rv2719c* to be a regulator of the *Mtb* cell division. Consequently, it plays a role in the transition of the bacterium from the latent to the metabolically active growth state, which involves the regulation of cell division. This potential function supports the predicted importance of *Rv2719c* in the SOS response. If the DNA is damaged, the cell division is blocked until the DNA is repaired. *Rv2719c* could possibly be involved in this blockage.

# Chapter 4

# Effective Repression of the *Escherichia coli bgl* Operon by the Protein H-NS

In this chapter, we model the specific repression of the *E. coli β-glucoside* (*bgl*) operon by the histone-like nucleoid structuring protein H-NS. According to our model, specific repression of the *bgl* operon is caused by the interplay of two positive *feedback loops* in the regulatory network. Feedback loops can essentially influence the behavior of a regulatory network. Thus, before we provide details about the biological part of this chapter, we discuss some general aspects about the role of feedback loops in regulatory networks. We have already seen in Chapter 2 that a positive auto-regulation can cause the existence of multiple steady states. This is also the case in our model of the *bgl* operon, as we will see in Section 4.3. Generally, a feedback loop can contain more than one component. We define it as a *circuit* in the interaction graph of the regulatory network. The product of all edge labels in a circuit is defined as the *sign of the circuit*. Hence, a feedback loop or circuit is *positive* if it contains an even number of negatively labeled edges and *negative* otherwise. This sign has an intuitive interpretation: An external up-regulation of a component in a positive feedback loop is amplified, and it is inhibited if the sign of the loop is negative. The concept of feedback loops will again appear in Chapter 6 and will be elucidated with respect to different aspects.

Before we start modeling, we give a general remark about the experimental data: We do not model the temporal behavior of the system under consideration, since time series measurements are not available. All measurements are assumed to represent *steady states* of the system, in which the activities $x_{i,s}$, $i = 1, \ldots, n$, are constant. Setting the time derivatives in our general model

$$\dot{x}_i(t) = s_i - \gamma_i x_i(t) + \sum_{j=1}^{n} r_{ij}(x_j) \tag{4.1}$$

to zero leads to a set of algebraic equations of the form

$$x_{i,s} = \frac{s_i + \sum_{j=1}^{n} r_{ij}(x_{j,s})}{\gamma_i} = \frac{\text{production rate of variable } x_1}{\text{degradation rate of } x_i} \quad i = 1, \ldots, n. \tag{4.2}$$

For some proteins, it is experimentally difficult to measure their concentrations directly. In our case, we measure concentrations of *bgl-lacZ gene reporter fusions* in wild types (wt) and *hns* mutants ($\Delta hns$), which lack the protein H-NS. The *bgl-lacZ* reporter fusions are parts of the DNA including genes of our system together with their regulatory regions. The genes to be measured are replaced by the gene *lacZ*, which encodes for $\beta$-galactosidase. $\beta$-galactosidase can easily be detected. The transcription rate of *lacZ* equals the transcription rate of the gene of interest in these constructs. Thus, according to equation (4.2), the amount of $\beta$-galactosidase is proportional to the amount of the protein under consideration. The variables in our model are transcription rates and not steady state concentrations $x_{i,s}$ of gene products. This has a technical reason: Equal $\beta$-galactosidase concentrations measured in different reporter fusions, which refer to different genes, indicate equal transcription rates of these genes, but not automatically equal steady state concentrations, since the degradation rates can be different.

We start with a biological introduction in Section 4.1. The model is introduced in Section 4.2, and results are shown in Section 4.3. The chapter concludes with a discussion in Section 4.4.

## 4.1   Biological introduction

Many Enterobacteria such as *E. coli* are flexible and adapt to changes in environmental conditions. This adaptation is controlled by a network of pleiotropic regulators which regulate the production of many gene products at the same time. One of these regulators is the protein H-NS, an abundant prokaryotic transcription factor that affects expression of approximately 5% of all genes in *E. coli* [123]. Regulation mechanisms of these pleiotropic regulators are poorly understood. H-NS, for instance, represses some genes very efficiently, although its binding specificity is rather low. It is an open question by which mechanisms this efficiency is achieved. Prominent paradigms for such specific H-NS regulations are the *Salmonella typhimurium proU* operon and the *E. coli bgl* operon. The *proU* operon encodes a high affinity uptake system for osmoprotectants [44, 45]. H-NS efficiently represses this operon at low osmolarity. At high osmolarity, repression is relieved, and the operon is approximately 200-fold induced.

Here, we address the question of specific pleiotropic control by modeling the repression of the *E. coli bgl* operon by the protein H-NS. The genes of the *bgl* operon encode proteins needed for the fermentation of aryl-$\beta$,D-glucosidic sugars [151, 166]. The operon is silent in wild type strains. This means, the genes are only expressed in a negligible amount [124, 171] due to repression by H-NS [58, 59, 123]. Silencing is relieved in *hns* mutants, which lack the protein H-NS [171]. Expression of genes in the operon is controlled by several regulation mechanisms at different levels during transcription and translation. Details of these inhibition mechanisms are not yet completely understood [59], not only for the *bgl* operon, but for all genes regulated by H-NS or related pleiotropic regulators. Thus, an
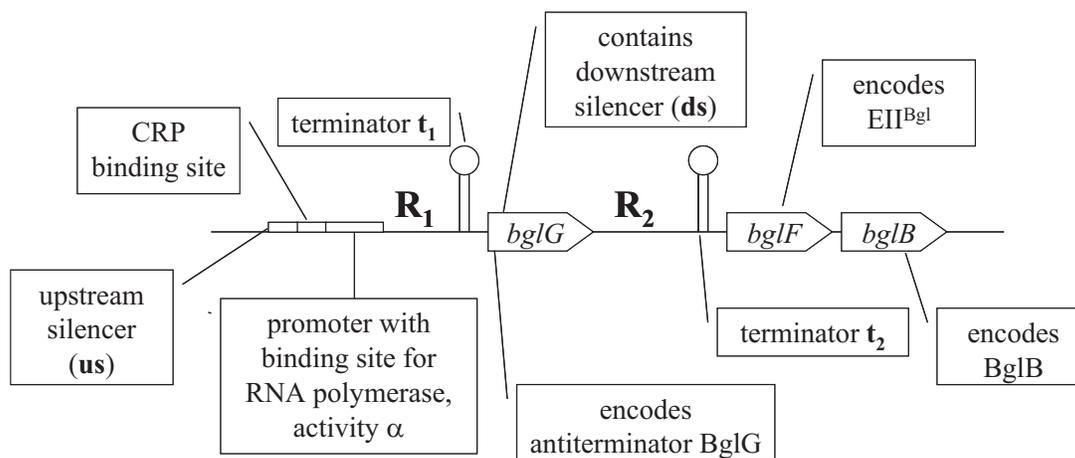
Figure 4.1: Regulation mechanisms of the *E. coli bgl* operon containing the genes *bglG, bglF* and *bglB*. The protein H-NS can bind upstream and downstream of the promoter. Two terminators $t_1$ and $t_2$ are RNA structures which can abort transcription elongation.

investigation via modeling these regulation processes might generally help to gain a deeper understanding about mechanisms of expression regulation that go beyond regulation of transcription initiation.

We focus our modeling on an observed phenomenon concerning measurements of the *bgl* operon: Expression of the operon does not correlate linearly with its cellular transcription rate. Within a range of promoter activities, a moderate, three-fold, increase in the promoter activity can result in 100-fold higher concentrations of operon proteins [58, 59, 95, 170]. Our model explains this threshold phenomenon by the interplay of two positive feedback loops. The first loop includes a binding site for H-NS located within *bglG*, the first gene in the operon. The influence of this loop on the transcription is amplified by a second loop, a positive auto-regulation of the gene product BglG. This auto-regulation also causes switch-like behavior and multi-stationarity.

## 4.2   Model

The *bgl* operon contains six genes *bglG, bglF, bglB, bglH, bglI* and *bglK*. The first three genes are required for the sugar metabolism [57]. We focus solely on the regulation of the first gene *bglG*. Figure 4.1 shows a scheme of the operon containing *bglG, bglF* and *bglB*. The regulations that we include in our model can be seen in Figure 4.2. Both figures are explained in the following. H-NS can bind to two specific binding sites: The first binding site, called *upstream silencer* (us), is located upstream of the promoter, the second one, called *downstream silencer* (ds), is located within the gene *bglG*. Binding of the catabolite regulator protein CRP to its CRP binding site facilitates binding of the RNA polymerase and thus transcription initiation. The affinity of the promoter to the RNA polymerase is
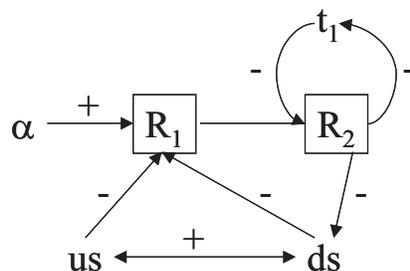
Figure 4.2: Simplified scheme of the regulations that are considered in our model. The transcription rate $R_1$ is affected by the promoter activity $\alpha$ and the silencers us and ds. The transcription rate $R_2$ influences the repression caused by binding of H-NS to the downstream silencer. Terminator $t_1$ can abort transcription and thus negatively regulates $R_2$. The active protein BglG, whose amount is approximated by $R_2$, acts in turn as an antiterminator and destroys the terminator structure. Upstream and downstream silencers mutually enhance each other.

denoted by $\alpha$ in Figure 4.2, and we refer to it as *promoter activity*.

Binding of H-NS to the DNA leads to structural changes, which affect transcription of the operon: An upstream silencer bounded by H-NS presumably prevents access to the promoter for CRP and the RNA polymerase [59]. Binding of H-NS at the downstream silencer is assumed to cause an RNA loop structure, which also inhibits transcription initiation [59, 123]. Both silencers mutually enhance each other: Repression of the operon is much more efficient when both silencers are bound, since binding of H-NS to close binding sites probably causes the formation of a DNA loop by 'zipping' the two sites together [59, 123, 170].

The model includes two different transcription rates: The transcription initiation rate $R_1$ downstream of the promoter and the transcription rate $R_2$ behind the gene *bglG*. Repression of transcription by H-NS is indicated by two negative regulations from the upstream and downstream silencers to $R_1$. The double arrow connecting upstream and downstream silencers accounts for their mutual enhancement.

Two transcriptional *terminators* $t_1$ and $t_2$ enclose *bglG*. A terminator is an RNA structure that can abort transcription. The protein BglG acts in turn as an antiterminator, which can destroy the terminator structure, by binding to specific RNA motifs called RAT [59, 83, 86, 172, 173]. The transcription rate $R_2$ is a measure for the concentration of the antiterminator BglG. Thus, the interaction graph contains a feedback loop: $R_2$ acts negatively on $t_1$ and $t_1$ inhibits $R_2$. Both regulations are summarized to a positive auto-regulation of $R_2$. Here, a threshold behavior is observed: BglG is limiting at low transcription rates, preventing expression of the operon, whereas above a threshold transcription rate, BglG efficiently antiterminates transcription [58]. The auto-regulation is thus modeled as a threshold regulation described by a Boolean function.

Efficiency of repression by the downstream silencer depends on the amount of incoming transcript [137, 138]. The higher $R_2$, the less efficient is the H-NS-downstream silencer

complex. This dependence defines the second positive feedback loop containing two negative regulations, from $R_2$ to the downstream silencer and from the downstream silencer to $R_1$. $R_2$ in turn increases with increasing transcription initiation rate $R_1$.

The second terminator $t_2$ and the two remaining operon genes *bglF* and *bglB* are not contained in the *bgl-lacZ* reporter fusions. The gene *bglF* encodes the enzyme EII$^{Bgl}$. This is a membrane transport protein, which negatively regulates BglG by phosphorylation and is itself controlled by the presence or absence of $\beta$-glucosidic substrates [33, 120, 173].

In the experiments used for parameter estimation, only parts of the regulatory network shown in Figure 4.2 are active. The remaining regulations are turned off, for example, by mutations. Thus it is possible to estimate parameters for our model successively, using different experiments for different regulation functions.

## 4.2.1 Regulation of the transcription rate $R_2$

We start modeling the positive auto-regulation of transcription rate $R_2$ including the terminator $t_1$. For reporter fusions which lack $t_1$, according to our regulatory network shown in Figure 4.2, there is no difference between the transcription initiation rate $R_1$ and transcription rate $R_2$. Otherwise, $R_2$ is assumed to be proportional to $R_1$, with a proportionality factor $c_{t_1} \in [0, 1]$ depending on the activity of the terminator. Taking the known threshold behavior in this regulation into account, we model $c_{t_1}$ as a Boolean function with a threshold value $R_2^{th}$:

$$R_2\left(R_1, t_1(R_2)\right) = \begin{cases} R_1 & \text{without } t_1 \\ c_{t_1}^{min} R_1 & \text{with } t_1 \text{ and } R_2 \leq R_2^{th} \\ c_{t_1}^{max} R_1 & \text{with } t_1 \text{ and } R_2 > R_2^{th} \end{cases} \tag{4.3}$$

The structure of $t_1$ and hence its negative effect on the transcription can be deleted by a mutation that stabilizes the BglG binding motif RAT. This mutation renders transcription of the operon independent of the terminator. Figure 4.3 shows a scheme of the experiments used for estimation of $c_{t_1}^{min}$ and $c_{t_1}^{max}$. The *bgl-lacZ* reporter fusion consists of the constitutive UV5 promoter $P_{UV5}$, the terminator and the reporter gene *lacZ*. Activity of $\beta$-galactosidase was measured in *Miller units* (MU), a standardized amount of $\beta$-galactosidase activity. In experiment 1C the terminator $t_1$ is RAT stabilized and thus inactive. We use this experiment as a reference, since $R_2 = R_1 = 4775$ MU in this case. In experiment 1A, the amount of the antiterminator BglG is low, and $t_1$ is assumed to be fully active. Hence, according to equation (4.3), transcription rate $R_2$ is given by $R_2 = c_{t_1}^{min} R_1$. We measure a $\beta$-galactosidase activity of 1490 MU, and the factor $c_{t_1}^{min}$ is the ratio

$$c_{t_1}^{min} = \frac{\beta\text{-galactosidase activity in exp. 1A}}{\beta\text{-galactosidase activity in exp. 1C}} = \frac{1490 \text{ MU}}{4775 \text{ MU}} \approx 0.3. \tag{4.4}$$

In experiment 1B, BglG is induced into the cell and effectively inhibits the terminator. Therefore the activity of $t_1$ is assumed to be reduced and $R_2 = c_{t_1}^{max} R_1$. The corresponding
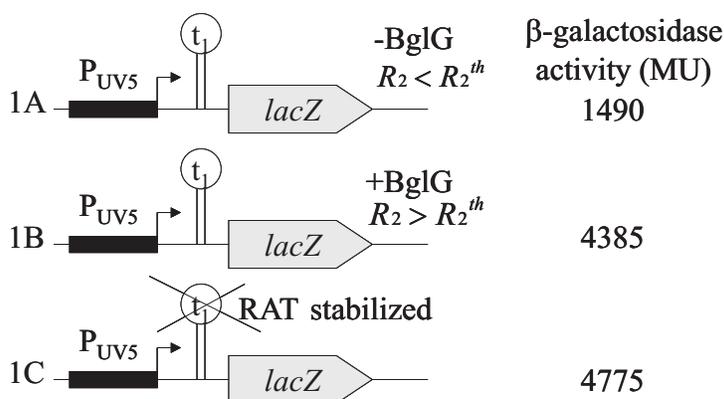
Figure 4.3: A *lacUV5* promoter, *t1*, *lacZ* fusion was integrated into the chromosomal *attB*-site, and the expression was determined of cells grown in minimal M9 glycerol medium supplemented with casaminoacids and B1 chromosome as described in [58]. BglG was provided in trans using plasmid pKESK18, and *bglG* expression was induced with 1 mM IPTG [58]. As a control, a construct with a *lacUV5* promoter and a RAT stabilized terminator $t_1$ was used, in which terminator $t_1$ was mutated by stabilization of the BglG binding motif RAT [138]. $\beta$-galactosidase activities were measured in Miller units and determined at least three times independently. Standard deviations were less than 10%.

measurements show that approximately 90% of the transcript passes $t_1$ and

$$c_{t_1}^{max} = \frac{\beta\text{-galactosidase activity in exp. 1B}}{\beta\text{-galactosidase activity in exp. 1C}} = \frac{4385 \text{ MU}}{4775 \text{ MU}} \approx 0.9. \qquad (4.5)$$

These experiments do not provide any information about the threshold value $R_2^{th}$. A value has to be set manually in our simulations. Results for different threshold values indicate that within a certain range, this value does not affect the qualitative results. Here, we demonstrate this for two threshold values. A more detailed analysis of the dependence of results on the threshold $R_2^{th}$ is provided in [154].

## 4.2.2   A positive feedback loop including the downstream silencer

Binding of H-NS to the downstream silencer causes a conformational change, which complicates transcription initiation. The activity of the silencer depends on the amount of incoming transcript, $R_2$ in this case [137]. This can be seen in the experiments in Figure 4.4. As no measurements for the amount of incoming transcript are available, we approximate this amount by the measurements in *hns* mutants. In the experiments shown in Figure 4.4, measurements were done using three reporter fusions with promoters $P_{lacI}$, $P_{UV5}$ and $P_{tac}$. $P_{lacI}$ is the weakest and $P_{tac}$ the strongest promoter. The DNA fragments contain the gene *bglG* including the downstream silencer and the reporter gene *lacZ*. $\beta$-galactosidase activity was measured in wild types (*left column*) and in *hns* mutants $\Delta hns$ (*right column*). The experiments characterize the positive feedback loop including $R_1$, $R_2$

β-galactosidase activity (LB)

| | | | | | wt | Δ*hns* |
|---|---|---|---|---|---|---|
| 2A | P$_{\text{lacI}}$ | ds | bglG | lacZ | 6 | 76 |
| 2B | P$_{\text{UV5}}$ | ds | bglG | lacZ | 400 | 961 |
| 2C | P$_{\text{tac}}$ | ds | bglG | lacZ | 2302 | 2787 |
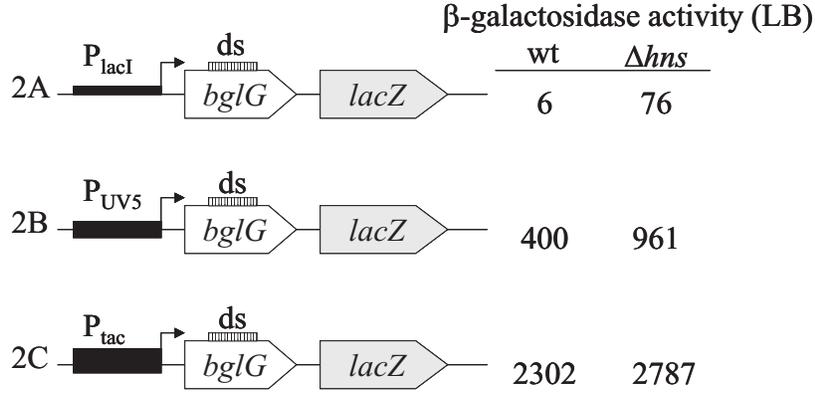
Figure 4.4: *bgl-lacZ* reporter fusions with three different promoters P$_{lacI}$, P$_{UV5}$ and P$_{tac}$. All constructs contain the genes *bglG* and *lacZ*. β-galactosidase activity was measured in wild type and *hns* mutant. Detailed information about growth medium and plasmids are provided in [137, 138].

and the downstream silencer. As the terminator is missing here, $R_1$ equals $R_2$. The influence of the downstream silencer on $R_1$ is described by a $R_2$-dependent repression factor $c_{ds}(R_2) \in [0, 1]$:

$$R_1(\alpha, ds(R_2)) = c_{ds}(R_2)\alpha \qquad (4.6)$$

The factor $c_{ds}(R_2)$ is described by a function that increases linearly with $R_2$ for small transcription rates and saturates at 1 for transcription rates exceeding an upper limit $R_2^*$, at which the downstream silencer becomes inactive:

$$c_{ds}(R_2) = \begin{cases} aR_2 + b & \text{wild type and } R_2 \leq \frac{1-b}{a} =: R_2^* \\ 1 & \textit{hns} \text{ mutant or } R_2 > R_2^* \end{cases} \qquad (4.7)$$

Using the least squares method, which minimizes the sum of squared errors between repression factors $c_{ds}(R_2)$ predicted by the model and the experimental values, the regression parameters $a$ and $b$ are estimated to be

$$a \approx 3 \cdot 10^{-4} \quad \text{and} \quad b \approx 0.1. \qquad (4.8)$$

The corresponding upper limit $R_2^*$ is given by $R_2^* = 3000$. Figure 4.5 shows the regression function (*continuous line*) and the experimental values (*dots*) for $c_{ds}(R_2)$, which equals the ratio of $R_1$ measurements in the wild type and in the *hns* mutant, in dependence of the incoming transcription rate in the *hns* mutant.

## 4.2.3 Regulation of the transcription initiation rate $R_1$

The regulatory network in Figure 4.2 indicates that $R_1$ is regulated by binding of H-NS to the two silencers and the promoter activity $\alpha$. Equation (4.6) presumes already a linear relation between $R_1$ and $\alpha$. We assume independent binding of H-NS to upstream and
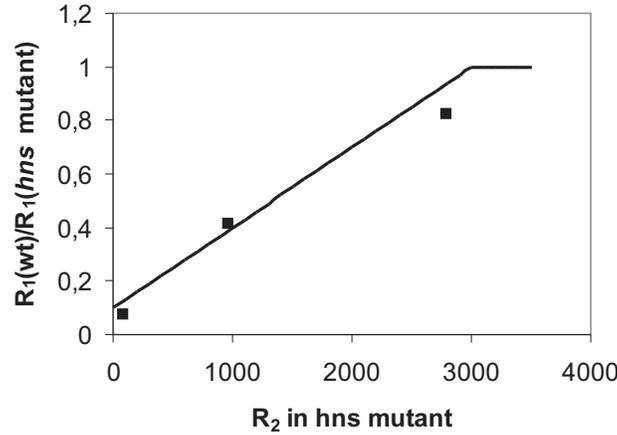
Figure 4.5: Three constructs with different promoters are used to estimate the influence of the downstream silencer (see Figure 4.4). Increasing transcription rates $R_2$ lower the efficiency of the downstream silencer. We describe this by a linear relation between $R_2$ and the repression factor $c_{ds}(R_2)$ and an upper limit $R_2^*$, at which the downstream silencer becomes inoperative.

downstream silencers and factorize their effects into a factor $c_{us}$ describing the influence of the upstream silencer and a factor $c_{ds}(R_2)$ that refers to repression through the downstream silencer. Mutual enhancement of both silencers is described by an additional repression factor $c_{coop}$. The parameterization for $R_1$ then reads:

$$R_1\left(\alpha, us, ds(R_2)\right) = \begin{cases} \alpha & \text{no silencers}/hns \text{ mutants} \\ c_{us}\alpha & \text{us, } \neg \text{ ds} \\ c_{ds}(R_2) & \neg \text{ us, ds} \\ c_{us}c_{ds}(R_2)c_{coop}\alpha & \text{both silencers present,} \end{cases} \tag{4.9}$$

with repression factors $c_{us}, c_{coop} \in [0,1]$. We use the two experiments shown in Figure 4.6 to estimate the repression factors $c_{us}$ and $c_{coop}$. Four DNA fragments with missing or inactive terminators are investigated in wild types (*left column*) and *hns* mutants (*right column*). The reporter construct in experiment 3B consists of the upstream silencer, the *bgl* promoter $P_{bgl}$ and the gene *lacZ*. According to equation (4.9), the factor $c_{us}$ is given by the ratio of the $\beta$-galactosidase activities in the wild type and in the *hns* mutant in this construct:

$$c_{us} \stackrel{(4.9)}{=} \frac{\beta\text{-galactosidase activity in wt in exp. 3B}}{\beta\text{-galactosidase activity in } \Delta hns \text{ in exp. 3B}} = \frac{128}{278} \approx 0.5 \tag{4.10}$$
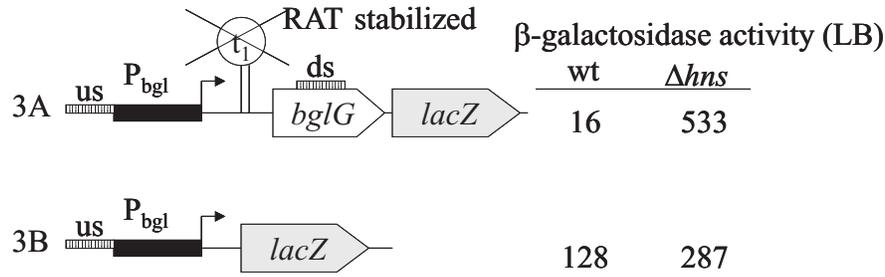
Figure 4.6: Measurements of $\beta$-galactosidase activity in wild type and *hns* mutant. **Experiment 3A:** *bgl-lacZ* fusion with promoter $P_{bgl}$, RAT stabilized (i.e. inactive) terminator, gene *bglG* including ds and reporter gene *lacZ*. **Experiment 3B:** *bgl-lacZ* fusion lacking the terminator and the gene *bglG*. More details about the experiments are given in [137, 138].

The first construct in Figure 4.6, experiment 3A, contains both silencers. The ratio of the amount of $\beta$-galactosidase in the wild type and in the *hns* mutant is given by

$$\frac{\beta\text{-galactosidase activity in wt in exp. 3A}}{\beta\text{-galactosidase activity in }\Delta hns\text{ in exp. 3A}} = \frac{16}{533} \overset{(4.9)}{=} c_{us}c_{ds}(R_2)c_{coop}$$

$$\approx \underbrace{0.5}_{c_{us}} \underbrace{\left(3 \cdot 10^{-4} \cdot 0.5 \cdot 533 + 0.1\right)}_{c_{ds}} c_{coop} \tag{4.11}$$

Here, we have approximated $R_2$ by the $\beta$-galactosidase activity in the *hns* mutant reduced by the factor $c_{us}$. Resolving equation (4.11) for $c_{coop}$ yields a value $c_{coop} \approx 0.3$.

## 4.2.4 Final model

Now we have everything at hand to specify equations for $R_1$ and $R_2$ in wild types with both silencers and terminator $t_1$:

$$R_1 = \begin{cases} c_{us}c_{coop}\left(aR_2 + b\right)\alpha & R_2 \leq R_2^* \\ c_{us}c_{coop}\alpha & R_2 > R_2^* \end{cases} \tag{4.12}$$

$$R_2 = \begin{cases} R_1 & \text{without terminator} \\ c_{t_1}^{max}R_1 & R_2 \leq R_2^{th} \\ c_{t_1}^{min}R_1 & R_2 > R_2^{th} \end{cases} \tag{4.13}$$

Inserting equation (4.13) into (4.12) leads to

$$R_1 = \begin{cases} c_{us}c_{coop}\left(aR_1 + b\right)\alpha & \text{no terminator and } R_2 \leq R_2^* \\ c_{us}c_{coop}\left(ac_{t_1}^{min}R_1 + b\right)\alpha & R_2 \leq R_2^* \text{ and } R_2 \leq R_2^{th} \\ c_{us}c_{coop}\left(ac_{t_1}^{max}R_1 + b\right)\alpha & R_2 \leq R_2^* \text{ and } R_2 > R_2^{th} \\ c_{us}c_{coop}\alpha & R_2 > R_2^* \end{cases} \tag{4.14}$$

Table 4.1: Estimated values for the model of *bgl* operon regulation

| parameter | $c_{us}$ | $c_{coop}$ | $c_{t_1}^{min}$ | $c_{t_1}^{max}$ | $a$ | $b$ | $R_2^*$ |
|---|---|---|---|---|---|---|---|
| estimated value | 0.5 | 0.3 | 0.3 | 0.9 | $3 \cdot 10^{-4}$ | 0.1 | 3000 |

Resolving (4.14) for the transcription rate $R_1$, we obtain $R_1$ as a function of the promoter activity $\alpha$:

$$R_1 = \begin{cases} \frac{c_{us}c_{coop}b\alpha}{1-c_{us}c_{coop}a\alpha} & \text{no terminator  and } R_2 \leq R_2^* \\ \frac{c_{us}c_{coop}b\alpha}{1-c_{us}c_{coop}ac_{t_1}^{min}\alpha} & R_2 \leq R_2^* \text{ and } R_2 \leq R_2^{th} \\ \frac{c_{us}c_{coop}b\alpha}{1-c_{us}c_{coop}ac_{t_1}^{max}\alpha} & R_2 \leq R_2^* \text{ and } R_2 > R_2^{th} \\ c_{us}c_{coop}\alpha & R_2 > R_2^* \end{cases} \tag{4.15}$$

The corresponding transcription rate $R_2$ is given by equation (4.13). Estimated parameters, which were used to carry out simulations in the following section, are listed in Table 4.1.

## 4.3   Results and discussion

### 4.3.1   Mutual enhancement of two feedback loops causes specific repression

We simulated the behavior of the transcription rate $R_2$ as a function of increasing promoter activity $\alpha$ in the wild type with upstream and downstream silencers (Figure 4.7). Figure A shows the behavior for a construct lacking the terminator, Figures B and C represent constructs including the terminator with threshold values $R_2^{th} = 100$ and $R_2^{th} = 50$, respectively. The non-linear increase up to $R_2 = 3000$ in all three plots is caused by the feedback loop including the downstream silencer. When this silencer becomes inactive for $R_2 > 3000$, $R_2$ is regulated solely by the terminator and the upstream silencer, which were modeled to have constant influences. Hence, $R_2(\alpha)$ is a linear function in this range. When the threshold $R_2^{th}$ is reached, the terminator causes an additional jump in $R_2$ in Figures B and C.

In order to explain the immense, 100-fold, increase in transcription rate $R_2$, which comes along with a three-fold increase in the promoter activity $\alpha$, we calculated the ratio of $R_2(3\alpha)$ and $R_2(\alpha)$ again as a function of $\alpha$. Figure 4.8 shows the predictions for a *bgl-lacZ* reporter fusion without terminator (Figure A) and with terminator and $R_2^{th} = 100$ (Figure B) and $R_2^{th} = 50$ (Figure C). In the construct without terminator, the ratio increases rapidly up to a maximum where $R_2(3\alpha)$ is about 20 times larger than $R_2(\alpha)$. A further increase in the promoter activity renders the downstream silencer inactive, and thus the positive feedback loop is turned off for transcription rate $R_2(3\alpha)$. Hence the ratio $R_2(3\alpha)/R_2(\alpha)$ decreases until the downstream silencer is as well turned off for transcription rate $R(\alpha)$. Then, both transcription rates are linearly related to $\alpha$, and hence the ratio is 3 independent of $\alpha$. In constructs containing the terminator, the maximal ratio is about 80 and thus four times higher than in the first figure lacking the terminator. For small promoter activity $\alpha$, the
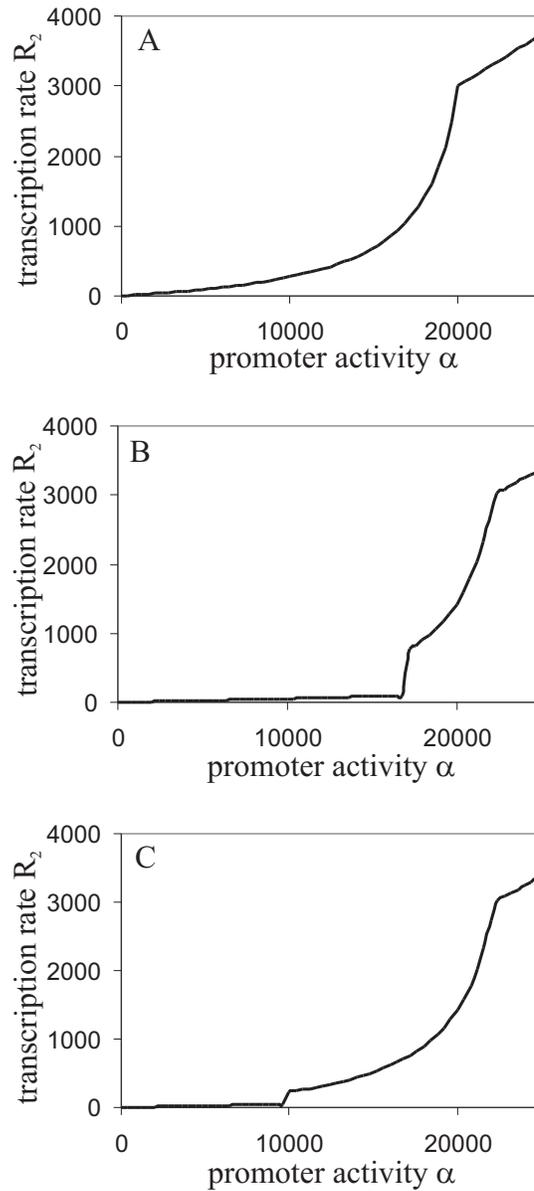
Figure 4.7: Transcription rate $R_2$ for increasing promoter activity $\alpha$. The non-linear increase is caused by the feedback-loop including the downstream silencer. $R_2$ increases linearly when this silencer becomes inoperative, that is, when the upper limit $R_2^* = 3000$ is exceeded. **A:** without terminator. **B:** with terminator and threshold $R_2^{th} = 100$. **C:** with terminator and threshold $R_2^{th} = 50$.
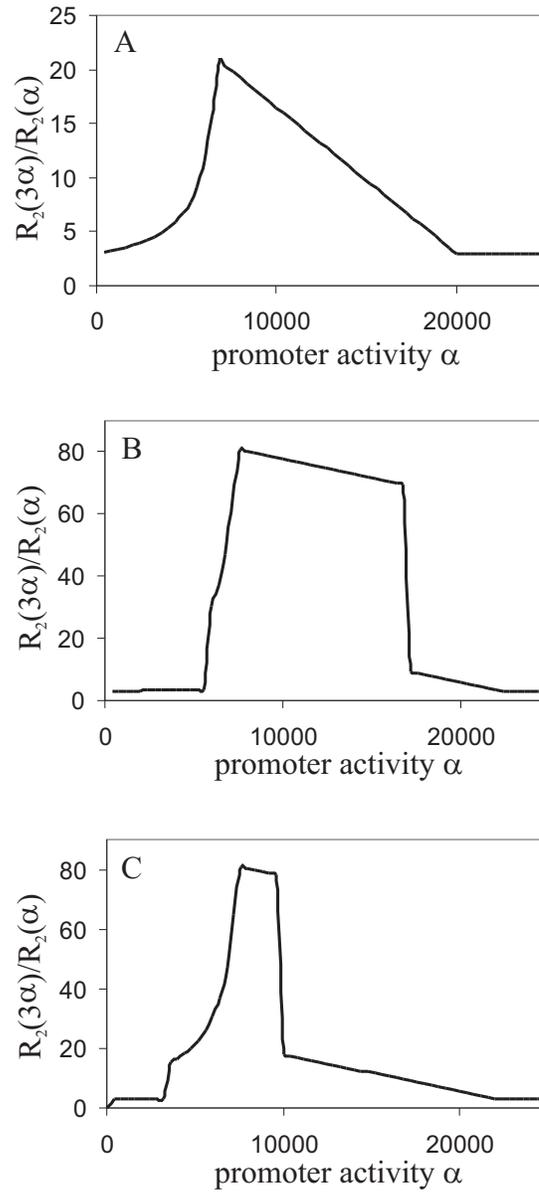
Figure 4.8: Ratio of transcription rates $R_2(3\alpha)$ and $R_2(\alpha)$ as a function of increasing promoter activity $\alpha$. **A:** without terminator. **B:** with terminator and threshold $R_2^{th} = 100$. **C:** with terminator and threshold $R_2^{th} = 50$.

ratio increases only moderately. A jump is observed when $R_2(3\alpha)$ reaches the threshold value $R_2^{th} = 100$ or $R_2^{th} = 50$, respectively, because $R_2(3\alpha)$ rapidly increases at this point. The ratio increases further until the positive feedback loop with the downstream silencer is turned off for $R_2(3\alpha)$. The second and third figures show high plateaus where the ratio does not change very much. On this plateaus, the terminator is only partly active for the high transcription rate $R_2(3\alpha)$, $c_{t_1}(R_2(3\alpha)) = c_{t_1}^{max}$, and fully active for the low transcription rate $R_2(\alpha)$, $c_{t_1}(R_2(\alpha)) = c_{t_1}^{min}$. The effect of both feedback mechanisms mutually enhance each other on this plateau. Thus, in constructs with terminator, this enhancement results in a four times higher ratio compared to the construct without terminator. The range of the promoter activity $\alpha$ in which this plateau is observed, is determined by $R_2^{th}$, as can be seen in the Figure. The ratio decreases when also the lower transcription rate $R_2(\alpha)$ reaches the threshold $R_2^{th}$, and it is the constant value 3 when the downstream silencer is inactive for both transcription rates, $R_2(3\alpha), R_2(\alpha) > R_2^*$.

### 4.3.2 Positive auto-regulation of the gene *bglG* leads to hysteresis

The non-linear positive feedback loop including $t_1$ entails an interesting property of our system: There exist two solutions for the transcription rates $R_1$ and $R_2$ in an interval $[\alpha_{min}, \alpha_{max}]$, a property called *multi-stationarity*. The system can switch between these two solutions when disturbed. Such a behavior is called *switch-like behavior*. A necessary condition for a system to show switch-like behavior is a non-linear positive feedback loop [43, 84, 188], as already demonstrated in example 2.7 in Chapter 2. We will once again return to this point in Section 6.

In one of the solutions, the terminator is fully active, in the second one, it is only partially active. Which of the solutions is realized depends on the direction of change in the promoter activity $\alpha$ and, so to speak, on the history of the system.

Figure 4.9 shows $R_2$ as a function of increasing and decreasing $\alpha$, respectively, for wild type cells (*left*) and *hns* mutants (*right*) and two threshold values $R_2^{th} = 100$ (*top*) and $R_2^{th} = 50$ (*bottom*). The system exhibits *hysteresis*: For increasing $\alpha$, the transcription rate $R_2$ increases moderately until $R_2^{th}$ is reached at a promoter activity $\alpha_{max}$. This causes a jump in $R_2$, which feeds back to amplify the effect of the positive feedback loop including the downstream silencer in the wild type. Accordingly, both transcription rates increase rapidly at this point. Contrary, when we start with a large $\alpha$ and slowly decrease the promoter activity, $R_2$ remains high and only falls below at a lower promoter activity $\alpha_{min} < \alpha_{max}$. The size of the interval $[\alpha_{min}, \alpha_{max}]$ depends on $R_2^{th}$, as can be seen in the Figure.

## 4.4 Concluding remarks

We have introduced a model for the specific repression of the *bgl* operon in *E. coli* by the protein H-NS. H-NS binds to two binding sites upstream and downstream of the promoter. Repression is further enhanced by RNA structures which terminate transcription elongation. Experiments in Dole *et al.* [59] indicate that transcription of genes in the operon
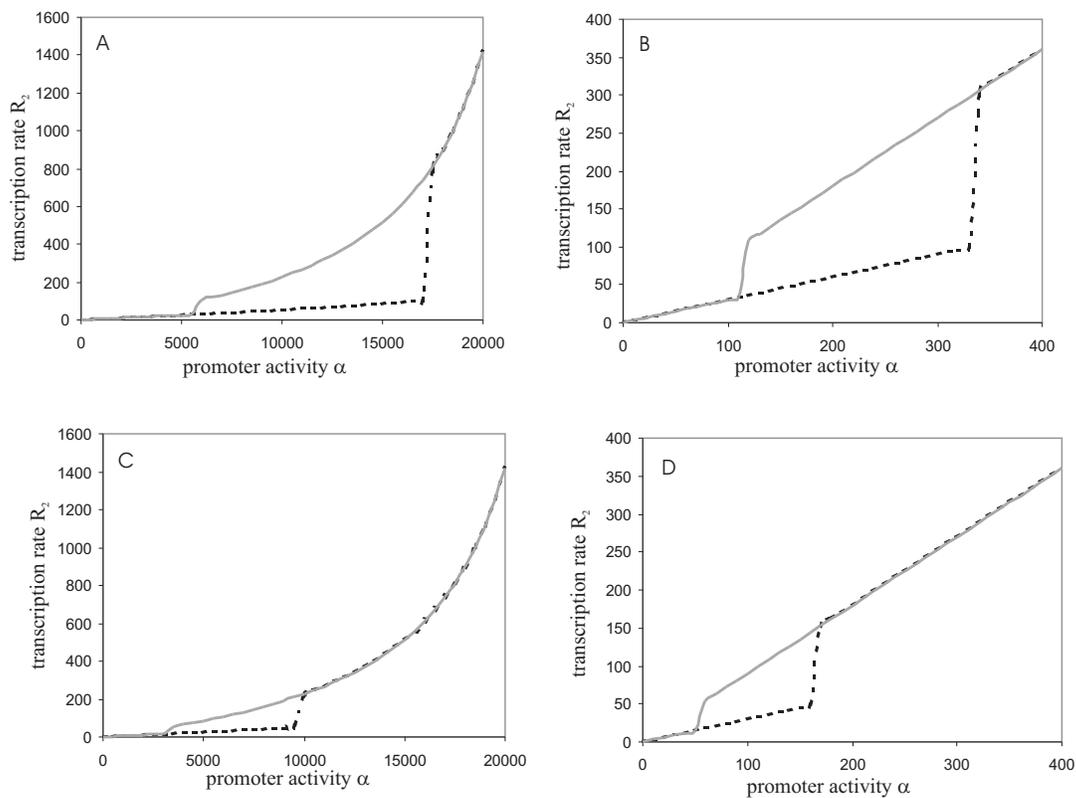
Figure 4.9: Change in transcription rate $R_2$ for increasing (*black dotted line*) and decreasing (*grey solid line*) promoter activity $\alpha$. The system has two stable steady states and shows hysteresis. **A:** wild type, $R_2^{th} = 100$, **B:** *hns* mutant, $R_2^{th} = 100$, **C:** wild type, $R_2^{th} = 50$, **D:** *hns* mutant, $R_2^{th} = 50$.

does not correlate linearly with promoter activity: A three-fold increase in the promoter activity can, for a certain range of promoter activities, lead to a 100-fold increase in the expression rate. According to our model, this non-linear behavior is ascribed to the interplay of two positive feedback loops including one of the silencers and a terminator structure. We used very simple regulation functions in our model. Nevertheless, the model is able to explain the observed behavior and, moreover, it is robust to changes in the parameterization. Important features that are needed to explain the behavior described above are the dependence of the repression by the downstream silencer, $c_{ds}$, on the transcription rate $R_2$, and the mutual enhancement of both feedback loops. A second property of our model is the ability to show hysteresis, which is due to the threshold regulation of the terminator on $R_2$.

Although our model is able to explain the observed non-linearity, the effect is less pronounced than in the experiment. The predictions show at most an 80-fold increase. However, we made several simplifying assumptions, most of which reduce the threshold phenomenon. In particular, the model could be extended with respect to the following aspects, provided that data are available for parameter estimation:

1. There are some publications indicating that the positive influence of the protein BglG on the expression of the operon is two-fold: It functions as an antiterminator and destroys terminator structures, and it is assumed to stabilize its own RNA [58, 59, 86]. The first function is well-known and already included in our model, whereas the second one is not assured and we neglect it[1]. Inclusion of this additional stabilizing function would lead to a further increase in the ratio $R_2(3\alpha)/R_2(\alpha)$.

2. The influence of the upstream silencer on the transcription initiation rate $R_1$ was modeled as a constant $c_{us}$. This is a simplification that neglects competitive binding of the RNA polymerase and H-NS. Increasing the promoter activity $\alpha$ would actually favor binding of the polymerase rather than binding of H-NS upstream. Accordingly, the efficiency of the upstream silencer should decrease with increasing promoter activity. Including this dependence into the model would again increases the ratio $R_2(3\alpha)/R_2(\alpha)$.

3. Finally, if both silencers become less efficient when the promoter activity increases, this should decrease as well their mutual enhancement, expressed by the repression factor $c_{coop}$ in the model. This factor was assumed to be constant in our model, even for promoter activities where the downstream silencer is inoperative.

Finally, we remark that we can in fact hope that our results about repression mechanisms by H-NS are transferable to other genes regulated by H-NS. Concerning the *proU* operon, for example, mechanisms have been shown to be very similar to *bgl* regulation [46, 141], and interestingly, repression of the operon also involves upstream and downstream binding sites for H-NS.

---

[1]Personal communication with Prof. Dr. Karin Schnetz, Cologne.

# Chapter 5

# A Bayesian Regularized Approach for Network Inference

This chapter introduces an approach based on *Bayesian statistics* to infer gene regulatory networks from time series data. Chapters 3 and 4 have shown that an inclusion of biological knowledge into the model can lead to biologically meaningful quantitative conclusions in spite of small datasets available for parameter estimation. In this chapter, we show a different way to deal with sparse data. Rather than adapting our model to a certain regulatory subsystem by including specific biological knowledge, we present an inference approach which restricts the parameter space by taking into account general properties of biological networks.

In a Bayesian learning approach, model parameters are described as *random variables* having some known *prior distribution*, in case of continuous variables usually given as a probability density function, which reflects 'degrees of belief' due to decision theoretic rather than the classical frequentistic interpretation. Experimental data influence this belief. Therefore, these data are used to convert the prior distribution into an *a posteriori probability distribution* (posterior), thereby revising our opinion about the true parameter values [60]. This posterior is usually also given as a density function. Bayesian learning investigates this posterior, which can, according to Bayes' formula, be calculated in terms of the prior distribution and the likelihood function determined by the experimental data. In order to apply a Bayesian learning approach, we have to embed our deterministic differential equation model into a stochastic framework and specify a prior distribution over model parameters. This distribution is chosen to reflect our expectation of outcome. We will use a *hierarchical* distribution over regulation strengths, which is specifically designed to favor sparse networks with only a few significant regulations. This prior distribution drastically reduces the parameter space and thus successfully avoids the typical problem of overfitting. The aim of our approach is to reconstruct the interaction graph from time series data. Moreover, our approach can provide estimates for kinetic parameters that are not yet experimentally accessible.

*Bayesian approaches* have frequently been used during the last few years, since they

can take advantage of several theories. They take into account the probabilistic nature of regulatory processes and handle noisy datasets. Moreover, any knowledge about the system at hand can in principle be included into the inference process by specifying degrees of belief in form of appropriate prior distributions. This knowledge can exist in terms of data from previous experiments, or in form of information from experts, such as statistical properties of the systems. Modeling this information with probability distributions does not require to fix certain values, but to express the uncertainty about this information in form of a distribution. Therefore, a Bayesian approach enables the modeler to weight the information according to their belief. So, in contrast to a maximum likelihood estimation, the result of a Bayesian approach depends on the subjective perception of the modeler about the reliability of the information included into the learning process.

Bayesian approaches have been established in recent years to infer regulatory networks from experimental data [10, 11, 13, 117, 160]. Beal *et al.* [10], for example, use linear state space models, a class of dynamic Bayesian networks, to reverse engineer transcriptional interactions from time series microarray data. They applied the method to the response of a human T-cell line to drug treatment. Rogers *et al.* [160] apply a sparse Bayesian regression algorithm to reconstruct network topologies from knock-out experiments, in which a set of genes is inoperative. They use a linear model and an a priori probability distribution that restricts the number of regulators for each gene in the network. The work of Bernard and Hartemink [13] is especially interesting, since they integrate multiple types of data into the inference process. Gene expression data are used to define the likelihood function, and transcription factor binding location data are modeled as prior probability distributions over edge weights. They showed that the inclusion of both data types could considerably improve the results compared to maximum likelihood estimates which include only one single data type.

All works mentioned use Bayesian networks or related models to describe gene regulatory networks. Bayesian networks are not offhand appropriate to describe the dynamic behavior of these networks, as described in Chapter 2. In contrast, differential equations are particularly suited for this task. In this chapter, we present a new inference approach which combines both, a differential equation model and a Bayesian approach.

Before we embed our differential equation model into a stochastic framework in Section 5.2, we start with a general introduction into Bayesian learning methods in Section 5.1. The approach is evaluated on a simulated and a real dataset in Sections 5.3 and 5.4, respectively. A comparison with a maximum likelihood estimation shows that a Bayesian approach with appropriate prior distributions over model parameters can prevent the typical problem of overfitting. Therefore, it improves network inference, in particular, if the data is noisy and only few time points are available, which is the typical setting when analyzing microarray data.

An introduction into statistical methods including Bayesian methods can be found in [14, 60, 66, 115]. Examples for applications in bioinformatics are given in Ewens and

Grant [66]. The book of Leonard and Hsu [115] also provides a practical guidance for the application of Bayesian techniques, in particular for numerical sampling methods. Duda *et al.* [60] embed the Bayesian learning approach into more general pattern classification approaches. This book also contains a comparison of maximum likelihood and Bayesian parameter estimation as well as examples for commonly used prior distributions. Basic terms of *measure theory*, which are defined in Section 5.1, are explained in [64].

## 5.1 Probability and measure theory - Basic terms

**Definition 5.1.1** [$\sigma$-algebra] Let $\Omega$ be a set and $\Sigma$ a set of subsets of $\Omega$ with the following properties:

1. $\Omega \in \Sigma$

2. $A \in \Sigma \Rightarrow \bar{A} := \Omega \setminus A \in \Sigma$

3. $A_n \in \Sigma,\ n \in \mathbb{N} \Rightarrow \bigcup_{n \in \mathbb{N}} A_n \in \Sigma$

Then, $\Sigma$ is denoted *$\sigma$-algebra over $\Omega$*.

$\Sigma$ is a set of subsets of a set $\Omega$, which contains the set $\Omega$ itself and is closed under complementation and countable unions of its elements. Properties 1 and 2 imply that $\Sigma$ must also contain the empty set, $\emptyset \in \Sigma$. A tuple $\mathcal{F} = (\Omega, \Sigma)$ of a set $\Omega$ and a $\sigma$-algebra $\Sigma$ over $\Omega$ is called a *measurable space*.

**Definition 5.1.2** [Measure, probability measure] A *measure* is a function $\mu : \Sigma \to \mathbb{R}_{0,+}$ with

1. $\mu(\emptyset) = 0$

2. $\mu(\cup_i A_i) = \sum_i \mu(A_i)$ for a countable set of pairwise disjoint sets $A_i \in \Sigma$

If additionally $\mu(\Omega) = 1$ holds, then $\mu$ is a *probability measure*.

**Definition 5.1.3** [Measure space, probability space] A triple $(\Omega, \Sigma, \mu)$ of a set $\Omega$, a $\sigma$-algebra $\Sigma$ over $\Omega$ and a measure $\mu$ is called a *measure space*. If $\mu$ is a probability measure, then $(\Omega, \Sigma, \mu)$ is called a *probability space*.

In a probability space, elements of the set $\Omega$ describe *observations* or *possible outcomes* of a chance experiment, and we also refer to $\Omega$ as the *sample space* of this experiment. The set $\Sigma$ is the set of *events*, and the function $\mu$ assigns probabilities to these events.

An important example is the probability space $(\Omega, \Sigma, \mu)$ with $\Omega = \mathbb{R}$ and the following types of events:

- *Point set event:* The experimental outcome takes a specific real value $v$.

- *Half-space event:* The outcome takes a value in an open or closed half-space, that is, $(-\infty, w)$, $(v, \infty)$, $(-\infty, w]$ or $[v, \infty)$.

- *Interval event:* The outcome takes a value in an interval limited by two real numbers $v$ and $w$. As for half-space events, this interval can be open, closed, or half-open.

The *Borel algebra* $\mathcal{B}(\mathbb{R})$ is the smallest $\sigma$-algebra of the set of real numbers which contains such interval events. Its elements are called *Borel sets*. We take $\mu$ to be the *Lebesgue measure*, which assigns an interval $(a, b)$ with $a, b \in \mathbb{R}$ its length $|b - a|$.

The concept of *random variables* is needed, if elements of the set $\Omega$ are not real numbers. A real valued random variable is a function which assigns real numbers to outcomes of a chance experiment. We need two more definitions for a formal introduction of a random variable:

**Definition 5.1.4** [Measurable set] A subset $A$ of a set $\Omega$ with $\sigma$-algebra $\Sigma$ is *measurable*, if $A \in \Sigma$.

For example, elements of the Borel set are Lebesgue-measurable.

**Definition 5.1.5** [Measurable function] A function $X : \Omega_1 \to \Omega_2$ between two measurable spaces $\mathcal{F}_1(\Omega_1, \Sigma_1)$ and $\mathcal{F}_2(\Omega_2, \Sigma_2)$ is *measurable*, if

$$\forall A \in \Sigma_2 : X^{-1}(A) \in \Sigma_1. \tag{5.1}$$

**Definition 5.1.6** [Random variable] Let $(\Omega_1, \Sigma_1, \mu)$ a probability space and $(\Omega_2, \Sigma_2)$ a measurable space. A *random variable* $X$ is a measurable function $X : \Omega_1 \to \Omega_2$.

In case of *real valued random variables*, the range of $X$ is the set of real numbers, and the corresponding $\sigma$-algebra is $\mathcal{B}(\mathbb{R})$. Here, we give an alternative definition for real valued random variables:

**Definition 5.1.7** [Real valued random variable] Let $(\Omega, \Sigma, \mu)$ a probability space. A *real valued random variable* is a function $X : \Omega \to \mathbb{R}$ with the property that for an $a \in \mathbb{R}$, the set of observations with $X(\omega) \le a$ is an element of $\Sigma$:

$$\forall a \in \mathbb{R} : \{\omega | X(\omega) \le a\} \in \Sigma \tag{5.2}$$

In the following, we assume that all random variables are real valued random variables.

Now we can ask about the *probability* of events such as $\Pr(\omega \in \Omega : X(\omega) \in [a, b])$. These probabilities are defined on the range $\mathbb{R}$ of the random variable $X$, and thus it is convenient to write shortly $\Pr(X \in [a, b])$, which equals $\mu([a, b])$. A *probability distribution*

assigns probabilities to every event. This distribution can be described by the *cumulative distribution function*

$$F_X(x) := \Pr(X \le x) = \mu((-\infty, x]), \tag{5.3}$$

or by the Lebesgue-integrable *probability density function* (density) $f_X(x)$, which, if it exists, determines the probability of $X$ to take a value in the interval $[x, x + dx]$ for small $dx$,

$$f_X(x)dx := P(x \le X \le x + dx) = \mu([x, x + dx]). \tag{5.4}$$

This implies that $f_X(x) \ge 0$ for all $x \in \Omega$, and the integral over the whole sample space $\Omega$ sums to one:

$$\int_\Omega f_X(x)dx = \mu(\mathbb{R}) = 1. \tag{5.5}$$

The set of all $x$ such that $f_X(x) > 0$ is defined as the *support of* $f_X(x)$. The cumulative distribution $F_X(x)$ and the density $f_X(x)$ are related via

$$F_X(x) = \int_{-\infty}^x f_X(x')dx'. \tag{5.6}$$

The *expected value* of a function $g(x)$ defined on the range of $X$ under the distribution $f_X(x)$ is given by

$$\mathcal{E}(g(x)) := \int_\Omega g(x)f_X(x)dx. \tag{5.7}$$

In particular, the expected value of the identity function $g(x) = x$ is the *mean* $m_X$ of $f_X(x)$,

$$m_X := \int_\Omega x f_X(x)dx. \tag{5.8}$$

Similarly, the *variance* is defined by

$$\sigma_X^2 := \int_\Omega (x - m_X)^2 f_X(x)dx. \tag{5.9}$$

Two well-known probability distributions are the *Normal* or *Gaussian distribution* and the *gamma distribution*. The density of the Normal distribution is given by

$$f_X : \mathbb{R} \to (0, \frac{1}{\sqrt{2\pi}\sigma}], \quad f_X(x) = \frac{1}{\sqrt{2\pi}\sigma} \exp\left[-\frac{1}{2}\left(\frac{x - m_X}{\sigma_X}\right)^2\right], \tag{5.10}$$

with mean $m_X$ and variance $\sigma_X^2$. For a normally distributed random variable $X$, we will use the common notation $X \sim \mathcal{N}(m_X, \sigma_X^2)$. The density of the gamma distribution is given by

$$g_X : \mathbb{R} \to \mathbb{R}_{0,+}, \quad g_X(x) = \begin{cases} \frac{1}{\Gamma(\alpha)}\lambda^\alpha x^{\alpha-1}e^{-\lambda x} & \text{for } x \ge 0 \\ 0 & \text{for } x < 0 \end{cases} \tag{5.11}$$

(a) shape parameter $\alpha = 0.5$

(b) shape parameter $\alpha = 0.8$

(c) shape parameter $\alpha = 1.1$
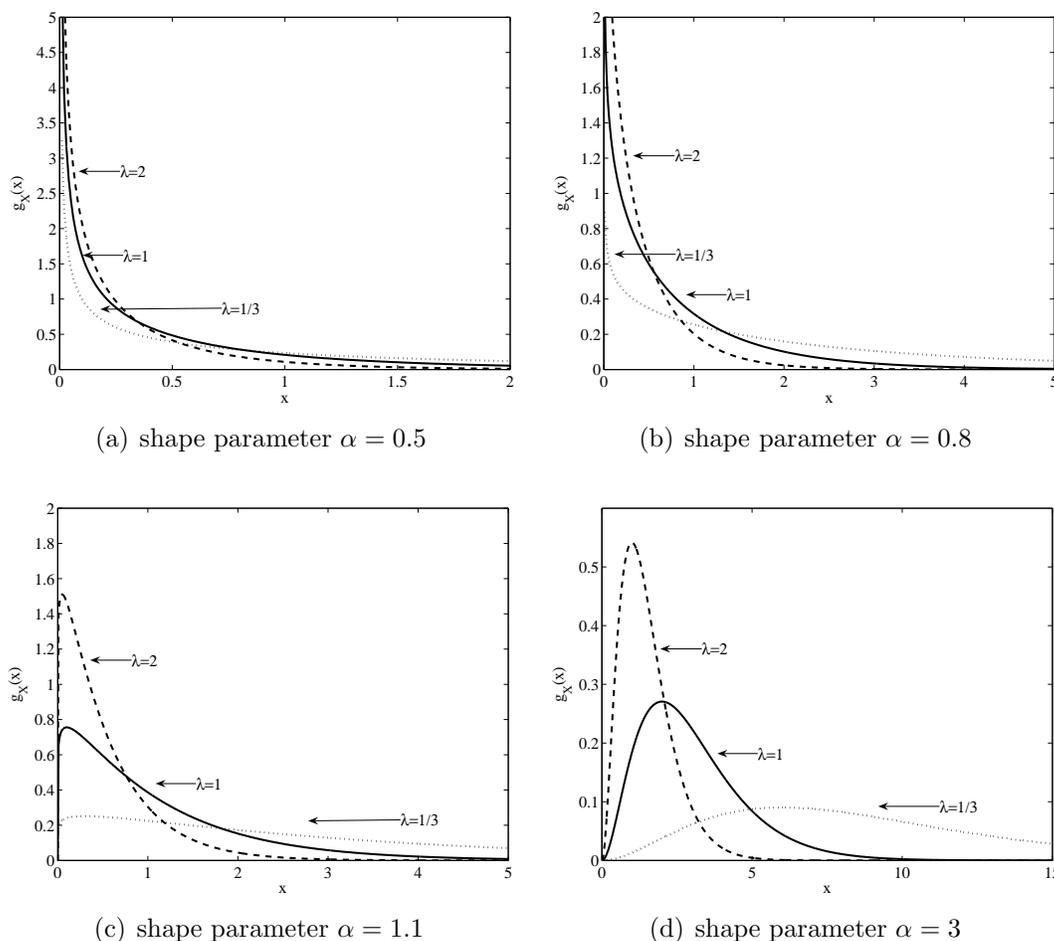
(d) shape parameter $\alpha = 3$

Figure 5.1: Gamma distributions $g_X(x)$ with different shape and rate parameters.

with *shape parameter* $\alpha > 0$ and *rate parameter* $\lambda > 0$. $\Gamma(\alpha)$ denotes the *Gamma function*, which is for positive $\alpha$ defined by

$$\Gamma(\alpha) := \int_0^\infty e^{-t} t^{\alpha-1} dt. \tag{5.12}$$

The gamma distribution is skewed with mean $m_X = \frac{\alpha}{\lambda}$ and maximum $x_M = \frac{\alpha-1}{\lambda}$. The variance is $\sigma_X^2 = \alpha/\lambda^2$. Figure 5.1 shows gamma distributions for different shape and rate parameters. These distributions can qualitatively be distinguished according to their shape parameter: $\lim_{x\to 0} g_X(x) = \infty$ for distributions with $\alpha < 1$ and $g_X(0) = 0$ if $\alpha > 1$. A shape parameter $\alpha = 1$ corresponds to an exponential distribution.

Given a set of $n$ real valued random variables $X_1, \ldots, X_n$, we can define a probability density function that is associated to the set as a whole, the *joint probability density function* $f_{X_1,\ldots,X_n}(x_1, \ldots, x_n)$. This function assigns a probability to an observation of

these random variables $\tilde{x} := (X_1 = \tilde{x}_1, \ldots, X_n = \tilde{x}_n)$ to be in a domain $D \subseteq \mathbb{R}^n$,

$$\Pr(\tilde{x} \in D) = \int_D f_{X_1,\ldots,X_n}(\tilde{x}_1, \ldots, \tilde{x}_n) d\tilde{x}_1 \ldots d\tilde{x}_n. \tag{5.13}$$

The probability density function $f_{X_i}(\tilde{x}_i)$ that is associated to one single $X_i$, the *marginal probability density function*, can be deduced from the joint distribution by integration over the remaining variables:

$$f_{X_i}(\tilde{x}_i) = \int f_{X_1,\ldots,X_n}(\tilde{x}_1, \ldots, \tilde{x}_n) d\tilde{x}_1 \ldots d\tilde{x}_{i-1} d\tilde{x}_{i+1} \ldots d\tilde{x}_n. \tag{5.14}$$

The variables $X_1, \ldots, X_n$ are *independent*, if their joint probability density function equals the product of the marginal density functions:

$$X_1, \ldots, X_n \text{ independent} \quad \Leftrightarrow \quad f_{X_1,\ldots,X_n}(\tilde{x}_1, \ldots, \tilde{x}_n) = \prod_{i=1}^{n} f_{X_i}(\tilde{x}_i) \tag{5.15}$$

Finally, the *conditional probability density function* $f_{X|Y}(\tilde{x}|\tilde{y})$ of two real random variables $X$ and $Y$ represents the probability density of $\tilde{x}$ given that $Y = \tilde{y}$. For constant $\tilde{y}$, $f_{X|Y}(\tilde{x}|\tilde{y})$ defines a probability density function over $\tilde{x}$. If in turn $\tilde{x}$ is constant, $f_{X|Y}(\tilde{x}|\tilde{y})$ is the *likelihood function* $\mathcal{L}(\tilde{y})$ over $\tilde{y}$. For $f_Y(\tilde{y}) \neq 0$, the conditional probability density is defined by the ratio of the joint probability density $f_{X,Y}(\tilde{x}, \tilde{y})$ and the marginal density $f_Y(\tilde{y})$,

$$f_{X|Y}(\tilde{x}|\tilde{y}) := \frac{f_{X,Y}(\tilde{x}, \tilde{y})}{f_Y(\tilde{y})}. \tag{5.16}$$

Writing equation (5.16) with exchanged random variables $X$ and $Y$ and eliminating $f_{X,Y}(\tilde{x}, \tilde{y})$ leads to *Bayes' formula*:

$$f_{X|Y}(\tilde{x}|\tilde{y}) = \frac{f_{Y|X}(\tilde{y}|\tilde{x}) f_X(\tilde{x})}{f_Y(\tilde{y})} \tag{5.17}$$

with a marginal density

$$f_Y(\tilde{y}) = \int f_{Y|X}(\tilde{y}|\tilde{x}) f_X(\tilde{x}) d\tilde{x}. \tag{5.18}$$

Equation (5.17) relates the two conditional probability densities $f_{X|Y}(\tilde{x}|\tilde{y})$ and $f_{Y|X}(\tilde{y}|\tilde{x})$. In many books, Bayes' formula is derived for discrete random variables, and the function $f$ denotes a probability rather than a density. A proof that it also holds for densities can be found in [143]. Moreover, it also holds for vectorial random variables $X, Y \in \mathbb{R}^n$.

In the following, we will shortly write $p(x)$ for $f_X(x)$ and $p(x|y)$ for $f_{X|Y}(x|y)$. Equations are given for continuous random variables, and to obtain the corresponding equations for discrete variables, integrals have to be replaced by sums.

## 5.1.1   Maximum likelihood and Bayesian parameter estimation

In a *Bayesian learning approach*, we are given a set $\mathcal{M}$ of models and a set $\mathcal{D}$ of experimental data. In addition, prior information about these models is encoded in an *a priori probability distribution* (*prior*) $p(m)$, $m \in \mathcal{M}$. This prior reflects our expectation of outcome before we have seen the data. Elements in $\mathcal{D}$ are understood as realizations of random variables, whose distributions $p(\mathcal{D}|m)$ are conditional on the underlying model $m$. Bayes' formula is then used to express the conditional probability distribution of a model $m$ given the data $\mathcal{D}$, $p(m|\mathcal{D})$, in terms of the likelihood function $\mathcal{L}_{\mathcal{D}}(m) = p(\mathcal{D}|m)$ and the prior $p(m)$,

$$p(m|\mathcal{D}) = \frac{p(\mathcal{D}|m)p(m)}{p(\mathcal{D})} = \frac{\mathcal{L}_{\mathcal{D}}(m)p(m)}{p(\mathcal{D})}. \tag{5.19}$$

The left hand side of equation (5.19) is called *a posteriori probability distribution* (*posterior*). It is proportional to the product of the conditional probability distribution $p(\mathcal{D}|m)$ and the prior $p(m)$. The denominator is given by marginalizing over $\mathcal{M}$,

$$p(\mathcal{D}) = \int_{\mathcal{M}} p(\mathcal{D}|m)p(m)dm, \tag{5.20}$$

and denoted *evidence*. It states to which degree the data reflects the model class $\mathcal{M}$ and the prior distribution $p(m)$. In the worst case, if $p(\mathcal{D}|m)$ and $p(m)$ have non-overlapping supports, the integral becomes zero and equation (5.19) does not hold any longer.

The evaluation of the integral in equation (5.20) often is the computationally most difficult task of a Bayesian approach [14]. It is usually performed numerically with *Monte Carlo techniques* [60].

The set $\mathcal{M}$ of models is frequently restricted to contain only functions which have the same parameterization, and a model $m$ is characterized by a parameter vector $\omega$. This converts the problem of learning a probability density function to one of estimating this vector $\omega$. In a *maximum a posteriori* (MAP) approach, the posterior (5.19) is maximized with respect to $\omega$, which leads to a point estimator $\hat{\omega}_{MAP}$:

$$\hat{\omega}_{MAP} \quad := \quad arg\max_{\omega} p(\omega|\mathcal{D}) \tag{5.21}$$

$$\stackrel{(5.19)}{=} \quad arg\max_{\omega} \frac{\mathcal{L}_{\mathcal{D}}(\omega)p(\omega)}{p(\mathcal{D})} \tag{5.22}$$

$$= \quad arg\max_{\omega} \mathcal{L}_{\mathcal{D}}(\omega)p(\omega) \tag{5.23}$$

$$= \quad arg\min_{\omega} \left(-\ln\mathcal{L}_{\mathcal{D}}(\omega) - \ln p(\omega)\right) \tag{5.24}$$

In the MAP approach, a calculation of the evidence is not required, since it appears as an $\omega$-independent scaling factor in equation (5.19). It is often convenient to minimize the negative logarithm of the posterior, in particular, if the posterior is given by a product of independent distributions, since in this case products convert into sums.

We compare the results of our Bayesian approach with results of the standard *maximum likelihood estimation* (MLE), in which the optimal parameter $\hat{\omega}_{MLE}$ is assumed to maximize the likelihood function $\mathcal{L}_{\mathcal{D}}(\omega)$,

$$
\begin{aligned}
\hat{\omega}_{MLE} &:= \arg\max_{\omega} \mathcal{L}_{\mathcal{D}}(\omega) & (5.25) \\
&= \arg\min_{\omega} \left( -\ln \mathcal{L}_{\mathcal{D}}(\omega) \right). & (5.26)
\end{aligned}
$$

Comparing both estimators, $\hat{\omega}_{MLE}$ and $\hat{\omega}_{MAP}$, the logarithm of the prior $p(\omega)$ over network parameters functions as an additional *penalty* or *regularization term* in equation (5.24).

## 5.2 A Bayesian learning framework

We will use the idea of Bayesian learning to estimate parameters for our gene regulatory network model described in Chapter 2. We are given a dataset $\mathcal{D} = \{\tilde{x}(t)\}_{\substack{t=z\cdot\Delta t \\ z=0,\dots,T}}$, $\tilde{x}(t) = (\tilde{x}_1(t), \dots, \tilde{x}_n(t)) \in \mathbb{R}^n$ of gene expression values of $n$ genes and $T+1$ equally distant time points. Expression values $\tilde{x}_i(t)$ are interpreted as random variables, which originate from an underlying deterministic process, and are randomly disturbed during the measurement process. The deterministic system is described by the ODE model in our approach. Elements of the dataset $\mathcal{D}$ are determined by the model and a stochastic noise term, which corresponds to random perturbations due to measurement errors.

We start with the ODE model derived in Chapter 2,

$$
\dot{x}_i(t) = s_i - \gamma_i x_i(t) + \sum_{j=1}^{n} k_{ij} \frac{x_j(t)^{m_{ij}}}{x_j(t)^{m_{ij}} + \theta_{ij}^{m_{ij}}} \qquad i = 1, \dots, n. \tag{5.27}
$$

This system contains $2n + 3n^2$ parameters, namely synthesis and degradation rates $s_i$ and $\gamma_i$ for each component, and, for each of the $n^2$ possible regulations, regulation strength $k_{ij}$, Hill-coefficient $m_{ij}$ and threshold value $\theta_{ij}$. These parameters are collected in a parameter vector $\omega \in \mathbb{R}^{2n+3n^2}$.

In order to compare model predictions and experimental data, we have to evaluate the solutions $x_i(t)$ of system (5.27) for given initial concentrations $\tilde{x}_i(0)$. For this, we integrate equation (5.27) numerically, using *Euler integration*, where time derivatives of the left hand side in equation (5.27) are approximated by difference quotients:

$$
\dot{x}_i(t) \approx \frac{x_i(t + \Delta t) - x_i(t)}{\Delta t}. \tag{5.28}
$$

Resolving for $x_i(t + \Delta t)$ yields a recursive formula for the expression level of gene $i$ at time $t + \Delta t$:

$$
x_i(t + \Delta t) = x_i(t) + \Delta t \underbrace{\left[ s_i + \gamma_i x_i(t) + \sum_{j=1}^{n} k_{ij} \frac{x_j(t)^{m_{ij}}}{x_j(t)^{m_{ij}} + \theta_{ij}^{m_{ij}}} \right]}_{=:h_i(\omega, x(t))} \tag{5.29}
$$

To indicate that $x_i(t)$ depends on the model parameters $\omega$ to be estimated, we will use the notation $h_i(\omega, x(t))$ for the expression on the right hand side of equation (5.29) in the following. To model elements of the dataset $\mathcal{D}$, we add a noise term $\eta_\xi$ to this expression, which converts the deterministic differential equation model into a stochastic model,

$$\tilde{x}_i(t + \Delta t) = h_i(\omega, \tilde{x}(t)) + \eta_\xi. \tag{5.30}$$

We assume that all noise terms for each network component and every time point are uncorrelated and normally distributed with mean zero and variance $\sigma_\xi^2$, $\eta_\xi \sim \mathcal{N}(0, \sigma_\xi^2)$. Thus, the variables $\tilde{x}_i(t + \Delta t)$ in equation (5.30) are realizations of independent real valued random variables . These variables are drawn from a Normal distribution with mean $h_i(\omega, \tilde{x}(t))$ defined by the discretized differential equation and the measurement $\tilde{x}(t)$ at the precedent time point, and a variance $\sigma_\xi^2$, $\tilde{x}_i(t + \Delta t) \sim \mathcal{N}(h_i(\omega, \tilde{x}(t)), \sigma_\xi^2)$. We will subsequently refer to the corresponding standard deviation $\sigma_\xi$ as 'noise level'. The assumption of independence is motivated by the assumption that the noise stems from several different, independent sources. Here, as stated in the beginning of this section, we neglect intrinsic noise due to stochastic regulation processes, and implicitly assume that the system acts deterministically, and that the variance observed in the data results solely from independent measurement errors.

The corresponding likelihood function $\mathcal{L}_\mathcal{D}(\omega)$ is given as a product of individual probabilities over $T + 1$ time points and all network components,

$$\mathcal{L}_\mathcal{D}(\omega) = \qquad\qquad \prod_{i=1}^{n} \prod_{t=0}^{T} p(\tilde{x}_i(t)|\omega) \tag{5.31}$$

$$= \; p(\tilde{x}(0)) \prod_{i=1}^{n} \prod_{t=0}^{T-1} \frac{1}{\sqrt{2\pi}\sigma_\xi} \exp\left[ -\frac{1}{2} \left( \frac{h_i(\omega, \tilde{x}(t)) - \tilde{x}_i(t+\Delta t)}{\sigma_\xi} \right)^2 \right]. \tag{5.32}$$

The probability density $p(\tilde{x}(0))$ over the initial concentration vector $\tilde{x}(0)$ is assumed to be a product of $n$ delta functions which peak at $\tilde{x}_i(0)$:

$$p(\tilde{x}(0)) = \prod_{i=1}^{n} p(\tilde{x}_i(0)) = \prod_{i=1}^{n} \delta(\tilde{x}_i(0)). \tag{5.33}$$

The *maximum likelihood estimator* $\hat{\omega}_{MLE}$, which maximizes equation (5.32), also minimizes the sum of squared errors between model predictions $h_i(\omega, \tilde{x}(t))$ and experimental data $\tilde{x}_i(t + \Delta t)$, $i = 1, \ldots, n$ and $t = 0, \ldots, T - 1$:

$$\hat{\omega}_{MLE} \;=\; arg \min_{\omega} \left( -\ln \mathcal{L}_\mathcal{D}(\omega) \right) \tag{5.34}$$

$$=\; arg \min_{\omega} \sum_{i=1}^{n} \sum_{t=0}^{T-1} \left[ h_i(\omega, \tilde{x}(t)) - \tilde{x}_i(t + \Delta t) \right]^2 \tag{5.35}$$

This can easily been seen by taking the logarithm of equation (5.32).

## 5.2.1  Prior distribution over network parameters

We express our prior belief about the real parameter values by a joint distribution $p(\omega)$, which is given as the product of independent distributions over each model parameter,

$$p(\omega) = \prod_{i=1}^{n} p(s_i) \prod_{i=1}^{n} p(\gamma_i) \prod_{i=1}^{n} \prod_{j=1}^{n} p(k_{ij}) \prod_{i=1}^{n} \prod_{j=1}^{n} p(\theta_{ij}) \prod_{i=1}^{n} \prod_{j=1}^{n} p(m_{ij}). \qquad (5.36)$$

This prior reflects that our prior belief about a model parameter is not affected by the value of a second parameter.

### Prior distributions over synthesis and degradation rates

We use independent gamma distributions for the parameters $s_i$ and $\gamma_i$, $i = 1, \ldots, n$, with a shape parameter $\alpha > 1$ and a rate parameter $\lambda > 0$ (see Figure 5.1). These distributions reflect our expectation that both parameters, synthesis and degradation rates, are positive and should not become too large. The assumption of independence is reasonable also from a biological point of view. The basal synthesis rate $s_i$ and the degradation rate $\gamma_i$ are model parameters which determine the behavior of gene product $i$ in case that all regulators of $i$ are absent. The basal synthesis rate $s_i$ describes the activity of the RNA polymerase without any transcription factors bound to the promoter region of gene $i$. Thus, $s_i$ does not depend on other network components. Degradation is also assumed to depend solely on the concentration of gene product $i$ itself and is therefore not affected by further network components.

### Prior distributions over threshold values and Hill-coefficients

We use delta prior distributions for the threshold values $\theta_{ij}$ and the Hill-coefficients $m_{ij}$, effectively fixing these parameters to constant values $\hat{\theta}_{ij}$ and $\hat{m}_{ij}$. Both parameters appear as non-linear terms in our model (5.27). If only few data points are available, we observed that they are hard to learn from a numerical point of view. In particular, large Hill-coefficients increase the stiffness of the differential equation system. We will detail this aspect later in Chapter 8. In principle, both parameters could also be described by gamma distributions, and they can be integrated in the optimization process as well, if the dataset is sufficiently large. However, it is not a difficult task to find biologically plausible limits for both parameters. In Chapter 2 we have seen that $m_{ij}$ corresponds to the number of proteins forming a complex. Most proteins are known to act as monomers, dimers or tetramers [121]. Thus $m_{ij}$ is assumed to lie within an interval $[1, 4]$. A variation of $m_{ij}$ within this interval does not have much effect on the model, since $m_{ij}$ only determines the slope of the regulation function about the threshold value $\theta_{ij}$ (see Chapter 2). Values $m_{ij} > 1$ accounting for cooperative interaction among transcription factors are in fact interesting for a theoretical investigation of the model, since they can alter its qualitative dynamic behavior. We will see an example in Chapter 8.

Threshold values $\hat{\theta}_{ij}$ are set within the range of observed expression values of gene $j$, assuming that the regulation is active in the observed network. Microarray measurements are usually given as normalized log-ratios with mean 0. In our model, the observations $\tilde{x}(t)$ are directly the ratios of concentrations. Thus the mean 0 of the log-ratios transforms to 1, and we choose $\hat{\theta}_{ij} = 1$ for all $i, j = 1, \ldots, n$ in this case.

**Prior distributions over regulation strengths**

For the regulation strengths $k_{ij}$, a specifically designed prior distribution is used [105]. This distribution favors sparse networks, in which most of the edges correspond to very small interaction strengths, and $k_{ij}$ only differs significantly from zero when the data warrants it. This is obtained with a *hierarchical prior distribution*. The regulation strengths $k_{ij}$, $i, j = 1, \ldots, n$ are assumed to be normally distributed with mean zero and a variance $\sigma^2$, $k_{ij} \sim \mathcal{N}(0, \sigma^2)$. The standard deviation $\sigma$ is itself modeled as a random variable, hence the whole distribution is called *hierarchical*. For $\sigma$ we use a gamma distribution, which has its maximum close to zero and rapidly decreases for increasing values. This is achieved with a shape parameter $1 < \alpha < 1 + \epsilon$. Accordingly, the marginal probability for a regulation strength $k_{ij}$ can be calculated by integrating over the range of the random variable $\sigma$ (see also [103]),

$$p(k_{ij}) = \int_0^\infty p(k_{ij}|\sigma)p(\sigma)d\sigma \tag{5.37}$$

$$= \int_0^\infty \frac{1}{\sqrt{2\pi}\sigma} \exp\left(-\frac{k_{ij}^2}{2\sigma^2}\right) \frac{\lambda^\alpha \sigma^{\alpha-1} e^{-\lambda\sigma}}{\Gamma(\alpha)} d\sigma \tag{5.38}$$

$$= \frac{\lambda^\alpha}{\sqrt{2\pi}\Gamma(\alpha)} \int_0^\infty \sigma^{\alpha-2} \exp\left(-\lambda\sigma - \frac{k_{ij}}{2\sigma^2}\right) d\sigma. \tag{5.39}$$

## 5.2.2   Optimization problem

We have specified the likelihood function $\mathcal{L}_\mathcal{D}(\omega)$ and the prior $p(\omega)$. The resulting objective function $F_{MAP}$, the negative logarithm of the posterior, which has to be minimized with respect to $\omega$ in order to obtain $\hat{\omega}_{MAP}$, is given by

$$F_{MAP}(\omega) \overset{(5.24)}{=} -\ln \mathcal{L}_\mathcal{D}(\omega) - \ln p(\omega)$$

$$= -\underbrace{\sum_{i=1}^n \sum_{t=1}^T \ln p(\tilde{x}_i(t)|\omega)}_{\text{log likelihood}}$$

$$-\underbrace{\left(\sum_{i=1}^n \ln p(s_i) + \sum_{i=1}^n \ln p(\gamma_i) + \sum_{i=1}^n \sum_{j=1}^n \ln p(k_{ij})\right)}_{\text{log prior}} \tag{5.40}$$

with probability densities

$$p(\tilde{x}_i(t)|\omega) = \frac{1}{\sqrt{2\pi}\sigma_\xi} \exp\left[ -\frac{1}{2}\left( \frac{h_i(\omega, \tilde{x}(t)) - \tilde{x}_i(t + \Delta t)}{\sigma_\xi}\right)^2\right], \quad (5.41)$$

$$p(s_i) = \frac{1}{\Gamma(\alpha_{s_i})} \lambda_{s_i}^{\alpha_{s_i}} s_i^{\alpha_{s_i}-1} exp(-\lambda_{s_i} s_i), \quad (5.42)$$

$$p(\gamma_i) = \frac{1}{\Gamma(\alpha_{\gamma_i})} \lambda_{\gamma_i}^{\alpha_{\gamma_i}} \gamma_i^{\alpha_{\gamma_i}-1} exp(-\lambda_{\gamma_i} \gamma_i), \quad (5.43)$$

$$\text{and} \quad p(k_{ij}) = \frac{\lambda^\alpha}{\sqrt{2\pi}\Gamma(\alpha)} \int_0^\infty \sigma^{\alpha-2} \exp\left( -\lambda\sigma - \frac{k_{ij}}{2\sigma^2}\right) d\sigma. \quad (5.44)$$

The first term in equation (5.40) corresponds to the logarithm of the likelihood function (log likelihood). It is a sum over all data points, which is weighted by the inverse of the variance $\sigma_\xi^2$ (compare equation (5.32)) and fits the parameter vector $\omega$ to the data $\mathcal{D}$. The remaining terms refer to the logarithm of the prior distributions (log prior). In comparison to the maximum likelihood objective function (equation (5.35)), these terms act as regularization terms, which penalize parameter vectors $\omega^*$ with small prior densities $p(\omega^*)$. For increasing sample size, the log likelihood becomes the dominating term in equation (5.40), and hence the difference between the two estimates $\hat{\omega}_{MLE}$ and $\hat{\omega}_{MAP}$ decreases.

## 5.3 Results on simulated data

### 5.3.1 Data simulation

We simulated time series for a network of seven genes with interaction graph $G = (V, E)$ as shown in Figure 5.2. This network was designed according to the cell cycle network in the yeast *S. cerevisiae*, which is used as a reference network in the following Section 5.4. Parameters used in the simulation were $s_i = 1$ and $\gamma_i = 0.1$ for $i = 1, \ldots, n$. Parameters of the regulation functions were set to $k_{ij} = \pm 2$ with signs according to the edge labels in the graph in Figure 5.2, $\theta_{ij} = 5$ and $m_{ij} = 2$ for $i, j = 1, \ldots, n$.

Data simulation was carried out with time steps $\Delta t = 1$. We used the discretized model (5.30) to simulate several time series with different initial concentration vectors $x(0)$ and three time points each. Initial concentrations $x_i(0)$, $i = 1, \ldots, n$, were drawn from a uniform distribution over the interval $[0, 5]$. We varied the noise level $\sigma_\xi$ and the number of time points used for learning.

### 5.3.2 Parameter estimation

Conjugate gradient descent was carried out to minimize the objective function $F_{MAP}(\omega)$ (5.40). For more details see also [60, 67, 103, 152]. Derivatives of the log likelihood in $F_{MAP}$ with respect to model parameters $\omega$ were included into this program and are listed in Appendix B. Derivatives of the log prior are given in [103]. The integrals in the prior
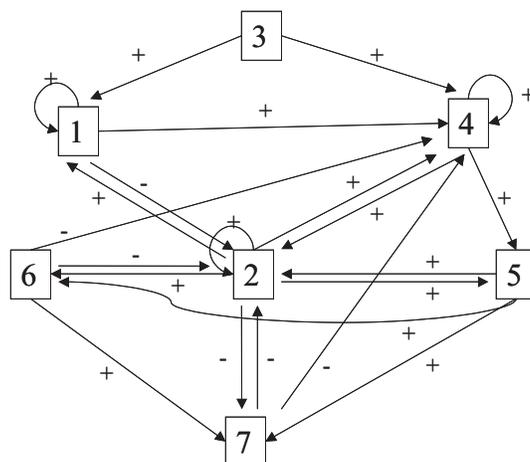
Figure 5.2: Structure of the network that was used to simulate datasets according to equation (5.30)

distributions over regulation strengths (equation (5.39)) had to be carried out numerically (see [103]).

The threshold values $\theta_{ij}$ and the Hill-coefficients $m_{ij}$ were fixed to values $\hat{\theta}_{ij} = 5$ and $\hat{m}_{ij} = 2$ for $i, j = 1, \ldots, n$. To test how strongly results depend on these parameters, we compared results using several different values, and observed no significant differences. Gradient descent was started with $s_i = \gamma_i = 0.1$. All regulation strengths $k_{ij}$ were initially set to 0. Parameters for gamma distributions over synthesis and degradation rates were set to $\alpha_{s_i} = 2$, $\lambda_{s_i} = 1$, $\alpha_{\gamma_i} = 1.0001$ and $\lambda_{\gamma_i} = 2$ for $i = 1, \ldots, n$. Parameters for the gamma distribution over standard deviations $\sigma$ in equation (5.39) were set to $\alpha = 1.2$ and $\lambda = 1.5$.

Figure 5.3 shows mean squared errors per estimated model parameter, i.e. synthesis and degradation rates $s_i$ and $\gamma_i$ and interaction strengths $k_{ij}$. The ML was compared with the MAP estimation for different noise levels and 40 time points (*left*) and 70 time points (*right*) used for learning. Shown are mean squared errors for synthesis and degradation rates in % (*top*) and mean squared errors for estimated interaction strengths (*bottom*), given as absolute values. It can be observed that $\hat{\omega}_{MAP}$ outperforms $\hat{\omega}_{MLE}$ especially for higher noise levels.

## 5.3.3   Inferred network structure

Since our method aims at the inference of the network structure and the estimation of parameters simultaneously, we performed a *receiver operator characteristics* (ROC) analysis to score the inferred regulations. For this, we set a threshold value $z$ for absolute values of the regulation strengths $k_{ij}$ and assume a regulation from $j$ to $i$ to be present if $|k_{ij}| \geq z$. ROC curves are obtained by varying $z$ from 0 to $\max\{|k_{ij}| \mid i, j = 1, \ldots, n\}$ and calculating the proportion of true positives among all positives (*sensitivity*) and the propor-
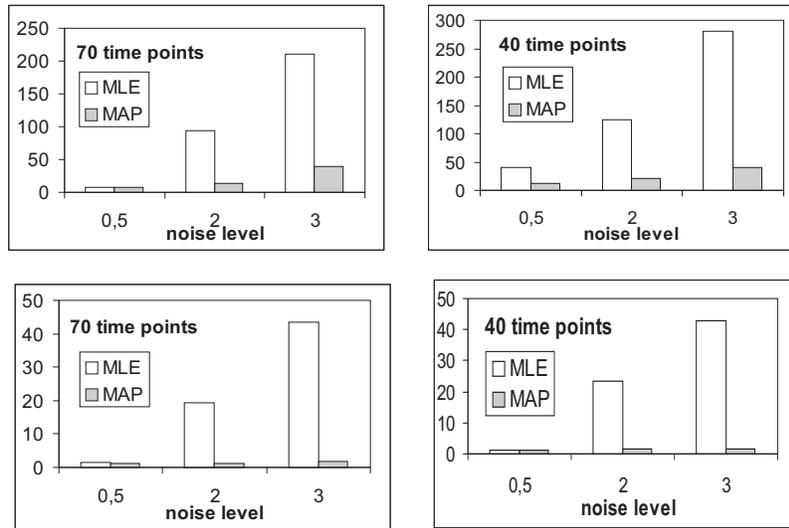
Figure 5.3: Mean squared errors (MSE) for estimated model parameters, $\hat{\omega}_{MLE}$ and $\hat{\omega}_{MAP}$. **Top:** MSE for synthesis and degradation rates $s_i$ and $\gamma_i$ are given in %. **Bottom:** MSE for interaction strengths $k_{ij}$ are given as absolute values.

tion of true negatives of all negatives (*specificity*) for the corresponding network structures.

Figure 5.4 shows ROC curves for noise levels $\sigma_\xi = \{2,3\}$ and 40 and 70 time points, respectively. As a high sensitivity and specificity are desirable, a good classifiers' ROC curve would be positioned in the upper left corner of the graph. Guessing would on average lead to a diagonal, where sensitivity equals 1-specificity.
Figure 5.4 indicates that MLE fails in case of 40 time points. Here, the corresponding ROC curves are not better than choosing edges randomly, whereas MAP is able to infer parts of the network structure. Not surprisingly, both approaches perform better when using 70 time points compared to the results obtained with 40 time points, and also here MAP outperforms MLE. Figure 5.5 shows the inferred networks for the ML (*left*) and the MAP (*right*) approach for a noise level $\sigma_\xi = 2$ and 70 time points. The 17 edges with highest weights are marked in bold. Solid lines indicate true positives, dashed lines false positives, and thin lines false negatives. Both approaches reveal many true regulations, 12 of 17 edges are true positives for MLE, 14 are found in the MAP approach.

The overall ROC performance can be represented by the *area under the curve* (AUC). This value is independent of the threshold $z$. The AUC lies between 0 and 1 and increases with increasing performance of the classifier. Random guessing whether an edge is present or not would on average yield an AUC value of 0.5. AUC values for $\hat{\omega}_{MLE}$ and $\hat{\omega}_{MAP}$ for different noise levels and a varying number of time points can be seen in Figure 5.6. The left plot shows how performance deteriorates with increasing noise level, for a fixed dataset size of 70 time points. The right plot shows the performance for an increasing number of

(a) $\sigma_\xi = 2, T = 40$                    (b) $\sigma_\xi = 3, T = 40$

(c) $\sigma_\xi = 2, T = 70$                    (d) $\sigma_\xi = 3, T = 70$
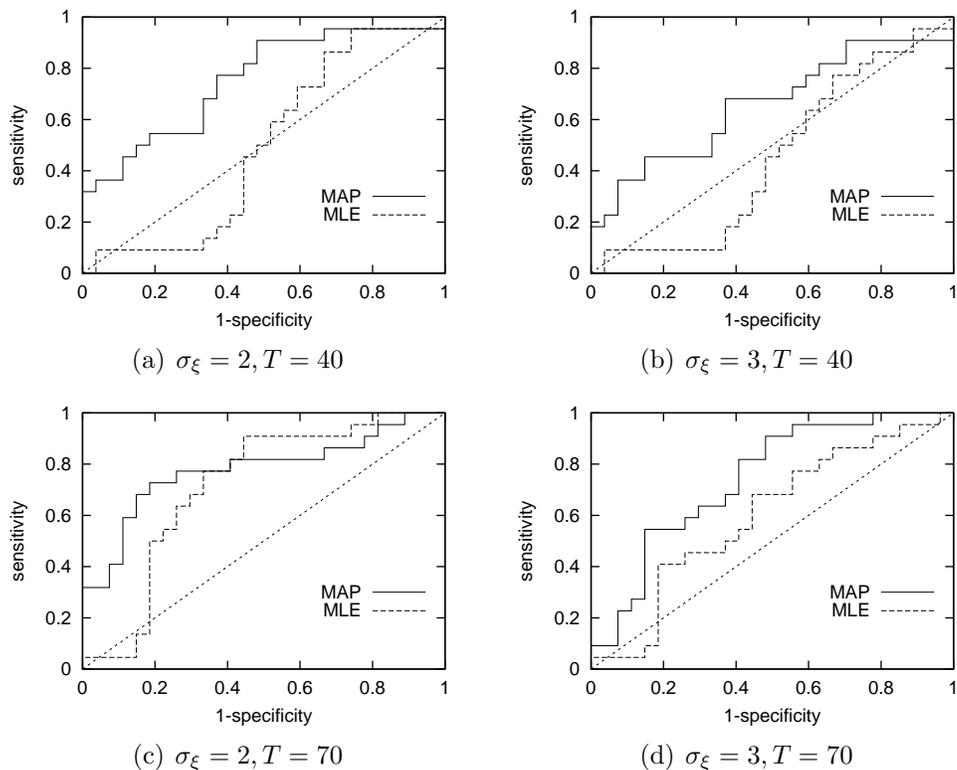
Figure 5.4: ROC curves for the Bayesian and the ML approach
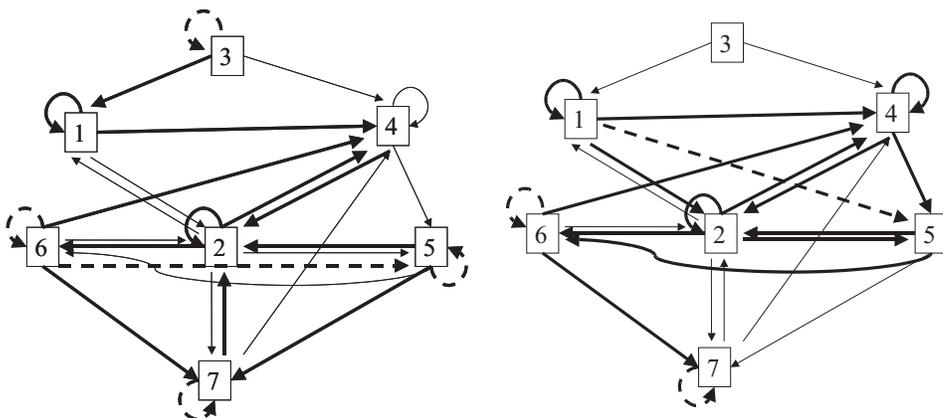


Figure 5.5: The 17 identified regulations with the highest regulation strengths for the MLE (*left*) and the MAP (*right*) approach. True positives are marked in *bold*, false positives are marked with *bold dashed lines*, false negatives correspond to *thin lines*. 70 time points were used for learning, the noise level $\sigma_\xi$ was set to $\sigma_\xi = 2$.
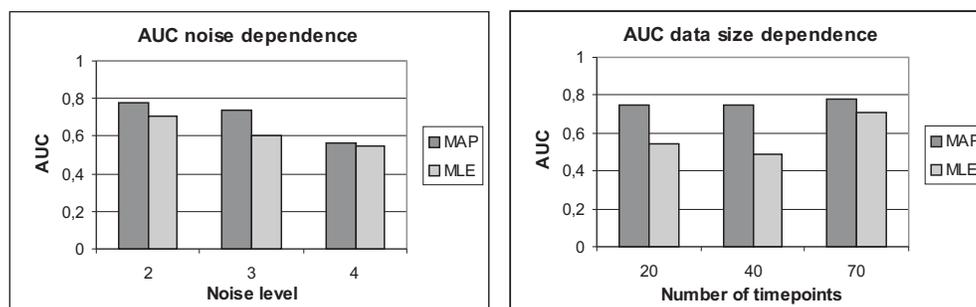
Figure 5.6: AUC values for the ML and MAP approach, with respect to varying noise levels (*left*, $T = 70$) and varying number $T$ of time points (*right*, with noise level $\sigma_\xi = 2$).

time points and a fixed noise level $\sigma_\xi = 2$. Although the ROC analysis is a very coarse-grained method to evaluate the performance of our approach, since it does not consider exact parameter values and even neglects values for several model parameters as synthesis or degradation rates, the AUC value turns out to be a good measure of the method's overall performance. Performance in ROC analysis correlates very well with mean squared errors of learned network parameters.

We conclude from our analysis of the simulated dataset that a Bayesian approach with an appropriate prior distribution improves network inference compared to a ML approach, especially in case of noisy datasets with only a few time points, typical for microarray measurements. Moreover, as seen in Figure 5.6, it reduces the minimal number of time points needed to draw meaningful conclusions.

## 5.4 Results on the yeast cell cycle

The cell cycle is one of the best known regulatory mechanisms. A proper function of the cell cycle machinery is essential for organisms to survive. Dysfunctions often lead to programmed cell death or to phenotypes that are not able to survive for a longer time or show significant changes in the cell cycle. As the cell cycle is highly conserved among eukaryotes, many key regulatory processes in yeast are also found in higher organisms, and it is often possible to draw conclusions from yeast experiments to higher eukaryotes. Surveys of control mechanisms of the yeast cell cycle can be found in [6, 30].

We applied our approach to a dataset of Spellman *et al.* [183], who measured gene expression values of the whole yeast genome containing about 6000 genes. They conducted a cluster analysis and reported approximately 800 genes to be cell cycle regulated. The dataset consists of log-ratios between synchronized cells and control experiments and contains 69 time points in total. These are divided into different time series due to three independent cell synchronization methods.

We analyzed measurements of eleven genes including Cln1, Cln2, Cln3, Clb5, Clb6,
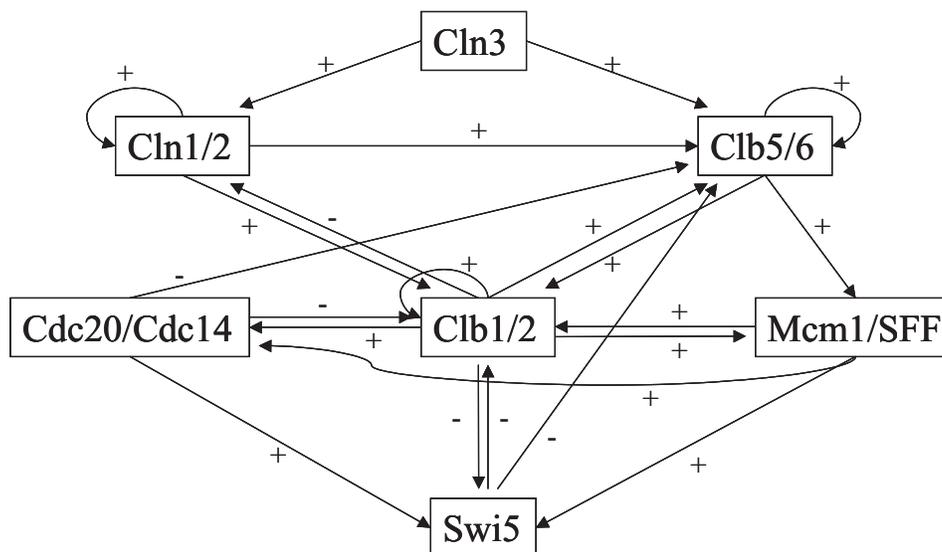
Figure 5.7: Regulatory network of the yeast cell cycle, which was used as a reference to evaluate our results. A descriptions for each interaction is given in Table C.1 in Appendix C.

Cdc20, Cdc14, Clb1, Clb2, Mcm1 and Swi5, which are known to be involved in the cell cycle [116]. In this and the following chapters, we will use the standard names for genes of the *S. cerevisiae* cell cycle. The corresponding systematic names and name descriptions are given in Table C.2 in Appendix C.

The reference network in Figure 5.7 was used for evaluation. It is a reduction of the regulatory network specified in Li *et al.* [116]. Details about this reduction and each single interaction of the reference network used here are detailed in Appendix C. Nodes which contain more than one gene were represented by their means, missing values were replaced by means of concentrations of consecutive and subsequent time points.

Gradient descent was started with $s_i = \gamma_i = 0.1$, $i = 1, \ldots, n$. All regulation strengths $k_{ij}$ were initially set to 0. Parameters for gamma distributions over synthesis and degradation rates were set to $\alpha_{s_i} = \alpha_{\gamma_i} = 0.01$, $\lambda_{s_i} = \lambda_{\gamma_i} = 0.1$, $i = 1, \ldots, n$. Parameters for the gamma distribution over standard deviations $\sigma$ in equation (5.39) were set to $\alpha = 1.7$ and $\lambda = 5$. Threshold values and Hill-coefficients were set to $\hat{\theta}_{ij} = 1$ and $\hat{m}_{ij} = 2$ for $i, j = 1, \ldots, n$.

Figure 5.8 shows ROC curves for $\hat{\omega}_{MLE}$ and $\hat{\omega}_{MAP}$. The corresponding AUC values are 0.61 and 0.68, respectively. This plot shows that both, MLE and MAP, are slightly better than guessing on average and reveal some of the main regulatory interactions. Inferred networks for the ML (*top*) and the MAP approach (*bottom*) can be seen in Figure 5.9. The 16 edges with highest inferred weights are shown in bold. True positives are indicated
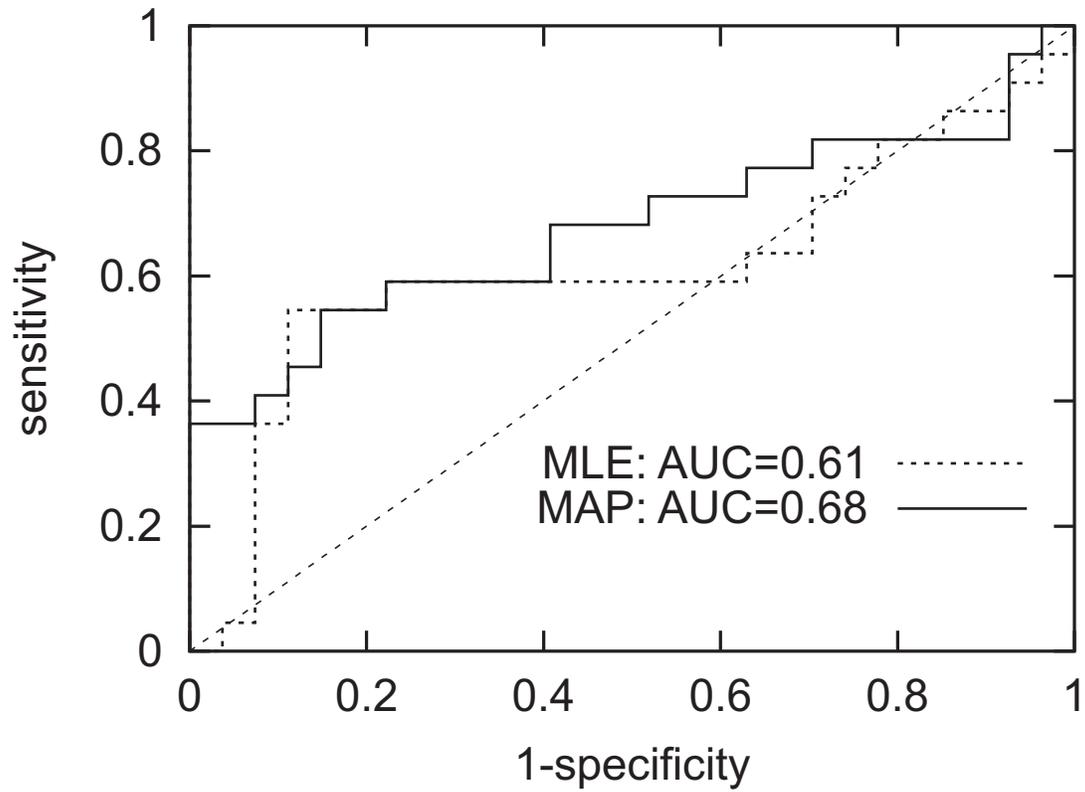
Figure 5.8: Receiver operator characteristics curve for the inferred regulatory network of the *Saccharomyces cerevisiae* cell cycle.

by continuous bold lines, dashed bold lines correspond to false positives, thin lines are referenced in the literature, but were not revealed in our approach. Many true regulations are revealed in both approaches. The MAP estimate identifies more true regulations than MLE between different genes. Interestingly, it reports a couple of auto-regulations, which are not contained in the reference network. It is not clear whether these regulations are artifacts resulting from strong prior distributions over synthesis and degradation rates, or if they are not yet stated in the literature.

## 5.5   Concluding remarks

This chapter presented a combination of an ODE model and a Bayesian learning approach. The method is generally able to infer dynamic phenomena of regulatory networks and to account for stochastic fluctuations. A Bayesian parameter estimation approach was defined, using prior distributions over model parameters. These distributions are used to integrate prior knowledge about the system into the inference process. In particular, we specified a hierarchical distribution over regulation strengths, which drives the solution to sparse networks. An analysis of simulated data indicates that the approach is able to prevent overfitting. Quantitative model parameters were correctly identified, and results are much better than maximum likelihood estimation, especially for few time points and a high noise level. Moreover, the underlying network structure was almost correctly identified. Hence, we concluded that the approach presented can deal with sparse data and provides an appropriate framework to analyze high-throughput data.

An application to a real-world dataset shows, here as well, that the Bayesian approach outperforms maximum likelihood estimation. However, although main regulations are revealed, the results are not as good as those for the simulated data. This becomes apparent in the ROC curves, which are worse than for the simulated dataset, and also, when taking the signs of edges into account, which have not been considered in the ROC analysis. Signs of inferred regulations using simulated data are conform with the real signs. However, some of the activating regulations in the yeast reference network have been identified as inhibitions in the inferred networks. The reasons for these differences between simulated and real data are manifold:

- First, the reference network does not only contain regulations via transcription factors, but also degradation control mechanisms and chemical modifications. These are not always reflected by mRNA concentrations. An improvement concerning this problem can only be reached by an inclusion of further information about regulation mechanisms at the post-transcriptional level. Such information can be information about transcription factor binding sites or protein-protein interaction data. In principle, the Bayesian approach provides a natural framework to include several data sources through prior distributions.

- The second problem is related to the kind of data used for estimation. The dataset consists of seven periodically expressed genes or gene clusters. The corresponding

(a) MLE



(b) MAP
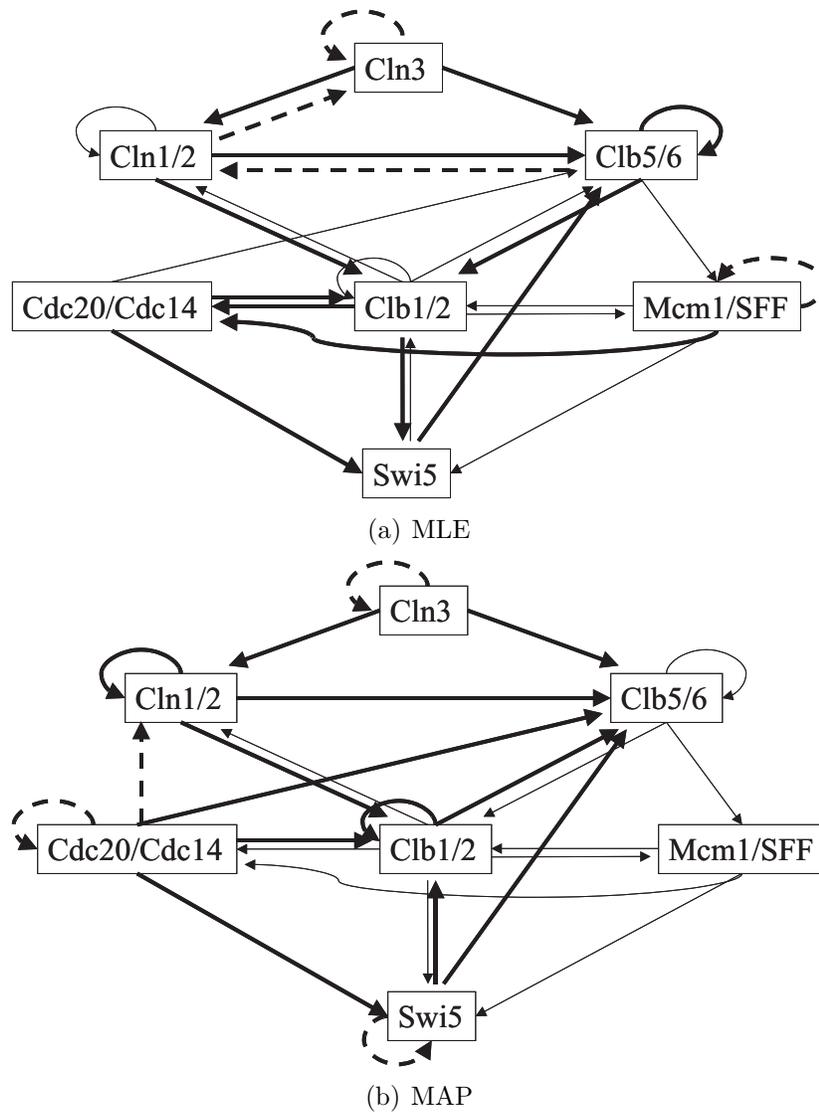
Figure 5.9: The 16 identified regulations with the highest regulation strengths for $\hat{\omega}_{MLE}$ (*top*) and $\hat{\omega}_{MAP}$ (*bottom*). True positives are marked in *bold*, false positives are marked with *bold dashed lines*, false negatives correspond to *thin lines*.

trajectory in the state space of the system covers only a small fraction of the whole state space. In principle, if we do only know the behavior of a system in such a small region of the state space, there might be several distinct networks which can all be used to generate very similar datasets. Thus, for network inference, it is generally better if the data points are distributed over a large range of the state space rather than concentrated in a small region [163]. Such data can for example be knock-out or mutant experiments, or measurements under different external conditions. In addition to this, biological networks are known to be redundant. This means, they contain many alternative mechanisms, such as different proteins which can take the same function, or alternative metabolic pathways. These alternative mechanisms make organisms flexible and robust against perturbations and dysfunctions. We will see in Chapter 7 that it is in fact possible to reproduce experimental gene expression time series using an inferred network whose structure differs from the reference network.

- Third, the Bayesian approach contains many parameters which have to be set manually. These include the noise level $\sigma_\xi$ and the parameters of the prior distributions. The noise term $\sigma_\xi$ corresponds to the noise due to the measurements. In the objective function $F_{MAP}$, the inverse of $\sigma_\xi$ appears as a prefactor in the log likelihood, which weights this term relative to the log prior. The higher this noise is set, the more is the inferred parameter vector $\hat{\omega}_{MAP}$ determined by the prior distribution, and the dataset $\mathcal{D}$ becomes less important.

  Parameters of the prior distributions can be interpreted in a similar way. They also have an indirect influence on the 'importance' of the log likelihood and the log prior in equation (5.40) relative to each other. Two extreme cases are flat prior distributions, which express that we have no prior knowledge about the system at hand, and delta distributions, which reflect that we are sure about model parameters even without having seen the dataset $\mathcal{D}$. In the first case, both estimators $\hat{\omega}_{MLE}$ and $\hat{\omega}_{MAP}$ are equal. In the second case, the posterior distribution equals the prior distribution, and $\hat{\omega}_{MAP}$ does not depend on the dataset $\mathcal{D}$.

  An appropriate choice of all these parameters is a technical issue. In general, of course, the better the prior information which is used for adjusting these values, the more can the result be improved compared to the maximum likelihood estimation. Obviously, it is more difficult to find appropriate parameters of prior distributions for the yeast cell cycle network than for the simulated datasets.

  There is no standard method how to choose prior distributions in a Bayesian approach. Methods to estimate parameters of these distributions from datasets, known as empirical Bayesian methods, have been developed [126]. In addition, a comparison between the prior and the posterior distribution can be helpful to gain experience in this setting: If the prior is 'strong' and differs much from a flat distribution, then prior and posterior distributions are very similar. The estimated parameter vector $\hat{\omega}_{MAP}$ mainly reflects the prior knowledge and does not contain much information

provided by the data. Contrary, if the prior is 'weak' because of lack of reliable prior knowledge, $\hat{\omega}_{MAP}$ is mainly determined by the data $\mathcal{D}$. If $\mathcal{D}$ is sparse, a weak prior distribution cannot prevent overfitting. In this case, we have to find a trade-off between the bias of the result caused by the prior and the expected variance of the result when using different datasets.

Finally, the evidence gives information to which degree the data reflects the prior knowledge. A small evidence indicates that the dataset does not support prior hypotheses, whereas a value around 1 means that prior information and information about the system provided by the dataset $\mathcal{D}$ are very conform. This can also be a useful information in the Bayesian setting.

- Finally, we have made some model assumptions which might be additional error sources. A derivative of the parameterized system of differential equations and the underlying assumptions such as additivity of regulatory influences, chemical equilibrium or first order degradation processes, have already been discussed in Chapter 2. The here suggested embedding of this model into a stochastic framework assumes independence of noise terms for all variables and also for consecutive time points. This neglects internal noise, which propagates over time. Similar to the postulated additive influence of different regulators, this assumption can also be seen as a trade-off between model complexity and tractability. We only consider noise due to the measurement process and assume that the system can still be described by a deterministic differential equation system. Thus, the presented framework does not contradict the assumptions and simplifications made to describe regulatory networks by ordinary differential equations. However, in principle it is possible to extend the model and include internal noise which affects consecutive time points. Such intrinsic noise is sometimes included in single cell models, which require single measurements of different cells to estimate parameters.

All in all, we conclude that a Bayesian approach in combination with a dynamic model provides an appropriate framework to analyze high-throughput data in general. In the future, the approach presented can technically be improved and extended in several ways. Dependence of the optimization on the initial parameter vector, for example, can be overcome by more exhaustive search algorithms such as genetic algorithms or simulated annealing [60]. Next, instead of maximizing the posterior, the whole distribution can be used to get information about the variance of the estimated parameters [103]. This is a major advantage of Bayesian methods compared to many other approaches, which usually lead to point estimates.

Numerical integration of the hierarchical prior distribution over regulation strengths is very time consuming. In future work, one could use a refined distribution with similar shape, which does not require this numerical integration. This would also allow to apply the approach to larger networks.

Last, statistical properties of gene regulatory networks can be included into the prior

distribution. Such networks are, for example, known to be *scale-free* [87]. This means, the degrees of nodes are exponentially distributed. Few genes, called hub genes, encode global regulators, which influence the expression of many other genes, whereas most of the genes have only marginal influences on other genes. Such properties are as well especially interesting for larger networks. Here, the random variables corresponding to regulation strengths are not mutually independent any longer.

# Chapter 6

# Circuits and Core Mechanisms

In Chapters 1 and 2 we have outlined the potential of differential equations to give insights into underlying mechanisms causing certain dynamic behaviors. In contrast to Boolean or Bayesian networks, ODE models for gene regulatory networks are based on underlying chemical binding processes. This allows to interpret results concerning qualitative dynamic behaviors in terms of these molecular processes, and to associate qualitative changes with kinetic rates. In this chapter, we will elucidate some concepts and results of the theory of ordinary differential equations and connect them to gene regulatory networks. In particular, we will focus on mechanisms which cause periodic behavior. We will introduce a *core network* model for the periodic expression of yeast cell cycle genes in Section 6.2, which will be analyzed afterwards.

Before we start introducing this model, Section 6.1 shows the tendency of our general model introduced in Chapter 2 to converge to a stable steady state. Results shown here are deduced from rather general properties of our system. Thus, they apply for a wide range of differential equation models proposed to describe regulatory networks. We will explain why *circuits* in the interaction graphs are a necessary condition for oscillations and multiple steady states.

The intention of this chapter is to show how an analysis of differential equations can facilitate the understanding and interpretation of observed dynamic phenomena. The results are very general and can be transferred to similar models for oscillating biological systems (see for example [72, 81, 167, 169, 194]).

The idea of *core mechanisms* which lead to complex dynamic behavior is not new [72, 81, 169]. A lot of different *core networks* have been proposed to describe various dynamic phenomena in biological systems. For example, the switch-like response of MAP kinase cascades has been explained by a positive auto-regulation [38, 69], and cellular rhythms such as the cell cycle or circadian oscillations have been described by differential equation models ([38] and references therein). Most of these models are two-component systems, which are much easier to analyze with respect to certain properties than systems with three or more variables [135]. The reason is that they are *planar* and have a two-dimensional state space. The existence of a periodic orbit is frequently shown using the

103

Poincaré-Bendixson Theorem [147], which is based on planar systems [203]. Generalizations of results obtained for two-component systems can be difficult. Thus, the behavior of differential equation systems with more than two variables can often only be investigated by means of simulations. This is the reason why most of the core models are reduced to two dimensions. Our core model for the yeast cell cycle also consists of two components, the periodically expressed cyclin-types CLN and CLB. We will further detail the difference between planar systems and higher dimensional systems in Chapter 9.

Of course, a reduction to two components poses a restriction to biological systems, and this is the main criticism of these models from many biologists. Thus, we start with a more comprehensive model of cell cycle regulations and show how it can, at least mathematically, be reduced to two dimensions. We will give reasons why such simplified models can be useful to describe mechanisms related to qualitative dynamic phenomena.

## 6.1 Convergence to a steady state

In this section, we discuss the importance of circuits for multi-stationarity and oscillations. We start with the ODE model derived in Chapter 2,

$$\dot{x}_i = f_i(x) = s_i - \gamma_i x_i + \sum_{j=1}^{n} k_{ij} \underbrace{\frac{x_j^{m_{ij}}}{x_j^{m_{ij}} + \theta_{ij}^{m_{ij}}}}_{r_{ij}(x_j)} \quad x \in U \subseteq \mathbb{R}^n, \quad i = 1, \ldots, n \qquad (6.1)$$

and parameters $s_i \geq 0$, $\gamma_i, m_{ij}, \theta_{ij} > 0$ and $k_{ij} \in \mathbb{R}$. For this chapter, we set the domain $U$ to be the positive orthant, $U = \mathbb{R}_+^n$. In Chapter 2, we graphically represented system (6.1) by an interaction graph $G(V, E)$, whose nodes correspond to variables, and an edge $e_{ij}$ indicates a regulation from variable $j$ to variable $i$. Edges in this graph are labeled according to the signs of the regulation strengths $k_{ij}$ in equation (6.1):

$$c(e_{ij}) = \begin{cases} + & \text{if } k_{ij} > 0 \\ - & \text{if } k_{ij} < 0 \end{cases} \quad \forall e_{ij} \in E \qquad (6.2)$$

Subsequently, we will use the following properties of the system:

1. **Monotonicity of the regulation functions:** A regulator $j$ has either an activating or an inhibiting effect on component $i$, it cannot exert both. Thus, a regulation function $r_{ij}(x_j)$, $i \neq j$ is either monotonically increasing or monotonically decreasing:

$$\text{activation:} \quad k_{ij} > 0 \quad \Rightarrow \quad \tfrac{dr_{ij}(x_j)}{dx_j} > 0 \quad \overset{i \neq j}{\Rightarrow} \quad \frac{\partial f_i(x)}{\partial x_j} > 0 \, \forall x_j \in \mathbb{R}_+ \qquad (6.3)$$

$$\text{inhibition:} \quad k_{ij} < 0 \quad \Rightarrow \quad \tfrac{dr_{ij}(x_j)}{dx_j} > 0 \quad \Rightarrow \quad \frac{\partial f_i(x)}{\partial x_j} < 0 \, \forall x_j \in \mathbb{R}_+ \qquad (6.4)$$

2. **Boundedness of regulation:** All regulation functions are bounded by 0 and the regulation strength $k_{ij}$. We have already seen that this boundedness leads to a trapping region in the state space (Chapter 2).

3. **The domain $U$ is an open convex set:** System (6.1) is defined on the positive orthant $\mathbb{R}^n_+$, which is an open convex set in $\mathbb{R}^n$.

The first property leads to a Jacobian matrix

$$J_f(x) = \left(\frac{\partial f_i(x)}{\partial x_j}\right)_{i,j=1,\ldots,n} =: (a_{ij}(x))_{i,j=1,\ldots,n} \tag{6.5}$$

which has constant signs almost everywhere in $U$. According to (6.3) and (6.4), the signs of the off-diagonal elements ($i \neq j$) are constant for all $x \in U$. The diagonal elements ($i = j$) are negative due to degradation for almost all $x \in U$. The only exception is a positive auto-regulation of a component $i$, which might exceed degradation and lead to a positive diagonal element $a_{ii} > 0$ in some interval $[x_i^{min}, x_i^{max}]$. We will see an example in Section 6.2. For the current section, we concentrate on systems with constant sign Jacobian matrices.

According to the Hartman-Grobman-Theorem (see Chapter 2), the stability of a hyperbolic fixed point $x_s$ of (6.1) is determined by the eigenvalues of the Jacobian matrix $J_f(x_s)$. A hyperbolic steady state is asymptotically stable if the real part of all eigenvalues $\lambda$ of $J_f(x_s)$ is negative, $\Re(\lambda) < 0$. The eigenvalues of a steady state and thus its stability are determined solely by the circuits in the interaction graph [84]. This can be seen by the determinant of $J_f(x_s)$. For this, we introduce the following definitions for an interaction graph $G(V, E)$ with sign-labeled edges. Corresponding definitions for matrices can be found in a more general form in [128].

**Definition 6.1.1** [Circuit] A *circuit* $C$ of an interaction graph $G(V, E)$ is a connected (not necessarily induced) subgraph $G' = (V', E')$ with vertices $V' = \{v_{i_1}, \ldots, v_{i_k}\}$. Each vertex in $G'$ has degree two, and $(v_{i_z}, v_{i_{z+1}}) \in E'$ for $z = 1, \ldots, k-1$ and $(v_{i_k}, v_{i_1}) \in E'$.

We have also frequently used the term *feedback loop* for a circuit in previous chapters.

**Definition 6.1.2** [Semicircuit] A *semicircuit* of an interaction graph $G(V, E)$ is a circuit in the corresponding undirected graph, that is, a subgraph $G' = (V', E')$ with vertices $V' = \{v_{i_1}, \ldots, v_{i_k}\}$, such that each vertex has degree two and $v_{i_z}$ is adjacent to $v_{i_{z+1}}$ for $z = 1, \ldots, k-1$ and $v_{i_k}$ is adjacent to $v_{i_1}$.

**Definition 6.1.3** [Full circuit] A *full circuit* of an interaction graph $G(V, E)$ is a set $S_C$ of circuits in $G(V, E)$, such that each node $v \in V$ belongs to exactly one of the circuits in $S_C$.

**Definition 6.1.4** [Sign of a circuit] The *sign $\sigma_C$ of a circuit $C$* is defined as the sign of the product of edge labels in the circuit:

$$\sigma_C := \prod_{e_{ij} \in C} c(e_{ij}) \tag{6.6}$$

According to this definition, a circuit is negative, if the number of negatively labeled edges is odd.

Finally, we need

**Definition 6.1.5** [Weight of an edge, weight of a circuit] The *weight $w_{e_{ij}}(x)$ of an edge $e_{ij}$* in an interaction graph $G(V, E)$ at a state $x \in U$ is defined as

$$w_{e_{ij}}(x) := a_{ij}(x). \tag{6.7}$$

The *weight $w_C(x)$ of a circuit $C$* at a state $x \in U$ is given by the product of weights $w_{e_{ij}}(x)$ of the edges in the circuit:

$$w_C(x) := \prod_{e_{ij} \in C} w_{e_{ij}}(x) \tag{6.8}$$

Signs and weights of semicircuits are defined analogously. Note that the sign of the weight of a circuit equals the sign of the circuit and is constant for systems with constant sign Jacobian matrices. Thus, we can talk about *positive* and *negative* circuits in the interaction graph, independent of the state $x$.

The determinant of the Jacobian matrix $J_f(x)$ at a state $x$ is determined by the weights of the full circuits of the corresponding interaction graph, as illustrated in Figure 6.1 for three variables:

$$
\begin{aligned}
det\left(J_f(x)\right) \;=\; & \sum_{\mathcal{P} \in S_n} \left( sgn(\mathcal{P}) \prod_{i=1}^{n} a_{i,\mathcal{P}(i)}(x) \right) \\
\;=\; & a_{11}(x)a_{22}(x)a_{33}(x) + a_{21}(x)a_{32}(x)a_{13}(x) + a_{31}(x)a_{23}(x)a_{12}(x) \\
& -a_{31}(x)a_{13}(x)a_{22}(x) - a_{21}(x)a_{12}(x)a_{33}(x) - a_{11}(x)a_{32}(x)a_{23}(x)
\end{aligned}
\tag{6.9}
$$

The equality in equation (6.9) is the *Leibniz formula* for the determinant of squared matrices. $\mathcal{P}$ denotes an element in the set $S_n$ of permutations of the numbers $1, \ldots, n$ .

Two important statements about dynamical systems $\dot{x} = f(x)$ with constant sign Jacobian matrices $J_f(x)$ and a convex open domain $U \subseteq \mathbb{R}^n$ have been made by Thomas [190]. We will explain both in the following. Compact proofs of these statements were also given independently by Gouzé [84] and Snoussi [182].

**Proposition 6.1.6 (Positive circuits [190])** *If the interaction graph contains only circuits with non-positive weights, and there is at least one full circuit with weight $\neq 0$, then the system cannot have multiple steady states.*

The proposition states that the existence of a circuit $C$ with strictly positive sign, $\sigma_C > 0$, in the interaction graph is a necessary condition for the existence of multiple steady states.

**Proof [84].** We show that, if all circuits in the interaction graph are non-positive and there is at least one negative full circuit, the vector field $f(x)$ is injective. This implies proposition 6.1.6, since the equation $f(x) = 0$ has at most one solution in this case.
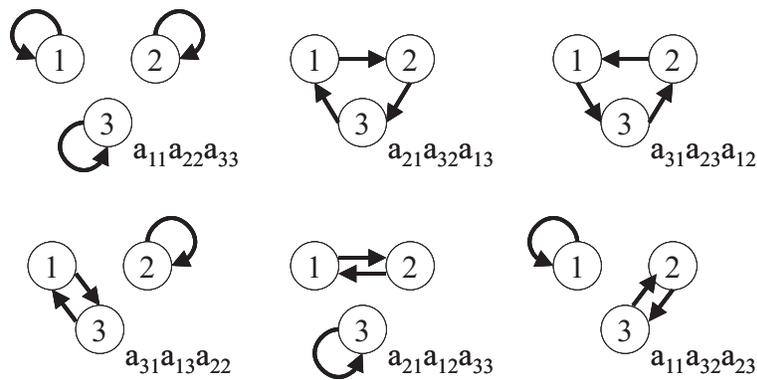
Figure 6.1: All possible full circuits and the corresponding weights of an interaction graph with three components. The characteristic polynomial of the Jacobian matrix $J_f(x)$ is given in terms of these weights.

First, we claim that if the interaction graph contains only non-positive circuits, then all terms in equation (6.9) have, independent of the number of variables, the same sign. If, moreover, the graph has at least one full circuit with weight $\neq 0$, then $det\,(J_f(x)) \neq 0$, and $J_f(x)$ is not singular in this case. In our model, such a full circuit is guaranteed by the degradation terms $-\gamma_i x_i$, which correspond to the first circuit in Figure 6.1.

Assume that there exist $x, y \in U$, $x \neq y$ and $f(x) = f(y)$. It can easily be seen by integrating along the segment $s_{xy}$ connecting $x$ and $y$, which can be parameterized by $s_{xy} = (1 - \alpha)x + \alpha y$, $\alpha \in [0, 1]$, that this leads to a contradiction:

$$0 = f(y) - f(x) = \int_0^1 J_f((1 - \alpha)x + \alpha y)(y - x)d\alpha =: A(x, y)(y - x) \qquad (6.10)$$

Equation (6.10) implies that the matrix $A(x, y)$ is singular. But the entries of the matrix $A(x, y)$ have the same signs as corresponding entries of $J_f(x)$, since the signs of the entries of $J_f(x)$ are constant along $s_{xy}$, which means that both matrices represent the same interaction graph. As the interaction graph of $f(x)$ was assumed to have at least one full circuit with weight $\neq 0$ and no positive circuits, all terms in $det(J_f(x))$ and in $det(A(x, y))$ have the same signs. Thus, $det(A(x, y)) \neq 0$ and hence $A(x, y)$ is not singular, which is a contradiction. $\square$

Here, the convexity of the domain $U$ is needed to guaranty that the path between the two states $x$ and $y$ lies entirely in $U$.

**Proposition 6.1.7 (Negative semicircuits [190])** *The existence of a semicircuit of length at least two with strictly negative weight is a necessary condition for the existence of a stable periodic orbit.*

This proposition can be proven by showing that each interaction graph with non-negative semicircuits is similar to a *cooperative system* [179]. A cooperative system is a system

which has a Jacobian matrix whose off-diagonal elements are non-negative, or, in other words, an interaction graph whose edges between different nodes are positively labeled. Many properties of such systems have been shown (see for example [96, 179, 180]). The most important property is that cooperative systems have a monotonous flow with respect to the partial ordering in $\mathbb{R}^n$ [96, 179]. This property can be generalized for systems with non-positive semicircuits [179]: These systems have a monotonous flow with respect to the partial ordering induced by some orthant $K$ of the coordinate system. We will illustrate this in the following. Any orthant $K$ of $\mathbb{R}^n$ can be written as

$$K = \{x \in \mathbb{R}^n : (-1)^{m_i} x_i \geq 0, i = 1, \ldots, n\}, \quad m_i \in \{0, 1\}, \tag{6.11}$$

and corresponds to a cone in $\mathbb{R}^n$, which, as such, generates a *partial ordering* $\leq_K$ in the usual fashion [179],

$$x \leq_K y \quad \Leftrightarrow \quad y - x \in K. \tag{6.12}$$

**Definition 6.1.8** [Order preserving flow [179]] A flow $\Phi_t(x)$ *preserves the partial ordering* $\leq_K$ in $\mathbb{R}^n$ if the following implication holds:

$$x, y \in E \text{ and } x \leq_K y \quad \Rightarrow \quad \Phi_t(x) \leq_K \Phi_t(y) \quad \forall t \geq 0. \tag{6.13}$$

Systems with an order preserving flow do not have stable periodic orbits [179].

**Example 6.1.9** [Order preserving flow] As an example, we consider the interaction graph $G(V, E)$ shown in Figure 6.2 (*left*), whose semicircuits of length $\geq 2$ are non-negative. The system might also include positive or negative auto-regulations, which are irrelevant here, and are thus not shown in Figure 6.2. A flow of a corresponding differential equation system preserves a partial ordering with respect to the following cone:

$$K = \{x \in \mathbb{R}^8 : (-1)^{m_i} x_i \geq 0, i = 1, \ldots, 8\}, \quad m = (1, 0, 1, 1, 0, 0, 1, 0) \tag{6.14}$$

We consider the corresponding undirected interaction graph (Figure 6.2 *right*). The set of nodes $V$ can be partitioned into two groups, such that edges between two different nodes in the same group are positively labeled in this undirected graph, and edges between the two groups are negatively labeled [84, 128]. The signs of auto-regulations can either be positive or negative. In the graph on the right hand side in Figure 6.2, the partition is indicated by white and grey nodes. Furthermore, we re-index the variables, such that the $k$ variables in the first group become variables $x_1, \ldots, x_k$, and the remaining $n - k$ variables in the second group become variables $x_{k+1}, \ldots, x_n$. The corresponding *signed-adjacency matrix $M$*, which we define for the undirected graph as

$$(m_{ij})_{i,j=1,\ldots,n} := \begin{cases} + & \text{positively labeled edge between } i \text{ and } j \\ - & \text{negatively labeled edge between } i \text{ and } j \\ 0 & \text{no edge between } i \text{ and } j \end{cases}, \tag{6.15}$$
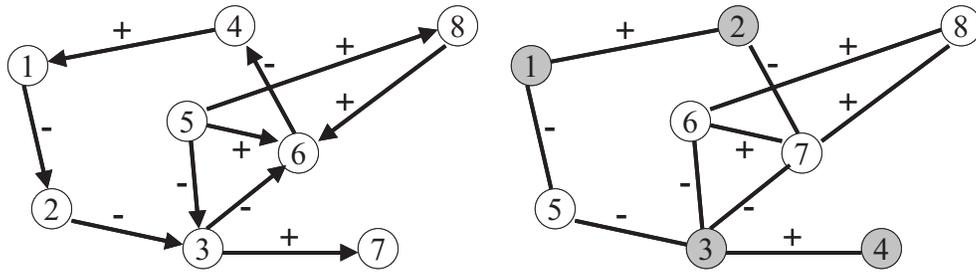
Figure 6.2: **Left:** An interaction graph $G(V, E)$ with non-negative circuits. The set $V$ of nodes can be partitioned into two groups, such that edges between two nodes in the same group are positively labeled, and edges between these two groups are negatively labeled. **Right:** Corresponding undirected graph with re-indexed nodes and a partition indicated by white and grey nodes.

has the following sign pattern:

$$M = \left( \begin{array}{cccc|cccc} ? & + & 0 & 0 & - & 0 & 0 & 0 \\ + & ? & 0 & 0 & 0 & 0 & - & 0 \\ 0 & 0 & ? & + & - & - & - & 0 \\ 0 & 0 & + & ? & 0 & 0 & 0 & 0 \\ \hline - & 0 & - & 0 & ? & 0 & 0 & 0 \\ 0 & 0 & - & 0 & 0 & ? & + & + \\ 0 & - & - & 0 & 0 & + & ? & + \\ 0 & 0 & 0 & 0 & 0 & + & + & ? \end{array} \right) =: \left( \begin{array}{c|c} A & -B \\ \hline -C & D \end{array} \right) \tag{6.16}$$

The matrices $B$ and $C$ are non-negative, and the matrices $A$ and $D$ correspond to cooperative systems. Going back to a directed graph, which is related to our model (6.1), $M$ defines the signs in the corresponding Jacobian matrix $J_f(x)$ for the directed interaction graph which has two edges $e_{i \to j}$ and $e_{j \to i}$ iff $e_{ij}$ is present in the undirected graph. Note that deleting one of the two edges in each pair $\{e_{i \to j}, e_{j \to i}\}$ does not change the properties of the system needed here to transform it into a cooperative system.

Changing signs of the variables in the second group (white nodes) transforms our system into a cooperative system:

$$\left( \begin{array}{c|c} I & 0 \\ \hline 0 & -I \end{array} \right) \left( \begin{array}{c|c} A & -B \\ \hline -C & D \end{array} \right) \left( \begin{array}{c|c} I & 0 \\ \hline 0 & -I \end{array} \right) = \left( \begin{array}{c|c} A & B \\ \hline C & D \end{array} \right) \tag{6.17}$$

If additionally all trajectories of such systems are bounded, as it is the case for our system (6.1), then almost every trajectory converges towards an equilibrium [84, 96]. 'Almost' means that all remaining trajectories have Lebesgue measure 0 [96]. Thus, from a practical point of view, every trajectory goes to an equilibrium[1].

---

[1]Interestingly, similar to the statements here, some relations between eigenvalues of the adjacency matrix of a graph and its structure have been stated in [199].

Propositions 6.1.6 and 6.1.7 emphasize the importance of circuits in regulatory systems. They are built on very general properties of the system of differential equations, and thus hold for many different models, also, for example, for non-additive regulation functions. Here, edge labels are defined as the signs of the corresponding entries in the Jacobian matrix. Thus, positive circuits generally account for multi-stationarity, and negative circuits are needed to show sustained oscillations.

In models for biological systems, multi-stationarity has been used to describe the processes of cell differentiation and switch-like behavior. Typically, a system with multiple steady states originating from a positive circuit can exhibit hysteresis. An example was given in the model for the regulation of the *E. coli bgl* operon in Chapter 4. Here, for a certain range of promoter activities, two stable steady states exist for the transcription rate $R_2$, and the behavior of the system at a previous time determines to which of these two states the system converges. Thus, the long-term behavior of the system depends on its history. This phenomenon is also named *memory* of the system [38]. In case of gene regulatory networks, temporary external influences can sometimes lead to permanent changes in expression patterns, which are inherited to the next generations. One refers to this mechanism as *epigenetic effect* [38]. Negative circuits are not only related to periodic behavior. They have also been shown to stabilize a steady state with respect to external influences. This phenomenon is known as *homeostasis* [38], and it is a fundamental characteristic of living organisms.

## 6.1.1   Analyzing circuits

After we pointed out how circuits can determine the qualitative behavior of a system, we justify the reduction of a system to a two-component circuit. For this, we consider once again systems with constant sign Jacobian matrices and a bounded trapping region in the state space. Moreover, we assume that external influences are not time-dependent, such that the system can be described by a system of autonomous first order differential equations. We will explain in which cases circuits can separately be analyzed, which can drastically reduce the dimension of the system under consideration. We will not give formal proofs, as this would go beyond the scope of this thesis, but only illustrate arguments. In the following, we partition the set of nodes $V$ of the interaction graph into a group $V^C$ of nodes belonging to a circuit, denoted by *circuit nodes*, and the group $V^{NC}$ of remaining nodes not belonging to a circuit, called *non-circuit nodes*. More specifically, we consider the following groups of non-circuit nodes:

1. **Group 1:** Non-circuit nodes that do not (directly or indirectly) influence circuit nodes. This means, there is no directed path from these nodes to any circuit node in the interaction graph. An example is illustrated in Figure 6.3. We consider a network of three nodes and an interaction graph shown in Figure 6.3 (*left*). Here, $V^C = \{x_1, x_2\}$ and $V^{NC} = \{x_3\}$. A trajectory of this system lies on a two-dimensional
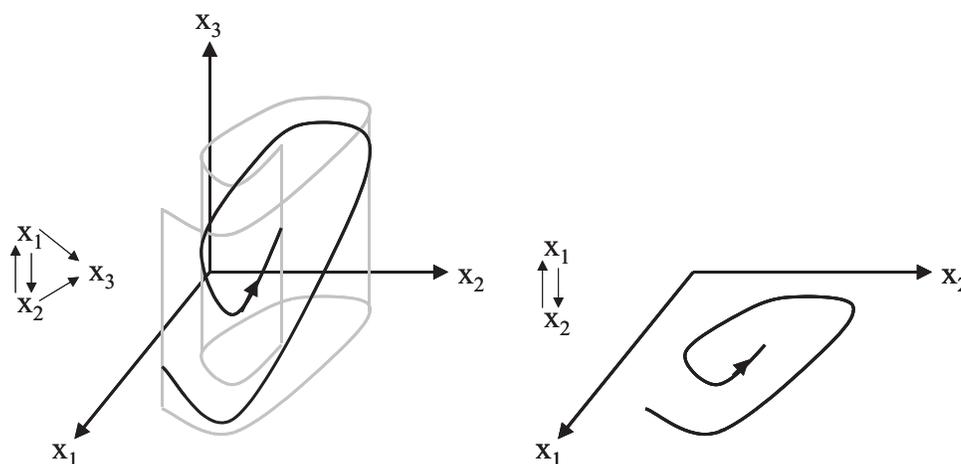
Figure 6.3: An example for a system with variable $x_3$ belonging to group 1 of non-circuit nodes. A trajectory of a corresponding differential equation system lies in a two-dimensional manifold perpendicular to the $x_1, x_2$-plane. The qualitative dynamic behavior of the system is solely determined by $V^C = \{x_1, x_2\}$.

manifold in the state space. Variable $x_3$ has no influence on the circuit variables $x_1$ and $x_2$, and hence the projection of the trajectory onto the $x_1, x_2$-plane does not dependent on $x_3$. Here, the subsystem with variables $x_1$ and $x_2$ can separately be analyzed.

2. **Group 2:** Non-circuit nodes that are not (directly or indirectly) influenced by circuits, but have themselves an influence on circuits. This means there are no directed paths from circuit nodes to these nodes, but there are in turn paths from these nodes to circuit nodes in the interaction graph. These nodes eventually converge to constant values in the trapping region. If their temporal behavior $x(t)$ is known, their influence can equivalently be described as an external influence when analyzing the dynamic behavior of the circuits. An example is shown in Figure 6.4. A non-circuit variable $x_3$ influences the circuit variables $x_1$ and $x_2$. Variable $x_3$ will converge to a constant value, and the trajectory of the system eventually lies on a two-dimensional manifold parallel to the $x_1, x_2$-plane. If the course $x_3(t)$ is known, it can be used to model the influence of $x_3$ on $x_1$ and $x_2$ as a time-dependent, but eventually constant, external signal, and the circuit containing $x_1$ and $x_2$ can be analyzed as a two-dimensional system.

3. **Group 3:** Nodes that lie on a path connecting two or more circuits. These nodes function as 'signal transmitters' between different circuits. However, also here it is sometimes possible to analyze the dynamic behavior of the circuits separately [169, 191]. An example is illustrated in Figure 6.5. Variable $x$ lies on a path connecting two circuits $C_1$ and $C_2$. $C_1$ is independent of the rest of the graph and can be analyzed separately. Knowing the behavior of $x$, we can also analyze circuit $C_2$ separately by
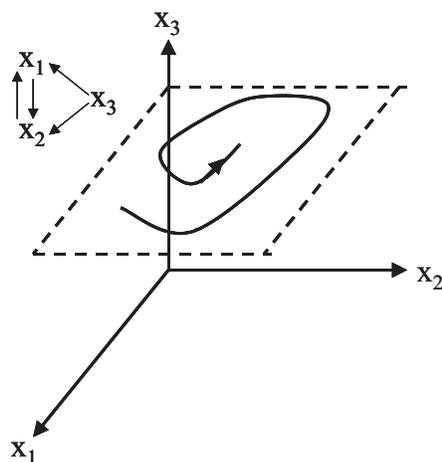
Figure 6.4: Non-circuit variable $x_3$ that belongs to group 2. It regulates the circuit variables $x_1$ and $x_2$ and eventually converges to a constant value. Thus, its influence on $x_1$ and $x_2$ can be described as an eventually constant external influence.
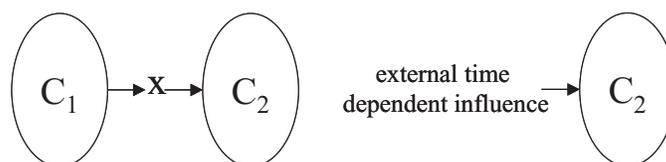


Figure 6.5: Variable $x$ lies on a path connecting two circuits $C_1$ and $C_2$. It belongs to group 3 of non-circuit nodes. Circuit $C_1$ does not depend on $x$ and can be analyzed separately (compare Figure 6.4). Also circuit $C_2$ can separately be analyzed provided that $x(t)$ can be determined in advance. In this case, the influence of $x$ can be described as an external influence acting on nodes belonging to circuit $C_2$.

> describing the influence of $x$ as an external influence. Unlike the external influence representing nodes belonging to group 2, this external influence does not necessarily converge to a constant value here, since it is influenced by other circuits.

Note that the differential equation systems which describe the circuits containing $x_1$ and $x_2$ in Figure 6.4 and the circuit $C_2$ in Figure 6.5 are potentially non-autonomous. Variables $x_3$ and $x$, which are modeled as external influences acting on the systems, may vary with time.

The examples discussed to analyze parts of a regulatory network separately can simplify the analysis, in particular, for systems that have disjoint circuits of at most two variables. Provided that the course of a node influencing a circuit can be determined in advance, the circuit can individually be analyzed as a planar system. However, it is only possible to determine the course of such nodes in advance, if the interaction graph contains no semicircuits. This is illustrated in Figure 6.6. Here, the two circuits $C_1$ and $C_2$ are interconnected by a semicircuit containing the variables $x_1$, $x_2$, $x_3$ and $x_4$. For an individual
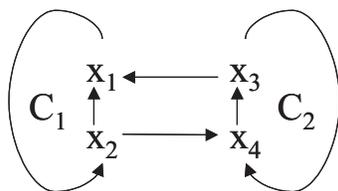
Figure 6.6: Two circuits $C_1$ and $C_2$ which are interconnected through a semicircuit with variables $x_1$, $x_2$, $x_3$ and $x_4$. These circuits cannot separately be analyzed.

analysis of circuit $C_1$, the course of $x_3$ has to be known, which is determined by circuit $C_2$. To analyze $C_2$ in turn, the behavior of variable $x_2$ is needed. Here, the two circuits cannot be analyzed separately. The situation is also more complex in case that circuits contain more than two components, or if several circuits are interlocked, that is, they have common nodes. In the first case, nodes in the circuit are frequently shrunken, such that the new circuit again contains at most two variables, and statements for planar systems can be used (see for example [32]). If the system comprises reactions at different time scales, such a reduction of variables can be achieved by a quasi-steady state approximation [68, 203]. If this is not the case, time delays are sometimes used to describe indirect regulations as time-delayed direct ones [194]. Time delays can be a major source of instabilities in negative circuits and have been shown to efficiently cause oscillations in biological systems [54, 167, 196]. An example for interlocked circuits has already been given in Chapter 4 of this thesis. Here, two positive feedback loops (circuits) with a common node mutually enhance each other. We will use several of these dimension reduction methods in the following section, where we will derive a core model for the yeast cell cycle.

## 6.2 An oscillating core model for the yeast cell cycle

Chemical reaction systems can be expected to have one or more steady states [194]. Biochemical oscillations that are built on such reaction kinetics usually arise when a trapping region in the state space contains one single steady state that is unstable [194]. An asymptotically stable limit cycle encloses this unstable steady state. According to the Hartman-Grobman Theorem introduced in Chapter 2, the stability of a steady state $x_s$ is determined by the eigenvalues of the Jacobian matrix $J_f(x_s)$. For a system with two variables,

$$J_f(x_s) = \begin{pmatrix} a_{11}(x_s) & a_{12}(x_s) \\ a_{21}(x_s) & a_{22}(x_s) \end{pmatrix}, \tag{6.18}$$

the eigenvalues $\lambda_{1,2}$ can be expressed in terms of the determinant $det(J_f(x_s))$ and the trace $tr(J_f(x_s))$,

$$\lambda_{1,2}(x_s) = \frac{tr\left(J_f(x_s)\right)}{2} \pm \sqrt{\left(\frac{tr\left(J_f(x_s)\right)}{2}\right)^2 - det\left(J_f(x_s)\right)}. \tag{6.19}$$

The steady state is unstable if at least one eigenvalue has a positive real part. In chemical reaction systems the elements on the diagonal are usually negative, reflecting degradation

or, in case of enzymatic reactions, transformations from one species to anything else [194]. For two-component systems, we have two characteristic sign patterns for Jacobian matrices $J_f(x_s)$ which can lead to unstable fixed points and thus cause oscillations [194]. These are

$$J_1(x_s) = \begin{bmatrix} + & + \\ - & - \end{bmatrix} \quad \text{and} \quad J_2(x_s) = \begin{bmatrix} + & - \\ + & - \end{bmatrix}. \tag{6.20}$$

Oscillators with the first pattern are called *substrate-depletion oscillators*, the second pattern characterizes an *activator-inhibitor oscillator*. In both oscillators the two components are involved in a negative circuit, and the first component exhibits a positive autoregulation. In this section, we derive an activator-inhibitor core model for the cell cycle of the budding yeast *S. cerevisiae*. Similar to the core model for the SOS response in *M. tuberculosis* in Chapter 3 and the model for the regulation of the *E. coli bgl* operon in Chapter 4, the circuits related to the dynamic behavior of the system comprise regulations on transcriptional and post-transcriptional level. Thus, the regulatory network includes mechanisms on different time scales. These differences can in fact stabilize periodic behavior, as we will demonstrate in Chapter 8 for the core network of the yeast cell cycle.

## 6.2.1   Model

**Regulation mechanisms in the *S. cerevisiae* cell cycle**

We start by considering the main regulations in the cell cycle of eukaryotic organisms, which are described for example in [2]. The cell cycle consists of four phases: During the *S-phase*, the DNA is duplicated, and in the *M-phase* the cell divides into two daughter cells. Between these phases, the cell persists in the genetically resting phases *G1* and *G2*. In the phase G1, cells increase in size and produce mRNAs and proteins. The G1 checkpoint, a cell cycle control mechanism, is activated during G1 to ensure that the cell can enter the S-phase. During G2, the cell continues to grow and produces new proteins. At the end of this phase, initiation of cell division is regulated by a second control mechanism, the G2 checkpoint. Thus, the two checkpoints coordinate cell growth with the DNA cycle. The cell cycle mechanisms are organized in a complicated regulatory network of *cyclin dependent kinases* (CDKs) and their cyclin partners. Binding of a cyclin to a CDK activates the kinase and leads to the phosphorylation of proteins that participate in different phases of the cell cycle. CDKs are permanently present in excess, whereas their cyclin partners are periodically accumulated and degraded during the cell cycle [194].

There is only one class of CDKs in budding yeast, denoted Cdc28. Cdc28 initiates entry into the S- or M-phase, depending on the class of cyclins bound to it. Nasmyth [139] has shown that the cell cycle in budding yeast is intimately connected to dynamic interactions between the class of G1-specific cyclins (CLN) and the class of mitotic cyclins (CLB). Thus, we build our model on interactions between these two classes. Regulation mechanisms are illustrated in Figure 6.7 and described in the following. A detailed description of regulation processes during the cell cycle in budding yeast can be found in [6, 30]. Expression of
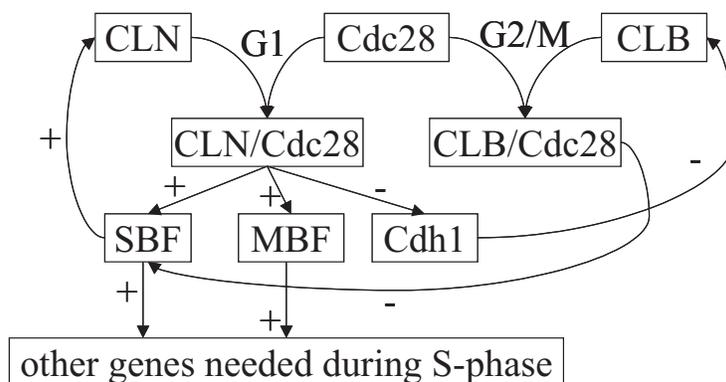
Figure 6.7: A scheme of the regulatory mechanisms during the cell cycle in budding yeast: During the phase G1, the active CLN/Cdc28 complex activates the transcription factor complexes SBF and MBF and inhibits Cdh1. In the G2/M phase, the CLB/Cdc28 complex inhibits SBF. This results in a decreased expression of S-phase genes.

the G1-specific cyclins Cln1, Cln2 and Cln3 (CLNs) peaks during the G1-phase, and the CLN/Cdc28 complex provides activation of the G1-specific transcription factor complexes MBF, a dimer consisting of the proteins Mbp1 and Swi6, and SBF, a complex of the proteins Swi4 and Swi6. MBF and SBF in turn regulate genes which act during the S-phase. As SBF also promotes transcription of the cyclins Cln1 and Cln2, CLN regulates itself auto-catalytically. Furthermore, CLN/Cdc28 inhibits the proteolytic enzyme Cdh1, which accelerates degradation of the mitotic cyclins Clb1 and Clb2 (CLB) by activating the anaphase promoting complex (APC). The mitotic cyclins Clb1 and Clb2 (CLB) are specifically expressed during the transition from the G2 to the M-phase, and form active heteromers with Cdc28. SBF is down-regulated by the CLB/Cdc28 complex.

We simplify these regulatory processes in the following way:

- We neglect the transcription factor complex MBF and the genes needed during the S-phase, which have no influence on the two cyclin classes CLN and CLB. All these components do not affect the dynamic behavior of the system, since they have no influence on any circuit in the regulatory network in Figure 6.7. According to our model, they belong to group 1 of the non-circuit nodes.

- The cyclin dependent kinase subunit Cdc28 is always present in excess, and its concentration can be assumed to be constant [6]. Processes are solely controlled by the concentration of CLN and CLB, which activate Cdc28. Thus, we also neglect Cdc28 and assume that the concentration of active cyclin/Cdc28 complexes is uniquely determined by the concentrations of the two cyclin classes CLN and CLB.

- The interaction graph on the left hand side in Figure 6.8 shows the remaining regulations. It consists of four components CLN ($x_1$), CLB ($x_2$), SBF ($x_3$) and Cdh1 ($x_4$), which are involved in two circuits: The negative feedback loop including all four
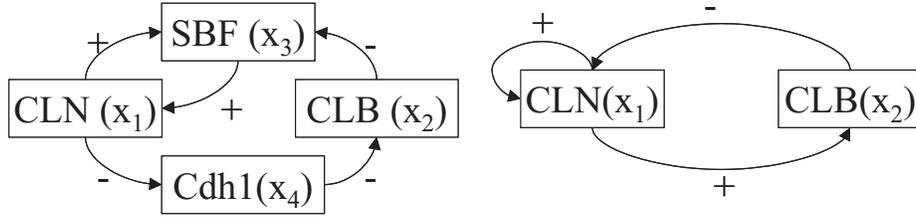
Figure 6.8: Simplified scheme of regulation mechanisms of the budding yeast cell cycle. The cyclin class CLN activates itself auto-catalytically by activating its own transcription factor SBF, and it is indirectly inhibited by CLB due to the negative regulation of CLB on SBF. CLB is indirectly activated by CLN, since CLN/Cdc28 inhibits Cdh1, which in turn promotes degradation of CLB. **Left:** Simplified network of four components. **Right:** Two-component core model.

components ($x_1 \xrightarrow{-} x_4 \xrightarrow{-} x_2 \xrightarrow{-} x_3 \xrightarrow{+} x_1$) and the positive feedback loop including $x_1$ and $x_3$ ($x_1 \xrightarrow{+} x_3 \xrightarrow{+} x_1$). In the following, we will use the quasi-steady state approximation to simplify this network to a two-component network with interaction graph as shown in Figure 6.8 (*right*). Here, the two negative regulations from $x_1$ to $x_4$ and from $x_4$ to $x_2$ have been summarized to a single positive regulation from $x_1$ to $x_2$, and the positive regulation from $x_2$ to $x_3$ and the negative regulation from $x_3$ to $x_1$ appear as a single negative regulation from $x_2$ to $x_1$. Moreover, the two positive regulations between $x_1$ and $x_3$ are modeled as a positive auto-regulation of $x_1$.

We use the following equations to describe the dynamic behavior of the four component system shown in Figure 6.8 (*left*):

$$\dot{x}_1(t) \;=\; s_1 - \gamma_1 x_1(t) + r_{1,3}(x_3) \tag{6.21}$$

$$\dot{x}_2(t) \;=\; s_2 - \tilde{\gamma}_2(x_4)x_2 \tag{6.22}$$

$$x_3(t) \;=\; r_{3,12}(x_1, x_2) \tag{6.23}$$

$$x_4(t) \;=\; r_{4,1}(x_1) \tag{6.24}$$

Here, the temporal change of variable $x_1$ is described by a basal synthesis rate, a first order degradation term and a regulation function $r_{1,3}(x_3)$, which refers to transcriptional regulation through $x_3$. Component $x_2$ is produced with a basal rate $s_2$. Also here, degradation is modeled as a first order process proportional to $x_2$. Degradation control through $x_4$ is expressed by a degradation rate $\tilde{\gamma}_2(x_4)$ which depends on $x_4$. Variables $x_3$ and $x_4$ describe activities of SBF and Cdh1, respectively. According to the interactions we include in our model, both components are solely regulated through chemical modification. These alter the activity, but have no direct influence on the amount of SBF and Cdh1 in the cell. Thus, the total concentration of both components is assumed to be constant, which is also verified in [6]. Equations (6.23) and (6.24) suggest that both variables are uniquely determined by $x_1$ and $x_2$, which is described by the regulation functions $r_{3,12}(x_1, x_2)$ and

$r_{4,1}(x_1)$. We will verify these regulation functions later. This assumption includes a quasi-steady state approximation. Chemical modification of both components by $x_1$ and $x_2$ is fast compared to the time scale of the system, which is determined by the transcriptional regulation of $x_1$ and the degradation control of $x_2$. Thus, these modifications are described as a chemical reaction in equilibrium. We have already introduced a QSSA in Chapter 2 for gene regulatory networks. Here, we assumed binding of a transcription factor to its specific DNA binding site to be fast compared to the process of gene expression. Analogously to the reaction kinetics which we used to model gene regulatory networks, we describe the probabilities of a single transcription factor complex SBF ($x_3$) to undergo a reaction with the cyclins CLN ($x_1$) or CLB ($x_2$), respectively, by sigmoidal functions. Binding of $x_1$ to $x_3$ leads to an activation of SBF through phosphorylation. This activation can be abolished by binding of $x_2$. Thus, the probability of a transcription factor complex to be active, denoted $P_3^a(x_1, x_2)$, can be written as

$$P_3^a(x_1, x_2) = P_3(x_1 \text{ has bound}) - P_3(x_1 \text{ and } x_2 \text{ have bound}). \quad (6.25)$$

Assuming that binding of $x_1$ and binding of $x_2$ to SBF are independent processes, which is the case if they have non-overlapping binding sites, the second term in equation (6.25) is the product of the two probabilities $P_3(x_1 \text{ has bound})$ and $P_3(x_2 \text{ has bound})$, and $P_3^a(x_1, x_2)$ is given by

$$
\begin{aligned}
P_3^a(x_1, x_2) &= P_3(x_1 \text{ has bound})\,[1 - P_3(x_2 \text{ has bound})] & (6.26) \\
&= \frac{x_1^{m_{31}}}{x_1^{m_{31}} + \theta_{31}^{m_{31}}} \left( 1 - \frac{x_2^{m_{32}}}{x_2^{m_{32}} + \theta_{32}^{m_{32}}} \right) & (6.27) \\
&\propto \frac{x_1^{m_{31}}}{x_1^{m_{31}} + \theta_{31}^{m_{31}}} \cdot \frac{1}{x_2^{m_{32}} + \theta_{32}^{m_{32}}}. & (6.28)
\end{aligned}
$$

As already done in Chapter 2, we assume $P_3^a(x_1, x_2)$ to be a measure for the effect of $x_3$ on $x_1$, $r_{1,3}(x_3) := k_{13} P_3^a(x_1, x_2)$. The QSSA states that $x_3$ can be expressed in terms of $x_1$ and $x_2$, and thus variable $x_3$ is eliminated in our model.

The QSSA is also used to eliminate variable $x_4$. Cdh1 is involved in the degradation of $x_2$. Its activity is inhibited by $x_1$. However, it only binds the APC, which is responsible for $x_2$-degradation, during G1. For the rest of the cell cycle, Cdh1 is inhibited through phosphorylation by the kinase Cdc28. The probability $P_4^a(x_1)$ for a single enzyme Cdh1 ($x_4$) to be active is modeled by

$$
\begin{aligned}
P_4^a(x_1) &= 1 - P_4(x_1 \text{ has bound}) \\
&= 1 - \frac{x_1^{m_{41}}}{x_1^{m_{41}} + \theta_{41}^{m_{41}}} & (6.29) \\
&\propto \frac{1}{x_1^{m_{41}} + \theta_{41}^{m_{41}}},
\end{aligned}
$$

which is taken as a measure for the amount of active Cdh1 and for the effect on the degradation of $x_2$, $\tilde{\gamma}_2 := \gamma_2 P_4^a(x_1)$. The QSSA effectively summarizes the two negative

regulations in the four-component interaction graph in Figure 6.7 to one single positive regulation from $x_1$ onto $x_2$.

**Final core model**

To introduce our final two-component core model, we set the Hill-coefficients to $m_{31} = m_{41} = 2$ and $m_{32} = 1$, suggesting that CLN binds as a dimer and CLB as a monomer. These Hill-coefficients are copied from a similar model in [194]. Our final core model, which contains the two cyclins CLN (variable $x_1$) and CLB (variable $x_2$), is written as

$$\dot{x}_1 = s_1 + k_{11} \frac{x_1^2}{x_1^2 + \theta_{11}^2} \frac{1}{\theta_{12} + x_2} - \gamma_1 x_1$$

$$\dot{x}_2 = s_2 - \gamma_2 \frac{1}{\theta_{21}^2 + x_1^2} x_2. \tag{6.30}$$

Here, we have changed the indices of the regulation strength $k_{31}$ to $k_{11}$ and of the threshold values $\theta_{41}$ and $\theta_{32}$ to $\theta_{21}$ and $\theta_{12}$, respectively, to adapt the originally four-component model to the two-component model. The corresponding interaction graph is shown on the right hand side in Figure 6.8. The positive auto-regulation of component $x_1$ due to the positive feedback loop between CLN and SBF is inhibited by $x_2$. Degradation of $x_2$, which is promoted by the enzyme Cdh1, is prevented by $x_1$ by phosphorylation and thereby activation of the enzyme.

## 6.2.2   Properties of the core model

In this subsection, we analyze the dynamic behavior of the core model (6.30). We use the Poincaré-Bendixson Theorem to demonstrate that the model can show periodic behavior for certain parameter vectors

$$\omega := (s_1, s_2, \gamma_1, \gamma_2, k_{11}, \theta_{11}, \theta_{12}, \theta_{21}) \in \mathbb{R}_+^8. \tag{6.31}$$

For the following theorem, we remember that a trajectory $\Gamma(x_0)$ is uniquely defined by an initial state $x_0 \in E$, and the forward trajectory $\Gamma^+(x_0)$ corresponds to the set of states of the system for given $x_0$ and positive time $t \in \mathbb{R}_+$ (Chapter 2).

**Theorem 6.2.1 (Poincaré-Bendixson Theorem [147])** *Suppose that $f \in C^1(E)$ where $E$ is an open subset of $\mathbb{R}^2$ and that the system $\dot{x} = f(x)$ has a trajectory $\Gamma(x_0)$, $x_0 \in E$, with $\Gamma^+(x_0)$ contained in a compact subset $F$ of $E$. Then if $\omega(\Gamma(x_0))$ contains no fixed point of the system, $\omega(\Gamma(x_0))$ is a periodic orbit.*

**Trapping region in $\mathbb{R}_+^2$**

According to the Poincaré-Bendixson Theorem, in order to prove the existence of a periodic orbit for our system, we have to show the existence of an initial state $x_0 \in E$, whose forward trajectory $\Gamma^+(x_0)$ is contained in a compact subset $F \in \mathbb{R}_+^2$ in the state space, and whose
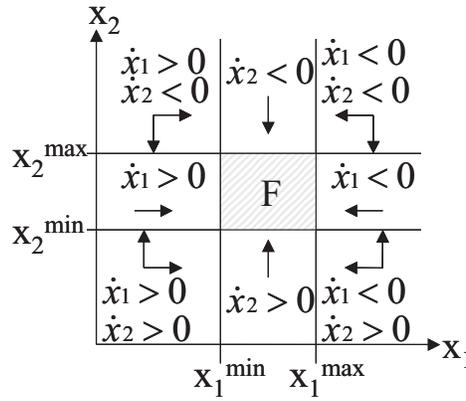
Figure 6.9: Every trajectory of the core network model (6.30) eventually reaches the trapping region $F$, which is bounded by $x_1^{min}$, $x_1^{max}$, $x_2^{min}$ and $x_2^{max}$. These bounds partition the state space into regions which can be characterized by the signs of the vector field components, as indicated here by arrows.

$\omega$-limit set $\omega(\Gamma(x_0))$ does not contain any fixed points. The initial state $x_0$ belongs to the basin of attraction of the periodic orbit $\omega(\Gamma(x_0))$. In fact, if such an $F$ exists, the basin of attraction is the whole state space in our model. We first show the existence of a compact trapping region for system (6.30). We have already shown that a trapping region exists for the additive model introduced in Chapter 2. The bounds of the trapping region in the core model cannot be calculated separately for each component. They are mutually dependent due to degradation of $x_2$, which is controlled by $x_1$. The idea is illustrated in Figure 6.9. We show the existence of lower and upper bounds $x_i^{min}$ and $x_i^{max}$ for each component $i = 1, 2$, such that whenever $x_i(0) < x_i^{min}$ or $x_i(0) > x_i^{max}$, then $\dot{x}_i(t) > 0$ or $\dot{x}_i(t) < 0$, respectively, and the system moves towards these bounds. These bounds are determined by the following estimations for $\dot{x}_1$ and $\dot{x}_2$ in system (6.30):

$$\dot{x}_1 = s_1 - \gamma_1 x_1 + k_{11} \underbrace{\frac{x_1^2}{x_1^2 + \theta_{11}^2} \frac{1}{x_2 + \theta_{12}}}_{\geq 0} \geq s_1 - \gamma_1 x_1. \qquad (6.32)$$

Thus, if $x_1 < x_1^{min} := \frac{s_1}{\gamma_1}$, then $\dot{x}_1 > 0$, and the trajectory moves towards this lower bound. For an upper bound $x_1^{max}$ we have

$$\dot{x}_1 = s_1 - \gamma_1 x_1 + k_{11} \underbrace{\frac{x_1^2}{x_1^2 + \theta_{11}^2}}_{\leq 1} \underbrace{\frac{1}{x_2 + \theta_{12}}}_{\leq \theta_{12}^{-1}} \leq s_1 - \gamma_1 x_1 + \frac{k_{11}}{\theta_{12}}. \qquad (6.33)$$

If we insert an $x_1 > x_1^{max} := \frac{1}{\gamma_1}\left(s_1 + \frac{k_{11}}{\theta_{12}}\right)$ into our core model (6.30), then $\dot{x}_1 < 0$, and the $x_1$-component of the corresponding forward trajectory $\Gamma^+(x)$ decreases monotonically.

Similarly, we can find a lower bound for $x_2$:

$$\dot{x}_2 = s_2 - \gamma_2 \underbrace{\frac{1}{x_1^2 + \theta_{21}^2}}_{\leq \theta_{21}^{-2}} x_2 \geq s_2 - \frac{\gamma_2}{\theta_{21}^2} x_2. \tag{6.34}$$

Hence, a lower bound for $x_2$ is given by $x_2^{min} := \frac{s_2 \theta_{21}^2}{\gamma_2}$, and $\dot{x}_2 > 0$ if $x_2 < x_2^{min}$.

The upper bound for $x_2$ depends on $x_1$.

$$\dot{x}_2 = s_2 - \gamma_2 \frac{1}{x_1^2 + \theta_{21}^2} x_2, \tag{6.35}$$

which is, for fixed $x_1$, negative if

$$x_2 > x_2^{max}(x_1) := \frac{s_2}{\gamma_2} \left( x_1^2 + \theta_{21}^2 \right). \tag{6.36}$$

Thus, the bound $x_2^{max}(x_1)$ increases with $x_1^2$. We know that $x_1$ is eventually bounded. This means, for every $x_0$ there exists a $t^*(x_0) > 0$, such that for all $t > t^*(x_0)$ $x_1(t) < x_1^{max}$. Thus for all $t > t^*(x_0)$, whenever $x_2 > x_2^{max}(x_1^{max})$, then $\dot{x}_2 < 0$, and $x_2^{max}(x_1^{max})$ is the desired upper bound. Note that both lower bounds are positive, and the core model is a positive system.

## A limit cycle around an unstable fixed point

All trajectories eventually converge to the trapping region bounded by $x_i^{min}$ and $x_i^{max}$, $i = 1, 2$. Hence, the $\omega$-limit sets of the system, which determine the long-term behavior, are contained in $F$. To investigate these limit sets, we calculate the *nullclines* of our system, which are given by setting $\dot{x}_1$ and $\dot{x}_2$ in system (6.30) independently to zero and resolving for $x_2$. We will denote the $x_1$-nullcline by $x_2^a(x_1)$ and the $x_2$-nullcline by $x_2^b(x_1)$, respectively:

$$\dot{x}_1(t) \stackrel{!}{=} 0 \quad \Rightarrow \quad x_2^a(x_1) = \frac{k_{11}}{\gamma_1 x_1 - s_1} \frac{x_1^2}{x_1^2 + \theta_{11}^2} - \theta_{12} \qquad x_1\text{-nullcline} \tag{6.37}$$

$$\dot{x}_2(t) \stackrel{!}{=} 0 \quad \Rightarrow \quad x_2^b(x_1) = \frac{s_2}{\gamma_2} \left( \theta_{21}^2 + x_1^2 \right) \qquad x_2\text{-nullcline} \tag{6.38}$$

Note that it is not always possible to resolve the corresponding equations for $x_2$.

Nullclines can help to investigate fixed points of planar dynamical systems. The course of the $x_1$-nullcline gives information about fixed points of $x_1$ for given $x_2$ and vice versa. Thus, the fixed points of a differential equation system are intersections of nullclines. Moreover, along the $x_1$-nullcline $\dot{x}_1 = 0$, and the vector field is parallel to the $x_2$-axis. Analogously, the vector field is parallel to the $x_1$-axis on the $x_2$-nullcline. Nullclines partition the state space into regions in which the signs of vector field components do not change. Figure 6.10 shows the trapping region and the nullclines $x_2^a(x_1)$ and $x_2^b(x_1)$ of system (6.30) in the state space. The $x_2$-nullcline monotonically increases, which reflects
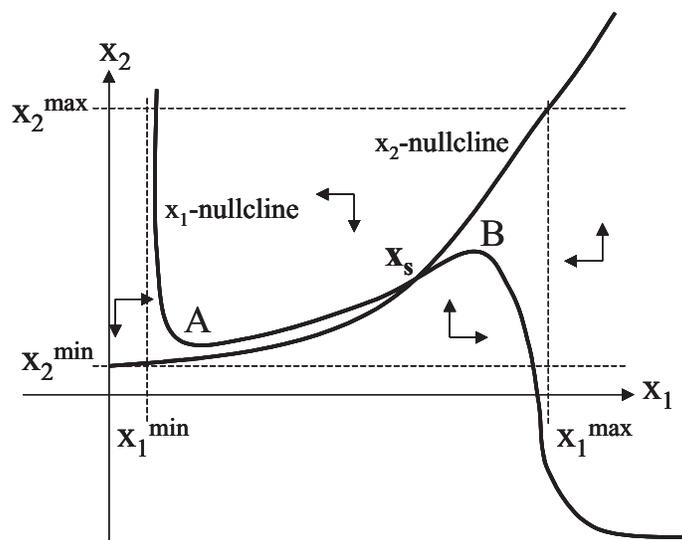
Figure 6.10: Nullclines of the core model (6.30). They partition the state space into regions in which two components of the vector field have constant signs, as indicated by the arrows. The system has an unstable fixed point $x_s$ in the trapping region. $A = (x_1^A, x_2^A)$ and $B = (x_1^B, x_2^B)$ denote the local minimum and maximum of the $x_1$-nullcline.

the positive regulation from $x_1$ to $x_2$. The $x_1$-nullcline increases between A and B due to the positive auto-regulation. For $x_1 < x_1^A$ or $x_1 > x_1^B$, degradation dominates the positive auto-regulation, and $x_2^a(x_1)$ decreases in this regions. Here, the sign of $a_{11}$ in the Jacobian matrix depends on the state $x$. Arrows in Figure 6.10 represent the signs of the two vector field components. Here, the system has a single fixed point $x_s$. The sign pattern of the Jacobian matrix $J_f(x_s)$ is

$$J_f(x_s) = \begin{bmatrix} + & - \\ + & - \end{bmatrix}, \tag{6.39}$$

which can also be seen in Figure 6.10. The condition $a_{11} = \frac{\partial f_1}{\partial x_1} > 0$, which is due to the auto-regulation of component $x_1$, is necessary for $x_s$ to be unstable. This means, the intersection of the two nullclines must be between the two local extrema of the $x_1$-nullcline. If we assume that such an unstable $x_s$ exists for a parameter set $\omega$, which will subsequently be verified by a concrete example, the Poincaré-Bendixson Theorem guarantees the existence of a stable periodic orbit.

The basin of attraction of the limit cycle in our system is the whole $\mathbb{R}_+^n$, and the system shows periodic behavior for an arbitrary initial condition $x_0$. This can be seen in Figure (6.10): We have shown that every trajectory reaches the trapping region limited by $x_i^{min/max}$, $i = 1, 2$. Further, the system has only one single fixed point, which was assumed to be unstable. Hence, the Poincaré-Bendixson Theorem states that $\omega(\Gamma(x_0))$ is a periodic orbit for each $x_0 \in U$.

A parameter set $\omega$ for which $x_s$ is indeed unstable is given by

$$\omega = (0.038, 0.072, 0.38, 0.0072, 3.8, 1.0, 1.0, 0.1). \tag{6.40}$$

This parameter vector has been adapted from the model in [194], and we will see in the following chapter that the oscillating region in the parameter space is rather small. The corresponding courses for the two components $x_1$ and $x_2$ are shown in Figure 6.11. For the simulation, we used Euler integration with a time step $\Delta t = 1$. The origin of these oscillations is intuitively clear. Component $x_1$ increases auto-catalytically when $x_2$ is small. Abundant $x_1$ stimulates accumulation of $x_2$, which in turn inhibits the production of $x_1$. Thus $x_1$ disappears and hence also $x_2$ decreases. This enables $x_1$ to increase again.

### Inference of an oscillating core model

In this subsection, we provide the basis to infer an oscillating regulatory network for the yeast cell cycle from experimental data. We will estimate parameters for the core model (6.30) using the dataset introduced in Chapter 5. For this, we embed the core model into a stochastic framework, as we have shown in Chapter 5. We will maximize the likelihood function $\mathcal{L}_\mathcal{D}(\omega)$ with $\omega \in \mathbb{R}_+^8$ to obtain parameters $\hat{\omega}_{MLE}$, which will be used as a starting point to extend the network by further components and regulations in Chapter 7. We start with the discretized core model

$$x_1(t + \Delta t) \;=\; \underbrace{x_1(t) + \Delta t \left[ s_1 + k_{11} \frac{x_1(t)^2}{x_1(t)^2 + \theta_{11}^2} \frac{1}{\theta_{12} + x_2(t)} - \gamma_1 x_1(t) \right]}_{=:h_1(\omega, t, x_0)} \tag{6.41}$$

$$x_2(t + \Delta t) \;=\; \underbrace{x_2(t) + \Delta t \left[ s_2 - \gamma_2 \frac{1}{\theta_{21}^2 + x_1(t)^2} x_2(t) \right]}_{=:h_2(\omega, t, x_0)} \tag{6.42}$$

and describe time series measurements of $x_1$ and $x_2$ as random variables by adding normally distributed noise terms to the hypotheses $h_i(\omega, t, x_0)$, $i = 1, 2$:

$$\tilde{x}_i(t + \Delta t) = h_i(\omega, t, x_0) + \eta_\xi, \quad \eta_\xi \sim \mathcal{N}(0, \sigma_\xi^2), \quad t = 0, \ldots, T - 1. \tag{6.43}$$

The corresponding likelihood function is given by

$$\mathcal{L}_\mathcal{D}(\omega) = \prod_{i=1}^{2} \prod_{t=0}^{T-1} \frac{1}{\sqrt{2\pi}\sigma_\xi} \exp\left[ -\frac{1}{2} \left( \frac{h_i(\omega, t, x_0) - \tilde{x}_i(t + \Delta t)}{\sigma_\xi^2} \right)^2 \right]. \tag{6.44}$$

In contrast to the likelihood function introduced in the previous chapter, the mean $h_i(\omega, t, x_0)$ of the normal distribution over the random variable $x(t + \Delta t)$ is recursively defined. This increases the computing time for the optimization and is thus not appropriate for larger networks. However, the objective function (6.44) is better suited to capture the temporal evolution of the system.
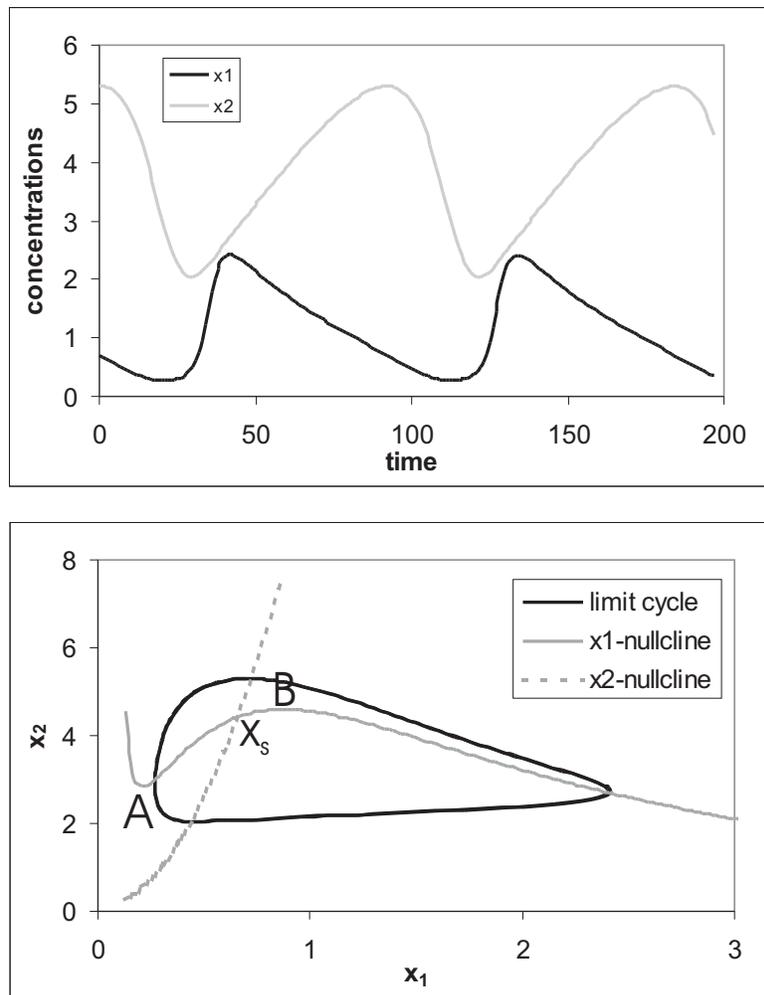
Figure 6.11: System (6.30) shows periodic behavior for the parameter vector $\omega$ given in (6.40) and all initial conditions. **Top:** Courses of $x_1(t)$ and $x_2(t)$ for initial concentrations $x_{1,0} = 0.7$ and $x_{2,0} = 5.3$. **Bottom:** Nullclines in the state space. The interior of the stable limit cycle contains an unstable fixed point $x_s$ between the minimum $A = (x_1^A, x_2^A)$ and the maximum $B = (x_1^B, x_2^B)$ of the $x_1$-nullcline.

We used the $\alpha$-factor synchronization experiments in the dataset of Spellman *et al.* [183]. The time series in this experiment contains 18 time points, measured every seven minutes over two cell cycles. Variable $x_1$ was represented by the mean of the Cln1 and Cln2 concentrations, variable $x_2$ by the mean of the Clb1 and Clb2 concentrations. The correlation of both pairs is very high in all four time series. Missing values were replaced by means of expression values of precedent and subsequent time points. The initial concentration vector $x_0$ was set to $\tilde{x}_0$. Note that we have to approximate the concentration of the cyclins by their mRNA concentrations, which is certainly not a good approximation for CLB.

For the maximization of equation (6.44), we used the Generalized Reduced Gradient (GRG2) algorithm. We started the optimization with a converging model $\omega_{initial} = (0.01, 0.01, 0.001, 0.001, 0, 1, 1, 0.1)$ with stable steady state $(x_{1,s}, x_{2,s}) = (10, 10.1)$. The inferred parameter vector $\hat{\omega}_{MLE}$ is

$$\hat{\omega}_{MLE} = (0.0, 0.0544, 0.3636, 0.0399, 2.1032, 0.0, 1.1703, 0.1). \tag{6.45}$$

A simulation using the inferred parameter vector $\hat{\omega}_{MLE}$ (*continuous lines*) along with the experimental data (*dots*) is shown in Figure 6.12. The ML approach was able to infer a core model that shows sustained oscillations. While the course of CLN is in good agreement with the experimental data, the simulated course of CLB seems to be shifted to the left, and also the oscillation amplitude is smaller than the experimental data suggest. The result of the optimization depends on the initial vector, which has been chosen somewhat arbitrarily here. Oscillating behavior is not learned for all initial parameter sets. The reason for this will be investigated in the following chapter.

## 6.3 Concluding remarks

In the first part of this chapter, we investigated some general properties of differential equation models for regulatory networks. We concentrated on systems of differential equations which have constant sign Jacobian matrices and are stable by means of the existence of a bounded trapping region in the state space. Thus, linear models as introduced in Chapter 2 are excluded. Systems which belong to this class, such as the non-linear model introduced in Chapter 2, tend to converge to a unique steady state. Circuits in the corresponding interaction graph are necessary to capture more complex dynamic behaviors. In particular, a positive circuit is required for multi-stationarity, and a negative circuit of at least two nodes can cause periodic behavior [190]. Circuits determine the qualitative dynamic behavior of the network. Moreover, we illustrated why disjoint circuits in an interaction graph can be analyzed separately, which can drastically reduce the number of variables of a dynamic system. In Section 6.2, we used the results from the previous Section 6.1 to derive a core model for cell cycle regulations in budding yeast. Variables of this model are the G1 specific cyclins, which accumulate during G1 and initiate entry into the S-phase, and the mitotic cyclins, which promote initiation into the M-phase. Based on chemical reaction kinetics and a QSSA, we derived a two-component differential equation system with a sign
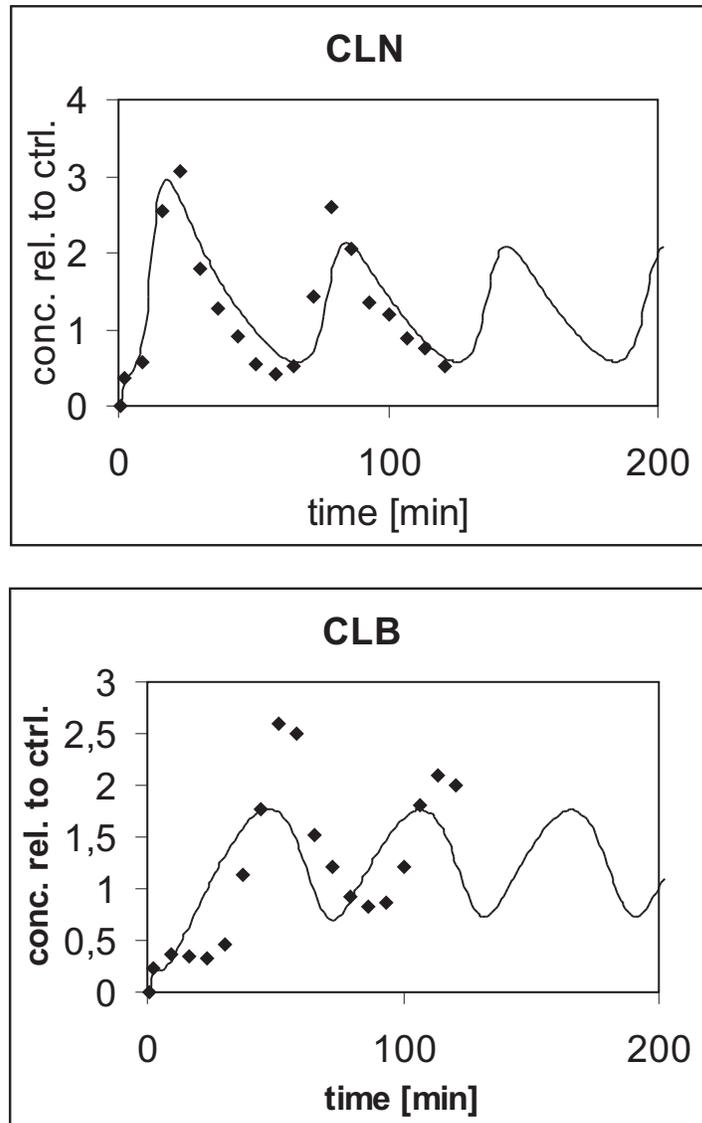
Figure 6.12: Course of inferred core network of the yeast cell cycle (*continuous lines*) along with experimental data (*dots*). **Top:** Course of CLN. **Bottom**: Course of CLB.

pattern of the Jacobian matrix typical for an activator-inhibitor oscillator. This model was analyzed in the state space. It is able to capture the observed periodic expression of the two cyclin classes. Similar to Chapter 5, we embedded this model into a probabilistic framework and used the $\alpha$-factor-synchronization experiments of the microarray dataset from Spellman *et al.* [183] to estimate model parameters by maximizing the likelihood function. This inferred core model will be used as a starting point to extend the network in the following chapter.

Regulation mechanisms of the yeast cell cycle have extensively been studied experimentally, and different models for these regulations have been proposed (see for example [29, 30, 148, 161, 195]). Many of these models are far more complex than the two-component model introduced here. The model of Chen *et al.* [30] for example contains about 30-40 variables. However, a comparison is difficult, since parameter estimation in [30] was mainly done using knockout experiments, which are not publicly available. One can distinguish between two model classes: Models which explain the periodic behavior by a stable limit cycle in the state space [80, 109], and models which are based on bistability phenomena [9, 91, 195]. For the latter models, different steady states correspond to different cell cycle phases. A varying external parameter, which is related to the mass of the cell, causes the system to switch between these states. Our model belongs to the class of limit cycle models. Both model classes are not necessarily contradictory [161]. They can be closely related [148]. Modeling variable $x_2$ in our model (6.30) as an external parameter, our model also shows bistable behavior. This can be seen in Figure 6.10. The $x_1$-nullcline has two stable steady states separated by an unstable steady state between A and B. We will return to this point in the following section.

Although our core model introduced here is built on regulations of the *S. cerevisiae* cell cycle, it has many characteristic properties that are common for models of cellular rhythms [81]. The course of the nullclines, for example, is typical for many models used to explain period behavior in regulatory networks. The underlying mechanisms causing the periodic behavior of these models is usually a destabilization of a steady state [23, 81], which requires feedback loops in the interaction graph, non-linear regulation functions and cooperative regulations, corresponding to Hill-coefficients greater than 1 [63, 81, 167]. Thus, the analysis of our model gives general insights into possible mechanisms causing periodic behavior or multi-stationarity.

# Chapter 7

# About Learning Oscillating Gene Networks: Difficulties and Problems

The Bayesian approach introduced in Chapter 5 aims at the inference of the interaction graph of a regulatory network. Here, prior distributions over network parameters were defined to prevent overfitting and to drive the solution to sparse networks in which most of the interaction strengths are in the proximity of zero. An analysis of simulated data has shown that this approach can outperform the classical maximum likelihood estimation in case of sparse and noisy datasets. However, the inferred models tend to converge to a steady state and are thus not appropriate to capture the dynamic behavior of the system. Reasons for this have been investigated in the previous Chapter 6. Moreover, the importance of circuits has been discussed, and we derived a core model for the yeast cell cycle. This core model is assumed to explain the underlying mechanisms of periodic expression of genes involved in the cell cycle. The model was built on two components, and oscillations arise around an unstable steady state. A necessary condition for the existence of a limit cycle is the existence of a negative circuit of at least two components and a non-linear positive auto-regulation of one of the components. Here, we exploit the theory of differential equations in order to understand mechanisms causing certain kinds of dynamic behaviors. Usually, most of these models are built on only two components and thus neglect many regulations of the system. We have seen in Chapter 6 that this can be a reasonable start to understand dynamic phenomena.

This chapter combines the approaches from Chapter 5 and Chapter 6 in order to infer regulatory networks of more than two components, which show periodic behavior. We start with the maximum likelihood estimation for the core model and extend this for further components and regulations using the Bayesian approach. Thus, we hope to infer a model which reliably predicts important interactions among cell components and at the same time captures the system's dynamic behavior. The method is explained in Section 7.1. We will show results on a simulated dataset. An extension of the core network for further components poses interesting new problems concerning the *robustness* of oscillations. Small perturbations of the core network in terms of variations of parameter values or of additional

127

external influences can easily stabilize the unstable steady state and thus destroy the limit cycle. We will apply a *bifurcation analysis* in order to explain this phenomenon in Section 7.2. Here, the limit sets of a system of differential equations are studied in dependence of model parameters. A comprehensive analysis of the core model helps to understand why it is difficult to infer an oscillating system.

Finally, results of network inference on the Spellman dataset [183] are shown in Section 7.3. The chapter ends with a summary and conclusions in Section 7.4.

## 7.1   Inference of an oscillating network

### 7.1.1   Method

We consider a model which consists of the core network for the *Saccharomyces cerevisiae* cell cycle introduced in Chapter 6 and is extended by further regulations and components:

$$\dot{x}_1 \;=\; s_1 - \gamma_1 x_1 + k_{11}\frac{x_1^2}{x_1^2 + \theta_{11}^2}\cdot\frac{1}{\theta_{12} + x_2} + \sum_{j=3}^{n} k_{1j}\frac{x_j^{m_{1j}}}{x_j^{m_{1j}} + \theta_{1j}^{m_{1j}}} \tag{7.1}$$

$$\dot{x}_2 \;=\; s_2 - \gamma_2\frac{1}{x_1^2 + \theta_{21}^2}x_2 + \sum_{j=3}^{n} k_{2j}\frac{x_j^{m_{2j}}}{x_j^{m_{2j}} + \theta_{2j}^{m_{2j}}} \tag{7.2}$$

$$\dot{x}_i \;=\; s_i - \gamma_i x_i + \sum_{j=1}^{n} k_{ij}\frac{x_j^{m_{ij}}}{x_j^{m_{ij}} + \theta_{ij}^{m_{ij}}} \quad i = 3,\dots,n \tag{7.3}$$

Systems (7.1), (7.2) and (7.3) describe a regulatory network of $n$ components (Figure 7.1). Equations (7.1) and (7.2) consist of the core network from Chapter 6, which is extended by further sigmoidal regulations from the remaining components $x_3,\dots,x_n$. System (7.3) corresponds to the model introduced in Chapter 2 and describes the temporal behavior of the remaining network components. The qualitative behavior of the network is assumed to be determined by the core network, indicated by bold arrows between the core variables $x_1$ and $x_2$ and from the core network to the remaining nodes. This core network is assumed to act relatively independent from the rest of the network, meaning that the regulation strengths $k_{ij}$ are small for $i = \{1,2\}$ and $j = 3,\dots,n$ and for $i,j \geq 3$, indicated by thin lines in Figure 7.1. This assumption justifies the network inference in two separate steps described below. In the following, we will use the subscript 'core' to refer to the core network.

To infer an oscillating regulatory network, we proceed in a two step process. First, we estimate parameters for the core model (7.1) and (7.2) with a predefined structure. As described in the previous chapter, this is done by maximizing the likelihood function $\mathcal{L}_{\mathcal{D}_{core}}(\omega_{core})$ given in (6.44) with respect to the parameters

$$\omega_{core} := (s_1, s_2, \gamma_1, \gamma_2, k_{11}, \theta_{11}, \theta_{12}, \theta_{21}) \in \mathbb{R}_+^8 \tag{7.4}$$
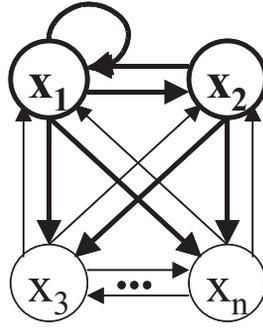
Figure 7.1: Extended network described by equations (7.1), (7.2) and (7.3). The core variables $x_1$ and $x_2$ are assumed to determine the qualitative behavior of the cell cycle network. Accordingly, the bold arrows between $x_1$ and $x_2$ and from the core network to remaining nodes indicate strong regulations, whereas thin lines from the remaining nodes $x_3, \ldots, x_n$ to the core network and between remaining nodes correspond to weaker regulations.

of the core model:

$$\hat{\omega}_{core} = arg \max_{\omega_{core}} \mathcal{L}_{\mathcal{D}_{core}}(\omega_{core}) \qquad \text{subject to } \omega_{core} \in \mathbb{R}^8_+. \tag{7.5}$$

Here, the subset $\mathcal{D}_{core} \subset \mathcal{D}$ contains the experimental data of the core network, that is, concentration time series of the two cyclin classes CLN (variable $x_1$) and CLB (variable $x_2$).

The vector $\hat{\omega}_{core}$ is used as a starting point to extend the core network by further components and interactions in a second step. The structure of the extended interaction graph is unknown and should be learned from the data. Therefore, we use the Bayesian approach explained in Chapter 5 to obtain a parameter vector $\hat{\omega}$ for the extended network. In comparison, results of the maximum likelihood estimation are shown as well.

## 7.1.2 Results on simulated data

### Data simulation

We simulated a network with seven components and an interaction graph given in Figure 5.2. For the core network including the variables $x_1$ and $x_2$ we used the parameter vector

$$\omega_{core} = (0.038, 0.072, 0.38, 0.0072, 3.8, 1, 1, 0.1), \tag{7.6}$$

which has already been used in the previous section.

Parameters for components $x_3, \ldots, x_7$ in system (7.3) were set to $s_i = 0$ and $\gamma_i = 1.9$ for $i = 3, \ldots, 6$, $s_7 = 3.8$ and $\gamma_7 = 0.38$. Regulation strengths, Hill-coefficients and threshold values were set to $k_{ij} = \pm 3.8$ for $j = \{1, 2\}$ and $i \notin \{1, 2\}$, i.e. edges from core network components to remaining nodes, and $k_{ij} = \pm 0.38$ for the remaining regulations.

This parameter choice for the regulation strengths reflects the assumption that the core network components are the main regulators (Figure 7.1). Hill-coefficients and thresholds were set to $m_{ij} = 2$ and $\theta_{ij} = 1$. For these parameters, the seven-component network shows periodic behavior. The noise level $\sigma_\xi$ was set to 0.1 and 0.5, respectively.

For inference of the parameter vector $\hat{\omega}_{core}$, we used a single time series. We show results for 50 and 70 time points and noise levels $\sigma_\xi = 0.1$ and $\sigma_\xi = 0.5$. As already observed before, a single time series is not appropriate to infer parameters $\hat{\omega}$ for the extended network. Thus, we simulated 50 and 200 time series consisting of two time points each. Initial concentrations $x_i(0)$ were randomly chosen from a uniform distribution over the interval $[0, 5]$.

### Core model

We start the optimization process with $\omega_{core,initial} = (0.1, 0.1, 0.1, 0.1, 0, 1, 1, 1)$. For this parameter set, the system converges quickly to its steady state $x_{core,s} := (x_{1,s}, x_{2,s}) = (1, 2)$.

Simulations using the estimated model parameters $\hat{\omega}_{core}$ are shown in Figure 7.2. The oscillating behavior is learned in all four cases. However, the inferred models show significant differences in the oscillation amplitudes of both components. For a low noise level, $\sigma_\xi = 0.1$, the inferred models have a limit cycle around an unstable fixed point and show sustained oscillations, whereas for higher noise levels, $\sigma_\xi = 0.5$, the fixed points are stable, and the oscillations are damped. Figure 7.2 also gives an impression of the amount and quality of data needed to infer parameters which cause the system to exhibit sustained oscillations.

### Extended model

As a starting point for the optimization of the posterior distribution, for the parameters of the core network, we used the maximum likelihood estimator $\hat{\omega}_{core}$, which was obtained using the dataset with 70 time points and a noise level $\sigma_\xi = 0.1$ (Figure 7.2(b)):

$$\hat{\omega}_{core} = (0.0178, 0.0850, 0.3957, 0.0088, 4.2356, 0.9770, 1, 0) \qquad (7.7)$$

Starting points for the remaining parameters were set to $s_i = 0.01$, $\gamma_i = 0.1$, $k_{ij} = 0$, $\hat{\theta}_{ij} = 1$ and $\hat{m}_{ij} = 2$. Synthesis and degradation rates were learned without prior distribution. Parameters for the prior distributions over regulation strengths were set to $\lambda = 1.3$ and $\alpha = 10$. In the first two steps of the optimization process, the prior distribution was not taken into account. The gradient descent stops when the error change is three times smaller than $10^{-5}$ or when a maximum number of 300 steps is reached. The noise level for the optimization was set to $\sigma_{noise} = 0.1$.

First, we observe that the datasets used for learning provide enough information to reconstruct the interaction graph. The inferred network structure fits the original structure very well, and the corresponding AUC values are close to 1 for all four datasets.

(a) 70 time points, $\sigma_\xi = 0.1$      (b) 70 time points, $\sigma_\xi = 0.1$

(c) 50 time points, $\sigma_\xi = 0.1$      (d) 50 time points, $\sigma_\xi = 0.1$

(e) 70 time points, $\sigma_\xi = 0.5$      (f) 70 time points, $\sigma_\xi = 0.5$

(g) 50 time points, $\sigma_\xi = 0.5$      (h) 50 time points, $\sigma_\xi = 0.5$
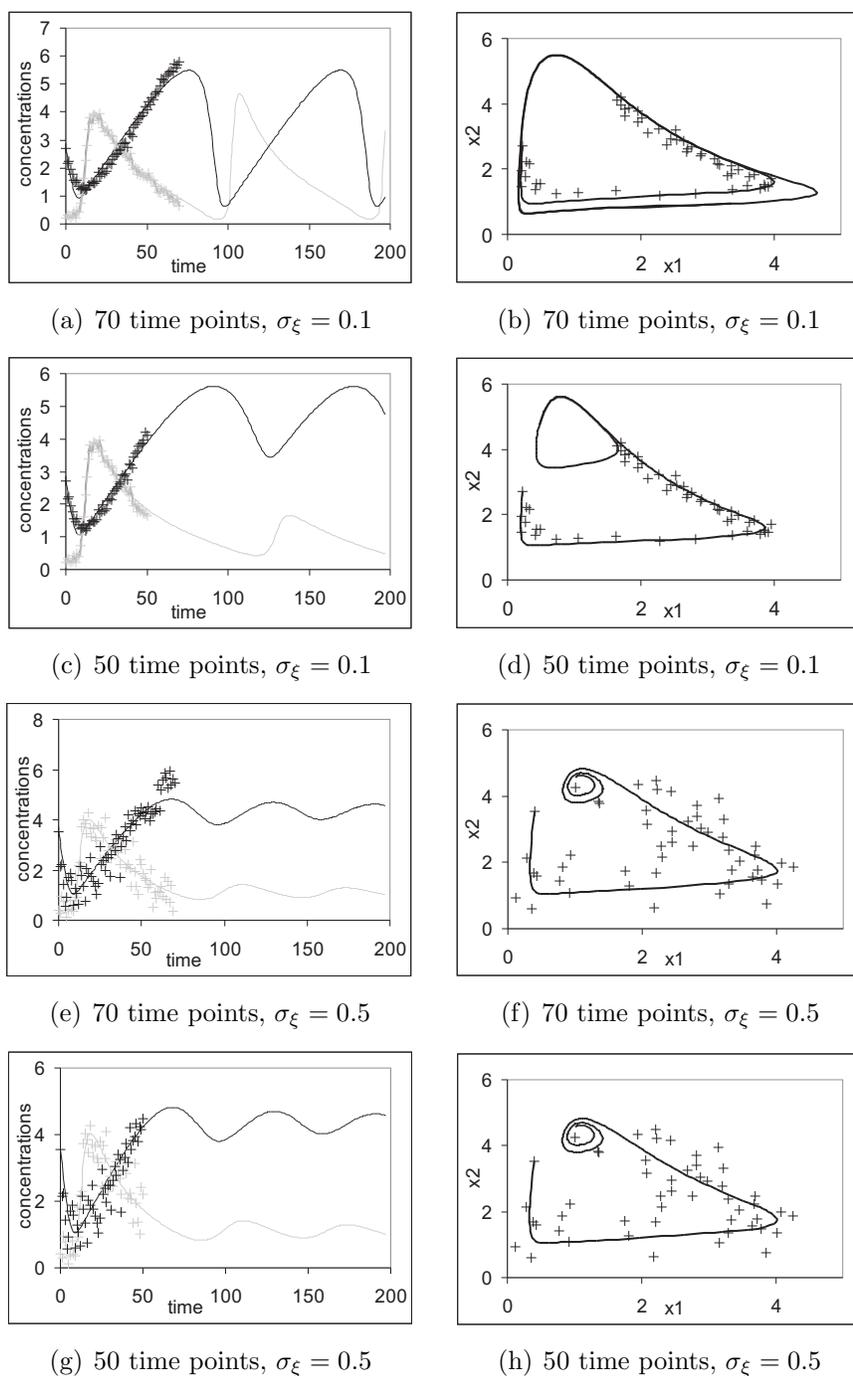
Figure 7.2: Simulations with the estimated parameter vector $\hat{\omega}_{core}$ and different noise levels $\sigma_\xi$ and numbers of time points used for the estimation. **Left:** Courses of $x_1$ (grey line) and $x_2$ (black line) along with the data used for the parameter estimation (grey and black crosses, respectively). **Right:** Trajectories in the state space.

(a) 100 time points, $\sigma_\xi = 0.01$      (b) 400 time points, $\sigma_\xi = 0.1$
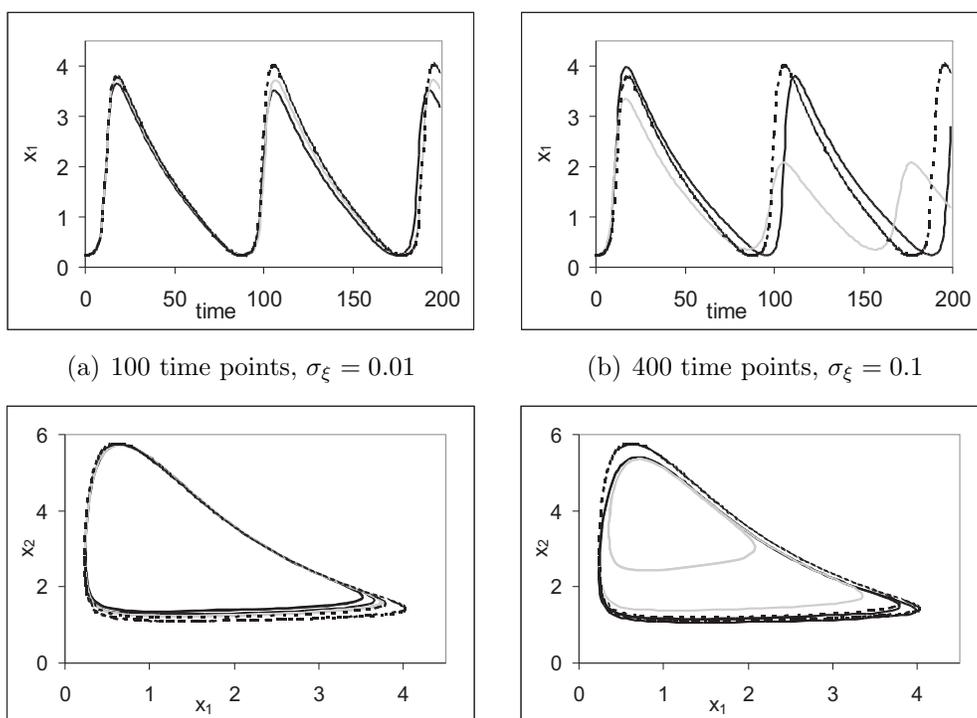
Figure 7.3: Behavior of the simulated network. Shown is the course of the model without noise (*dotted line*), the course with parameters derived with MLE (*grey line*) and the corresponding course with the Bayesian approach (*black continuous line*). **Top:** Course of $x_1$. **Bottom:** Projection of the trajectory onto the $x_1$-$x_2$-plane.

Now we concentrate on the inferred dynamic behavior. Figure 7.3 shows a comparison between the MAP and the MLE approach for different noise levels and numbers of time points used for learning. The upper figures show the inferred course of $x_1$ for the MLE (*grey line*) and the MAP approach (*black line*) along with course of the undisturbed original model (*black dotted line*). A projection of the trajectory onto the $x_1$-$x_2$-plane is shown in the lower graphs. We observe no significant difference between both approaches for low noise and 100 time points used for learning, but the MAP approach outperforms MLE in the case of higher noise, as both oscillation periods and amplitudes better fit the course of the original model. Courses of other network components show a similar behavior.

The results indicate that the inference of a large oscillating network from experimental data is much more difficult than the reconstruction of the network structure. While the network structure is perfectly learned from the dataset used here, results on the core network already indicate that much larger datasets are needed to learn periodic behavior with our model. The qualitative dynamic behavior of the model seems to be sensitive to parameter changes. An explanation for this is provided in the following Section.

## 7.2 Bifurcation analysis

A concept of stability which refers to a property of a system in the parameter space is investigated in the bifurcation theory of differential equations. Here, we ask about changes of the qualitative behavior of a differential equation system $\dot{x} = f(x)$ when changing the vector field $f$. We will refer to this stability concept as *structural stability* or *robustness*. Parameter sets for which $f$ is not structurally stable are called *bifurcation sets*. The idea of structural stability was first formulated by Andronov and Pontryagin in 1937 [147]. Loosely speaking, a vector field $f$ is structurally stable, if for any vector field $g$ near $f$, both vector fields are topologically equivalent (for further details about topological equivalence see [85, 147]). In this section, we will apply methods from *bifurcation theory* to our core network model and use the results to explain why it is difficult to infer an oscillating network. We will see that a stable limit cycle only exists in a small region of the parameter space. Before we show results for the core model in Subsection 7.2.2, we will introduce the two most important bifurcations which occur in our core model in Subsection 7.2.1, *saddle-node* and *Hopf bifurcations*.

### 7.2.1 Saddle-node and Hopf bifurcation

We consider the stability of the phase portrait of a differential equation

$$\dot{x} = f(x, \mu), \quad x \in E, \, \mu \in J, \, f \in \mathcal{C}^1(E \times J) \tag{7.8}$$

with $E$ being an open subset of $\mathbb{R}^n$, $J \in \mathbb{R}$ an interval and $\mu$ the *bifurcation parameter*. A value $\mu_0 \in J$ is a *bifurcation value*, if $f(x, \mu_0)$ is not structurally stable [147]. This means, the qualitative dynamic behavior of the system changes in a small neighborhood around $\mu_0$. Such a change can be caused by different mechanisms. We will explain two of these, *saddle-node* and *Hopf bifurcations*. Both are *local* bifurcations, which occur near an equilibrium point or a periodic orbit.

#### Saddle-node bifurcation

The Hartman-Grobman Theorem introduced in Chapter 2 states that the stability of a hyperbolic fixed point $x_s(\mu)$ is determined by the signs of the real parts of the eigenvalues of $J_f(x_s(\mu))$. It is stable if all real parts are negative. Thus, a stable fixed point $x_s(\mu)$ becomes unstable when an eigenvalue $\lambda^*(x_s(\mu))$ of $J_f(x_s(\mu))$ crosses the imaginary axes, that is, if $x_s(\mu)$ is non-hyperbolic, because $\Re(\lambda^*(x_s(\mu)) = 0$. A *saddle-node bifurcation* occurs at $\mu_0$ if $J_f(x_s(\mu_0))$ has a simple eigenvalue $\lambda^*(x_s(\mu_0))$ with zero real part. An example is the system

$$\dot{x} = \mu - x^2 \quad x, \mu \in \mathbb{R}. \tag{7.9}$$

It has a stable and an unstable fixed point $x_s(\mu) = \pm\sqrt{\mu}$ for $\mu > 0$. These collide at $\mu_0 = 0$, and $x_s(\mu_0) = 0$ is a non-hyperbolic equilibrium point. The system does not have any fixed points for $\mu < 0$.

**Hopf bifurcation**

A *Hopf bifurcation* occurs if the change of stability of $x_s(\mu)$ is caused by a simple pair of purely imaginary eigenvalues. Here, $x_s(\mu)$ looses stability, and a periodic orbit is created. An example is given by the differential equation system

$$\dot{x} = -y + x(\mu - x^2 - y^2)$$
$$\dot{y} = x + y(\mu - x^2 - y^2). \tag{7.10}$$

This system has a single equilibrium point $x_s(\mu) = 0$, which is stable for $\mu < 0$ and unstable for $\mu > 0$. Hence, $\mu_0 = 0$ is the bifurcation value. In system (7.10), a stable limit cycle occurs when $\mu$ passes the bifurcation value $\mu_0$. We distinguish between *supercritical* and *subcritical* Hopf bifurcations. The Hopf bifurcation at $\mu_0$ in system (7.10) is supercritical. In contrast, at a subcritical Hopf bifurcation an *unstable* limit cycle is created.

**Bifurcation diagram**

The behavior of a differential equation system can graphically be represented by a *bifurcation diagram*. Here, the limit sets of the differential equation system are plotted as a function of the bifurcation parameter $\mu$. If the state space has dimension $\geq 2$, one coordinate of the limit sets is usually depicted for graphical representation. Figure 7.4 shows bifurcation diagrams of system (7.9) (Figure 7.4(a)), system (7.10) (Figure 7.4(b)) and a subcritical Hopf bifurcation (Figure 7.4(c)). System (7.9) has a stable and an unstable fixed point for $\mu > 0$ and no fixed points for $\mu < 0$. System (7.10) has a stable fixed point $x_s = 0$ for $\mu < 0$, which becomes unstable for $\mu > 0$. A stable limit cycle occurs at the bifurcation value $\mu_0 = 0$. Here, minimum and maximum values of the $x$-component of this limit cycle are shown. The Hopf bifurcation of system (7.10) is supercritical. In comparison, the typical bifurcation diagram of a subcritical Hopf bifurcation at $\mu_0 = 0$ is shown in Figure 7.4(c). As before, the stable fixed point $x_0 = 0$ becomes unstable at $\mu_0 = 0$. An unstable and a stable limit cycle exist in an interval $[a, 0]$. The stable one continues for $\mu > 0$. Thus, there are two different $\omega$-limit sets in the interval $[-a, 0]$, and the systems can exhibit hysteresis: Starting in the steady state $x_s(\mu) = 0$ for a bifurcation parameter $\mu < 0$ and increasing $\mu$, the system rests in this state until it becomes unstable at $\mu_0 = 0$. Here, the system jumps to the stable limit cycle and starts to oscillate. In contrast, starting with a bifurcation parameter $\mu > 0$, the system only converges to the stable fixed point $x_s(\mu) = 0$ when the stable limit cycle disappears at $a < 0$. The unstable limit cycle separates the basins of attractions for the two $\omega$-limit sets of the system.

Usually, bifurcation diagrams have to be created numerically. A bifurcation program is started in an $\omega$-limit set, which is continued by small variations of the bifurcation parameter. The stability of the limit set is determined in each step. Courses of two limit sets emanating from the same bifurcation value $\mu_0$ have to be continued separately in these programs. A bifurcation diagram consists of sets of numerically calculated points. Most programs have an implemented algorithm, which adapts the step size $\Delta\mu$ automatically.

(a) saddle-node     (b) supercritical Hopf     (c) subcritical Hopf
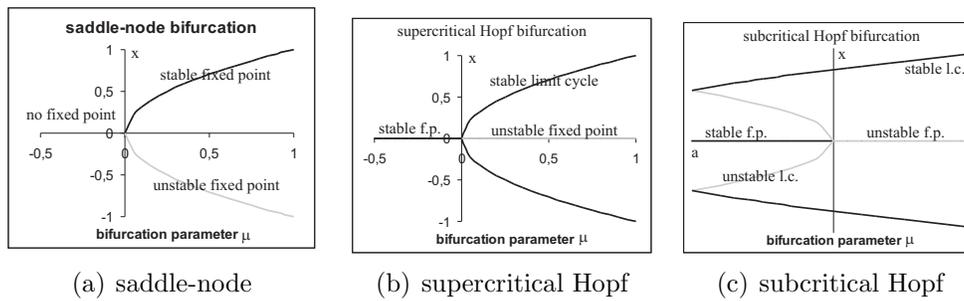
Figure 7.4: Bifurcation diagrams for *7.4(a)* a saddle-node bifurcation (system (7.9)), *7.4(b)* a supercritical Hopf bifurcation (system (7.10)) and *7.4(c)* a subcritical Hopf bifurcation.
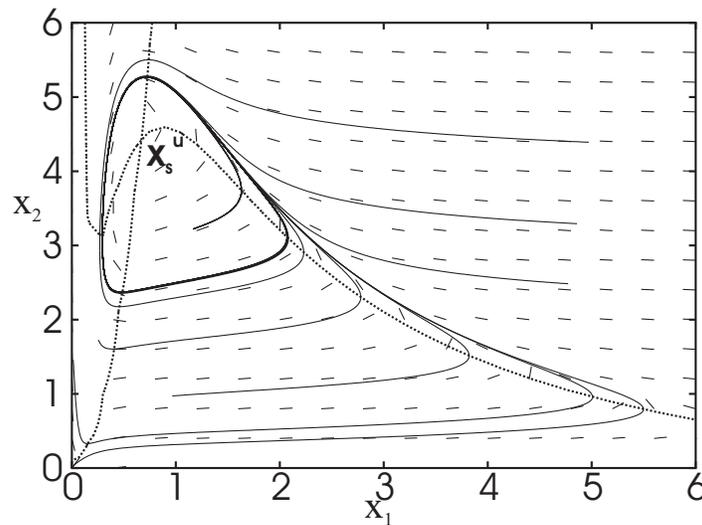


Figure 7.5: Phase portrait of core model described by equations (7.1) and (7.2) and parameters given in equation (7.6). A globally stable limit cycle exists around an unstable fixed point $x_s^u$. Nullclines of the system are drawn as dotted lines.

Thus, if the step size is large, a limit set in a bifurcation diagram is displayed as a set of points rather than a function of $\mu$. This can also be seen in the bifurcation diagrams shown in the following subsection.

## 7.2.2   Bifurcation analysis of the core model

Now we apply a bifurcation analysis to our core system (7.1) and (7.2) with parameter vector $\hat{\omega}_{core}$ specified in (7.6). For this parameter set, the system exhibits sustained oscillations. The corresponding stable limit cycle and the vector field of the system are shown in Figure 7.5. The nullclines of the system are shown as well (*dotted lines*). The fixed point $x_s^u$, given as the intersection of these nullclines in the interior of the limit cycle, is unstable.

In the following subsections, we consider the influence of each model parameter on the

qualitative behavior of equations (7.1) and (7.2) separately, and use them consecutively as bifurcation parameters. In order to understand these bifurcation diagrams, it is convenient to consider the dependence of intersections of the nullclines on the bifurcation parameters. According to the Poincaré-Bendixson Theorem, a unique unstable fixed point guarantees the existence of a stable limit cycle for our system. In the parameter ranges where these oscillations occur, we will also look at the oscillation period.

Analysis is carried out with the open source program XPPAUT, a tool for simulations and analysis of dynamical systems [65]. The bifurcation diagrams show limit sets of variable $x_1$ in the core system described by (7.1) and (7.2).

### Basal synthesis rate $s_1$

Figure 7.6 shows the behavior of the system in dependence of the basal synthesis rate $s_1$. The bifurcation diagram is shown in Figure 7.6(a). We detect a saddle-node bifurcation at $s_1^{SN}$ and a Hopf bifurcation at $s_1^{HB}$. For $s_1 < s_1^{SN}$, the system has a stable steady state $x_s^s$ and two unstable steady states $x_s^u$. The stable steady state is globally stable and attracts all trajectories. The corresponding phase portrait is shown in Figure 7.6(c). At a value $s_1^{SN}$, a saddle-node (SN) bifurcation occurs, and the stable steady state $x_s^s$ and one of the unstable steady states $x_s^u$ disappear. The system shows periodic behavior and oscillates around the remaining unstable steady state. The period T of these oscillations is shown in Figure 7.6(b). A further increase of $s_1$ leads to a decrease of the period and the amplitude of the oscillations. Finally, the single unstable steady state $x_s^u$ becomes stable at a Hopf bifurcation value $s_1^{HB}$, and the limit cycle disappears (Figure 7.6(d)).

### Basal synthesis rate $s_2$

The behavior of the system for varying basal synthesis rate $s_2$ can be seen in Figures 7.7 and 7.8. For small $s_2$, the system has a unique fixed point $x_s$. This fixed point becomes unstable between a supercritical and a subcritical Hopf bifurcation at $s_2^{HB1}$ and $s_2^{HB2}$, respectively. Hence, the system oscillates in this interval (Figure 7.7(a)). Figure 7.7(b) shows the oscillation period T. The nullclines and their intersection $x_s$ are shown in Figure 7.8 for three parameter values $s_2 = 0.02 < s_2^{HB1}$, $s_2$ between the two bifurcation values, $s_2^{HB1} < s_2 = 0.072 < s_2^{HB2}$, and a value $s_2 = 0.3 > s_2^{HB2}$. Only variable $x_2$ and thus only the $x_2$-nullcline depend on $s_2$. The Figure shows that the larger the synthesis rate $s_2$, the larger is the $x_2$-coordinate of the fixed point, $x_2^s$, for given $x_1$.

### Degradation rate $\gamma_1$

The bifurcation parameter in Figure 7.9 is the degradation rate $\gamma_1$. For small degradation rates $\gamma_1$, the system has a unique stable fixed point $x_s$, which decreases with increasing $\gamma_1$ (Figure 7.9(a)). This fixed point becomes unstable at a Hopf bifurcation value $\gamma_1^{HB}$, and the system oscillates between this Hopf bifurcation (HB) and a saddle-node bifurcation (SN) at $\gamma_1^{SN}$. The period of this oscillation can be seen in Figure 7.9(b). For $\gamma_1 > \gamma_1^{SN}$, the system has a globally stable fixed point $x_s^s$. Figures 7.9(c) and 7.9(d) show the intersections of

(a) Bifurcation diagram

(b) Oscillation period T

(c) Convergence for $s_1 < s_1^{SN}$

(d) Convergence for $s_1 > s_1^{HB}$
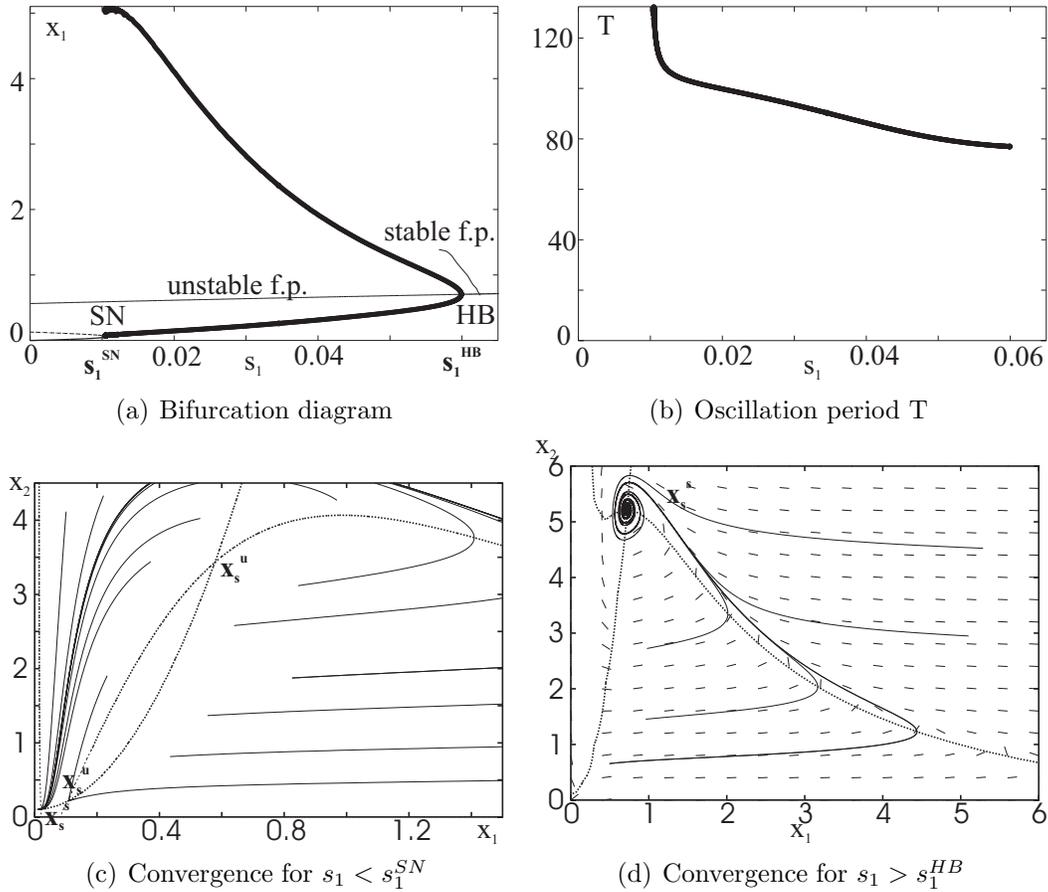
Figure 7.6: Behavior of core system (equations (7.1) and (7.2)) in dependence of the degradation rate $s_1$. Stable oscillations occur in an interval between a saddle-node (SN) and a Hopf bifurcation (HB). **Figure 7.6(a):** Bifurcation diagram. **Figure 7.6(b):** Oscillation period. **Figure 7.6(c):** Phase portrait for $s_1 < s_1^{SN}$. All trajectories converge to the unique stable fixed point $x_s^s$. **Figure 7.6(d):** Phase portrait for $s_1 > s_1^{HB}$. The system has a unique globally stable fixed point $x_s^s$, which attracts all trajectories.

(a) Bifurcation diagram

(b) Oscillation period T
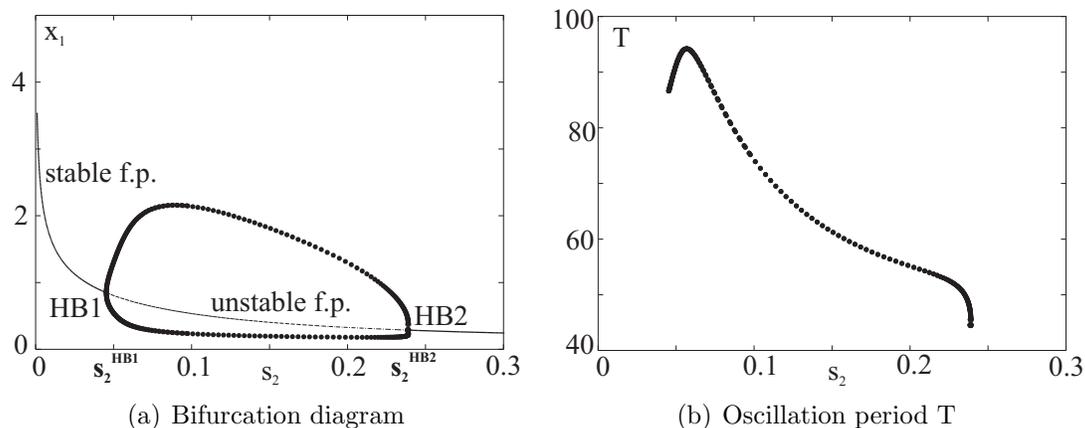
Figure 7.7: Bifurcation diagram and oscillation period for bifurcation parameter $s_2$. The system shows oscillations between two Hopf bifurcations HB1 and HB2 and bifurcation values $s_2^{HB1}$ and $s_2^{HB2}$, respectively.
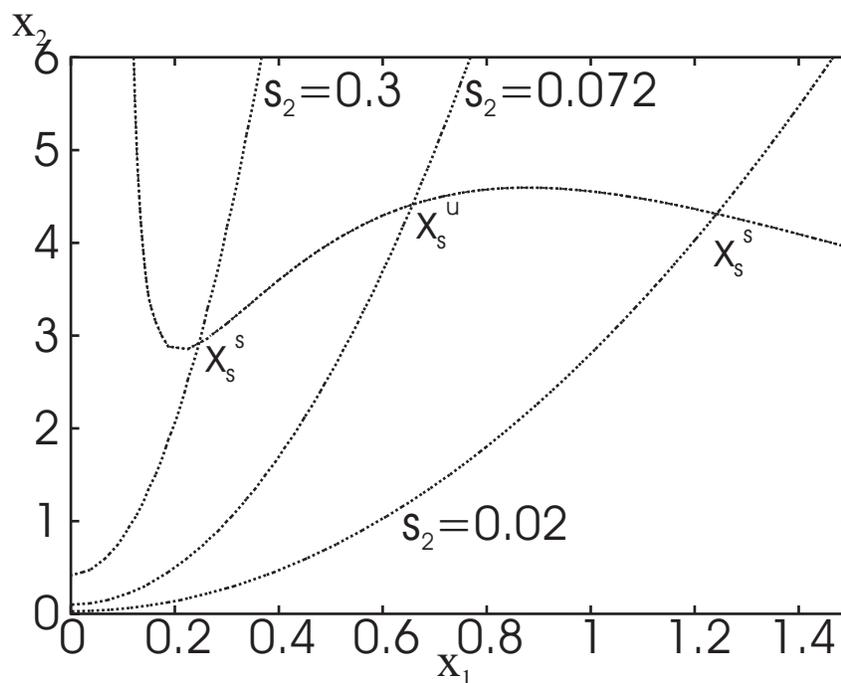


Figure 7.8: Intersection of nullclines for varying parameter $s_2$. The system has a unique fixed point $x_s$, which is stable for $s_2 < s_2^{HB1}$, represented here by $s_2 = 0.02$, and $s_2 > s_2^{HB2}$, represented by $s_2 = 0.3$, and unstable between the two Hopf bifurcations (here $s_2 = 0.072$).

(a) Bifurcation diagram

(b) Oscillation period T

(c) Steady state of the system

(d) Saddle-node bifurcation
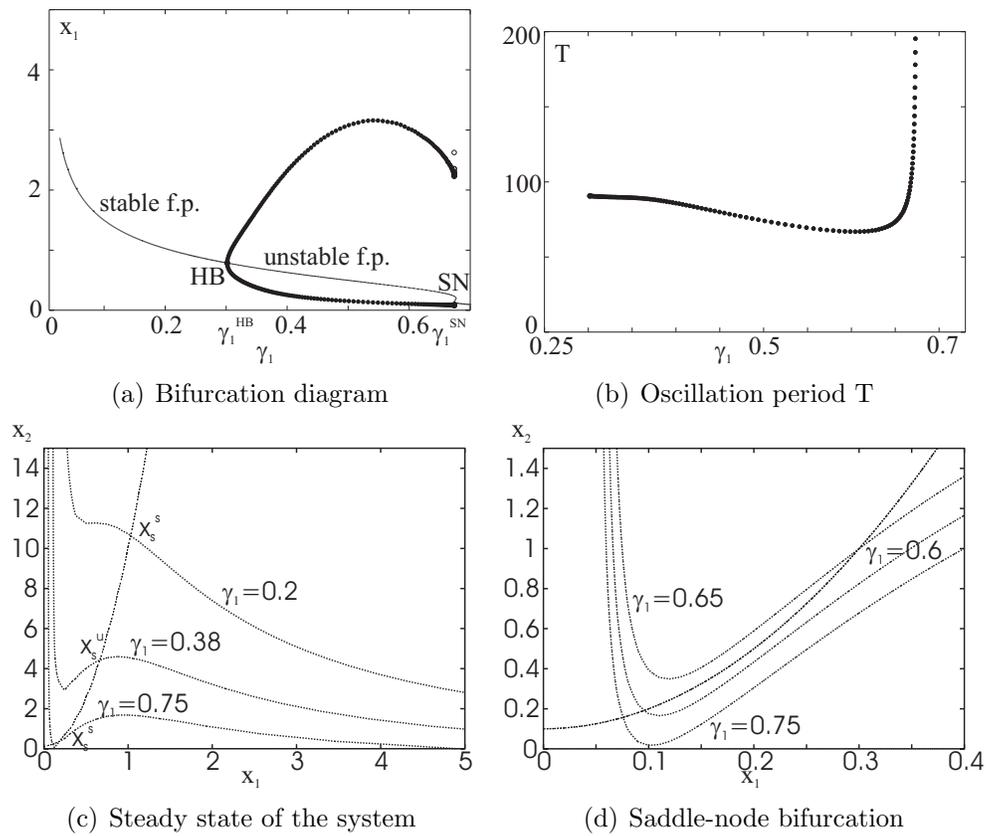
Figure 7.9: Behavior of the core system (equations (7.1) and (7.2)) in dependence of the degradation rate $\gamma_1$. **Figure 7.9(a):** Bifurcation diagram. **Figure 7.9(b):** Oscillation period. **Figure 7.9(c):** Intersection of the nullclines for parameter values $\gamma_1 = 0.2 < \gamma_1^{HB}$, $\gamma_1^{HB} < \gamma_1 = 0.38 < \gamma_1^{SN}$ and $\gamma_1 = 0.75 > \gamma_1^{SN}$. **Figure 7.9(d):** Course of the nullclines in the neighborhood of the saddle-node bifurcation.

nullclines for different degradation rates $\gamma_1$. The region $\gamma_1 < \gamma_1^{HB}$ is represented by $\gamma_1 = 0.2$ in Figure 7.9(c), the value $\gamma_1 = 0.38$ refers to the oscillating region between the Hopf and the saddle-node bifurcations, and $\gamma_1 = 0.75$ represents the region $\gamma_1 > \gamma_1^{SN}$. Figure 7.9(d) explains the appearance of the saddle-node bifurcation in Figure 7.9(a) at a larger scale. For $\gamma_1 = 0.6 < \gamma_1^{SN}$, the unique fixed point is unstable. The course of the $x_1$-nullcline drops with increasing $\gamma_1$, whereas $x_2$ and thus also the $x_2$-nullcline is independent of $\gamma_1$. In a very small region, the nullclines intersect three times, and the system has three fixed points. The system has a unique stable fixed point for both values $\gamma_1 = 0.65$ and $\gamma_1 = 0.75$.

## Degradation rate $\gamma_2$

Figure 7.10 shows the behavior of the system with bifurcation parameter $\gamma_2$. Also here, oscillations occur between two Hopf bifurcations HB1 and HB2 at $\gamma_2^{HB1}$ and $\gamma_2^{HB2}$, respec-

(a) Bifurcation diagram

(b) Oscillation period T

(c) Subcritical Hopf bifurcation

(d) Subcritical Hopf bifurcation
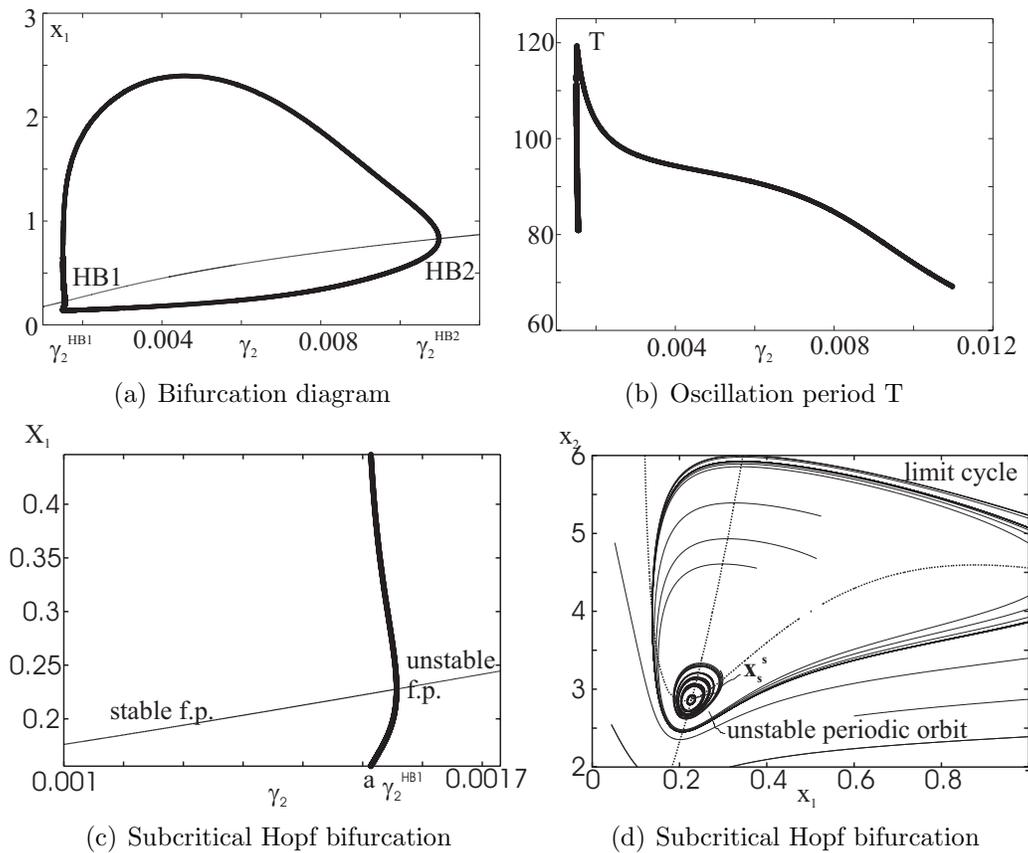
Figure 7.10: Behavior of the core system (equations (7.1) and (7.2)) in dependence of the degradation rate $\gamma_2$. The system has a stable limit cycle between a subcritical and a supercritical Hopf bifurcation HB1 and HB2. **Figure 7.10(a):** Bifurcation diagram. **Figure 7.10(b):** Oscillation period. **Figure 7.10(c):** The Hopf bifurcation HB1 at $\gamma_2^{HB1}$ is subcritical and the system has two $\omega$-limit sets for $\gamma_2 \in [a, \gamma_2^{HB1}]$. **Figure 7.10(d):** Phase portrait for $\gamma_2 \in [a, \gamma_2^{HB1}]$. The system has a stable steady state and a stable limit cycle. The basins of attraction are separated by an unstable limit cycle.

tively (Figure 7.10(a)). HB1 is subcritical. Accordingly, different limit sets coexist for an interval $\gamma_2 \in I := [a, \gamma_2^{HB1}]$, which is indicated in Figure 7.10(c). The phase portrait for an $s_2 \in I$ is shown in Figure 7.10(d). The two basins of attraction for the stable steady state $x_s^s$ and the limit cycle are separated by an unstable limit cycle around $x_s^s$.

### Parameters of the regulation functions

Bifurcation diagrams and oscillation periods for the remaining parameters in the core system (equations (7.1) and (7.2)) are illustrated in Figures 7.11, 7.12, 7.13 and 7.14. Also here, the parameter regions in which the system shows oscillations are limited by Hopf bifurcations.
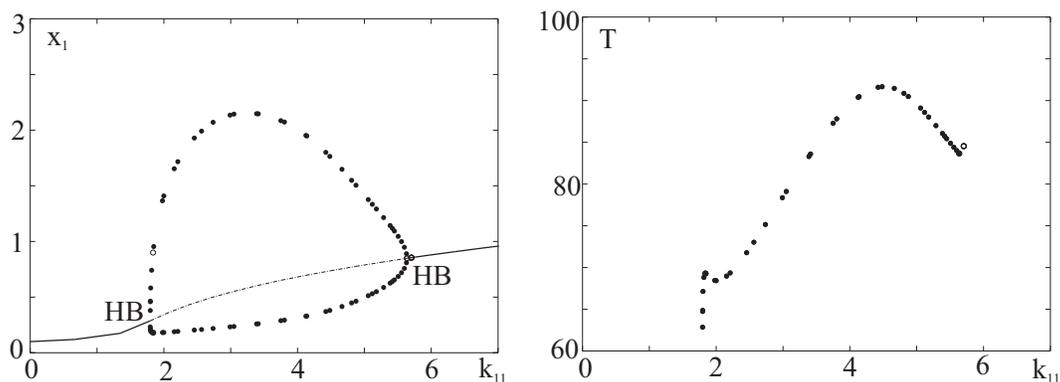
Figure 7.11: Bifurcation diagram (*left*) and oscillation period $T$ (*right*) for bifurcation parameter $k_{11}$. The Hopf bifurcation on the left hand side is subcritical, the one on the right hand side supercritical.
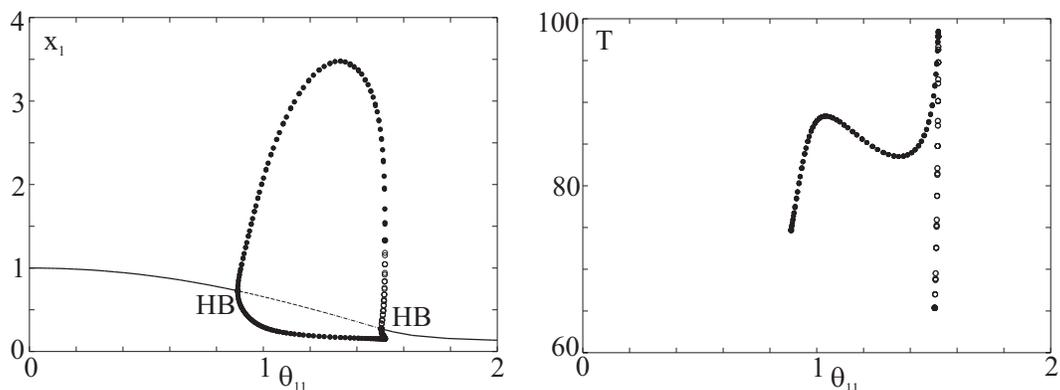


Figure 7.12: Bifurcation diagram (*left*) and oscillation period $T$ (*right*) for bifurcation parameter $\theta_{11}$. The Hopf bifurcation on the left hand side is supercritical, the one on the right hand side subcritical. Empty circles indicate that the limit cycle emanating from the subcritical Hopf bifurcation is unstable.
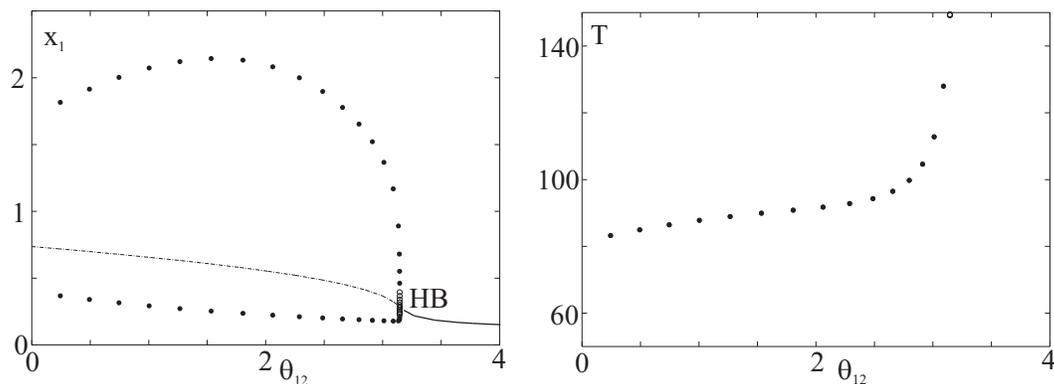
Figure 7.13: Bifurcation diagram (*left*) and oscillation period $T$ (*right*) for bifurcation parameter $\theta_{12}$. The unstable fixed point for $\theta_{12} < \theta_{12}^{HB}$ becomes stable at the subcritical Hopf bifurcation $\theta_{12}^{HB}$.
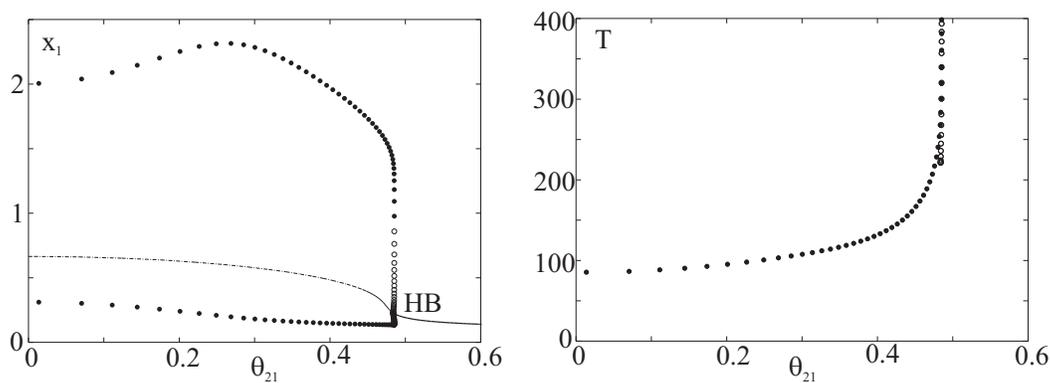


Figure 7.14: Bifurcation diagram (*left*) and oscillation period T (*right*) for bifurcation parameter $\theta_{21}$. The system has an unstable fixed point for $\theta_{21} < \theta_{21}^{HB}$, which becomes stable at the subcritical Hopf bifurcation $\theta_{21}^{HB}$.
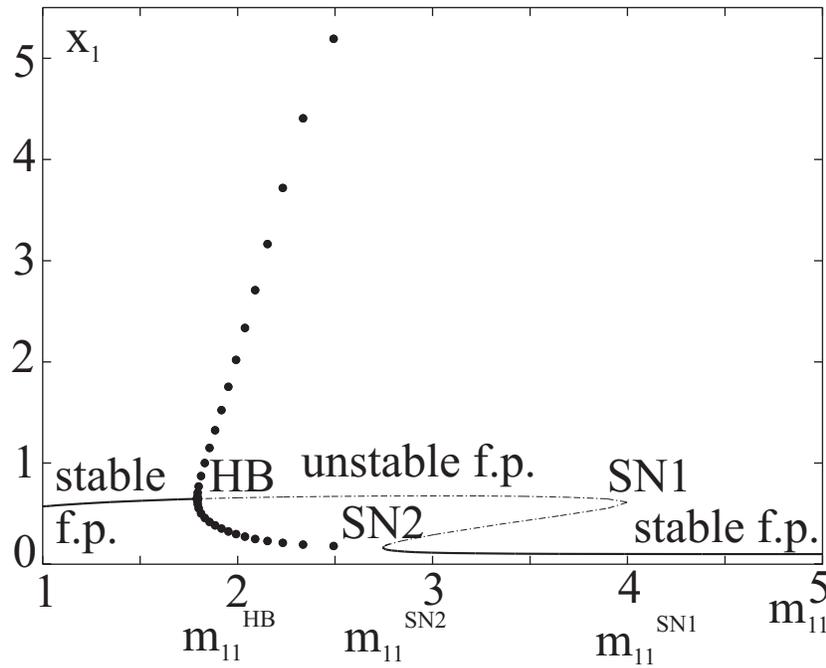
Figure 7.15: Bifurcation diagram for bifurcation parameter $m_{11}$. A limit cycle exists between the Hopf bifurcation at $m_{11}^{HB}$ and the saddle-node bifurcation at $m_{11}^{SN2}$.

## Cooperative interaction is required for periodic behavior

Figure 7.15 shows the bifurcation diagram with Hill-coefficient $m_{11}$, which was set to $m_{11} = 2$ in the core system, as the bifurcation parameter. The interval in which a limit cycle exists is limited by a supercritical Hopf bifurcation at $m_{11}^{HB}$ and a saddle-node bifurcation at $m_{11}^{SN2}$. Outside this interval, the system converges to a stable fixed point. Two unstable and one stable steady state exist between the two saddle-node bifurcations at $m_{11}^{SN2}$ and $m_{11}^{SN1}$. Figure 7.16 shows the nullclines for different bifurcation parameters. For $m_{11} = 1.7 < m_{11}^{HB}$ (*grey continuous lines*) and $m_{11} = 4.2 > m_{11}^{SN2}$ (*grey dashed lines*), the system has a single stable fixed point. The parameter $m_{22} = 2$ lies between $m_{11}^{HB}$ and $m_{11}^{SN1}$ and represents the oscillating region (*black continuous lines*). Here, the nullclines intersect in a single point that is unstable. Finally, there are three intersections of the nullclines in the interval $[m_{11}^{SN1}, m_{11}^{SN2}]$, represented by $m_{11} = 3$ in the Figure (*black dashed lines*). Two of them are unstable, the third one is globally stable.

Independent of all other parameters of the core network, a Hill-coefficient $m_{11} > 1$ is a necessary condition for the existence of periodic solutions. We will show this in the following.

A necessary condition for $J_f(x_s)$ to have purely imaginary eigenvalues and thus to undergo a Hopf bifurcation required for oscillations is $a_{11}(x_s) > 0$ [194], as already demon-
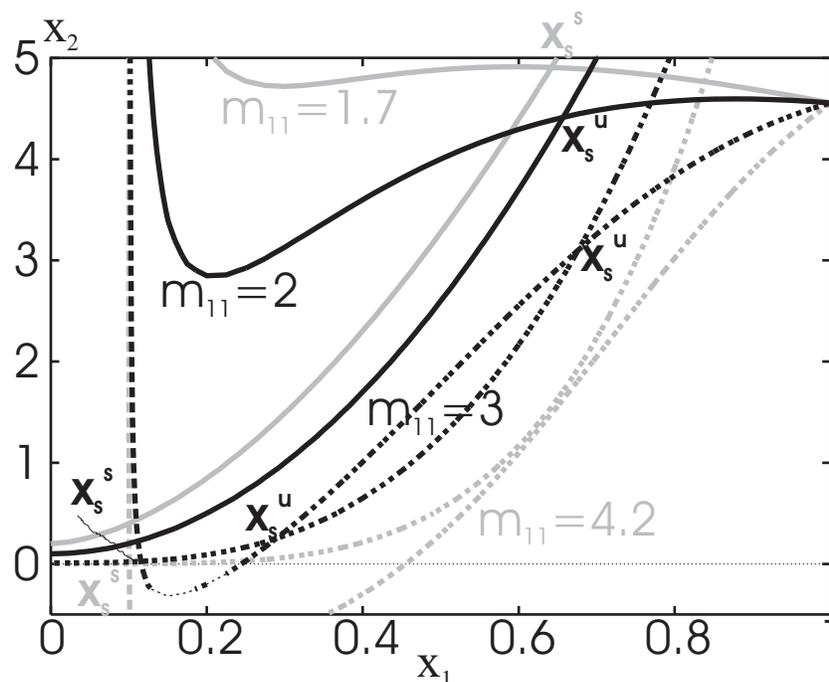
Figure 7.16: Nullclines of the core model for different Hill-coefficients $m_{11}$. For $m_{11} = 1.7 <$ $m_{11}^{HB}$ (*grey continuous lines*), the nullclines intersect once, which is a stable fixed point $x_s^s$ of the system. The system oscillates for values $m_{11}$ between the Hopf bifurcation value $m_{11}^{HB}$ and the saddle-node bifurcation at $m_{11}^{SN2}$, represented by $m_{11} = 2$ (*black continuous lines*). Here, the nullclines intersect in a single unstable fixed point $x_s^u$. The system has two unstable and a stable fixed point between two saddle-node bifurcations $m_{11}^{SN2}$ and $m_{11}^{SN1}$, here represented by $m_{11} = 3$ (*black dashed lines*). The stable fixed point is globally attracting. Finally, there is one single stable fixed point for values $m_{11} > m_{11}^{SN1}$, here $m_{11} = 4.2$ (*grey dashed lines*).

strated in Chapter 6. Since $x_s$ lies on the $x_1$-nullcline, which is given by

$$x_2^a(x_1, m_{11}) = \frac{k_{11}}{\gamma_1 x_1 - s_1} \frac{x_1^{m_{11}}}{x_1^{m_{11}} + \theta_{11}^{m_{11}}} - \theta_{12}, \tag{7.11}$$

the derivative of $x_2^a(x_1, m_{11})$ with respect to $x_1$ has to be positive for some value $x_1$ in the trapping region $F$, which is bounded by $x_i^{min}$ and $x_i^{max}$, $i = 1, 2$,

$$\exists x_1 \in I := \left( x_1^{min} = \frac{s_1}{\gamma_1}, x_i^{max} = \frac{s_1 + k_{11}}{\gamma_1} \right) : \quad \frac{\partial x_2^a(x_1, m_{11})}{\partial x_1} > 0. \tag{7.12}$$

This derivative is given by

$$\begin{aligned}
\frac{\partial x_2^a(x_1, m_{11})}{\partial x_1} &= -\frac{k_{11}\gamma_1}{(\gamma_1 x_1 - s_1)^2} \frac{x_1^{m_{11}}}{x_1^{m_{11}} + \theta_{11}^{m_{11}}} + \frac{k_{11}}{\gamma_1 x_1 - s_1} \frac{\partial}{\partial x_1} \frac{x_1^{m_{11}}}{x_1^{m_{11}} + \theta_{11}^{m_{11}}} \\
&= \frac{k_{11}}{\gamma_1 x_1 - s_1} \left[ -\frac{\gamma_1}{\gamma_1 x_1 - s_1} \frac{x_1^{m_{11}}}{x_1^{m_{11}} + \theta_{11}^{m_{11}}} + \frac{\partial}{\partial x_1} \frac{x_1^{m_{11}}}{x_1^{m_{11}} + \theta_{11}^{m_{11}}} \right].
\end{aligned} \tag{7.13}$$

It is a continuous function in $I$. Moreover,

$$\lim_{x_1 \to (x_1^{min})^+} \frac{\partial x_2^a(x_1, m_{11})}{\partial x_1} \to -\infty. \tag{7.14}$$

Hence, in order to fulfill condition (7.12), the intermediate value theorem states the existence of an $x_1^*$ that is a zero of (7.13),

$$\left. \frac{\partial x_2^a(x_1, m_{11})}{\partial x_1} \right|_{x_1^*} = 0. \tag{7.15}$$

This leads to

$$-\frac{k_{11}\gamma_1}{(\gamma_1 x_1^* - s_1)^2} \frac{(x_1^*)^{m_{11}}}{(x_1^*)^{m_{11}} + \theta_{11}^{m_{11}}} + \frac{k_{11}}{\gamma_1 x_1^* - s_1} \left. \frac{\partial}{\partial x_1} \frac{x_1^{m_{11}}}{x_1^{m_{11}} + \theta_{11}^{m_{11}}} \right|_{x_1^*} = 0. \tag{7.16}$$

Inserting

$$\left. \frac{\partial}{\partial x_1} \frac{x_1^{m_{11}}}{x_1^{m_{11}} + \theta_{11}^{m_{11}}} \right|_{x_1^*} = \frac{m_{11}\theta_{11}^{m_{11}}}{x_1^*((x_1^*)^{m_{11}} + \theta_{11}^{m_{11}})} \frac{(x_1^*)^{m_{11}}}{(x_1^*)^{m_{11}} + \theta_{11}^{m_{11}}} \tag{7.17}$$

into equation (7.16) yields

$$-\frac{k_{11}\gamma_1}{(\gamma_1 x_1^* - s_1)^2} \frac{(x_1^*)^{m_{11}}}{(x_1^*)^{m_{11}} + \theta_{11}^{m_{11}}} + \frac{k_{11}}{\gamma_1 x_1^* - s_1} \frac{m_{11}\theta_{11}^{m_{11}}}{x_1^*((x_1^*)^{m_{11}} + \theta_{11}^{m_{11}})} \frac{(x_1^*)^{m_{11}}}{(x_1^*)^{m_{11}} + \theta_{11}^{m_{11}}} = 0, \tag{7.18}$$

which, by multiplying with $\frac{(\gamma_1 x_1^* - s_1)^2((x_1^*)^{m_{11}} + \theta_{11}^{m_{11}})^2 x_1^*}{(x_1^*)^{m_{11}} k_{11}\gamma_1}$, becomes

$$\underbrace{(x_1^*)^{m_{11}+1} - (m_{11} - 1)\theta_{11}^{m_{11}} x_1^* + m_{11}\theta_{11}^{m_{11}} \frac{s_1}{\gamma_1} = 0.}_{=:f(x_1^*, m_{11})} \tag{7.19}$$

For $0 < m_{11} \leq 1$, $f(0, m_{11}) > 0$ and for $x_1^* \geq 0$, $\partial f(x_1^*, m_{11})/\partial x_1^* \geq 0$. Thus, there is no real solution for $x_1^*$ in this case. Accordingly, cooperative interaction expressed by a Hill-coefficient $m_{11} > 1$ is necessary for a Hopf bifurcation and thus for oscillating behavior in our model.

In summary, the bifurcation analysis of the core model shows that, for each network parameter, the oscillating region is only a small interval bounded by Hopf and saddle-node bifurcations. This certainly complicates the inference of an oscillating network. It also raises the question about mechanisms stabilizing oscillating expression of cell cycle genes. However, it is possible to infer an oscillating network with our approach using the Spellman dataset, as will be shown in the following section.

## 7.3  Results on the yeast cell cycle

In this section, we show results for the yeast cell cycle and point out additional difficulties, which do not occur when analyzing simulated data, and which are thus related to the real dataset and the model. For parameter estimation of the yeast cell cycle network, we used the alpha-factor synchronization experiments of the Spellman dataset [183], which we already used for the inference of the core model in the previous chapter. Parameters $\hat{\omega}_{core}$ inferred in Chapter 6 were taken as a starting point for the optimization of the posterior distribution for the extended network. Remaining parameters were set to $s_i = 0.01$, $\gamma_i = 0.1$, $k_{ij} = 0$, $\hat{\theta}_{ij} = 1$ and $\hat{m}_{ij} = 2$. Synthesis and degradation rates were learned without prior distribution. Parameters for the prior distributions over regulation strengths were set to $\lambda = 1.3$ and $\alpha = 5$. In the first two steps of the optimization process, the prior distribution was not taken into account. Gradient descent stops when the error change is three times smaller than $10^{-3}$ or when a maximum number of 300 steps is reached. The noise level for the optimization was set to $\sigma_\xi = 0.2$.

Figure 7.17 shows the inferred network structure. The 21 edges with strongest interaction strengths are marked in bold. Bold continuous lines correspond to true positives, bold dashed lines to false positives. Thin lines indicate false negatives. 15 of 21 true regulations are revealed. These include the three regulations $x_1 \to x_1$, $x_1 \to x_2$ and $x_2 \to x_1$ of the core network, which were already fixed in advance. Figure 7.18 shows inferred courses (*dashed lines*) for all seven network components, together with the linearly interpolated experimental data (+). Our inferred model fits the amplitudes of most genes very well, whereas the oscillation periods of the experimental data is approximately 10-20 minutes longer than the period of the inferred model. The reason for this requires further investigation.
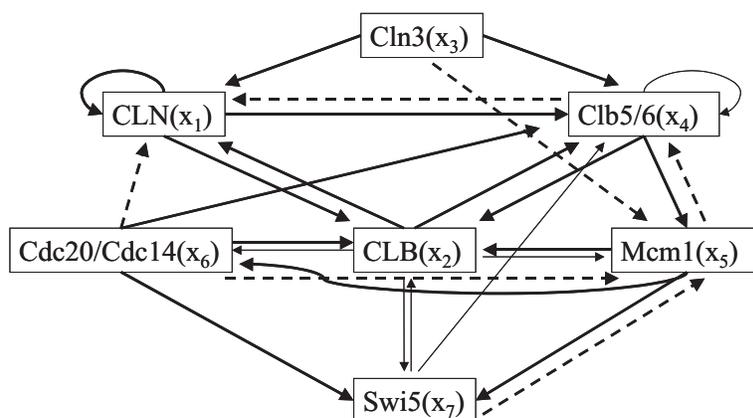
Figure 7.17: Network structure of the inferred yeast cell cycle network. The 21 regulations with the strongest interaction strengths are marked in bold. 15 of them are true positives (*bold continuous lines*), 6 are false positives (*bold dashed lines*), and *thin lines* appear in the reference network, but are not revealed in our approach.

## 7.4 Concluding remarks

Differential equations are frequently used to infer gene regulatory or, more general, bio-chemical networks. However, linear models, which have severe limitations concerning their qualitative dynamic behavior, are the most often used models for network inference. Evaluation of results frequently focuses on a comparison of the inferred interaction graph with a reference network from literature, as it was also done in Chapter 5. However, differential equation models are very detailed compared to other model classes introduced in Chapter 1. Thus, we can hope to learn more than just the interaction graph. They can also provide an explanation for the observed dynamic behavior in terms of quantitative reaction parameters. Differential equation models also have often been used for this purpose, but frequently only with models of two or three components. These models are assumed to represent very simplified core mechanisms in living systems, which determine the qualitative dynamic behavior. We motivated in Chapter 6 why a reduction to only two components can be useful to get insights into mechanisms causing qualitative behaviors. However, an interesting question is how these core models can be extended to obtain a more realistic model of the system under consideration, which includes for example more components or more interactions. Here, we presented such an extension of our core model. The aim was to infer a regulatory network which captures periodic behavior and at the same time reveals interactions between network components. For this purpose, we used the core model derived in Chapter 6, which was assumed to determine the qualitative behavior of the system, and extended this model for further regulations and components using the Bayesian approach described in Chapter 5. This approach tries to combine the advantage of differential equation models to explain dynamic behaviors and the advantage of a Bayesian approach to deal with sparse datasets. However, results on simulated data show already that, using the introduced model, it is difficult to infer a large oscillating network from 'experimen-
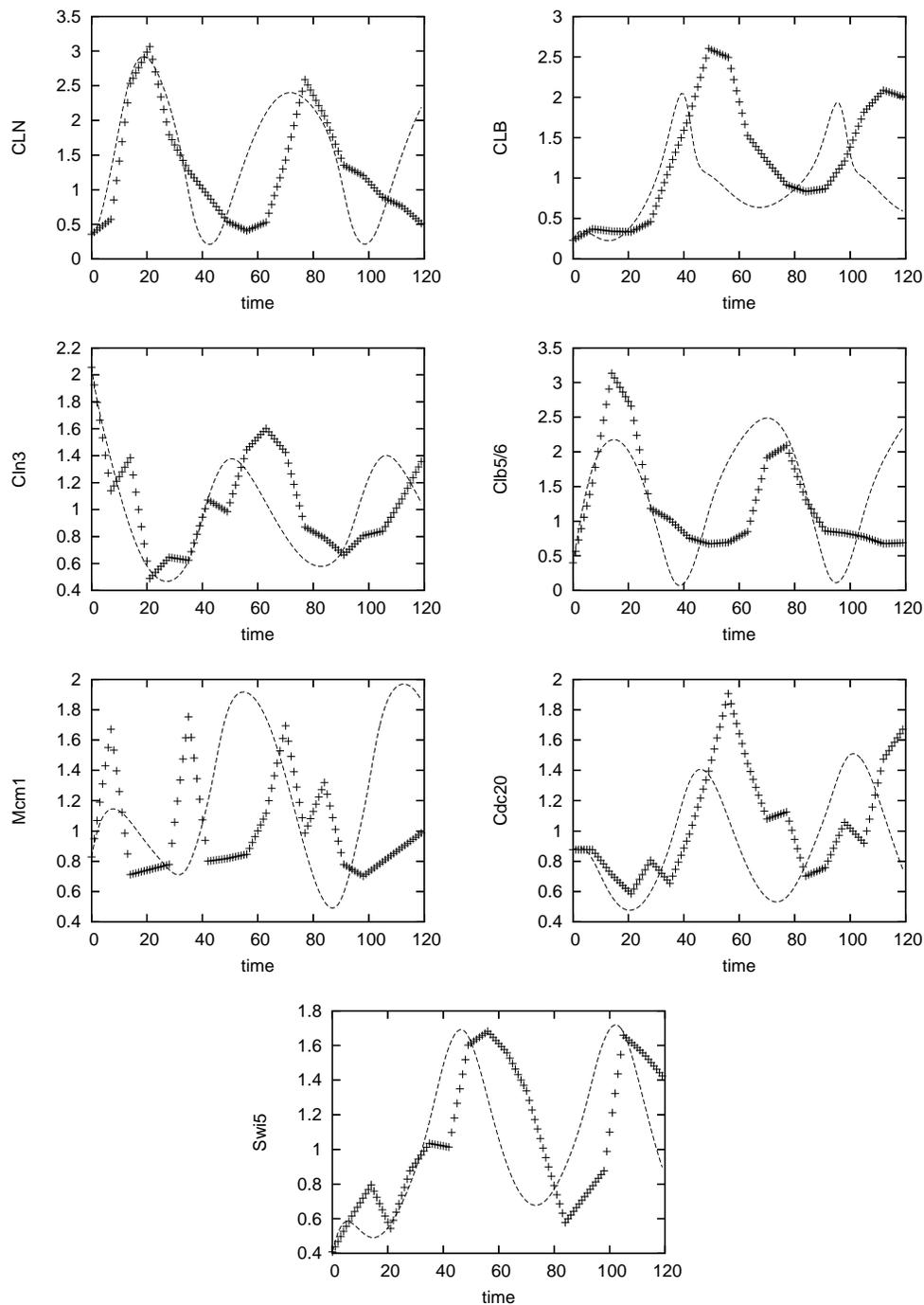
Figure 7.18: Simulated courses (*dashed lines*) with inferred model parameters of all seven genes included in our model and interpolated experimental values which were used for learning (*crosses*). Time is given in minutes.

tal' data. We are only able to capture the periodic behavior when using large datasets with a small noise level. With these datasets, the interaction graph is already perfectly reconstructed. The behavior of the core model is very sensitive to parameter changes. In order to explain this sensitivity, we applied a bifurcation analysis. Here, the parameters of the core network were consecutively used as bifurcation parameters, and the qualitative behavior of the system was analyzed with respect to variations in these parameters. We observed for all parameters that a limit cycle only exists in a small interval, which is limited by Hopf and saddle-node bifurcations. Outside this interval, the system converges to a steady state. This analysis shows that a negative feedback loop in the interaction graph is in fact a necessary condition for a stable periodic orbit, but it is by no means sufficient. The quantitative parameter values are important for periodic behavior in our model. The bifurcation diagrams provide an explanation why it is difficult to learn periodic behavior. Additionally, they give information about the dependence of the oscillation amplitude on the model parameters. Generally, within the parameter regions in which the core network oscillates, the amplitude varies in a wide range, whereas the oscillation period is relatively insensitive to parameter changes. This is a typical property of both, activator-inhibitor and substrate-depletion oscillators.

We used the microarray dataset from Spellman *et al.* [183] to infer a regulatory network for the yeast cell cycle with our approach. Here, we were able to infer an oscillating regulatory network. However, there are several problems which, together with the results of the core network analysis, raise interesting questions:

First, results are more sensitive to changes in parameters of the prior distributions used in the Bayesian approach than results for the simulated datasets. This makes inference difficult on the one hand, and it also raises doubts about the reliability of estimation results for real datasets on the other hand. These doubts affect the model, since the approach works much better on simulated data. It probably indicates that the dynamics of cell processes is much more complicated than suggested in the presented model and as can be learned from microarray data. Further mechanisms such as the interrelation of transcriptional and post-transcriptional regulation processes or transport processes are probably important to stabilize periodic behavior. Thus, it is an interesting question to what extend microarray studies alone can be used to learn something about the dynamic behavior of biochemical networks.

The objective function that was optimized in order to estimate model parameters in the Bayesian approach in Chapter 5 does not seem to be appropriate to learn the dynamic behavior of the system. The optimization problem interprets measurements of consecutive time points, $x(t)$ and $x(t + \Delta t)$, as a set of independent input-output pairs. The temporal order of all these pairs is not taken into account. However, already in Chapter 6, when inferring parameters for the core model, it turns out that it is difficult to learn oscillations with this objective function. Therefore, we introduced another objective function, which includes the temporal order of all measurements in the time series and which facilitates the learning of periodic, or any other dynamic behavior. The corresponding new

optimization problem is much harder in terms of computational costs, and it is thus not feasible for networks of more than two or three components. This raises the question how the optimization problem has to be formulated in order to learn qualitative dynamic behaviors.

A comparison of the inferred time series for the yeast genes with the inferred network structure uncovers a further problem of network inference from experimental data: The inferred model is able to reconstruct the experimentally observed courses, although the corresponding inferred interaction graph differs from the reference network. Contrary to the simulated dataset, a satisfying simulation of the dynamic behavior does not necessarily imply a correctly learned interaction graph. This can probably also be explained with the kind of data used for learning: The simulated dataset contains many short time series with different initial conditions, whereas the real dataset only represents a limit cycle, which provides less information about the underlying dynamical system. Thus, the size of the dataset that is required to get reasonable results depends considerably on the kind of data. Measurements on the system for varying conditions or experiments on mutants probably provide much more information than a single time series measured in a properly working cell.

Finally, we have seen in the bifurcation diagrams that oscillations only occur in a small region of the parameter space. They are thus sensitive to parameter changes, which makes inference difficult. On the other hand, the cell cycle, as many other biological oscillators, has to work properly for varying conditions [203]. For example, binding energies vary with temperature and pressure, and binding of transcription factors is actually a discrete stochastic process underlying fluctuations [203]. Thus, biological oscillators seem to be more robust than our core model. Which mechanisms are important for this robustness in a cell and how can we modify our model accordingly to account for these mechanisms? These questions will be taken up in the following chapter.

# Chapter 8

# Robustness of Oscillations

At the beginning of this chapter, we recapitulate results of the previous chapters that are relevant to motivate the following work. In Chapter 2 we derived a model for regulatory networks. This model is characterized by monotonous bounded regulation functions and first order degradation terms. These properties ensure that all trajectories eventually reach a bounded trapping region in the state space. Moreover, the model belongs to differential equation systems which have constant sign Jacobian matrices almost everywhere in the state space. Accordingly, we have illustrated in Chapter 6 that our model has the tendency to converge to a steady state. Circuits in the interaction graph are related to more complex dynamic behavior such as multi-stationarity and oscillations. These behaviors typically occur through a destabilization of the steady state, which can result in multiple steady states or in a limit cycle. A negative semicircuit containing at least two components is necessary for a limit cycle. In a two-component network, we need additionally a positive auto-regulation of at least one of the two components. We introduced an activator-inhibitor oscillator for the yeast cell cycle. Given parameters for this model which guarantee the existence of a limit cycle, the periodic behavior of the system is very stable, since the basin of attraction for this limit cycle is the whole state space. This is one possible way to define stability of the long-term behavior of a system. Here, the system is analyzed in the state space, and the stability of limit sets is related to the size of the basins of attraction of these sets. However, regarding the parameter estimation problem, it is convenient to introduce a different stability concept. Since initial conditions are usually specified by the experimental data used for estimation, but in turn the parameters of the model are not known, stability of dynamic behaviors should refer to the parameter space rather than to the state space. We refer to this concept of stability as *structural stability* or *robustness*. According to this, a limit set of a differential equation system is stable if the region in the parameter space in which this limit set exists is large.

Looking at the bifurcation diagrams in Chapter 7, we can imagine that an objective function used for the parameter estimation is generally smoother in regions in which the system's qualitative behavior does not change than around bifurcation values. The temporal behavior of the system, and thus also the value of the objective function, changes

abruptly, for example, at a subcritical Hopf bifurcation. This complicates parameter esti-
mation and, in case of local search methods, emphasizes the dependence of the estimation
result on the initial parameter vector $\omega_{init}$. Thus, we can expect the result $\hat{\omega}$ to be more
robust when increasing the neighborhood of $\hat{\omega}$ in which the qualitative behavior does not
change. On the other hand, this conception of robustness also relates inference results to
variations due to noise in the datasets used. Ideally, $\hat{\omega}$ should be robust with respect to
small variations in the dataset. This is the case if $\hat{\omega}$ is far away from bifurcation values.
Since the region for oscillations are rather small in our core model, structural stability
poses a problem here. Although we were able to reconstruct an oscillating model in the
previous chapter, results are structurally not very stable and depend considerably on initial
parameter vectors $\omega_{init}$ and on the datasets used. A bifurcation analysis discloses reasons
for this. This brought up interesting questions:
Which mechanisms lead to structurally stable oscillations in a cell, and how do we have to
modify our models to account for these stabilizing mechanisms?
The current chapter addresses these questions and discusses different mechanisms to in-
crease the robustness of oscillations. We illustrate ideas and concepts using the core model
derived in Chapter 6, but statements and concepts can also be transfered to other oscil-
lating regulatory network models with limit cycles emanating from Hopf bifurcations and
are not specific for the yeast cell cycle.

In Section 8.1, we explicitly model time scale differences between the temporal changes
of network components and show that these can affect both the robustness and the am-
plitude of oscillations. Section 8.2 shows that oscillations can also be made more robust
by an inclusion of time-delays. Both sections are inspired by Chen and Aihara [32], who
set up an activator-inhibitor model for a genetic regulatory system and investigated the
effect of time scale differences and time delays on the periodic behavior of this system. All
statements given in [32] refer to their two-component model, which includes time scale dif-
ferences and which is analyzed using first order perturbation theory. However, the proofs
given in [32] are based on rather general properties of their specific model and can thus
be generalized and applied to other oscillating regulatory systems as well. In particular,
contrary to [32], we do not consider time scale differences in Section 8.2.

In Section 8.3, we investigate a system of interlocked negative circuits of more than two
components. This section can be seen as an excursion towards additional difficulties when
increasing the number of variables. We use the stability theory of Liapunov in order to
show that the system has a unique steady state, which is globally attracting for a large set
of parameters. The construction of the Liapunov function is copied from Mees and Rapp
[130]. This result emphasizes again the tendency of the introduced model to converge to
a steady state. Finally, the chapter concludes with a summary and a discussion of results
in Section 8.4.

We start again with the two-component core model, which was introduced in Chapter

6 and which will be extended in Sections 8.1 and 8.2:

$$\dot{x}_1 = f_1(x) = s_1 + k_{11}\frac{x_1^2}{x_1^2 + \theta_{11}^2}\frac{1}{\theta_{12} + x_2} - \gamma_1 x_1$$
$$\dot{x}_2 = f_2(x) = s_2 - \gamma_2\frac{1}{\theta_{21}^2 + x_1^2}x_2,$$

$$(8.1)$$

with domain $E = \mathbb{R}_+^2$ and a parameter vector

$$\omega := (s_1, s_2, \gamma_1, \gamma_2, k_{11}, \theta_{11}, \theta_{12}, \theta_{21}) \in \mathbb{R}_+^8. \tag{8.2}$$

# 8.1  Different time scales - Relaxation oscillations

In Chapters 6 and 7 we have analyzed the nullclines of system (8.1). Intersections of these nullclines correspond to steady states of the system. A necessary condition for a steady state $x_s$ of our model to be unstable is $\frac{\partial f_1}{\partial x_1} = a_{11}(x_s) > 0$. In the following, we will show that this becomes a sufficient condition if the temporal change of both variables happens on different time scales. This is the case when the production and/or degradation rate of one of the components is much smaller than the corresponding rates of the second component. Examples for such differences are manifold. Consider for instance two genes which are regulated by the same transcription factor. Binding of this transcription factor to the promoter region of the first gene is highly specific (which corresponds to a small threshold value $\theta$ in the sigmoidal regulation function), whereas binding to the specific site in the promoter region of the second gene is unspecific (the threshold value which corresponds to this regulation is much higher). The transcription factor will much more often bind to the first binding site, and thus the effect on the expression of the first gene is much higher than on the second one. The protein concentration of the first gene is much more sensitive to changes in the transcription factor concentration than the second one, in particular in case that the transcription factor concentration is low. Thus, when changing the transcription factor concentration, the first gene is the fast variable and the second gene the slow variable. In general, in a chemical reaction system, different time scales can be associated with different binding affinities or reaction rates, which can also affect post-transcriptional regulations.

Subsection 8.1.1 discusses the effect of time scale differences on the eigenvalues of the Jacobian matrix $J_f(x_s)$ at a fixed point $x_s$. This concept is applied to our core model in Subsection 8.1.2. Stiffness of a system of differential equations in connection with large time scale differences is finally discussed in Subsection 8.1.3.

## 8.1.1  Linear stability analysis in two dimensions

Consider a two-dimensional model with a fast and a slow component, which is assumed to have a fixed point $x_s$. We account for time scale differences by introducing a time scale

parameter $\epsilon$, which represents the ratio of the slow and the fast time scales. Thus, the larger the difference between the two time scales, the smaller is $\epsilon$. Variable $x_1$ is assumed to represent the fast component, and our model is written as

$$
\begin{aligned}
\dot{x}_1 &= f_1(x) \\
\dot{x}_2 &= \epsilon f_2(x)
\end{aligned}
\tag{8.3}
$$

with continuously differentiable functions $f_1(x)$ and $f_2(x)$. The factor $\epsilon$ accounts for the time scale differences between these two components and is denoted *time scale parameter*. It is chosen such that the order of magnitude of $f_1(x)$ is supposed to be the same as the order of magnitude of $f_2(x)$. For small $\epsilon$, the temporal changes of $x_1$ and $x_2$ happen on different time scales. On the slow time scale $\Delta t$ appropriate to describe the change of variable $x_2$, we can apply the quasi-steady state approximation to $x_1$ and set $\dot{x}_1 \approx 0$, which was done for the binding reaction of transcription factors to DNA in Chapter 2. The change of $x_1$ has to be considered on the fast time scale, given by time steps of order $\epsilon \Delta t$. On this time scale, the change of the slow variable $x_2$ is only marginal between two time steps, such that we can set $\dot{x}_2 \approx 0$. This was also done in Chapter 2, when we considered the binding reaction of transcription factors and the DNA to derive the sigmoidal regulation function. Here, we assumed the total transcription factor concentration $[TF]_t$ to be constant.

The nullclines, given by $\dot{x}_1 = 0$ and $\dot{x}_2 = 0$, respectively, and therefore also the set of steady states, are independent of $\epsilon$ and are thus the same as in the core system without time scale differences, that is, system (8.3) with time scale parameter $\epsilon = 1$. However, their stability and hence the qualitative dynamic behavior depends on $\epsilon$.

The Jacobian matrix $J_f(x_s)$ of the steady state $x_s$ of system (8.3) is written as

$$
J_f(x_s) = \begin{pmatrix} a_{11}(x_s) & a_{12}(x_s) \\ \epsilon a_{21}(x_s) & \epsilon a_{22}(x_s) \end{pmatrix}
\tag{8.4}
$$

with eigenvalues

$$
\begin{aligned}
\lambda_{1,2}(x_s) =& \frac{tr\left(J_f(x_s)\right)}{2} \pm \sqrt{\left(\frac{tr\left(J_f(x_s)\right)}{2}\right)^2 - det\left(J_f(x_s)\right)} \\
=& \frac{a_{11}(x_s) + \epsilon a_{22}(x_s)}{2} \\
& \pm \sqrt{\left(\frac{a_{11}(x_s) + \epsilon a_{22}(x_s)}{2}\right)^2 - \left(\epsilon a_{11}(x_s) a_{22}(x_s) - \epsilon a_{12}(x_s) a_{21}(x_s)\right)}.
\end{aligned}
\tag{8.5}
$$

Now we investigate the stability of the fixed point $x_s$ for large time scale differences. In the limit $\epsilon \to 0$, we can use *singular perturbation theory* to analyze system (8.3) [32]. We

linearize the eigenvalues $\lambda_{1,2}(x_s)$ about $\epsilon = 0$:

$$\lambda_1(x_s) \quad = \quad a_{11}(x_s) + \frac{a_{12}(x_s)a_{21}(x_s)}{a_{11}(x_s)}\epsilon + \mathcal{O}(\epsilon^2) \tag{8.6}$$

$$\lambda_2(x_s) \quad = \quad \left(a_{22}(x_s) - \frac{a_{12}(x_s)a_{21}(x_s)}{a_{11}(x_s)}\right)\epsilon + \mathcal{O}(\epsilon^2). \tag{8.7}$$

For small $\epsilon$, $a_{11}(x_s)$ is the dominating term in (8.6). Thus, if $\epsilon$ is sufficiently small, the sign of $\lambda_1(x_s)$ is determined by the sign of $a_{11}(x_s)$. Moreover, $|\lambda_2(x_s)| \ll |\lambda_1(x_s)|$ in the limit $\epsilon \to 0$, since $\lambda_1(x_s) = \mathcal{O}(1)$ and $\lambda_2(x_s) = \mathcal{O}(\epsilon)$. These properties of $\lambda_1$ and $\lambda_2$ are used to draw conclusions for our model in the following subsection.

## 8.1.2 Application to our model

Our core model (8.1) has at least one fixed point $x_s$, since the $x_1$-nullcline $x_2^a(x_1)$ : $(x_1^{min}, x_1^{max}) \to \mathbb{R}_+$ is surjective, which guarantees an intersection with the $x_2$-nullcline $x_2^b(x_1) : \mathbb{R}_+ \to \mathbb{R}_+$. We have already illustrated this in Chapters 6 and 7. Including the time scale parameter $\epsilon$, our core system is written as

$$\dot{x}_1 = f_1(x) = s_1 + k_{11}\frac{x_1^2}{x_1^2 + \theta_{11}^2}\frac{1}{\theta_{12} + x_2} - \gamma_1 x_1$$

$$\dot{x}_2 = f_2(x) = \epsilon\left[s_2 - \gamma_2\frac{1}{\theta_{21}^2 + x_1^2}x_2\right]. \tag{8.8}$$

In our model (8.1), and hence also in (8.8), the product $a_{12}(x)a_{21}(x)$ is negative for all $x \in E$. This product is the weight of the negative feedback loop including both variables $x_1$ and $x_2$. Furthermore, due to the degradation term $-\gamma_2(x_1)x_2$, $a_{22}(x) < 0$ everywhere in the state space. Thus, the condition $a_{11}(x_s) < 0$ implies that $tr(J_f(x_s)) < 0$ and $det(J_f(x_s)) > 0$. In this case, the real parts of both eigenvalues are negative, and $x_s$ is stable independent of $\epsilon$. Hence, in our system (8.1), $a_{11}(x_s) > 0$ is necessary for the occurrence of a Hopf bifurcation and thus for the existence of a stable limit cycle.

For small $\epsilon$, $a_{11}(x_s)$ is the dominating term in (8.6). Thus, if $\epsilon$ is sufficiently small, then $a_{11}(x_s) > 0$ implies $\lambda_1(x_s) > 0$, which states that in the limit $\epsilon \to 0$, $a_{11}(x_s) > 0$ is indeed a sufficient condition for $x_s$ to be unstable. As a consequence, whenever the core system has a single fixed point between the minimum A and the maximum B of the $x_1$-nullcline (Figure 6.10), this fixed point can be destabilized and hence oscillating behavior can be induced by decreasing the time scale parameter $\epsilon$.

To illustrate the influence of $\epsilon$ on system (8.3), we apply a bifurcation analysis with bifurcation parameter $\epsilon$ and model parameters

$$\hat{\omega}_{core} = (0.038, 0.072, 0.38, 0.0072, 3.8, 1, 1, 0.1). \tag{8.9}$$

We have already used this parameter set in the bifurcation analysis in Chapter 7. For these parameters and an $\epsilon = 1$, the system has a single steady state at $x_s = (0.66, 4.41)$.
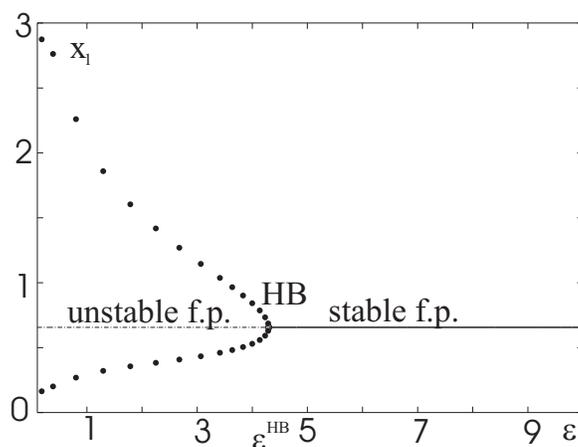
Figure 8.1: Bifurcation diagram for system (8.1) with time scale parameter $\epsilon$ and model parameters given in equation (8.9). The system undergoes a supercritical Hopf bifurcation at $\epsilon^{HB} = 4.3$.

The bifurcation diagram is shown in Figure 8.1. The steady state $x_s$ of the system is independent of $\epsilon$ and thus parallel to the $x$-axis. However, its stability depends on $\epsilon$. A supercritical Hopf bifurcation occurs at $\epsilon^{HB} \approx 4.3$. For $\epsilon < \epsilon^{HB}$, $x_s$ is unstable and the system exhibits stable oscillations. The smaller $\epsilon$, the larger is the oscillation amplitude. When $\epsilon > \epsilon^{HB}$, $x_s$ becomes globally stable.

Figure 8.2 shows the long-term behavior of the system for different values of $\epsilon$. The limit cycle and the nullclines of the system are shown on the left hand side, corresponding courses for variable $x_1$ are shown on the right hand side. The larger $\epsilon$, the smaller are amplitude and period of the oscillation. For large time scale differences, represented by $\epsilon = 0.1$ in Figure 8.2, the system exhibits so-called *relaxation oscillations*: It moves slowly along the $x_1$-nullcline where $x_1$ is in a quasi-steady state, and the system is determined by the dynamics of $x_2$. At the points where the steady state of $x_1$ vanishes, the system quickly 'jumps' to the new steady state. The system is determined by the fast time scale during this transition. This is also reflected in Figure 8.2: The increase of variable $x_1$ from its lowest to its highest value is very fast, as can be seen in the course on the right hand side for $\epsilon = 0.1$. The slow component $x_2$ on the other hand does not change much during this transition, indicated by the course of the limit cycle for $\epsilon = 0.1$ in the Figure on the left hand side, which proceeds almost parallel to the $x_1$-axis during this transition. Subsequently, the system evolves along the $x_1$-nullcline, where $x_1$ slowly decreases and $x_2$ increases. When the system reaches the local maximum of the $x_1$-nullcline, the stable steady state for $x_1$ vanishes when $x_2$ increases further, and the system undergoes a second fast transition during which $x_1$ decreases.
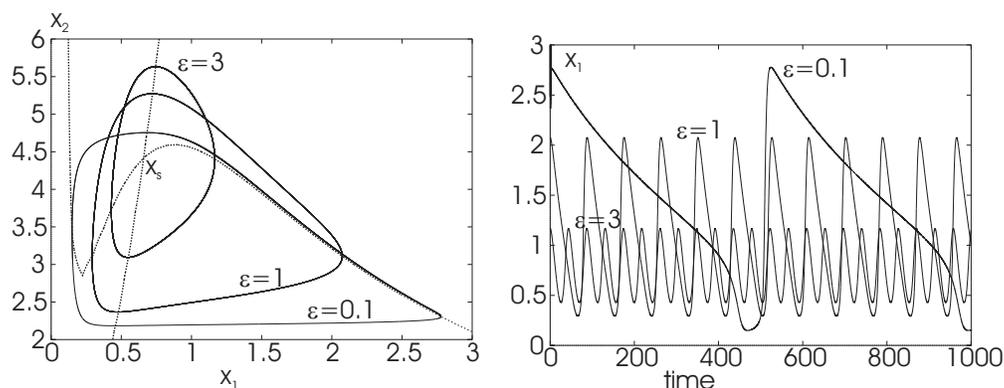
Figure 8.2: Dependence of the amplitude and the period of the oscillations on the time scale parameter $\epsilon$. **Left:** Limit cycles and nullclines of system (8.1) in the state space for different time scale parameters $\epsilon = 0.1, 1, 3$. **Right:** corresponding courses of component $x_1$. The smaller $\epsilon$, the smaller are amplitude and period of the oscillations.

### 8.1.3 Stiffness due to time scale differences

Large time scale differences can lead to *stiff differential equation systems.* Stiffness, similar to the stability of a fixed point, refers to properties of real parts of eigenvalues of the Jacobian matrix $J_f(x)$, which is constant only for linear systems. Accordingly, the term stiffness is only 'globally' defined for linear differential equations. Stiffness refers to the ratio of the real parts of the smallest and the largest eigenvalue. A linear system $\dot{x}(t) = Ax(t)$ is said to be stiff, if all real parts of eigenvalues of $A$ are negative and differ in several orders of magnitude, that is, if this ratio is $\gg 1$,

$$\frac{\max_{\lambda \in \Lambda(A)} |\Re(\lambda)|}{\min_{\lambda \in \Lambda(A)} |\Re(\lambda)|} \gg 1. \tag{8.10}$$

Here, $\Lambda(A)$ is the set of eigenvalues of the matrix $A$, called the *spectrum* of $A$. In Chapter 2 we have seen that the solution of the linear system is a linear combination of exponential functions $e^{\lambda t}$. Thus, a trajectory of the system rapidly moves towards the linear subspace spanned by the eigenvector corresponding to the eigenvalues with large absolute value of the real parts, and then slowly moves on this subspace towards the fixed point $x_s = 0$. The system is first determined by the fast time scale until the fast components are in a quasi-steady state. Then, the system evolves on the slow time scale. Numerical integration methods with a fixed step size $\Delta t$ are not appropriate for such stiff systems, since a suitable $\Delta t$ for the slow movement is larger than a suitable $\Delta t$ for the fast movement of the system.

For non-linear systems, stiffness is not globally defined, but refers to the linearization $\dot{x} \approx J_f(x^*)(x - x^*)$ about a state $x^*$. In our general model introduced in Chapter 2 and also in the core model (8.1), stiffness is very sensitive to changes of the Hill-coefficients. A

small increase of the Hill-coefficient $m_{ij}$ in a regulation function

$$r_{ij}(x_j) \propto \frac{x_j^{m_{ij}}}{x_j^{m_{ij}} + \theta_{ij}^{m_{ij}}} \tag{8.11}$$

leads to a large change of the derivative $\partial r_{ij}(x_j)/\partial x_j$ around the threshold value $\theta_{ij}$. This affects the entry $a_{ij}$ of the Jacobian matrix $J_f(x)$ and hence the eigenvalues of the system. The sensitive dependence of the eigenvalues on the Hill-coefficients $m_{ij}$ and the threshold values $\theta_{ij}$ might be the reason for the observed numerical problems in Chapter 5 when including both parameters as variables to be optimized into the conjugate gradient descent.

**Summary**

We have investigated how the stability of a fixed point $x_s$ of a planar system depends on time scale differences between the two variables. In the limit of large time scale differences, which corresponds to $\epsilon \to 0$ in our model, we can linearize the eigenvalues of the Jacobian matrix $J_f(x_s)$ about $\epsilon$, which differ in one order of magnitude. Thus, large time scale differences are related to stiffness of the system. The dynamic behavior of our core model depends on this time scale parameter. We demonstrated this for a fixed parameter vector $\hat{\omega}_{core}$. Here, both oscillation amplitude and period increase when $\epsilon$ decreases. Moreover, the system undergoes a Hopf bifurcation at which the unstable fixed point $x_s$ becomes globally stable. Finally, we could show that the condition $a_{11}(x_s) > 0$, which is in our core model necessary to destabilize a stable fixed point, becomes a sufficient condition in the limit $\epsilon \to 0$.

## 8.2 Time-delays

In this section, we account for time-delays, which refer, for example, to transcription, translation and translocation processes in a cell. Time-delays become important in biochemical networks that include regulations on transcriptional and post-transcriptional level. Gene expression is a slow process compared to a chemical modification of a protein such as phosphorylation. This can be described by a time-delay $\tau$ accounting for the duration between binding of a transcription factor to its binding site and the effect it has on the concentration of the corresponding protein.

Time-delays have been shown to efficiently cause oscillations in biological systems (see for example [23, 32, 167, 191, 194], [38] and references therein). Similar to a time scale parameter $\epsilon$, a time-delay $\tau$ can destabilize a stable steady state $x_s$ of a system via a Hopf bifurcation, since the eigenvalues of the Jacobian matrix $J_f(x_s)$ depend on $\tau$ [82, 89, 111]. We start this section with an introduction about linear stability analysis of a delay differential equation system in Subsection 8.2.1. The concepts are used to analyze the stability of fixed points of our core model (8.1). In Subsection 8.2.2, we show that time-delays can in fact cause a Hopf bifurcation in our system and hence lead to periodic

behavior. An introduction to delay differential equations is given in [82, 89, 111]. Parts of the contents in Subsection 8.2.1 can be found in [111].

## 8.2.1 Linear stability analysis in delay differential equations

A delay differential equation (DDE) is written as

$$\dot{x}(t) = f(x(t), z(t)), \tag{8.12}$$

where $z(t)$ is a functional of the past history of $x(t)$ [194]. We concentrate on discrete time-lags of the form

$$z(t) = x(t - \tau). \tag{8.13}$$

In contrast, for a distributed time-lag, $z(t)$ is a weighted integral over previous states of the system. In the following, we use the common short notations $x$ for $x(t)$ and $x^\tau$ for $z(t)$.

In order to get a unique solution of an ordinary differential equation $\dot{x} = f(x)$, $x \in \mathbb{R}^n$ and $f \in \mathcal{C}^1$, one has to specify an initial state vector $x(0) \in \mathbb{R}^n$ of $n$ components. In contrast, in order to solve a DDE system with discrete time-lag of the form (8.13), one has to specify an initial function $f_0(t) : [-\tau, 0] \to \mathbb{R}^n$, which describes the behavior of the system in the time interval $[-\tau, 0]$. Thus, a DDE system maps functions defined on a time interval $[t - \tau, t]$ onto functions on the interval $[t, t + \tau]$ [111]. A global analysis of a DDE is more difficult than of the corresponding ODE with time-delay $\tau = 0$. However, some analysis techniques of finite-dimensional systems can be adapted to infinite-dimensional systems. In particular, a DDE and its corresponding ODE have the same set of steady states, and we can apply the Hartman-Grobman Theorem to analyze the stability of a steady state $x_s$ in terms of the real parts of its eigenvalues for both systems [82]. For this, the system has to be linearized about $x_s$. The response to a small perturbation $\Delta x(t)$ of the system in the state $x_s$, which persists over a time interval of length $\tau$, is described by

$$\frac{d}{dt}\Delta x(t) = f(x_s + \Delta x, x_s + \Delta x^\tau) \approx J_f(x_s)\Delta x + J_f^\tau(x_s)\Delta x^\tau. \tag{8.14}$$

Here, $\Delta x = x - x_s$ is the perturbation of the system at time $t$, and $\Delta x^\tau = x^\tau - x_s$ denotes the perturbation at time $t - \tau$. The Jacobian matrices $J_f(x_s)$ and $J_f^\tau(x_s)$ are defined as

$$J_f(x_s) \quad := \quad \left( \frac{\partial f_i(x, x^\tau)}{\partial x_j} \bigg|_{x_s} \right)_{i,j=1,\dots,n} =: (a_{ij}(x_s))_{i,j=1,\dots,n} \tag{8.15}$$

$$\text{and} \quad J_f^\tau(x_s) \quad := \quad \left( \frac{\partial f_i(x, x^\tau)}{\partial x_j^\tau} \bigg|_{x_s} \right)_{i,j=1,\dots,n} =: \left( a_{ij}^\tau(x_s) \right)_{i,j=1,\dots,n}. \tag{8.16}$$

Inserting the ansatz

$$\Delta x = e^{\lambda t} v \tag{8.17}$$

into (8.14) leads to

$$\lambda v = \left[ J_f(x_s) + e^{-\lambda \tau} J_f^\tau(x_s) \right] v. \tag{8.18}$$

Thus, $v$ is an eigenvector of the matrix $\left[J_f(x_s) + e^{-\lambda\tau}J_f^\tau(x_s)\right]$ with associated eigenvalue $\lambda$, which is characterized by the characteristic equation

$$\chi(\lambda) = det\left[J_f(x_s) + e^{-\lambda\tau}J_f^\tau(x_s) - \lambda I\right] = 0. \tag{8.19}$$

Different from the characteristic equation of an ODE, which is a polynomial in $\lambda$, the characteristic equation of a DDE contains exponential functions, here the term $e^{-\lambda\tau}J_f^\tau(x_s)$, and can have an infinite number of roots [111].

We consider the characteristic polynomial $\chi(\lambda)$ for a steady state $x_s$ of a two-component system of the form

$$\begin{aligned}
\dot{x}_1 &= f_1(x_1, x_2^\tau) \\
\dot{x}_2 &= f_2(x_1, x_2)
\end{aligned} \tag{8.20}$$

with a variable $x_1$ that depends on the state of variable $x_2$ at a previous time $t - \tau$. In biochemical networks, this is for example the case when protein concentrations are regulated by binding of transcription factors to their promoter regions. Here, the time-delay $\tau$ corresponds to the time between binding of the transcription factors and the effect it has on the concentration of the active protein. In eukaryotic cells, such time-delays can also be used to incorporate transport or diffusion processes into the model.

For system (8.20), the Jacobian matrices $J_f(x_s)$ and $J_f^\tau(x_s)$ in equation (8.19) are given by

$$J_f = \begin{pmatrix} \left.\frac{\partial f_1(x_1, x_2^\tau)}{\partial x_1}\right|_{x_s} & \left.\frac{\partial f_1(x_1, x_2^\tau)}{\partial x_2}\right|_{x_s} \\ \left.\frac{\partial f_2(x_1, x_2)}{\partial x_1}\right|_{x_s} & \left.\frac{\partial f_2(x_1, x_2)}{\partial x_2}\right|_{x_s} \end{pmatrix} = \begin{pmatrix} a_{11} & 0 \\ a_{21} & a_{22} \end{pmatrix} \tag{8.21}$$

$$J_f^\tau = \begin{pmatrix} \left.\frac{\partial f_1(x_1, x_2^\tau)}{\partial x_1^\tau}\right|_{x_s} & \left.\frac{\partial f_1(x_1, x_2^\tau)}{\partial x_2^\tau}\right|_{x_s} \\ \left.\frac{\partial f_2(x_1, x_2)}{\partial x_1^\tau}\right|_{x_s} & \left.\frac{\partial f_2(x_1, x_2)}{\partial x_2^\tau}\right|_{x_s} \end{pmatrix} = \begin{pmatrix} 0 & a_{12}^\tau \\ 0 & 0 \end{pmatrix}. \tag{8.22}$$

Here, we have dropped the dependence of the matrix entries $a_{ij}$ on the steady state $x_s$.

Inserting these matrices into (8.19) leads to

$$\chi(\lambda) = \underbrace{(a_{11} - \lambda)(a_{22} - \lambda)}_{=:f(\lambda)} - \underbrace{e^{-\lambda\tau}a_{12}^\tau a_{21}}_{=:g_\tau(\lambda)} = 0. \tag{8.23}$$

A zero $\lambda$ of $\chi(\lambda)$ is given as the intersection of the two functions $f(\lambda)$ and $g_\tau(\lambda)$. In order to investigate the influence of a time-delay $\tau > 0$ in comparison to the corresponding ordinary differential equation with $\tau = 0$ on the stability of a fixed point $x_s$, we have to consider how the signs of the real parts of $\lambda$ depend on $\tau$. For this, we write $g_\tau(\lambda)$ as a function $g(\lambda, \tau)$ of the two variables $\lambda$ and $\tau$ and calculate the derivative of equation (8.23) with respect to $\lambda$:

$$\frac{df(\lambda)}{d\lambda} - \frac{dg(\lambda, \tau)}{d\lambda} = 0 \tag{8.24}$$

Inserting

$$\frac{df(\lambda)}{d\lambda} = 2\lambda - (a_{11} + a_{22}) \tag{8.25}$$

$$\text{and} \quad \frac{dg(\lambda,\tau)}{d\lambda} = \frac{\partial g(\lambda,\tau)}{\partial\tau} \cdot \frac{d\tau}{d\lambda} + \frac{\partial g(\lambda,\tau)}{\partial\lambda}$$

$$= -\lambda a_{12}^{\tau} a_{21} e^{-\lambda\tau} \left(\frac{d\tau}{d\lambda}\right) - \tau a_{12}^{\tau} a_{21} e^{-\lambda\tau} \tag{8.26}$$

$$= e^{-\lambda\tau} a_{12}^{\tau} a_{21} \left[ -\lambda\left(\frac{d\tau}{d\lambda}\right) - \tau \right] \tag{8.27}$$

into (8.24) and resolving for the derivative $d\tau/d\lambda$ leads to

$$\frac{d\tau}{d\lambda} = \frac{-2\lambda + (a_{11} + a_{22})}{\lambda a_{12}^{\tau} a_{21}} e^{\lambda\tau} - \frac{\tau}{\lambda}. \tag{8.28}$$

Since we are interested in the change of $\Re(\lambda)$ in dependence of $\tau$, described by $d\Re(\lambda)/d\tau$, we consider the real parts of both sides in equation (8.28), which have to be equal,

$$\Re\left[\frac{d\tau}{d\lambda}\right] = \Re\left[\frac{-2\lambda + (a_{11} + a_{22})}{\lambda a_{12}^{\tau} a_{21}} e^{\lambda\tau} - \frac{\tau}{\lambda}\right]. \tag{8.29}$$

Expressing the derivative $d\lambda/d\tau$ in polar corrdinates, $d\lambda/d\tau := R\exp(i\Phi)$, the real part of the left hand side of (8.28) evolves to

$$\Re\left[\frac{d\tau}{d\lambda}\right] = \Re\left[\left(\frac{d\lambda}{d\tau}\right)^{-1}\right] = \Re\left[\frac{1}{Re^{i\phi}}\right] = \frac{1}{R^2}\Re\left[Re^{i\phi}\right]$$

$$= \frac{1}{\left|\frac{d\lambda}{d\tau}\right|^2}\Re\left[\frac{d\lambda}{d\tau}\right] = \frac{1}{\left|\frac{d\lambda}{d\tau}\right|^2}\frac{d\Re(\lambda)}{d\tau}. \tag{8.30}$$

Taking the real part of the right hand side of equation (8.28), we obtain the following relation:

$$\Re\left[\frac{-2\lambda+(a_{11}+a_{22})}{\lambda a_{12}^{\tau} a_{21}} e^{\lambda\tau} - \frac{\tau}{\lambda}\right] \qquad \Big/ \cdot \frac{\bar{\lambda}}{\bar{\lambda}}$$

$$= \Re\left[\frac{-2\lambda\bar{\lambda}+(a_{11}+a_{22})\bar{\lambda}}{\lambda\bar{\lambda} a_{12}^{\tau} a_{21}} e^{\lambda\tau} - \frac{\tau\bar{\lambda}}{\lambda\bar{\lambda}}\right] \qquad \Big/ \lambda\bar{\lambda} = |\lambda|^2$$

$$= \frac{1}{|\lambda|^2}\Re\left[\frac{-2|\lambda|^2+(a_{11}+a_{22})\bar{\lambda}}{a_{12}^{\tau} a_{21}} e^{\lambda\tau} - \tau\bar{\lambda}\right]$$

$$= \frac{1}{|\lambda|^2}\left(\frac{1}{a_{12}^{\tau} a_{21}}\Re\left[\left(-2|\lambda|^2 + (a_{11}+a_{22})\bar{\lambda}\right)e^{\lambda\tau}\right] - \tau\Re(\bar{\lambda})\right) \tag{8.31}$$

Inserting (8.30) and (8.31) into (8.29) and multiplying both sides by $\left|\frac{d\lambda}{d\tau}\right|^2$, the derivative $d\Re(\lambda)/d\tau$ is given by

$$\frac{d\Re(\lambda)}{d\tau} = \underbrace{\frac{\left|\frac{d\lambda}{d\tau}\right|^2}{|\lambda|^2}}_{=:c>0} \cdot \left(\frac{1}{a_{12}^{\tau} a_{21}}\Re\left[\left(-2|\lambda|^2 + (a_{11}+a_{22})\bar{\lambda}\right)e^{\lambda\tau}\right] - \tau\Re(\bar{\lambda})\right). \tag{8.32}$$

Inserting $\lambda = iv$ into (8.32), we show that this derivative is positive for all $\lambda$ in a neighborhood of the imaginary axis:

$$\frac{d\Re(iv)}{d\tau} = \frac{c}{a_{12}^\tau a_{21}} \left[-2v^2 \cos(v\tau) + (a_{11} + a_{22})v \sin(v\tau)\right]. \tag{8.33}$$

The sin- and cos-terms can be eliminated by calculating the real and imaginary parts of $\chi(iv)$ (equation (8.23)), which both have to become zero, and resolving for $\cos(v\tau)$ and $\sin(v\tau)$, respectively:

$$\Re(\chi(iv)) = 0 \quad \Rightarrow \quad \cos(v\tau) = \frac{a_{11}a_{22} - v^2}{a_{12}^\tau a_{21}} \tag{8.34}$$

$$\Im(\chi(iv)) = 0 \quad \Rightarrow \quad \sin(v\tau) = \frac{v(a_{11} + a_{22})}{a_{12}^\tau a_{21}} \tag{8.35}$$

Finally, we get the following expression for an eigenvalue $\lambda = iv$ on the imaginary axis:

$$\frac{d\Re(iv)}{d\tau} = \frac{c}{(a_{12}^\tau a_{21})^2} \left[2v^4 + v^2(a_{11}^2 + a_{22}^2)\right] > 0 \tag{8.36}$$

This is a very nice result. It states that if the time-delay $\tau$ in system (8.20) is increased and causes an eigenvalue $\lambda$ of the Jacobian matrix $J_f(x_s)$ to cross the imaginary axis, this crossing always happens from left to right. Hence, an unstable fixed point $x_s^u$ of an ordinary differential equation can never be stabilized through a time-delay $\tau$. However, a fixed point $x_s$ that is stable in the ODE system can become unstable through a time-delay.

## 8.2.2  Application to our model

We include a time-delay $\tau$ into our core model (8.1) and show how it influences the behavior of the system. Variable $x_1$ is assumed to depend on the state of variable $x_2$ at a previous time point $x_2(t - \tau)$ (Figure 8.3):

$$\begin{aligned}
\dot{x}_1 &= f_1(x_1, x_2^\tau) = s_1 - \gamma_1 x_1 + k_{11}\frac{x_1^2}{x_1^2 + \theta_{11}^2}\frac{1}{\theta_{12} + x_2^\tau} \\
\dot{x}_2 &= f_2(x_1, x_2) = s_2 - \gamma_2\frac{x_2}{x_1^2 + \theta_{21}^2}
\end{aligned} \tag{8.37}$$

Figure 8.4 shows the influence of $\tau$ on the limit cycle in the state space for parameter $\hat{\omega}_{core}$ given in equation (8.9). Initial conditions were set to $(x_1, x_2) = (0,0)$ for $t \in [-\tau, 0]$. The amplitudes of both variables increase with increasing $\tau$. Corresponding time courses for both variables are shown in Figure 8.5. It can be seen that also the oscillation period increases with increasing delay $\tau$.

Next, we demonstrate that a time-delay $\tau > 0$ can indeed destabilize a stable fixed point $x_s$ in our model by causing two complex conjugate eigenvalues to cross the imaginary
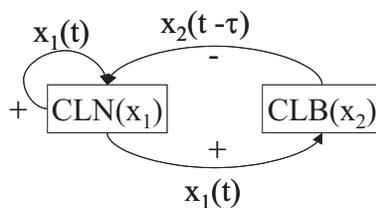
Figure 8.3: Interaction graph of the two-component model (8.8). Variable $x_1$ depends on its own state and on the state of $x_2$ at time $t - \tau$. Variable $x_2$ is negatively influenced by $x_1$.
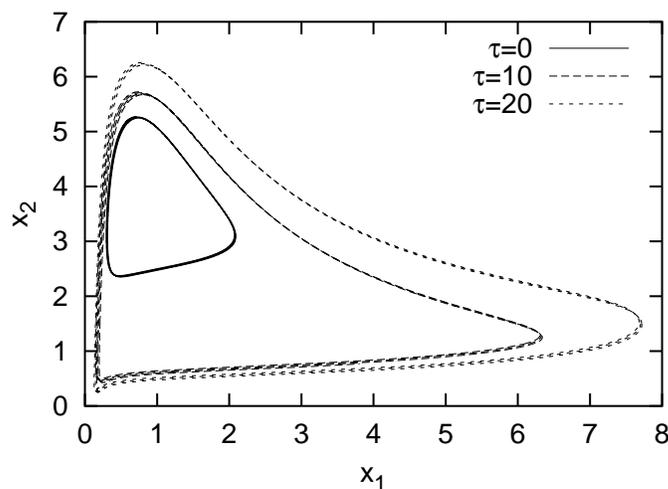


Figure 8.4: Effect of the time-delay $\tau$ in system (8.37) for values $\tau = 0, 10, 20$. Initial conditions were set to $(x_1, x_2) = (0, 0)$ for $t \in [-\tau, 0]$. The oscillation amplitude increases with increasing time-delay $\tau$. Transients are not shown.
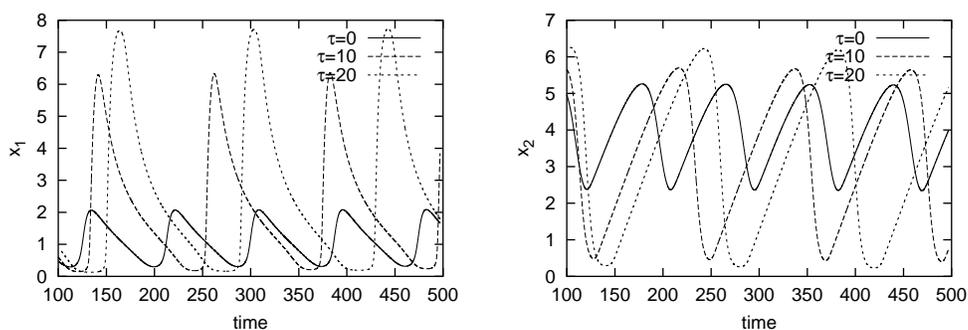


Figure 8.5: Effect of the time-delay $\tau$ in system (8.37) on the courses of variables $x_1$ (*left*) and $x_2$ (*right*). The oscillation period and the amplitude increase with increasing parameter $\tau$. Transients are not shown.
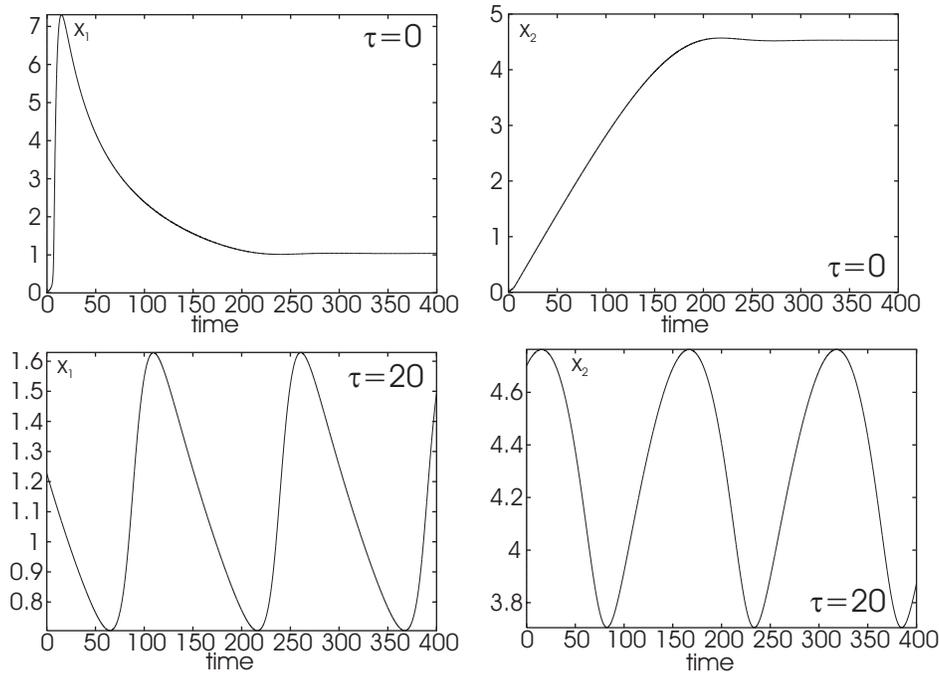
Figure 8.6: A time-delay can destabilize a stable fixed point $x_s$ of a planar system and can lead to sustained oscillations. Here: Convergence of system (8.37) for $\tau = 0$ (*top*) and periodic behavior for $\tau = 20$ (*bottom*). Parameters are given in equation (8.9), $s_2$ was changed to $s_2 = 0.03$. Initial conditions were set to $(x_1, x_2) = (0, 0)$ for $t \in [\tau, 0]$ in both simulations. In the lower figures, the transients are not shown.

axis from left to right, which corresponds to a Hopf bifurcation. For this, we set the synthesis rate $s_2$ to $s_2 = 0.03$, which causes the system to converge to a stable fixed point $x_s = (1.04, 4.53)$. The corresponding courses of $x_1$ and $x_2$ are shown in Figure 8.6 (*top*). For $\tau = 20$, $x_s$ is unstable and the system shows periodic behavior (Figure 8.6 (*bottom*)). Thus, there is a critical time-delay $0 < \tau_{crit} < 20$ at which $x_s$ looses its stability. The condition $a_{11} > 0$ can also be overcome by a time-delay $\tau$. This means, positive auto-regulation of one of the two components is no longer necessary for oscillations in DDEs. In fact, $a_{11}(x_s) < 0$ for the parameters used in the above described example. This can be seen by calculating $a_{11}(x_s)$ and inserting the values given in equation (8.9) and the fixed point $x_s = (1.04, 4.53)$:

$$a_{11}(x_s) = \frac{\partial f_1(x_1, x_2^\tau)}{\partial x_1}\bigg|_{x_s} = -\gamma_1 + k_{11}\frac{2x_{1,s}\theta_{11}^2}{(x_{1,s}^2 + \theta_{11}^2)^2}\frac{1}{\theta_{12} + x_{2,s}} = -5.01 \cdot 10^{-2} \qquad (8.38)$$

**Summary**
In this Section, we have shown that time-delays can destabilize a fixed point $x_s$ of a planar system. Applying these results to the core model, we demonstrated that amplitude and period of the oscillation increase with increasing time-delay. Moreover, the condition

$a_{11} > 0$ required for a Hopf bifurcation in the core model can be overcome by a critical time-delay $\tau^{crit}$, whose value depends on the model parameters $\hat{\omega}_{core}$. We concluded that the inclusion of a time-delay $\tau$ is an efficient way to increase robustness of oscillations.

## 8.3  An excursion to higher dimensions

This section shall give an insight how higher dimensional systems can be analyzed. Here again, we concentrate on the determination of fixed points and a method to analyze their stability using *Liapunov functions*.

We consider the following system, which corresponds to the general additive model derived in Chapter 2 with an interaction graph shown in Figure 8.7:

$$
\begin{aligned}
\dot{x}_1 &= s_1 + k_{1,1}\frac{x_1^{m_{1,1}}}{x_1^{m_{1,1}} + \theta_{1,1}^{m_{1,1}}} + k_{1,n}\frac{x_n^{m_{1,n}}}{x_n^{m_{1,n}} + \theta_{1,n}^{m_{1,n}}} - \gamma_1 x_1 \\
&=: g_1(x_1, x_n) - \gamma_1 x_1 \\
\dot{x}_i &= s_i + k_{i,i}\frac{x_i^{m_{i,i}}}{x_i^{m_{i,i}} + \theta_{i,i}^{m_{i,i}}} + k_{i,i-1}\frac{x_{i-1}^{m_{i,i-1}}}{x_{i-1}^{m_{i,i-1}} + \theta_{i,i-1}^{m_{i,i-1}}} + k_{i,n}\frac{x_n^{m_{i,n}}}{x_n^{m_{i,n}} + \theta_{i,n}^{m_{i,n}}} - \gamma_i x_i \\
&=: g_i(x_{i-1}, x_i, x_n) - \gamma_i x_i \qquad i = 2, \ldots, n - 1 \\
\dot{x}_n &= s_n + k_{n,n}\frac{x_n^{m_{n,n}}}{x_n^{m_{n,n}} \theta_{n,n}^{m_{n,n}}} + k_{n,n-1}\frac{x_{n-1}^{m_{n,n-1}}}{x_{n-1}^{m_{1,n-1}} + \theta_{n,n-1}^{m_{n,n-1}}} - \gamma_n x_n \\
&=: g_n(x_{n-1}, x_n) - \gamma_n x_n
\end{aligned}
\tag{8.39}
$$

with $s_i, \gamma_i > 0$, $k_{i,i}, k_{i,n} \leq 0$ for $i = 1, \ldots, n$, $k_{i,i-1} > 0$ for $i = 2, \ldots, n$ and $k_{1,n} < 0$. Moreover, in order to restrict the domain of system (8.39) to be $\mathbb{R}_+^n$, we set $|s_1| > |k_{1,n}|$, $|s_2| > |k_{j,n}|$ and $|s_n| > |k_{n,n}|$. We will also use the short hand notation

$$
\dot{x} = g(x) - Gx, \quad x \in \mathbb{R}_+^n, \tag{8.40}
$$

with $g : \mathbb{R}_+^n \to \mathbb{R}_+^n$, $g(x) := (g_1, \ldots, g_n)$ and $G$ is the $n \times n$ diagonal matrix which contains the degradation rates on the diagonal, $G := diag(\gamma_i)$.

The interaction graph in Figure 8.7 consists of interlocked negative circuits, each of which contains exactly one negative regulation. The conditions for the parameters state that the weight of edge $e_{1,n}$ is non-zero, $w_{e_{1,n}} \neq 0$, whereas the remaining inhibitions are allowed to have weight 0. The same holds for all auto-regulations, which have to be non-positive, $w_{e_{i,i}} \leq 0$.

In Chapter 2, we have already shown the existence of a trapping region for system (8.40). Here, lower and upper bounds are given by

$$
\begin{array}{ll}
x_1^{min} = \frac{1}{\gamma_1}(s_1 + k_{1,1} + k_{1,n}) & x_1^{max} = \frac{s_1}{\gamma_1} \\
x_i^{min} = \frac{1}{\gamma_j}(s_i + k_{i,i} + k_{i,n}) & x_i^{max} = \frac{1}{\gamma_i}(s_i + k_{i,i-1}) \\
x_n^{min} = \frac{1}{\gamma_n}(s_n + k_{n,n}) & x_n^{max} = \frac{1}{\gamma_n}(s_n + k_{n,n-1}).
\end{array}
\tag{8.41}
$$
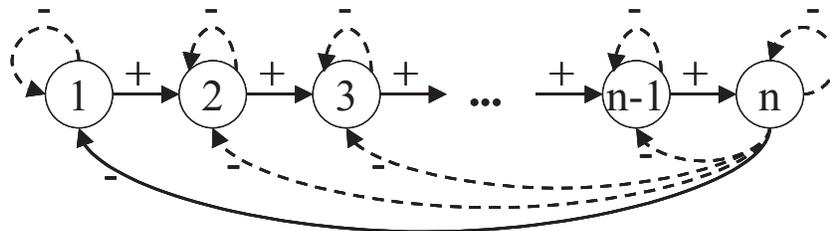
Figure 8.7: Interaction graph of multiple interlocked negative circuits. We describe this system by the general model derived in Chapter 2. The corresponding differential equation system is given in (8.39), and as a short version in (8.40). Continuous lines have non-zero weights, the weights of the dashed lines are also allowed to be zero.

In the following, we show that system (8.40) has a unique equilibrium $x_s \in \mathbb{R}_+^n$ within this trapping region. This equilibrium is globally stable for a large region in the parameter space. As we have seen in Chapter 6, uniqueness of $x_s$ also follows from the fact that the interaction graph does not contain positive circuits. To show that $x_s$ is globally stable, we will construct an appropriate Liapunov function for this system. Its existence implies that no periodic solution can exist [130]. Here, we will also see that periodic behavior is promoted by slow degradation processes. The proofs shown here are adapted to our system from Mees and Rapp [130], who give general results for multiple loop feedback inhibition systems.

We will need the concept of Liapunov functions and understand how they are related to the stability of a fixed point $x_s$ of a system $\dot{x} = f(x)$. This is explained in Subsection 8.3.1. The existence of a unique fixed point is shown in Subsection 8.3.2. Finally, in Subsection 8.3.3, we present a Liapunov function to investigate the stability of this unique fixed point.

## 8.3.1   Liapunov functions

The Hartman-Grobman Theorem, which was introduced in Chapter 2, allows to characterize the stability of steady states in terms of eigenvalues of the linearization about these fixed points. This is only possible if the steady state $x_s$ is hyperbolic, that is, all eigenvalues of the Jacobian matrix $J_f(x_s)$ have eigenvalues $\lambda$ with non-zero real part, $\Re(\lambda) \neq 0$. *Liapunov's method* is an alternative method to investigate the stability of a fixed point $x_s$, which does not require to calculate the eigenvalues of $J_f(x_s)$ and is also applicable for non-hyperbolic fixed points. The method relies on finding a positive definite function $V : U \rightarrow \mathbb{R}_{0,+}$, called *Liapunov function*, which decreases along solution curves of the differential equation [85]. This function can be used to determine if $x_s$ is stable or asymptotically stable. Moreover, it can provide information about the basins of attraction for asymptotically stable fixed points [5, 85, 97].

**Theorem 8.3.1 (Liapunov's method [97])** *Let $x_s$ be a fixed point for a differential equation of the form $\dot{x} = f(x)$, $x \in \mathbb{R}^n$ and a smooth function $f : U \subseteq \mathbb{R}^n \rightarrow \mathbb{R}^n$.*

*Let $V : W \to \mathbb{R}$ be a differentiable function defined on some neighborhood $W \subseteq U$ of $x_s$
such that:*
*(P1) $V(x_s) = 0$ and $V(x) > 0$ $\forall x \neq x_s$*
*(P2) The* orbital derivative, *that is, the derivative along the solution curve $x(t)$, is non-
positive:*

$$\dot{V}(x) := \sum_{i=1}^{n} \frac{\partial V(x)}{\partial x_i} \cdot \dot{x}_i = \sum_{i=1}^{n} \frac{\partial V(x)}{\partial x_i} f_i(x) \leq 0 \quad in \; W \setminus \{x_s\}. \tag{8.42}$$

*Then $x_s$ is stable. Moreover, if strictly*
*(P3) $\dot{V}(x) < 0$ in $W \setminus \{x_s\}$,*
*then $x_s$ is asymptotically stable. If $W = U$ in condition (P3), then $x_s$ is said to be globally
asymptotically stable.*

A function $V$ which fulfills conditions (P1) and (P2) is called a *smooth weak Liapunov
function in the small.* It can be used to show that trajectories in a neighborhood $W$ of
$x_s$ remain in a neighborhood for $t \geq 0$. If the stricter condition (P3) holds, then $V$ is a
*smooth strict Liapunov function in the small.* Its existence states that trajectories in a
neighborhood $W$ of $x_s$ converge to $x_s$ for $t \geq 0$. The neighborhood $W$ of a smooth strict
Liapunov function belongs to the basin of attraction of $x_s$, which is stated by the following
theorem:

**Theorem 8.3.2 (Basin of attraction [97])** *Let $x_s \in U$ be a fixed point of a dynamical
system $\dot{x} = f(x)$ with a continuously differentiable function $f : U \to \mathbb{R}^n$ and $U \subseteq \mathbb{R}^n$ an
open subset of $\mathbb{R}^n$. Let furthermore $V : W \to \mathbb{R}$ be a Liapunov function for $x_s$, defined on
a neighborhood $W$ of $x_s$. Let $P \subset W$ be a neighborhood of $x_s$ which is closed in $U$. Suppose
that $P$ is positively invariant, i.e. for $x \in P$, the forward trajectory $\Gamma^+(x) \in P$, and that
there is no trajectory in $P \setminus \{x_s\}$ on which $V$ is constant. Then $x_s$ is asymptotically stable,
and $P$ is contained in the basin of attraction of $x_s$, $P \subset B(x_s)$.*

Thus, if the neighborhood $W$ equals the domain of the differential equation, and (P1) and
(P3) are fulfilled, we refer to $V$ as a *global strict Liapunov function.* The existence of
such a global strict Liapunov function implies global asymptotic stability of $x_s$, and every
trajectory approaches $x_s$ for $t \to \infty$ [97].

**Example 8.3.3** [Liapunov function] As an example, we construct Liapunov functions for
the one-dimensional system

$$\dot{x} = f(x) = 0.1 - 0.5x + \frac{x^5}{x^5 + 1} \quad x \in \mathbb{R}_+, \tag{8.43}$$

which describes a system with linear degradation and positive sigmoidal auto-regulation.
The fixed points of this system have already been investigated using the Hartman-Grobman
Theorem in Chapter 2. It has two stable fixed points $x_s^1$ and $x_s^3$ and an unstable fixed point
$x_s^2$. Figure 8.8 shows the function $f(x)$ and three functions $V1$, $V2$ and $V3$ for each fixed

point, respectively:

$$V1(x): \quad (0, x_{2,s}) \to \mathbb{R}_{0,+}: \quad x \mapsto (x - x_{1,s})^2, \tag{8.44}$$

$$V2(x): \quad (x_{1,s}, x_{3,s}) \to \mathbb{R}_{0,+}: \quad x \mapsto (x - x_{2,s})^2 \tag{8.45}$$

$$V3(x): \quad (x_{2,s}, \infty) \to \mathbb{R}_{0,+}: \quad x \mapsto (x - x_{3,s})^2 \tag{8.46}$$

We consider the stable fixed point $x_{1,s}$ and the corresponding function $V1(x)$. $V1$ is a Liapunov function for $x_{1,s}$. Condition (P1) is fulfilled, and in the domain of $V1(x)$, $\partial V1(x)/\partial x$ and $f(x)$ have opposite signs: For $x < x_{1,s}$, $\partial V1(x)/\partial x < 0$ and $f(x) > 0$, for $x > x_{1,s}$, $\partial V1(x)/\partial x > 0$ and $f(x) < 0$. Hence, according to equation (8.42), $\dot{V}1(x) < 0$, and $x_{1,s}$ is asymptotically stable. The basin of attraction includes the interval $(0, x_{2,s})$, which is the domain of $V1$. It is also the maximal domain and therefore the whole basin of attraction of $x_{1,s}$, which can in this example easily be read off the signs of the vector field $f(x)$. We can analogously show that $x_{3,s}$ is stable as well. $V3$ is the corresponding Liapunov function for $x_{3,s}$. Also here, $(x_{2,s}, \infty)$ is the basin of attraction of $x_{3,s}$. Contrary, the signs of $\partial V2(x)/\partial x$ and $f(x)$ are both negative for $x < x_{2,s}$, and they are both positive for $x > x_{2,s}$. Thus, $\dot{V}2(x) > 0$, and $V2(x)$ is not a Liapunov function for $x_{2,s}$. Indeed, $x_{2,s}$ is unstable. This can be seen, since $V2(x)$ is a Liapunov function for the stable fixed point $y_{2,s}$ of the system $\dot{y} = -f(y)$ with reversed vector field. Stable fixed points of this system are unstable in the original system $\dot{x} = f(x)$[1].

In general, finding a suitable Liapunov function can be a hard task. The norm $\|x - x_s\|^2$, which was also used in our example, is often a good candidate, since it fulfills condition (P1). It is, however, not always appropriate to verify the conditions (P2) or (P3). For our system (8.40), we use a more general scalar product as a Liapunov function.

## 8.3.2 Existence of a unique fixed point in $\mathbb{R}_+^n$

System (8.40) has a unique fixed point $x_s \in \mathbb{R}_+^n$. We show this for each single variable. A fixed point $x_s$ of system (8.40) is characterized by $\dot{x}_{s,i} = 0$, which leads to $g(x) = Gx$. For variable $x_1$ we have

$$\forall x_n =: \kappa \in \mathbb{R}_+: \quad g_1(0, \kappa) = s_1 + k_{1,n} \frac{\kappa^{m_{1,n}}}{\kappa^{m_{1,n}} + \theta_{1,n}^{m_{1,n}}} > 0. \tag{8.47}$$

Moreover, $g_1(x_1, \kappa)$ is monotonically decreasing with respect to $x_1$,

$$\frac{\partial g_1(x_1, \kappa)}{\partial x_1} = k_{1,1} \frac{\partial}{\partial x_1} \left( \frac{x_1^{m_{1,1}}}{x_1^{m_{1,1}} + \theta_{1,1}^{m_{1,1}}} \right) \leq 0, \tag{8.48}$$

since $k_{1,1} \leq 0$ and $x_1^{m_{1,1}}/(x_1^{m_{1,1}} + \theta_{1,1}^{m_{1,1}})$ is a monotonically increasing function. Thus, $g_1(x_1, \kappa) = \gamma_1 x_1$ has a unique solution $x_{s,1}^\kappa$ for each value $x_n = \kappa \in \mathbb{R}_+$. Moreover, $\partial x_{s,1}^\kappa(\kappa)/\partial \kappa < 0$, because of the negative regulation strength $k_{1,n} < 0$.

---

[1]Personal communication with Dr. Daniel Weiss, Mathematical Institute, University of Cologne.
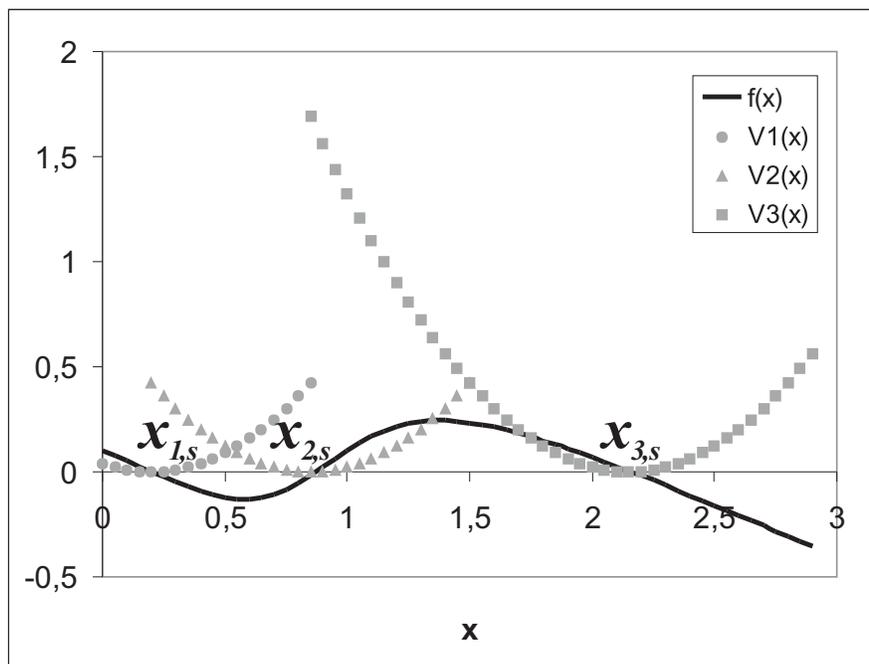
Figure 8.8: Function $f(x)$ in system (8.43) (*black continuous line*). It has three zeros $x_{1,s}$, $x_{2,s}$ and $x_{3,s}$, which correspond to fixed points of system (8.43). The quadratic functions $V1$, $V2$ and $V3$ are candidates for Liapunov functions of $x_{1,s}$, $x_{2,s}$ and $x_{3,s}$, respectively, since they fulfill condition (P1) in Theorem (8.3.1). Additionally, condition (P3) holds for $V1$ and $V3$, which identifies both functions as Liapunov functions for $x_{1,s}$ and $x_{3,s}$, respectively. Hence, these two fixed points are asymptotically stable. $V2$ is not a Liapunov function for $x_{2,s}$, since neither (P2) nor (P3) are fulfilled.
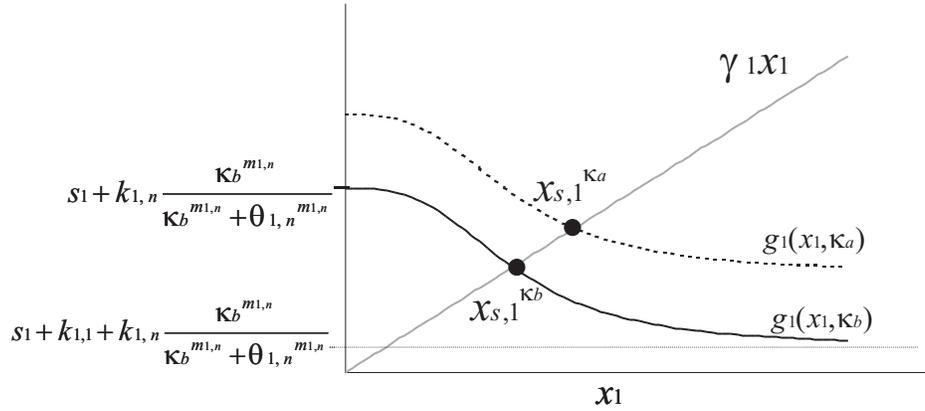
Figure 8.9: The fixed point $x_{s,1}^\kappa$ is the intersection of $\gamma_1 x_1$ and $g_1(x_1, \kappa)$. Here, $x_{s,1}^\kappa$ is shown for two different values $\kappa_a$ and $\kappa_b > \kappa_a$. Increasing $\kappa$ shifts $g_1(x_1, \kappa)$ downwards. As a consequence, $x_{s,1}^\kappa$ decreases.

Figure 8.9 illustrates the fixed point $x_{s,1}^\kappa$, which is the intersection of $\gamma_1 x_1$ and $g_1(x_1, \kappa)$, as a function of $x_1$ for two different values $\kappa_a$ and $\kappa_b > \kappa_a$. Increasing $\kappa$ shifts $g_1(x_1, \kappa)$ downwards. As a consequence, $x_{s,1}^\kappa$ decreases.

Similarly, for fixed $x_n = \kappa$, $g_2(x_{s,1}^\kappa, x_2, \kappa) = \gamma_2 x_2$ has a unique solution $x_{s,2}^\kappa$, which decreases with increasing $\kappa$, $\partial x_{s,2}^\kappa(\kappa)/\partial \kappa \leq 0$. This can be continued to obtain $x_{s,j}^\kappa$ for $j = 3, \ldots, n-1$. Finally, using the same arguments, also $g_n(x_{n-1}^\kappa, \kappa) = \gamma_n \kappa$ has a unique solution $\hat{\kappa}$. The unique fixed point is given by $x_s = (x_{s,1}^{\hat{\kappa}}, x_{s,2}^{\hat{\kappa}}, \ldots, x_{s,n-1}^{\hat{\kappa}}, \hat{\kappa})$.

### 8.3.3   Stability of the fixed point

We present a global strict Liapunov function $V(x)$ for system (8.39), which shows that $x_s$ is globally attracting in case of sufficiently large degradation rates [130].

Let

$$V(x) := \frac{1}{2} \langle \Delta x, G^{-1} \Delta x \rangle \quad \text{with } \Delta x := x - x_s. \tag{8.49}$$

We have to show that the so defined function $V(x)$ fulfills the properties (P1) and (P3) with domain $W = \mathbb{R}_+^n$. For this purpose, we write $V(x)$ as

$$V(x) = \frac{1}{2} \sum_{i=1}^{n} \frac{1}{\gamma_i} (x_i - x_{i,s})^2. \tag{8.50}$$

It is easy to see that $V(x_s) = 0$, $V(x) > 0$ for all $x \in \mathbb{R}_+^n \setminus \{x_s\}$ and $V(x) \in \mathcal{C}^1(\mathbb{R}_+^n)$. To

show $\dot{V}(x) < 0$, we calculate

$$\dot{V}(x) = \langle \nabla V(x), f(x) \rangle \tag{8.51}$$

$$= \left\langle \sum_{i=1}^{n} \left( \frac{\Delta x_i}{\gamma_i} \right) e_i, f(x) \right\rangle \tag{8.52}$$

$$= \sum_{i=1}^{n} \left( \frac{\Delta x_i}{\gamma_i} \right) \cdot f_i(x). \tag{8.53}$$

Inserting

$$f(x) = \dot{x} = \dot{x} - \dot{x}_s = \underbrace{g(x) - g(x_s)}_{=:\Delta g} - G \cdot \Delta x \tag{8.54}$$

into (8.53) leads to

$$\dot{V}(x) = \left[ \sum_{i=1}^{n} \left( \frac{\Delta x_i}{\gamma_i} \right) e_i \right] \cdot (\Delta g - G \cdot \Delta x)$$

$$= \sum_{i=1}^{n} \left( \frac{\Delta x_i}{\gamma_i} \Delta g_i \right) - \sum_{i=1}^{n} (\Delta x_i)^2 \tag{8.55}$$

$$= \langle \Delta x, G^{-1} \Delta g \rangle - \langle \Delta x, \Delta x \rangle .$$

This expression is negative if

$$\langle \Delta x, G^{-1} \Delta g \rangle < \langle \Delta x, \Delta x \rangle . \tag{8.56}$$

The Cauchy-Schwarz inequality states that

$$\langle \Delta x, G^{-1} \Delta g \rangle \leq \|\Delta x\| \cdot \|G^{-1} \Delta g\|, \tag{8.57}$$

and thus it is sufficient to show

$$\|G^{-1} \Delta g\| < \|\Delta x\|. \tag{8.58}$$

For this, we use a generalization of the mean value theorem, which estimates the difference between $f(x)$ and $f(y)$ with the supremum of derivatives on the segment joining two points $x \in \mathbb{R}^m$ and $y \in \mathbb{R}^m$ for a continuous function $f : \mathbb{R}^m \to \mathbb{R}^n{}^2$.

**Theorem 8.3.4 (Mean value theorem [55])** *Let $f : \mathbb{R}^m \to \mathbb{R}^n$ be a continuous function defined on a neighborhood of a segment $S$ joining two points $x_0$ and $x_0 + t$ of $\mathbb{R}^m$. If $f$ is differentiable at every point of $S$, then*

$$\|f(x_0 + t) - f(x_0)\| \leq \|t\| \sup_{0 \leq \xi \leq 1} \|f'(x_0 + \xi t)\|. \tag{8.59}$$

---

[2]The Theorem is more generally defined on two Banach spaces, which are vector spaces $V$ over the real or complex numbers and a norm $\| \cdot \|$, such that every Cauchy sequence in $V$ has a limit in $V$. For our purposes, it is sufficient to consider the vector space $\mathbb{R}^n$ with a vector norm $\| \cdot \|_V$, for example the Euclidean norm $\|x\|_2 = \sqrt{\sum_{i=1}^{n} |x_i|^2}$, and an operator-norm for a linear operator $f$ induced by this vector norm through $\|f\| := \sup_{\|x\|_V = 1} \|f(x)\|$.

If we identify $x_0 + t$ in Theorem 8.3.4 with $x$ and $x_0$ with $x_s$, then $t$ corresponds to $\Delta x$. Furthermore, we set $f := G^{-1}g$, which is smooth in $\mathbb{R}^n_+$, and obtain the following estimate according to Theorem 8.3.4:

$$\|G^{-1}\Delta g\| \leq \|\Delta x\| \sup_{0 \leq \xi \leq 1} \|J_{G^{-1}g}(x_s + \xi\Delta x)\|. \tag{8.60}$$

Thus, $x_s$ is globally asymptotically stable if

$$\sup_{0 \leq \xi \leq 1} \|J_{G^{-1}g}(x_s + \xi\Delta x)\| < 1 \quad \forall x \in \mathbb{R}^n_+. \tag{8.61}$$

This can always be fulfilled, for example, by increasing the degradation rates $\gamma_i$ in system (8.40). For this, we consider the Jacobian matrix $J_{G^{-1}g}(x)$ of the function $G^{-1}g(x)$:

$$G^{-1}g(x) = \begin{pmatrix} \frac{1}{\gamma_1}g_1(x_1, x_n) \\ \frac{1}{\gamma_2}g_2(x_1, x_2, x_n) \\ \vdots \\ \frac{1}{\gamma_n}g_n(x_{n-1}, x_n) \end{pmatrix}, \tag{8.62}$$

which is given by

$$J_{G^{-1}g}(x) = \begin{pmatrix} \frac{1}{\gamma_1}\frac{\partial g_1(x_1,x_n)}{\partial x_1} & 0 & \cdots & \cdots & \frac{1}{\gamma_1}\frac{\partial g_1(x_1,x_n)}{\partial x_n} \\ \frac{1}{\gamma_2}\frac{\partial g_2(x_1,x_2,x_n)}{\partial x_1} & \frac{1}{\gamma_2}\frac{\partial g_2(x_1,x_2,x_n)}{\partial x_2} & 0 & \cdots & \frac{1}{\gamma_2}\frac{\partial g_2(x_1,x_2,x_n)}{\partial x_n} \\ 0 & \ddots & \ddots & \ddots & \vdots \\ \vdots & \ddots & \ddots & \ddots & \vdots \\ 0 & \cdots & & \frac{1}{\gamma_n}\frac{\partial g_n(x_{n-1},x_n)}{\partial x_{n-1}} & \frac{1}{\gamma_n}\frac{\partial g_n(x_{n-1},x_n)}{\partial x_n} \end{pmatrix}. \tag{8.63}$$

Equation (8.63) shows that $\|J_{G^{-1}g}(x)\|$ decreases with increasing degradation rates for all $x \in \mathbb{R}^n_+$. Thus, condition (8.61), which assures global asymptotic stability of $x_s$, can always be fulfilled by multiplying $G$ with a sufficiently large number $\alpha \in \mathbb{R}_+$, since

$$G_2 = \alpha G_1 \quad \Rightarrow \quad \|J_{G_2^{-1}g}(x)\| = \frac{1}{\alpha}\|J_{G_1^{-1}g}(x)\|. \tag{8.64}$$

This shows that whenever system (8.40) oscillates, these oscillations can be destroyed by increasing the degradation rates. For single loop systems, it has been shown that an unstable fixed point $x_s$ is a sufficient condition for system (8.40) to show periodic behavior [130]. Unfortunately, Liapunov's method only provides sufficient conditions for $x_s$ to be stable. So, even if condition (8.61) is not fulfilled for the fixed point $x_s$, this does not necessarily mean that $x_s$ is unstable[3].

---

[3]Actually, Liapunov functions can also be used to show that a fixed point is unstable [4], but this is beyond the scope of this thesis here.

**Summary**

In this section, we considered a system of $n$ components with an interaction graph of interlocked negative circuits shown in Figure 8.7. This system has a unique fixed point $x_s$. We presented a Liapunov function for the system and showed that $x_s$ is globally stable for sufficiently large degradation rates. In contrast to an analysis of the stability of a fixed point $x_s$ via linearizing about $x_s$, the fixed point does not need to be hyperbolic, and the eigenvalues of $J_f(x_s)$ do not have to be calculated. Albeit the fixed point $x_s$ is not explicitly given here, the Liapunov function allows for conclusions about the stability $x_s$.

# 8.4 Concluding remarks

We investigated some theoretical aspects of differential equation models with monotonous bounded regulation functions, which are related to the robustness of periodic behavior. We have shown two different model extensions to increase this robustness, time scale differences and time-delays. Both extensions aim at the destabilization of a stable fixed point $x_s$, whose stability is characterized by properties of the Jacobian matrix $J_f(x_s)$. Thus, we concentrated our analysis on the effect of time scale differences and time-delays on the characteristic equation of $J_f(x_s)$. Both extensions were investigated for two-dimensional systems, and we illustrated effects on the core model derived in Chapter 6.

In Section 8.1, we included a time scale parameter $\epsilon$ into the model, which accounts for time scale differences in the temporal change of system variables. If the time scale differences in a dynamical system are sufficiently large, which corresponds to a small value $\epsilon \ll 1$, singular perturbation theory can be used to describe the dynamic behavior of the system. We used a Taylor expansion for the eigenvectors of the Jacobian matrix and demonstrated that the condition $a_{11}(x_s) > 0$, which corresponds to a positive auto-regulation of component $x_1$ in our core system and which is necessary for the system to show sustained oscillations, becomes a sufficient condition when $\epsilon$ is sufficiently small. According to this mechanism, for any system with the same qualitative course of nullclines, if it has a single stable fixed point $x_s$ between minimum and maximum of the $x_1$-nullcline, $x_s$ can be destabilized, causing the system to oscillate, by choosing $\epsilon$ sufficiently small.

A bifurcation analysis with bifurcation parameter $\epsilon$ and numerical simulations have shown that both amplitude and period of the oscillations can be increased by decreasing $\epsilon$. We also observe a change in the dynamic of the system, which is typical for systems with different time scales: The variables of the system change on two different time scales, which causes a 'jumping dynamic', and which is denoted by relaxation oscillation. Most of the time, the system evolves on the slow time scale. Here, the fast variables are in a quasi-steady state all the time. When this steady state vanishes at certain points in the state space, the system undergoes a transition to a new stable steady state. During this transition, the changes of the variables are determined by the time scale of the fast variables, and thus the states change rapidly until the new steady state for the fast variables is reached. From here on, the system continues again to move unhurriedly along the slow

manifold.

A duration between a cause and its effect on the temporal change of a variable was incorporated into our model in Section 8.2. Here, the system of ordinary differential equations becomes a time-delayed differential equation system, which complicates an analysis of the system in general. Fortunately, the stability of a fixed point $x_s$ can still be investigated via the characteristic equation of the Jacobian matrix $J_f(x_s)$. Different to ordinary differential equation systems, the characteristic equation is not a simple polynomial in terms of eigenvalues $\lambda$, but contains additional exponential terms. These terms can complicate the stability analysis. However, an inclusion of time-delays has turned out to be a very efficient way to increase the robustness of oscillations with respect to parameter variations. Similar to an increase in time scale differences, a time-delay can increase both, amplitude and period of the oscillation. In contrast to the first extension, the condition $a_{11}(x_s) > 0$, positive auto-regulation which exceeds degradation for component $x_1$ in the steady state $x_s$, is not even necessary in a time-delayed system. We demonstrated this with a concrete example using again the two-dimensional core system.

Finally, Section 8.3 analyzes the stability of a fixed point $x_s$ of a system with more than two variables. The general additive model derived in Chapter 2 was used to describe this regulatory network. This system has a predefined interaction graph, which consists of interlocked negative circuits. Here, analysis methods that were useful in order to understand phenomena in the planar core system can no longer be used. For example, a determination of fixed points, which has been done by searching for intersections of nullclines in the two-dimensional system, is more difficult here. Moreover, the Poincaré-Bendixson Theorem, which was used to prove the existence of a limit cycle in Chapter 6, is based on planar systems. Thus, a change from a two-variable system to higher dimensions can pose some difficulties, as will also be outlined in Section 9. However, monotonicity of the regulation functions in our general model and the special structure of the interaction graph considered here allowed to prove the existence of a unique fixed point $x_s$. Furthermore, we discussed the concept of *Liapunov functions*, which is an alternative way to investigate the stability of fixed points. We constructed a Liapunov function for our model which emphasizes the maintenance of the global asymptotic stability of the system's fixed point by fast degradation processes. In particular, in case that $x_s$ is not stable, increasing the degradation rates $\gamma$ has always a stabilizing effect. We conclude that periodic behavior is maintained by small degradation rates.

All extensions discussed in this chapter are biologically motivated. Time scale differences and time-delays become especially important in models for biochemical networks, which comprise transcriptional and post-transcriptional regulation processes. Here, we have to describe chemical modifications, which happen on a fast time scale, and at the same time regulation of gene expression via binding of transcription factors to the DNA, which are much slower. In addition, non-zero concentration gradients and transport processes via diffusion or active transport from the nucleus to the cytoplasm are important in

eukaryotic cells. Thus, although we have illustrated concepts with the core model, which was actually specifically derived for the yeast cell cycle machinery, results presented here can also be embedded into a more general framework.

# Chapter 9

# Conclusions

In the last chapter we will point out essential aspects of this work. A short summary and a discussion of results as well as technical improvements concerning the approaches used have already been addressed in the conclusion sections of each chapter. The main statements of this thesis are summarized in Section 9.1. In Section 9.2, we will retrospectively respond to consequences for the ultimate goal of constructing in silico models. Finally, Section 9.3 discusses perspectives for future work, which arise from the precedent conclusions.

## 9.1 Summary

In this thesis, we inferred biochemical networks from experimental data with the focus to investigate mechanisms related to the network's dynamic behavior. An introduction into this field was given in **Chapter 1**. Here, we described cellular regulation processes and frequently used approaches for network inference.

In **Chapter 2**, we developed a model for gene regulatory networks which interprets these networks as homogeneous chemical reaction systems. The system's dynamic was described by chemical reaction kinetics, resulting in a system of ordinary differential equations. More specifically, the expression rate of a gene was described to be regulated through binding of a transcription factor to a specific DNA binding site in the promoter region of this gene. This binding was modeled as a reversible binding reaction in chemical equilibrium, which comprises a quasi-steady state approximation. The resulting average number of transcription factor-binding site complexes was taken to be a measure for the effect on the expression rate of the regulated gene, resulting in a sigmoidal dependence of a gene's expression rate on the concentration of its transcription factors.

Given initial concentrations of all network components, this approach presumes that the temporal behavior of these concentrations is uniquely determined by a parameterized function, the unique solution of the differential equation system. This assumptions allows to use time series concentration data to estimate model parameters and is thus the basis for network inference with microarray data. The model was applied to three regulatory

subsystems in Chapters 3, 4 and 5.

**Chapter 3** focused on the response of the *Mycobacterium tuberculosis* DNA repair system. When the bacterium's DNA is damaged, a signal transduction pathway induces expression of SOS genes. These SOS genes are responsible to stop cell division and to repair DNA breaks before cell division continues. Besides a well-known core mechanism regulating these genes, an alternative mechanism specific for the Mycobacterium is assumed to act in concert with this core mechanism. Our study focused on this alternative core mechanism, whose components are not yet completely known. We built a model of the core network and estimated model parameters using gene expression time series of the bacterium's response to a treatment with DNA damaging drugs. Interaction information from literature and pairwise correlations of gene expression values were used to extend this network by further components and regulations. The behavior of the resulting extended network was compared with the core network, and we concluded that the gene $Rv2719c$, whose function was not yet annotated at that time, might play an important role in the DNA repair system. Further work supporting this hypothesis has independently been published by other groups in the meantime [20, 28].

Mathematically, the model describes the relaxation of a differential equation system to a stable fixed point after a temporary external perturbation, which is related to the DNA damaging signal. Such a relaxation can satisfactorily be captured by the model class used here.

Mechanisms of specific regulation by pleiotropic regulators in bacteria, which are known to bind unspecifically to the DNA, were addressed in **Chapter 4**. Specific repression of the *Escherichia coli bgl* operon by the global regulator protein H-NS, which was investigated here, serves as a paradigm for this specific control. The *bgl* operon encodes proteins for the fermentation of a certain sugar, and its expression is repressed by binding of H-NS to two DNA binding sites. Although binding of H-NS is relatively unspecific, repression of the operon is highly effective. The expression rate of the operon in *hns* mutants is about 100 times higher than expression in the wild type. Further, experiments indicate a threshold regulation: Within a certain range of promoter activities, the 100-fold repression can be released by a moderate (3-fold) increase in the promoter activity. We set up a model for this repression and used measurements of *bgl lacZ* reporter fusions to estimate parameters. According to the inferred model, specificity of repression is caused by the mutual enhancement of two interlocked positive circuits in the corresponding interaction graph. One of these circuits reflects the influence of aborting transcription elongation on transcription initiation via forming DNA loop structures. The second one includes the antiterminator protein BglG, a product of one of the operon genes, which can destroy DNA structures called terminators, thereby promoting the expression of the operon.

Due to these positive feedback loops, the model can show complex dynamic behavior. Such positive feedback loops are generally related to hysteresis and multi-stationarity. The observed threshold phenomenon is described by switches between two different stable steady states of the model.

While Chapters 3 and 4 addressed questions related to the systems under study, and the models include a lot of specific biological knowledge, **Chapter 5** deals with the typical problem to have many parameters to be estimated but at the same time only few measurements available. A formulation of the parameter estimation problem as an optimization problem is severely under-determined. Thus, it entails a restriction of the parameter space in order to formulate the parameter estimation problem as a well-defined optimization problem. We introduced a new Bayesian approach to reconstruct gene regulatory networks from time series concentration data. For this, the model was embedded into a probabilistic framework, interpreting the measured concentration values as random variables. Prior distributions over model parameters, formulated as probability density functions, were specified to prevent overfitting. In particular, a hierarchical distribution over interaction strengths favors small regulation strengths. Thus, it drives the solution to sparse networks, in which only few interactions have strengths differing considerably from zero. Parameters were estimated by maximizing the posterior probability with respect to model parameters. We compared results obtained with the Bayesian approach and the classical maximum likelihood estimation. Evaluation was done by means of a receiver operator characteristic analysis, which compares the structure of the inferred network with a reference network. Results on simulated data showed that the Bayesian approach can outperform maximum likelihood estimation, in particular in case of sparse and noisy datasets, which is the typical setting in microarray studies. An application on a real dataset of the *Saccharomyces cerevisiae* cell cycle showed that also here the Bayesian approach was better than maximum likelihood, and we revealed some of the main interactions of the cell cycle network. However, an analysis of this dataset turned out to be more difficult, and results are worse than on simulated datasets of the same size. We discussed several reasons for this.

An analysis of the networks inferred with the Bayesian approach revealed an interesting phenomenon, which was further investigated in the following chapters: While the structure of the networks were successfully learned, at least for the simulated data, most of the inferred models converge quickly to a steady state for both, the simulated and the yeast cell cycle network. Thus, although performing reasonable in the receiver operator characteristic analysis, the model seems not to be appropriate to capture the periodic expression of cell cycle genes. The theory of dynamical systems was used to explain this phenomenon and to investigate mechanisms causing oscillating behavior in chemical reaction systems. Our model, as well as many other systems of differential equations used to model regulatory networks, can be assigned to a class of dynamical systems having constant sign Jacobian matrices. Solutions of these systems tend to converge to steady states, which was explained in **Chapter 6**. According to this, circuits in the interaction graph are the most interesting structures related to dynamic behaviors such as multi-stationarity, hysteresis and oscillations. A positive circuit is necessary for a system to have more than just one steady state, and a negative circuit is required for a system to show periodic behavior. An example of a positive circuit causing multi-stationarity had already been given in the model for the regulation of the *bgl* operon in *E. coli* in Chapter 4.

Consequently, we introduced a two-component activator-inhibitor model, which was derived according to regulations of the yeast cell cycle. It comprises a negative circuit and a positive auto-regulation and is able to show sustained oscillations. This model was assumed to be the core mechanism that determines the system's qualitative dynamic behavior. According to this core model, periodic behavior of network components is related to a stable limit cycle in the corresponding differential equation system. Using microarray data of the yeast cell cycle, we were able to infer an oscillating model with a maximum likelihood estimation.

In **Chapter 7**, we extended the core model by further components and regulations using the Bayesian approach introduced in Chapter 5. In this connection, it turned out that the qualitative dynamic behavior of the core model is structurally not stable. Oscillations are sensitive to changes of model parameters. Results on simulated data gave an impression of the quality of datasets needed to capture oscillating behavior. The datasets have to be much better with respect to size and noise level compared to the data needed to infer the interaction graph. Although we were able to infer an oscillating seven-component network for the yeast cell cycle, also here results are quite sensitive to parameter variations. In this connection, a bifurcation analysis of the core network showed that a negative circuit in the interaction graph is far from sufficient to guarantee periodic behavior. This raised the question about mechanisms leading to robust sustained oscillations in a living organism and how to include these into the model.

Finally, extensions of the core model addressing these questions were proposed in **Chapter 8**. These extensions go beyond ordinary differential equations. We showed how different time scales and an inclusion of a time-delay, respectively, can increase the robustness of oscillations in the core network. The underlying mechanism in both extensions is the destabilization of a steady state that is stable in the original model, since the existence of a single unstable steady state implies the existence of a stable limit cycle in our model. This allowed to examine the system's temporal behavior by investigating solely the linearization about this steady state, which facilitated the analysis considerably, in particular, for delay differential equations. In case of large time scale differences, we used a Taylor expansion to analyze the qualitative behavior in terms of the eigenvalues of the linearization in the limit of large time scale differences. According to the Hartman-Grobman Theorem, eigenvalues are related to the stability of steady states, and thus they determine the qualitative temporal behavior of the system. Theoretical results and an application to the core model for the budding yeast cell cycle indicate that time scale differences and time-delays can maintain sustained oscillations of activator-inhibitor oscillator models and therefore might also play a role in stabilizing periodic behavior in general.

Chapter 8 also gave an insight into the analysis of higher-dimensional systems. We considered a system of $n$ components and interlocked negative circuits and showed that this system has a unique steady state, which is stable if degradation is not too slow. Stability was investigated here using Liapunov's method. We presented a Liapunov function, which allowed to analyze the stability of a fixed point without the need for explicitly linearizing

the system and calculating eigenvalues. Once more, results provided an explanation why it is difficult to model periodic behavior with autonomous chemical reaction systems.

## 9.2 In silico models - The ultimate goal

Here, we come back to the ultimate goal of systems biology, the in silico reconstruction of cellular systems, which was outlined in the beginning of this thesis. A realization of such in silico models requires an understanding of interactions between cell components. This can be achieved at different levels, and we will classify these into a qualitative level of an understanding about interactions of cell components, an understanding of the dynamic behavior and, finally, an understanding about the relation of experimental data and phenotypes, which is most interesting for medical practice.

### 9.2.1 Qualitative analysis

A first step from the characterization of single cell components towards a system-level understanding is the investigation of relations between these components. Microarray data are currently most often used for this purpose. Methods have been proposed to find genes which are differentially expressed under different conditions or in different probes and tissues. Results can help to group genes into functional modules, which refer to different regulation processes in the cell.

A further step is to describe functional dependencies between these components. In recent years, many top down approaches have been developed to infer regulatory networks. The main problem in this setting is to get biologically reasonable results in spite of sparse datasets, which renders classical regression methods useless. Thus, in order to formulate the parameter estimation problem as a well-defined optimization problem, the models are usually kept simple, meaning that they consist of preferably few parameters. Such simplified models are not always based on underlying regulation mechanisms.

The inferred networks reflect regulation processes which affect the amount of mRNAs. These are mainly transcriptional regulation processes, for example, transcription factors binding to specific binding sites in the promoter region of the regulated gene. Thus, microarray data provide insights into the regulation of transcription initiation. These top down approaches might be appropriate to reveal rough structures of the systems. For example, global transcription factors that regulate many genes or groups of commonly regulated genes might be detected. Thus, such approaches can provide a good starting point for further investigations.

### 9.2.2 Capturing the dynamic behavior

Learning the dynamic behavior of regulatory networks is often more complicated than the reconstruction of the interaction graph only. In general, neither the simplified models nor microarray data alone are sufficient to obtain an in-depth understanding of a system's

behavior or to predict complex behaviors [108]. Often, the observed dynamic behavior can only be explained by the interrelation between various regulation processes acting at the transcriptional and at the post-transcriptional level. All applications presented in this thesis are biochemical networks, which include transcriptional and post-transcriptional regulations. These post-transcriptional regulations affect the dynamic behavior of the systems considerably. Hence, they have to be included into a dynamic modeling approach.

A detailed understanding of dynamic cell processes poses a challenge in many aspects: First, it requires larger amounts of and, in particular, more accurate data compared to the datasets required to infer interactions between cell components. Second, mRNA concentration data have to be supplemented by further data containing information about post-transcriptional and post-translational regulation mechanisms. Both goals are perhaps beyond the scope of current experimental practices [108] and give thus the direction for future research. Third, the corresponding models generally have to be built in terms of underlying reaction processes. Moreover, since post-transcriptional regulation processes such as chemical modifications are fast processes compared to the regulation of transcription, the models have to include processes on different time scales, which has extensively been discussed in this thesis.

Consequently, a detailed analysis of the dynamic behavior of a regulatory network usually focuses on subnetworks of 10-15 components at most.

## 9.2.3 Relevance for medical applications

Finally, the highest level of understanding is the characterization of the phenotype from experimental data and the ability to predict the system's response to interventions. This level is required for applications in medical practice such as drug design, an investigation of side effects or personalized therapies on the basis of genome and proteome data. Some successes have already been achieved in this field: Herceptin, for example, is a drug against breast cancer, which is effective for only 16% of the patients. However, Herceptin is highly efficient for these patients. Gene tests are used to identify if a patient is among these 16%. Another example is the pain reliever Codein, which cannot be converted by about 10% of patients due to a lack of an enzyme and is thus useless for these patients.

Since drugs are related to an understanding of regulation mechanisms in eukaryotes, it is probably most important to go beyond mRNA data and investigate post-transcriptional and post-translational regulations, which characterize the proteome. In Chapter 1 we pointed out some differences between eukaryotes and prokaryotes concerning the regulation of gene expression. It is known that the main difference of both is not the number of genes, but the various regulation mechanisms, which are far more complex in eukaryotes. Thus, while using mRNA concentrations to characterize the proteome in prokaryotes might be reasonable, this is generally not the case in eukaryotes.

First, an eukaryotic cell has a complex spatial structure divided in different compartments, and concentrations are determined by diffusion and transport processes. Such

processes can result in a delayed reaction and might have a considerable influence on the system's dynamic behavior, as investigated in Chapter 8. Also transcription and translation happen spatially separated. Experimental techniques which provide information about protein concentrations within the cell are only gradually becoming feasible.

Second, only little is known so far about several post-transcriptional regulation mechanisms such as alternative splicing or the function of non-coding RNAs, which are assumed to influence gene expression as well. But many diseases such as Alzheimer's disease for example are related to defects in the proteome, such that high-throughput techniques and analysis methods that can accurately capture the proteome are required in the future.

A further difficulty poses the difference between experiments in test tubes (*in vitro*) and in living organisms (*in vivo*). A gene's function depends among other factors on the stage of development in which the gene is active. To investigate mechanisms in vivo, methods have been developed to manipulate the genome in mice. The aim of the International Mouse Mutagenesis Consortium (IMMC), an international project of genome research institutes, is the complete characterization of gene functions and the storage in public databases within the next decades.

## 9.3 Perspectives for future work

### 9.3.1 Top down approaches and multiple data sources

Resulting from the fact that the temporal behavior of most cellular regulatory systems is determined at the transcriptional and at the post-transcriptional level, microarray data presumably have to be supplemented by other data sources, which provide information about post-transcriptional and post-translational regulation processes. In Chapter 3, we have used an algorithm to extract regulatory subnetworks, which includes interaction information and gene expression data at the same time. Results indicate that this combination is indeed useful to facilitate network inference. Only recently, a couple of publications appeared, which propose inference approaches including multiple data sources such as literature information, transcription factor binding site data and gene expression measurements [13, 162, 187, 212, 215]. Many of these methods are multi-step procedures.

Bayesian approaches are particularly useful in this setting. As explained in Chapter 5, they provide a natural framework to include information from multiple data sources [13, 162, 187]. Thus, any knowledge about the system at hand can in principle be included into a Bayesian inference approach, which can lead to integrated models on the one hand, and which also helps to restrict the search space in order to formulate the parameter estimation problem as a well-defined problem on the other hand.

### 9.3.2   An analysis of core mechanisms

We pointed out the importance of circuits in the interaction graph for the qualitative behavior of the system. Many core networks based on positive and negative feedback mechanisms have already been proposed to explain the underlying mechanisms causing phenomena such as multi-stationarity and periodic behavior [8, 43, 203]. Most of them are two-component models. Activator-inhibitor or substrate-depletion oscillator models are used in order to explain sustained oscillations in biological systems. However, we have seen that these simplified models are not always structurally stable. This complicates network inference on the one hand, and it comprises a contradiction to robust dynamic behaviors in living organisms on the other hand. Thus, it is an interesting questions how these models can be extended in order to make qualitative dynamic behaviors more robust.

Here, we have investigated the robustness of oscillations and showed that large differences in the changing rates of system variables, expressed by small time scale parameters in the activator-inhibitor model presented, can destabilize a stable fixed point and thus lead to oscillations. The inclusion of a time-delay into the model seems to be even more effective in extending the region in the parameter space in which the system has a stable limit cycle, thereby stabilizing the periodic behavior.

Parameter estimation for these extensions, which go beyond ordinary chemical reaction systems, require spatiotemporal data to describe diffusion and transport processes. Further, an estimation of stochastic fluctuations in the regulation of gene expression is only possible with single cell experiments.

Questions concerning such extensions can be formulated more generally: To what extend is the simplified description of cellular systems as chemical reaction systems justified? And what are the limitations of this modeling in terms of capturing and unraveling dynamic phenomena? Once again, these questions are related to the question about what we can hope to learn from microarray data alone, independently from the sparsity problem.

### 9.3.3   From planar systems to higher dimensions

Most analyses presented in Chapters 6, 7 and 8 concentrate on the two-dimensional core network derived in Chapter 6. We have also argued in Chapter 6 that it is in some cases possible to analyze each circuit in the interaction graph separately and to reduce a single circuit to a two-component system.

While such planar systems are easier to analyze than higher-dimensional systems from a mathematical point of view, an extension by further variables might be desirable from a biological point of view. This is not always an easy task, and we will mention some difficulties here. Of course, planar systems have the advantage of a two-dimensional state space, which allows for a good graphical representation. Fixed points are given as intersections of nullclines, which partition the state space into regions in which the signs of the vector field components are constant. This has extensively been used throughout the thesis.

Eigenvalues of the Jacobian matrix $J_f(x_s)$ of a fixed point $x_s$ are solutions of a poly-

nomial of degree two, and hence, the stability of $x_s$ can easily be determined. Eigenvalues for Jacobian matrices of higher-dimensional systems usually have to be determined numerically.

Moreover, the $\mathbb{R}^2$ is topologically not equivalent to the $\mathbb{R}^n$ for $n \geq 3$ [147]. For planar systems, the Jordan curve Theorem, which states that any simple closed curve $\gamma$ separates the $\mathbb{R}^2$ into two disjoint open connected sets having $\gamma$ as their boundary, is frequently used to proof theorems about flows of planar systems. These proofs cannot be directly transfered to systems of higher dimension.

In general, the determination of the nature of limit sets of non-linear systems with more than two variables is still a challenging field, whereas the theory for planar systems is more complete [85, 147]. Peixoto's Theorem [85], for example, provides necessary and sufficient conditions for a planar system to be structurally stable. Also the Poincaré-Bendixson Theorem, which has been used to show the existence of a limit cycle for the core system, makes statements about planar systems. Here, we could even show that if a limit cycle exists, its basin of attraction is the whole state space. In contrast, one of the few methods of reliably establishing the existence of limit cycles in higher-dimensional systems is the Hopf bifurcation Theorem [98], which assures the existence of a limit cycle in a neighborhood of a Hopf bifurcation value $\mu_0$. However, this theorem, as well as the Hartman-Grobman Theorem, makes statements about a system's local behavior in a neighborhood of a limit set. They give no information about the basin of attraction.

Albeit these mathematical challenges, it would be interesting to investigate the relation between systems of interlocked feedback loops and the dynamic behavior. An extension of two component feedback loop models for further components have already been shown to affect the qualitative dynamic behavior. An example has been given in this thesis: In Chapter 4, we demonstrated that two interlocked positive circuits acting in concert can amplify switch-like behavior. This is in accordance with related work, in which a combination of two positive circuits was shown to accelerate switches and increase robustness [16, 18, 35]. Extensions of oscillatory models for further components have also already been investigated [119, 134]. For example, adding further components to a negative feedback loop can create an effect similar to the time-delay investigated in Chapter 8 [134]. We have shown that the inclusion of a time-delay can make the positive auto-regulation, which was necessary for destabilizing a stable fixed point in a two-component model, dispensable. A well-known oscillator model of ordinary differential equations without time-delays is the Goodwin oscillator [68]. This model consists of a single negative feedback loop of three components. A model of two interlocked circuits is also considered in [130]. In this model, oscillations can occur even without cooperative regulations, that is, with Hill-coefficients equal to one.

### 9.3.4 Robustness of regulatory networks

Robustness is an essential property of many biological systems, which has probably not emerged by chance, but is a result of evolution. Robustness of biological systems is phe-

nomenologically expressed by, for example, the adaptation of organisms to environmental changes and the insensitivity to specific kinetic rates. From the modeling point of view, robustness is related to negative feedback control mechanisms, redundancy, structurally stable intrinsic mechanisms and *modularity*, that is, the physical or functional insulation of subsystems, such that failure in one module does not affect other cell processes [108].

Thus, an understanding of mechanisms and principles underlying robustness of regulatory networks is essential for a system-level understanding of cellular networks.

Here, we have investigated robustness in terms of structural stability of qualitative dynamic behaviors with respect to parameter variations. This was exemplarily done for an oscillating system. For this purpose, we applied a bifurcation analysis, which is a powerful method to obtain statements about this robustness in dependence of only one or two variables at the same time. Programs for this already exist and are applicable if the model is built on only a few, say less than ten, parameters.

However, the creation of a single bifurcation diagram can computationally be very expensive. Moreover, variations of model parameters that reflect noise due to the measurement procedures or stochasticity of cell processes are more realistically modeled by small random perturbations of many parameters simultaneously. Accordingly, a bifurcation analysis is thus not always practicable to analyze the robustness of models containing a lot of variables and parameters.

Statistical models, which allow to vary several parameters simultaneously, would be desirable in this setting. This also raises the necessity of methods which can automatically classify models according to their qualitative behavior. Some work has already been done in this field [8, 43, 72, 203]. Vilar *et al.* [203], for example, investigated the noise resistance in a model for circadian oscillations. This model can, similar to the core model introduced in this thesis, exhibit hysteresis-based oscillations, and also here, in comparison to the oscillation period, the amplitude has been shown to be relatively insensitive to parameter variations. Craciun *et al.* [43] investigated conditions for a reaction network to show switch-like behavior. In Lu *et al.* [121], robustness was defined in terms of distances from the model parameter vector $\omega$ to a bifurcation hyperplane.

Finally, to broaden the current understanding of regulation processes in a cell and to take advantage also for medical applications is a high demand for the following decades. It requires further research in several directions comprising experimental techniques as well as analysis methods and can only be obtained by interdisciplinary cooperations between researchers.

# Appendix A

# Dependence of the chemical equilibrium on temperature - Arrhenius equation

Throughout this thesis, we assume constant equilibrium constants $K$ for all binding interactions. This assumption only holds if all external conditions like temperature or pH-values are constant. Thus, it is usually not possible to directly compare results from different experiments. The temperature dependence of a chemical reaction is often described by the *Arrhenius equation*,

$$K(\Delta G, T) \propto e^{-\frac{\Delta G}{T}}. \tag{A.1}$$

Here, $\Delta G$ denotes the *free enthalpy* of the binding reaction. Its sign characterizes whether a reaction in a test-tube happens spontaneously, which is the case if $\Delta G < 0$. Actually, the enthalpy is itself dependent on temperature. But equation (A.1) is often used as an empirical relation, and the dependence of $\Delta G$ on $T$ is neglected. In this form, it states that an increase in temperature or a decrease in the free enthalpy, for example caused by a catalyst, increases the rate of the reaction exponentially. This empirical equation (A.1) has already been used to describe binding processes of transcription factors to the DNA [56, 78, 168].

A derivation of the exact form of (A.1) is provided by the theory of statistical mechanics, which describes many-body systems with measurable thermodynamic variables such as pressure, temperature, chemical potential, entropy, volume or the number of particles. A set of these variables, which give a complete description of the system, is called *macro-state* of the system. This theory assumes that the system can be described by averaging over different *micro-states*, which provide the most detailed description of the system. For example, for an ideal gas, which consists of non-interacting, point-like particles, a micro-state is the information about space and momentum for each single particle, which corresponds to a point in the phase space of the system. The macro-state of the system includes knowledge about the number of particles, the volume and the temperature. A measurable

macro-state usually corresponds to many micro-states, but we do not know anything about these micro-states. We describe this lack of knowledge by an *ensemble* of systems with the same macro- but different micro-states. Thermodynamic variables correspond to averages over all systems in this ensemble. The exact dependence of $K$ on $T$ and $\Delta G$ is obtained by minimizing the total entropy $S$, which is here defined as $S := E/T$ with inner energy $E$, with respect to constant temperature and pressure.

This theory is similar to the assumptions underlying our model for gene regulatory networks derived in Chapter 2. Micro-states correspond to reaction processes between transcription factors and DNA binding sites in single cells. We observe a macro-state, which is assumed to be an average over many binding reactions. With this assumption, the system is described deterministically, although the underlying processes are in fact of stochastic nature.

# Appendix B

# Bayesian learning approach – Derivatives of the likelihood function

$$\hat{\omega}_{MLE} = arg\min_{\omega} \left( -\ln \mathcal{L}(\omega) \right)$$

$$= arg\min_{\omega} \left[ n(T-1)\ln\left(\sqrt{2\pi}\sigma_\xi\right) + \frac{1}{2\sigma_\xi^2} \sum_{i=1}^{n} \sum_{t=1}^{T-1} \left( h_i(\omega, \tilde{x}(t)) - \tilde{x}_i(t + \Delta t) \right)^2 \right]$$

$$= arg\min_{\omega} \underbrace{\frac{1}{2\sigma_\xi^2} \sum_{i=1}^{n} \sum_{t=1}^{T-1} \left( h_i(\omega, \tilde{x}(t)) - \tilde{x}_i(t + \Delta t) \right)^2}_{=:F_{MLE}(\omega)}$$

A necessary condition for a vector $\omega$ to minimize the objective function $F_{MLE}(\omega)$ is that all partial derivatives with respect to $\omega_a$, $a = 1, \ldots, 2n + 3n^2$ vanish:

$$\frac{\partial F_{MLE}(\omega)}{\partial \omega_a} \overset{!}{=} 0 \quad a = 1, \ldots, 2n + 3n^2 \tag{B.1}$$

This leads to the following equations:

**Derivatives with respect to synthesis rates $s_l$, $l = 1, \ldots, n$:**

$$\frac{\partial F_{MLE}(\omega)}{\partial s_l} = \frac{\partial}{\partial s_l} \left( \frac{1}{2\sigma_\xi^2} \sum_{i=1}^{n} \sum_{t=1}^{T-1} \left( h_l(\omega, \tilde{x}(t)) - \tilde{x}_l(t + \Delta t) \right)^2 \right)$$

$$= \frac{1}{\sigma_\xi^2} \sum_{t=1}^{T-1} \left( h_l(\omega, \tilde{x}(t)) - \tilde{x}_l(t + \Delta t) \right) \frac{\partial}{\partial s_l} \left( h_l(\omega, \tilde{x}(t)) - \tilde{x}_l(t + \Delta t) \right) \tag{B.2}$$

Inserting

$$\frac{\partial}{\partial s_l} \left( h_l(\omega, \tilde{x}(t)) - \tilde{x}_l(t + \Delta t) \right)$$

$$= \frac{\partial}{\partial s_l} \left( \tilde{x}_l(t) + \Delta t \left[ s_l - \gamma_l \tilde{x}_l(t) + \sum_{j=1}^{n} r_{lj}(\tilde{x}_j(t)) \right] - \tilde{x}_l(t + \Delta t) \right)$$

$$= \Delta t$$

into (B.2) leads to

$$\frac{\partial F_{MLE}(\omega)}{\partial s_l} = \frac{\Delta t}{\sigma_\xi^2} \sum_{t=1}^{T-1} \left( h_l(\omega, \tilde{x}(t)) - \tilde{x}_l(t + \Delta t) \right)$$

$$= \frac{\Delta t}{\sigma_\xi^2} \sum_{t=1}^{T-1} \left( \tilde{x}_l(t) + \Delta t \left[ s_l - \gamma_l \tilde{x}_l(t) + \sum_{j=1}^{n} r_{ij}(\tilde{x}_j(t)) \right] - \tilde{x}_l(t + \Delta t) \right).$$

**Derivatives with respect to degradation rates $\gamma_l$, $l = 1, \ldots, n$:**

$$\frac{\partial F_{MLE}(\omega)}{\partial \gamma_l} = \frac{\partial}{\partial \gamma_l} \left( \frac{1}{2\sigma_\xi^2} \sum_{i=1}^{n} \sum_{t=1}^{T-1} \left( h_l(\omega, \tilde{x}(t)) - \tilde{x}_l(t + \Delta t) \right)^2 \right)$$

$$= \frac{1}{\sigma_\xi^2} \sum_{t=1}^{T-1} \left( h_l(\omega, \tilde{x}(t)) - \tilde{x}_l(t + \Delta t) \right) \frac{\partial}{\partial \gamma_l} \left( h_l(\omega, \tilde{x}(t)) - \tilde{x}_l(t + \Delta t) \right)$$

(B.3)

Inserting

$$\frac{\partial}{\partial \gamma_l} \left( h_l(\omega, \tilde{x}(t)) - \tilde{x}_l(t + \Delta t) \right)$$

$$= \frac{\partial}{\partial \gamma_l} \left( \tilde{x}_l(t) + \Delta t \left[ s_l - \gamma_l \tilde{x}_l(t) + \sum_{j=1}^{n} r_{lj}(\tilde{x}_j(t)) \right] - \tilde{x}_l(t + \Delta t) \right)$$

$$= -\Delta t \tilde{x}_l(t)$$

into (B.3) leads to

$$\frac{\partial F_{MLE}(\omega)}{\partial \gamma_l} = \frac{\Delta t}{\sigma_\xi^2} \sum_{t=1}^{T-1} \left( h_l(\omega, \tilde{x}(t)) - \tilde{x}_l(t + \Delta t) \right) \left( -\tilde{x}_l(t) \right)$$

$$= \frac{\Delta t}{\sigma_\xi^2} \sum_{t=1}^{T-1} \left( \tilde{x}_l(t) + \Delta t \left[ s_l - \gamma_l \tilde{x}_l(t) + \sum_{j=1}^{n} r_{ij}(\tilde{x}_j(t)) \right] - \tilde{x}_l(t + \Delta t) \right) \left( -\tilde{x}_l(t) \right).$$

**Derivatives with respect to regulation strengths $k_{lz}$, $l, z = 1, \ldots, n$:**

$$\frac{\partial F_{MLE}(\omega)}{\partial k_{lz}} = \frac{\partial}{\partial k_{lz}} \left( \frac{1}{2\sigma_\xi^2} \sum_{i=1}^{n} \sum_{t=1}^{T-1} \left( h_l(\omega, \tilde{x}(t)) - \tilde{x}_l(t + \Delta t) \right)^2 \right)$$

$$= \frac{1}{\sigma_\xi^2} \sum_{t=1}^{T-1} \left( h_l(\omega, \tilde{x}(t)) - \tilde{x}_l(t + \Delta t) \right) \frac{\partial}{\partial k_{lz}} \left( h_l(\omega, \tilde{x}(t)) - \tilde{x}_l(t + \Delta t) \right)$$

(B.4)

Inserting

$$\frac{\partial}{\partial k_{lz}} \left( h_l(\omega, \tilde{x}(t)) - \tilde{x}_l(t + \Delta t) \right)$$

$$= \frac{\partial}{\partial k_{lz}} \left( \tilde{x}_l(t) + \Delta t \left[ s_l - \gamma_l \tilde{x}_l(t) + \sum_{j=1}^{n} r(\tilde{x}_j(t)) \right] - \tilde{x}_l(t + \Delta t) \right)$$

$$= \Delta t \frac{\tilde{x}_z(t)^{m_{lz}}}{\tilde{x}_z(t)^{m_{lz}} + \theta_{lz}^{m_{lz}}}$$

into (B.4) leads to

$$\frac{\partial F_{MLE}(\omega)}{\partial k_{lz}} = \frac{\Delta t}{\sigma_\xi^2} \sum_{t=1}^{T-1} (h_l(\omega, \tilde{x}(t)) - \tilde{x}_l(t + \Delta t)) \frac{\tilde{x}_z(t)^{m_{lz}}}{\tilde{x}_z(t)^{m_{lz}} + \theta_{lz}^{m_{lz}}}$$

$$= \frac{\Delta t}{\sigma_\xi^2} \sum_{t=1}^{T-1} \left( \tilde{x}_l(t) + \Delta t \left[ s_l - \gamma_l \tilde{x}_l(t) + \sum_{j=1}^{n} r_{ij}(\tilde{x}_j(t)) \right] - \tilde{x}_l(t + \Delta t) \right)$$

$$\cdot \frac{\tilde{x}_z(t)^{m_{lz}}}{\tilde{x}_z(t)^{m_{lz}} + \theta_{lz}^{m_{lz}}}.$$

**Derivatives with respect to threshold values $\theta_{lz}$, $l, z = 1, \ldots, n$:**

$$\frac{\partial F_{MLE}(\omega)}{\partial \theta_{lz}} = \frac{\partial}{\partial \theta_{lz}} \left( \frac{1}{2\sigma_\xi^2} \sum_{i=1}^{n} \sum_{t=1}^{T-1} (h_l(\omega, \tilde{x}(t)) - \tilde{x}_l(t + \Delta t))^2 \right)$$

$$= \frac{1}{\sigma_\xi^2} \sum_{t=1}^{T-1} (h_l(\omega, \tilde{x}(t)) - \tilde{x}_l(t + \Delta t)) \frac{\partial}{\partial \theta_{lz}} (h_l(\omega, \tilde{x}(t)) - \tilde{x}_l(t + \Delta t))$$

(B.5)

Inserting

$$\frac{\partial}{\partial \theta_{lz}} \left( h_l(\omega, \tilde{x}(t)) - \tilde{x}_l(t + \Delta t) \right)$$

$$= \frac{\partial}{\partial \theta_{lz}} \left( \tilde{x}_l(t) + \Delta t \left[ s_l - \gamma_l \tilde{x}_l(t) + \sum_{j=1}^{n} r(\tilde{x}_j(t)) \right] - \tilde{x}_l(t) \right)$$

$$= -\Delta t k_{lz} \frac{\tilde{x}_z(t)^{m_{lz}}}{\tilde{x}_z(t)^{m_{lz}} + \theta_{lz}^{m_{lz}}} \frac{m_{lz} \theta_{lz}^{m_{lz}-1}}{\tilde{x}_z(t)^{m_{lz}} + \theta_{lz}^{m_{lz}}}$$

into (B.5) leads to

$$
\frac{\partial F_{MLE}(\omega)}{\partial \theta_{lz}}
$$

$$
= -\frac{\Delta t}{\sigma_\xi^2} \sum_{t=1}^{T-1} \left(h_l(\omega, \tilde{x}(t)) - \tilde{x}_l(t + \Delta t)\right) k_{lz} \frac{\tilde{x}_z(t)^{m_{lz}}(t)}{\tilde{x}_z(t)^{m_{lz}} + \theta_{lz}^{m_{lz}}} \frac{m_{lz}\theta_{lz}^{m_{lz}-1}}{\tilde{x}_z(t)^{m_{lz}} + \theta_{lz}^{m_{lz}}}
$$

$$
= -\frac{\Delta t}{\sigma_\xi^2} \sum_{t=1}^{T-1} \left(\tilde{x}_l(t) + \Delta t \left[s_l - \gamma_l \tilde{x}_l(t) + \sum_{j=1}^{n} r_{ij}(\tilde{x}_j(t))\right] - \tilde{x}_l(t + \Delta t)\right)
$$

$$
\cdot k_{lz} \frac{\tilde{x}_z(t)^{m_{lz}}}{\tilde{x}_z(t)^{m_{lz}} + \theta_{lz}^{m_{lz}}} \frac{m_{lz}\theta_{lz}^{m_{lz}-1}}{\tilde{x}_z(t)^{m_{lz}} + \theta_{lz}^{m_{lz}}}.
$$

# Appendix C

# Reference network

The *Saccharomyces cerevisiae* cell cycle - Reference network The reference network used to evaluate results of the Bayesian approach in Chapter 5 is shown in Figure C.2. It was deduced from the network shown in Li *et al.* [116] (Figure C.1) in the following way:

The transcription factor complexes SBF and MBF, which are post-transcriptionally modified by Cln3 and which active Cln1 and Cln2 and Clb5 and Clb6, respectively, were omitted. The paths Cln3 $\xrightarrow{+}$ SBF $\xrightarrow{+}$ Cln1/2 and Cln3 $\xrightarrow{+}$ MBF $\xrightarrow{+}$ Clb5/6 appear in our reference network as direct paths Cln3 $\xrightarrow{+}$ Cln1/2 and Cln3 $\xrightarrow{+}$ Clb5/6. Similarly, we summarized the regulations Clb1/2 $\xrightarrow{-}$ SBF $\xrightarrow{+}$ Cln1/2 and Clb1/2 $\xrightarrow{+}$ MBF $\xrightarrow{+}$ Clb5/6 to a single negative regulation Clb1/2 $\xrightarrow{-}$ Cln1/2 and a single positive regulation Clb1/2 $\xrightarrow{+}$ Clb5/6, respectively. We omitted the two proteins Cdh1 and Sic1 as well, and summarized corresponding regulations in the same way.
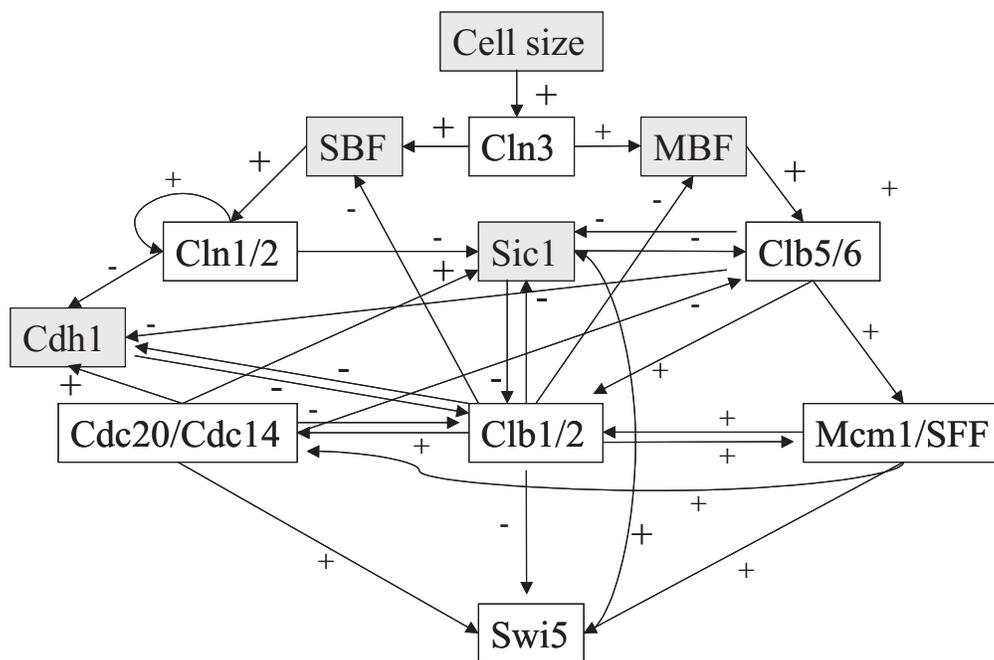
Figure C.1: Regulatory network of the budding yeast *Saccharomyces cerevisiae*, copied from Li *et al.* [116]. The cyclin Cln3 is assumed to be regulated by the cell size, which is described as a checkpoint in [116]. Further details about single interactions and corresponding references can be found in the supplement of [116]. A reduced version of this network was used as a reference to evaluate results of the Bayesian approach in Chapter 5.
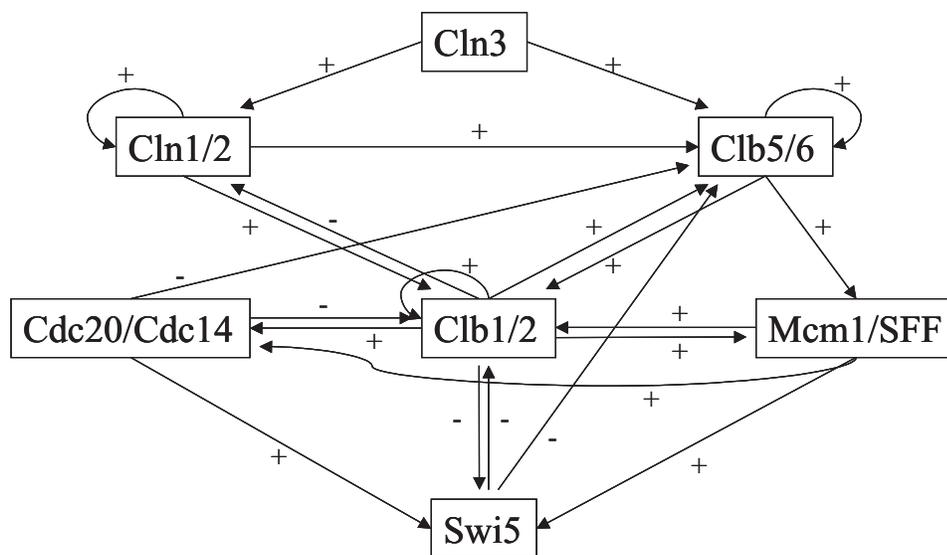


Figure C.2: Reduced regulatory network of the yeast cell cycle which was used as a reference network for the Bayesian approach. Interactions are deduced from the network in Figure C.1, and corresponding descriptions are provided in Tables C.1 and C.2.

Table C.1: Regulations in the reference network of the yeast cell cycle. Most descriptions and corresponding references are listed in the supplement of Li *et al.* [116].

| Regulation | Description |
| --- | --- |
| Cln3 → Cln1/2 | The Cln3/Cdc28-complex activates the transcription factor complex SBF by phosphorylation. SBF acts as a transcription factor for Clb1/2. |
| Cln3 → Clb5/6 | The transcription factor complex MBF is activated by Cln3 and facilitates transcription of Clb5/6. |
| Cln1/2 → Cln1/2 | Cln1/2 activates its own transcription factor complex SBF. |
| Cln1/2 → Clb5/6 | Cln1/2-Cdc28-complex triggers degradation of Sic1, which in turn inactivates the Clb5/6-Cdc28 complex. |
| Cln1/2 → Clb1/2 | Twofold regulation: Cln1/2-Cdc28-complex inhibits Cdh1, which accelerates degradation of Clb1/2. Moreover, Cln1/2-Cdc28 phosphorylates Sic1 for degradation, which in turn inactivates Clb1/2-Cdc28 by binding. |
| Clb1/2 → Cln1/2 | Clb1/2 inactivates the transcription factor complex SBF, which triggers transcription of Cln1/2 |
| Clb1/2 → Clb1/2 | Twofold regulation: Clb1/2 phosphorylate Sic1, which in turn inactivates Clb1/2. Additionally, Clb1/2 inactivates Cdh1 by phosphorylation, which in turn controls degradation of Clb1/2. |
| Clb1/2 → Clb5/6 | Clb1/2 phosphorylates Sic1, which inactivates the Clb5/6-Cdc28-complex. Maybe there is a further negative regulation from Clb1/2 to MBF, the transcription factor of Clb5/6. |
| Clb1/2 → Mcm1/SFF | Clb1/2 phosphorylates the complex. |
| Clb1/2 → Swi5 | Clb1/2 phosphorylates Swi5 such that it cannot enter the nucleus. |
| Clb1/2 → Cdc20 | Cdc20 is a subunit of the anaphase promoting complex (APC), which is activated by Clb1/2 by phosphorylation. |
| Clb5/6 → Clb1/2 | Twofold regulation: Clb5/6 phosphorylate Sic1 and Cdh1, which both inhibit Clb1/2. |
| Clb5/6 → Clb5/6 | Clb5/6 phosphorylates Sic1, Sic1 in turn inhibits the Clb5/6-Cdc28-complex. |
| Clb5/6 → Mcm1/SFF | Clb5/6 initiate DNA replication. In this phase G2/M, Mcm1/SFF is activated via binding of Ndd1. |
| Cdc20/14 → Clb1/2 | Direct interaction: Cdc20/APC degrades Clb1/2. Twofold indirect interaction: Cdc14 can dephosphorylate and thus activate Sic1 and Cdh1, which inhibit Clb1/2. |
| Cdc20/14 → Clb5/6 | Cdc20 presents Clb5/6 to the APC for ubiquination. Moreover, Cdc14 dephosphorylates Sic1, which inhibits Clb5/6. |
| Cdc14 → Swi5 | Cdc14 dephosphorylates and thus activates Swi5. |
| Mcm1/SFF → Clb1/2 | Mcm1/SFF is the transcription factor of Clb1/2. |
| Mcm1/SFF → Cdc20 | Transcription control is assumed to depend on Mcm1/SFF. |
| Mcm1/SFF → Swi5 | Mcm1/SFF is the transcription factor of Swi5. |
| Swi5 → Clb1/2 | Swi5 is the transcription factor of Sic1, which inhibits Clb1/2. |
| Swi5 → Clb5/6 | Swi5 is the transcription factor of Sic1, which inhibits Clb5/6. |

Table C.2: Yeast cell cycle genes included in our analysis. Information is copied from the *Saccharomyes* genome database SGD (http://www.yeastgenome.org).

| Standard name | systematic name | name description |
|---|---|---|
| Cdc14 | YFR028C | **C**ell **d**ivision **c**ycle |
| Cdc20 | YGL116W | **C**ell **d**ivision **c**ycle |
| Cdc28 | YBR160W | **C**ell **d**ivision **c**ycle |
| Cdh1 | YGL003C | **Cd**c20 **h**omolog |
| Clb1 | YGR108W | **C**y**c**lin **B** |
| Clb2 | YPR119W | **C**y**c**lin **B** |
| Clb5 | YPR120C | **C**y**c**lin **B** |
| Clb6 | YGR109C | **C**y**c**lin **B** |
| Cln1 | YMR199W | **C**y**clin** |
| Cln2 | YPL256C | **C**y**clin** |
| Cln3 | YAL040C | **C**y**clin** |
| MBF | | **M**lul cell cycle box **B**inding **F**actor |
| | | Transcription factor complex of Mbp1 and Swi6 |
| Mbp1 | YDL056W | **M**lul-box **b**inding **p**rotein |
| Mcm1 | YMR043W | **M**ini**c**hromosome **m**aintenance |
| SBF | | **S**wi4/Swi6 cell cycle box **B**inding **F**actor |
| | | Transcription factor complex of Swi4 and Swi6 |
| Swi4 | YER111C | **Swi**tching deficient |
| Swi5 | YDR146C | **Swi**tching deficient |
| Swi6 | YLR182W | **Swi**tching deficient |

# Bibliography

[1] R. Albert and H.G. Othmer. The topology of the regulatory interactions predict the expression pattern of the segment polarity genes in *Drosophila melanogaster*. *J. Theor. Biol.*, 223:1–18, 2003.

[2] B. Alberts, A. Johnson, J. Lewis, M. Raff, K. Roberts, and P. Walter, editors. *Molecular Biology of the Cell*. Garland Publishing, New York, 4. edition, 2002.

[3] U. Alon. *An introduction to systems biology - design principles of biological circuits*. Mathematical and Computational Biology Series. Chapman & Hall/CRC, London,UK, 2006.

[4] H. Amann. *Gewöhnliche Differentialgleichungen*. Walter de Gruyter, 1983.

[5] A. Bacciotti and L. Rosier. *Liapunov Functions and Stability in Control Theory*, volume 267 of *Lecture Notes in Control and Information Sciences*. Springer, 2001.

[6] J. Baehler. Cell-cycle control of gene expression in budding and fission yeast. *Annu. Rev. Genet.*, 39:69–94, 2005.

[7] M. Bansal, V. Belcastro, A. Ambesi-Impiombato, and D. di Bernardo. How to infer gene networks from expression profiles. *Mol. Syst. Biol.*, 3(78), 2007.

[8] N. Barkai and S. Leibler. Circadian clocks limited by noise. *Nature*, 403:267–268, 1999.

[9] D. Battogtokh and J.J. Tyson. Bifurcation analysis of a model of the budding yeast cell cycle. *Chaos*, 14(3):653–661, 2003.

[10] M.J. Beal, F. Falciani, Z. Ghahramani, C. Rangel, and D.L. Wild. A Bayesian approach to reconstructing genetic regulatory networks with hidden factors. *Bioinformatics*, 21(3):349–356, 2005.

[11] P. Beerli. Comparison of Bayesian and maximum-likelihood inference of population genetic parameters. *Bioinformatics*, 22(3):341–345, 2006.

[12] P. Berg and M. Singer, editors. *Dealing with genes*. University Science books, 1992.

[13] A. Bernard and A.J. Hartemink. Informative structure priors: joint learning of dynamic regulatory networks from multiple types of data. In *Pac. Symp. Biocomp. 2005 (PSB05)*, pages 459–470, New Jersey, 2005. World Scientific.

[14] M.R. Berthold and D.J. Hand. *Intelligent data analysis, an introduction.* Springer, 2. edition, 2003.

[15] H. Bolouri and E.H. Davidson. Modeling transcriptional regulatory networks. *BioEssays*, 24:1118–1129, 2002.

[16] S. Bornholdt. Less is more in modeling large genetic networks. *Science*, 310(5747):449–450, 2005.

[17] H. Boshoff, T.G. Myers, B.R. Copp, M.R. McNeil, M.A. Wilson, and C.E. Barry. The transcriptional response of *Mycobacterium tuberculosis* to inhibitors of metabolism: novel insights into drug mechanisms of action. *J. Biol. Chem.*, 279:40174–40184, 2004.

[18] O. Brandman, J.E. Ferrell, R. Li, and T. Meyer. Interlinked fast and slow positive feedback loops drive reliable cell decisions. *Science*, 310(21):496–498, 2005.

[19] I.N. Bronstein and K.A. Semendjajew. *Taschenbuch der Mathematik.* Verlag Harri Deutsch, 1957.

[20] P.C. Brooks, L.F. Dawson, L. Rand, and E.O. Davis. The *Mycobacterium*-specific gene Rv2719c is DNA damage inducible independently of RecA. *J. Bacteriol.*, 188(16):6034–6038, 2006.

[21] P.C. Brooks, F. Movahedzadeh, and E.O. Davis. Identification of some DNA damage-inducible genes of *Mycobacterium tuberculosis*: apparent lack of correlation with LexA binding. *J. Bacteriol.*, 183:4459–4467, 2001.

[22] S. Bulashevska and R. Eils. Inferring genetic regulatory logic from expression data. *Bioinformatics*, 21(11):2706–2713, 2005.

[23] N. Burić and D. Todorović. Dynamics of delay-differential equations modelling immunology of tumor growth. *Chaos, Solitons and Fractals*, 13:645–655, 2002.

[24] A. Burkovski. Ammonium assimilation and nitrogen control in *Corynebacterium glutamicum* and its relatives: an example for new regulatory mechanisms in actinomycetes. *FEMS Microbiol. Rev.*, 27:617–628, 2003.

[25] A. Burkovski. I do it my way: regulation of ammonium uptake and ammonium assimilation in *Corynebacterium glutamicum. Arch. Microbiol.*, 179:83–88, 2003.

[26] M. Caberlin, M. Mackey, and N. Nigam. Invariant manifolds in a dynamical model for gene transcription. preprint, 2002.

[27] L. Cabusora, E. Sutton, A. Fulmer, and C.V. Forst. Differential network expression during drug and stress response. *Bioinformatics*, 21(12):2898–2905, 2005.

[28] A. Chauhan, H. Lofton, E. Maloney, J. Moore, M. Fol, M.V.V.S. Madiraju, and M. Rajagopalan. Interference of *Mycobacterium tuberculosis* cell division by Rv2719c, a cell wall hydrolase. *Mol. Microbiol.*, 62(1):132–147, 2006.

[29] B.-S. Chen, Y.-C. Wang, W.-S. Wu, and W.-H. Li. A new measure of the robustness of biochemical networks. *Bioinformatics*, 21(11):2698–2705, 2005.

[30] C.C. Chen, L. Calzone, A. Csikasz-Nagy, F.R. Cross, B. Novak, and J.J. Tyson. Integrative analysis of cell cycle control in budding yeast. *Mol. Biol. Cell*, 15(8):3841–3862, 2004.

[31] K.-C. Chen, T.-Y. Wang, H.-H. Tseng, C.-Y.F. Huang, and C.-Y. Kao. A stochastic differential equation model for quantifying transcriptional regulatory network in *Saccharomyces cerevisiae*. *Bioinformatics*, 21(12):2883–2890, 2005.

[32] L. Chen and K. Aihara. A model of periodic oscillation for genetic regulatory systems. *IEEE Transactions on Circuits and Systems*, 49(10), 2002.

[33] Q. Chen, P.W. Postma, and O. Amster-Choder. Dephosphorylation of the *Escherichia coli* transcriptional antiterminator BglG by the sugar sensor BglF is the reversal of its phosphorylation. *J. Bacteriol.*, 182(7):2033–2036, 2000.

[34] T. Chen, H.L. He, and G.M. Church. Modeling gene expression with differential equations. *Pac. Symp. Biocomp.*, 4:29–40, 1999.

[35] V. Chickarmane, B.N. Kholodenko, and H.M. Sauro. Oscillatory dynamics arising from competitive inhibition and multisite phosphorylation. *J. Theor. Biol.*, 244:68–76, 2007.

[36] V. Chickarmane, S.R. Paladugu, F. Bergmann, and H.M. Sauro. Bifurcation discovery tool. *Bioinformatics*, 21(18):3688–3690, 2005.

[37] D.-Y. Cho, K.-H. Cho, and B.-T. Zhang. Identification of biochemical networks by S-tree based genetic programming. *Bioinformatics*, 22(13):1631–1640, 2006.

[38] O. Cinquin and J. Demongeot. Roles of positive and negative feedback in biological systems. *C.R. Biol.*, 325(11):1085–1095, 2002.

[39] S.J. Cokus, D. Haynor, N. Gronbech-Jensen, and M. Pellegrini. Modelling the network of cell cycle transcription factors in the yeast *Saccharomyces cerevisiae*. *BMC Bioinformatics*, 7(381), 2006.

[40] S.T. Cole and *et al.* Deciphering the biology of *Mycobacterium tuberculosis* from the complete genome sequence. *Nature*, 393:537–544, 1998.

[41] J. Collado-Vides and R. Hofestädt, editors. *Gene Regulations and Metabolism - Postgenomic Computational Approaches.* MIT Press, 2002.

[42] G.M. Cooper and R.E. Hausman, editors. *The Cell: A Molecular Approach.* ASM Press and Sinauer Associates, 4. edition, 2007.

[43] G. Craciun, Y. Tang, and M. Feinberg. Understanding bistability in complex enzyme-driven reaction networks. *Proc. Natl. Acad. Sci.*, 103(23):8697–8702, 2006.

[44] L.N. Csonka. A third L-proline permease in *Salmonella typhimurium* which functions in media of elevated osmotic strength. *J. Bacteriol.*, 151:1433–1443, 1982.

[45] L.N. Csonka and W. Epstein. Osmoregulation. In F.C. Neidhardt, R. Curtiss, J.L. Ingraham, E.C.C. Lin, K.B. Low, B. Magasanik, W.S. Reznikoff, M. Riley, M. Schaechter, and H.E. Umbarger, editors, *Escherichia coli and Salmonella. Cellular and Molecular Biology*, pages 1210–1223. ASM Press, Washington D.C., 2. edition, 1996.

[46] C.S. Dattananda, K. Rajkumari, and J. Gowrishankar. Multiple mechanisms contribute to osmotic inducibility of *proU* operon expression in *Escherichia coli*: demonstration of two osmoresponsive promoters and of a negative regulatory element within the first structural gene. *J. Bacteriol.*, 173:7481–7490, 1991.

[47] E.O. Davis, E.M. Dullaghan, and L. Rand. Definition of the mycobacterial SOS box and use to identify LexA-regulated genes in *Mycobacterium tuberculosis*. *J. Bacteriol.*, 184(12):3287–3295, 2002.

[48] H. de Jong. Modeling and simulation of genetic regulatory systems: A literature review. *J. Comp. Biol.*, 9(1):67–103, 2002.

[49] H. de Jong, J. Geiselmann, C. Hernandez, and M. Page. Genetic network analyzer: qualitative simulation of genetic regulatory networks. *Bioinformatics*, 19(3):336–344, 2003.

[50] H. de Jong, J.-L. Gouzé, C. Hernandez, M. Page, T. Sari, and J. Geiselmann. Qualitative simulation of genetic regulatory networks using piecewise-linear models. *Bull. Math. Biol.*, 66(2):301–340, 2004.

[51] H. de Jong and M. Page. Qualitative simulation of large and complex genetic regulatory systems. In W. Horn, editor, *Proceedings of the 14th European Conference on Artificial Intelligence (ECAI2000), Berlin*, pages 191–195, Amsterdam, 2000. IOS press.

[52] P. De Leenheer and D. Aeyels. Stability properties of equilibria of classes of cooperative systems. *IEEE Transactions on Automatic Control*, 46(12):1996–2001, 2001.

[53] P. D'Haeseler, X. Wen, S. Fuhrman, and R. Somogyi. Linear modeling of mRNA expression levels during cns development and injury. *Pac. Symp. Biocomp.*, pages 41–52, 1999.

[54] B.F. Dibrov, A.M. Zhabotinsky, and B.N. Kholodenko. Dynamic stability of steady states and static stabilization in unbranched metabolic pathways. *J. Math. Biol.*, 15:51–63, 1982.

[55] J. Dieudonné. *Foundations of modern analysis.* Academic Press, New York, 1960.

[56] M. Djordjevic, A.M. Sengupta, and B.I. Shraiman. A biophysical approach to transcription factor binding site discovery. *Genome Research*, 13:2381–2390, 2003.

[57] S. Dole. *Multiple level regulation of the Escherichia coli bgl operon.* PhD thesis, Institute for Genetics, University of Cologne, 2001.

[58] S. Dole, S. Kühn, and K. Schnetz. Post-transcriptional enhancement of *Escherichia coli bgl* operon silencing by limitation of BglG-mediated antitermination at low transcription rates. *Mol. Microbiol.*, 43(1):217–226, 2002.

[59] S. Dole, V. Nagarajavel, and K. Schnetz. The histone-like nucleoid structuring protein H-NS represses the *Escherichia coli bgl* operon downstream of the promoter. *Mol. Microbiol.*, 52(2):589–600, 2004.

[60] R.O. Duda, P.E. Hart, and D.G. Stork, editors. *Pattern classification.* John Wiley & Sons, 2. edition, 2001.

[61] E.M. Dullaghan, P.C. Brooks, and E.O. Davis. The role of multiple SOS boxes upstream of the *Mycobacterium tuberculosis lexA* gene - identification of a novel DNA-damage-inducible gene. *J. Microbiol.*, 148:3609 –3615, 2002.

[62] J. Dziadek, M.V.V.S. Madiraju, S.A. Rutherford, M.A.L. Atkinson, and M. Rajagopalan. Physiological consequences associated with overproduction of *Mycobacterium tuberculosis* FtsZ in mycobacterial hosts. *J. Microbiol.*, 148:961–971, 2002.

[63] M.B. Elowitz and S. Leibler. A synthetic oscillatory network of transcriptional regulators. *Nature*, 403:335–338, 2000.

[64] J. Elstrodt. *Maß- und Integrationstheorie.* Springer, 2005.

[65] B. Ermentrout. *Simulating, Analyzing, and Animating Dynamical Systems: A guide to XPPAUT for Researchers and Students.* SIAM, Philadelphia, USA, 2002.

[66] W.J. Ewens and R.Grant Gregory. *Statistical Methods in Bioinformatics.* Statistics for Biology and Health. Springer, 2. edition, 2005.

[67] U. Faigle, W. Kern, and G. Still. *Algorithmic Principles of Mathematical Programming.* Kluwer Academic Publishers, Dordrecht/Boston/London, 2002.

[68] C.P. Fall, E.S. Marland, J.M. Wagner, and J.J. Tyson, editors. *Computational Cell Biology*, volume 20 of *Interdisciplinary Applied Mathematics*. Springer series, 2005.

[69] J.E. Ferrell and E.M. Machleder. The biochemical basis of an all-or-none cell fate switch in xenopus oocytes. *Science*, 280:895–898, 1998.

[70] N. Friedman, M. Linial, I. Nachman, and D. Pe'er. Using Bayesian networks to analyze expression data. *J. Comp. Biol.*, 7(3–4):601–620, 2000.

[71] N. Friedman, K. Murphy, and S. Russell. Learning the structure of dynamical probabilistic networks. In *Proceedings of the 14th Annual Conference on Uncertainty in Artificial Intelligence*, pages 139–147, San Francisco, CA, USA, 1998. Morgan Kaufmann Publishers.

[72] E. Fung, W.W. Wong, J.K. Suen, T. Bulter, S. Lee, and J.C. Liao. A synthetic gene-metabolic oscillator. *Nature*, 435:118–122, 2005.

[73] A.C. Gavin and *et al.* Functional organization of the yeast proteome by systematic anaylsis of protein complexes. *Nature*, 415(6868):141–147, 2002.

[74] J. Gebert. *Modellierung genregulatorischer Netzwerke mit stückweise linearen Differenzialgleichungen*. PhD thesis, Center for Applied Computer Science, University of Cologne, 2007.

[75] J. Gebert and N. Radde. A new approach for modeling prokaryotic biochemical networks with differential equations. In D. Dubois, editor, *AIP Conference Proceedings of 7th International Conference on Computing Anticipatory Systems (CASYS05)*, volume 839, pages 526–533, 2006.

[76] J. Gebert, N. Radde, U. Faigle, J. Strösser, and A. Burkovski. Modeling and simulation of nitrogen regulation in *Corynebacterium glutamicum*. to appear in Discrete Applied Mathematics, Special Issue 'Networks in Computational Biology', 2007.

[77] J. Gebert, N. Radde, and G.-W. Weber. Modelling gene regulatory networks with piecewise linear differential equations. *to appear in the special issue (feature cluster) Challenges of Continuous Optimization in Theory and Applications of European Journal of Operational Research*, 18(3), 2007.

[78] U. Gerland, D. Moroz, and T. Hwa. Physical constraints and functional characteristics of transcription factor-DNA interaction. *Proc. Natl. Acad. Sci.*, 99(19):12015–12020, 2002.

[79] L. Glass and S.A. Kauffman. The logical analysis of continuous, non-linear biochemical control networks. *J. Theor. Biol.*, 39:103–129, 1973.

[80] A. Goldpeter. A minimal cascade model for the mitotic oscillator involving cyclin and cdc2 kinase. *Proc. Natl. Acad. Sci.*, 88:9107–9111, 1991.

[81] A. Goldpeter. Computational approaches to cellular rhythms. *Nature*, 420:238–245, 2002.

[82] K. Gopalsamy. Stability and oscillations in delay differential equations of population dynamics. In *Mathematics and its Applications*, volume 74. Kluwer Academic Publishers, 1992.

[83] B. Görke. Regulation of the *Escherichia coli* antiterminator protein BglG by phosphorylation at multiple sites and evidence for transfer of phosphoryl groups between monomers. *J. Biol. Chem.*, 278(47):46219—46229, 2003.

[84] J.-L. Gouzé. Positive and negative circuits in dynamical systems. *J. Biol. Sys.*, 6(21):11–15, 1998.

[85] J. Guckenheimer and P. Holmes. *Nonlinear oscillations, dynamical systems, and bifurcations of vector fields*. Number 42 in Applied Mathematical Sciences. Springer, 1990.

[86] A. Gulati and S. Mahadevan. The *Escherichia coli* antiterminator protein BglG stabilizes the 5' region of the *bgl* mRNA. *J. Biosci.*, 26(2):193–203, 2001.

[87] M. Gustafsson, M. Hörnquist, and A. Lombardi. Constructing and analyzing a large-scale gene-to-gene regulatory network - Lasso constrained inference and biological validation. *IEEE transcations on computational biology and bioinformatics*, 2(3):254–261, 2005.

[88] R. Guthke, U. Möller, M. Hoffmann, F. Thies, and S. Töpfer. Dynamic network reconstruction from gene expression data applied to immune response during bacterial infection. *Bioinformatics*, 21(8):1626–1634, 2005.

[89] I. Györi and G. Ladas. Oscillation theory of delay differential equations - with applications. In *Oxford Mathematical Monographs*. Oxford Science Publications, 1991.

[90] A.J. Hartemink, D.K. Gifford, T.S. Jaakkola, and R.A. Young. Combining location and expression data for principled discovery of genetic network models. *Pac. Symp. Biocomp.*, 7:437–449, 2002.

[91] L.H. Hartwell and T.A. Weinert. Checkpoints: controls that ensure the order of cell cycle events. *Science*, 246:629–634, 1989.

[92] J. Hasty, D. McMillen, F. Isaacs, and J.J. Collins. Computational studies of gene regulatory networks: *in numero* molecular biology. *Nat. Rev. Genet.*, 2:268–279, 2001.

[93] T. Herman. Industrial production of amino acids by coryneform bacteria. *J. Biotechnol.*, 104:155–172, 2003.

[94] J. Hershberger, M. Maxel, and S. Suri. Finding the $k$-shortest simple paths: a new algorithm and its implementation. In *Proc. of the 5th Workshop on ALgorithm ENgineering and EXperiments, ALENEX03*, pages 26–36, Baltimore, USA, 2003.

[95] C.F. Higgins, C.J. Dorman, D.A. Stirling, L. Waddell, I.R. Booth, G. May, and E. Bremer. A physiological role for DNA supercoiling in the osmotic regulation of gene expression in *Salmonella typhimurium* and *E. coli. Cell*, 52:569–584, 1988.

[96] M.W. Hirsch. Systems of differential equations that are competitive or cooperative II: convergence almost everywhere. *J. Math. Anal.*, 16(3):423–439, 1985.

[97] M.W. Hirsch and S. Smale. *Differential Equations, Dynamical Systems and Linear Algebra.* Academic Press, New York, 1974.

[98] E. Hopf. Abzweigung einer periodischen Lösung von einer stationären Lösung eines Differential-Systems. *Ber. Math. Phys.*, 94:1–22, 1942.

[99] S. Huang. Gene expression profiling, genetic networks, and cellular states: an integrating concept for tumorigenesis and drug discovery. *J. Mol. Med.*, 77:469–480, 1999.

[100] D. Husmeier. Sensitivity and specificity of inferring genetic regulatory interactions from microarray experiments with dynamic Bayesian networks. *Bioinformatics*, 19(17):2271–2282, 2003.

[101] F. Jacob and J. Monod. Genetic regulatory mechanisms in the synthesis of proteins. *J. Mol. Biol.*, 3:318–356, 1961.

[102] V.M. Jiménez and A. Marzal. Computing the $k$-shortest paths: a new algorithm and an experimental comparison. In *Lecture Notes in Computer Science 1668, 3rd International Workshop on Algorithm Engineering (WAE99)*, pages 15–29, London, UK, 1999.

[103] L. Kaderali. *A hierarchical bayesian approach to regression and its application to predicting survival times in cancer.* PhD thesis, Center for Applied Computer Science, University of Cologne, 2006.

[104] L. Kaderali and N. Radde. *Inferring gene regulatory networks from expression data*, volume 1 of *Studies in Computational Intelligence*, chapter 2. Springer-Verlag, Berlin, 2007.

[105] L. Kaderali, T. Zander, U. Faigle, J. Wolf, J.L. Schultze, and R. Schrader. CASPAR: a hierarchical Bayesian approach to predict survival times in cancer from gene expression data. *Bioinformatics*, 22(12):1495–1502, 2006.

[106] S. Kauffman. Metabolic stability and epigenesis in randomly constructed genetic nets. *J. Theor. Biol.*, 22:437–467, 1969.

[107] S. Kikuchi, D. Tominaga, M. Arita, K. Takahashi, and M. Tomita. Dynamic modeling of genetic networks using genetic algorithm and S-system. *Bioinformatics*, 19(5):643–650, 2003.

[108] H. Kitano. Systems biology: A brief overview. *Science*, 295:1662–1664, 2002.

[109] R.R. Klevecz, J. Bolen, G. Forrest, and D.B. Murray. A genomewide oscillation in transcription gates DNA replication and cell-cycle. *Proc. Natl. Acad. Sci.*, 101(5), 2004.

[110] M. Kloster, C. Tang, and N.S. Wingreen. Finding regulatory modules through large-scale gene-expression data analysis. *Bioinformatics*, 21(7):1172–1179, 2005.

[111] Y. Kuang. Delay differential equations - with applications in population dynamics. In *Mathematics in Science and Engineering*, volume 191. Academic Press, San Diego, 1993.

[112] E.S. Lander and *et al.* Initial sequencing and analysis of the human genome. *Nature*, 409(6822):860–921, 2001.

[113] L.S. Lasdon and A.D. Waren. Design and testing of a generalized reduced gradient code for nonlinear programming. *ACM Transactions on Mathematical Software*, 4(1):34–50, 1978.

[114] R. Laubenbacher and B. Stigler. A computational algebra approach to the reverse engineering of gene regulatory networks. *J. Theor. Biol.*, 229(4):523–537, 2004.

[115] T. Leonard and J.S.J. Hsu. *Bayesian methods. An analysis for statisticians and interdisciplinary researchers.* Cambridge series in statistical and probabilistic mathematics. Cambridge University Press, 1999.

[116] F. Li, T. Long, Y. Lu, Q. Ouyangm, and C. Tang. The yeast cell-cycle network is robustly designed. *Proc. Natl. Acad. Sci.*, 101:4781–4786, 2004.

[117] Y. Li, C. Campbell, and M. Tipping. Bayesian automatic relevance determination algorithms for classifying gene expression data. *Bioinformatics*, 18(10):1332–1339, 2002.

[118] S. Liang, S. Fuhrman, and R. Somogyi. Reveal, a general reverse engineering algorithm for inference of genetic network architectures. *Pac. Symp. Biocomp.*, 3:18–29, 1998.

[119] J.C.W. Locke, M.M. Southern, L. Kozma-Bognár, V. Hibbert, P.E. Brown, M.S. Turner, and A.J. Millar. Extension of a genetic network model by iterative experimentation and mathematical analysis. *Mol. Syst. Biol.*, 28:1–9, 2005.

[120] L. Lopian, A. Nussbaum-Shochat, K. O'Day-Kerstein, A. Wright, and O. Amster-Choder. The BglF sensor recruits the BglG transcription regulator to the membrane and releases it on stimulation. *Proc. Natl. Acad. Sci.*, 100(12):7099–7104, 2003.

[121] J. Lu, H.W. Engl, and P. Schuster. Inverse bifurcation analysis: Application to simple gene systems. *Alg. Mol. Biol.*, 1(11):11, 2006.

[122] D.G. Luenberger. *Introduction to Dynamic Systems: Theory, models and Applications.* J.Wiley & Sons, 1979.

[123] S. Madhusudan, A. Paukner, Y. Klingen, and K. Schnetz. Independent regulation of H-NS mediated silencing of the *bgl* operon at two levels: upstream by BglJ and LeuO and downstream by DnaKJ. *J. Microbiol.*, 151:3349–3359, 2005.

[124] S. Mahadevan, A.E. Reynolds, and A. Wright. Positive and negative regulation of the *bgl* operon in *Escherichia coli. J. Bacteriol.*, 169(6):2570–2578, 1987.

[125] L. Mao and H. Resat. Probabilistic representation of gene regulatory networks. *Bioinformatics*, 20(14):2258–2269, 2004.

[126] J.S. Maritz and T. Lwin. *Empirical Bayes Methods.* Chapman & Hall, 2. edition, 1989.

[127] K.G. Mawuenyega, C.V. Forst, K.M. Dobos, J.T. Belisle, J. Chen, E.M. Bradbury, A.R.M. Bradbury, and X. Chen. *Mycobacterium tuberculosis* functional network analysis by global subcellular protein profiling. *Mol. Biol. Cell*, 16:396–404, 2005.

[128] J. Maybee and J. Quirk. Qualitative problems in matrix theory. *SIAM Review*, 11(1):30–51, 1969.

[129] H.H. McAdams and A. Arkin. Stochastic mechanisms in gene expression. *Proc. Natl. Acad. Sci.*, 94:814–819, 1997.

[130] A.I. Mees and P.E. Rapp. Periodic metabolic systems: oscillations in multiple-loop negative feedback biochemical control networks. *J. Math. Biol.*, 5:99–114, 1978.

[131] T. Mestl, E. Plahte, and S.W. Omholt. A mathematical framework for describing and analysing gene regulatory networks. *J. Theor. Biol.*, 176:291–300, 1995.

[132] K. Missal, M.A. Cross, and D. Drasdo. Gene network inference from incomplete expression data: transcriptional control of hematopoietic commitment. *Bioinformatics*, 22(6):731–738, 2006.

[133] K. Murphy and S. Mian. Modelling gene expression data using dynamic Bayesian networks. Technical report, Computer Science Division, University of California, Berkeley, CA, USA, 1999.

[134] D.B. Murray, M. Beckmann, and H. Kitano. Regulation of yeast oscillatory dynamics. *Proc. Natl. Acad. Sci.*, 104(7):2241–2246, 2007.

[135] J.D. Murray. *Mathematical Biology - An introdcution*, volume 17 of *Interdisciplinary Applied Mathematics*. Springer series, 2002.

[136] I. Nachman, A. Regev, and N. Friedman. Inferring quantitative models of regulatory networks from expression data. *Bioinformatics*, 20(Suppl.1):i248–i256, 2004.

[137] V. Nagarajavel. *H-NS mediated repression of the E. coli bgl and proU operons*. PhD thesis, Institute for Genetics, University of Cologne, 2007.

[138] V. Nagarajavel, S. Madhusudan, S. Dole, A.R. Rahmouni, and K. Schnetz. Repression by binding of H-NS within the transcription unit. to appear in J. Biol. Chem., 2007.

[139] K. Nasmyth. At the heart of the budding yeast cell cycle. *Trends Genet.*, 12:405–412, 1996.

[140] H. Öktem, R. Pearson, and K. Egiazarian. An adjustable aperiodic model class of genomic interactions using continuous time Boolean networks (Boolean delay equations). *Chaos*, 13(4):1–8, 2003.

[141] D.G. Overdier and L.N. Csonka. A transcriptional silencer downstream of the promoter in the osmotically controlled *proU* operon of *Salmonella typhimurium*. *Proc. Natl. Acad. Sci.*, 89:3140–3144, 1992.

[142] L. Pagliaro and D.L. Taylor. 2-Deoxyglucose and Cytochalasin D Modulate Aldolase Mobility in Living 3T3 Cells. *J. Cell Biol.*, 118(4):859–863, 1992.

[143] A. Papoulis. *Probability, random variables and stochastic processes*. McGraw-Hill, 2. edition, 1984.

[144] J. Pearl. *Causality: Models, Reasoning and Inference*. Cambridge University Press, Cambridge, 2000.

[145] D. Pe'er. Bayesian network analysis of signaling networks: A primer. *Science STKE*, 281:pl4, 2005.

[146] D. Pe'er, A. Regev, G. Elidan, and N. Friedman. Inferring subnetworks from perturbed expression profiles. *Bioinformatics*, 17:215–224, 2001.

[147] L. Perko. *Differential Equations and Dynamical Systems*. Texts in Applied Mathematics. Springer series New York, 1991.

[148] V. Petrov, M. Peifer, and J. Timmer. Bistability and self-oscillations in cell cycle control. *International Journal of Bifurcation and Chaos*, 16(4):1057–1066, 2006.

[149] T.H. Pham, J.C. Clemente, K. Satou, and T.B. Ho. Computational discovery of transcriptional regulatory rules. *Bioinformatics*, 21(Suppl.2):ii101–ii107, 2005.

[150] N. Prakash and W. Wurst. Specification of midbrain territory. *Cell Tissue Res.*, 3(8):5–14, 2004.

[151] I. Prasad and S. Schaefler. Regulation of the $\beta$-glucoside system in *Escherichia coli* K12. *J. Bacteriol.*, 120:638–650, 1974.

[152] W.H. Press, S.A. Teukolsky, W.T. Vetterling, and B.P. Flannery. *Numerical Recipes in C++*. Cambridge University Press, Cambridge, 2002.

[153] M.-H. Qin, M.V.V.S. Madiraju, and M. Rajagopalan. Characterization of the functional replication origin of *Mycobacterium tuberculosis*. *Gene*, 233:121–130, 1999.

[154] N. Radde, J. Gebert, U. Faigle, R. Schrader, and K. Schnetz. Modeling feedback loops in the H-NS-mediated regulation of the *Escherichia coli bgl* operon. to appear in J. Theor. Biol., 2007.

[155] N. Radde, J. Gebert, and C.V. Forst. Systematic component selection for gene-network refinement. *Bioinformatics*, 22(21):2674–2680, 2006.

[156] N. Radde and L. Kaderali. Bayesian inference of gene regulatory networks using gene expression time series data. In S. Hochreiter and R. Wagner, editors, *Bioinformatics Research and Development*, volume 4414 of *Lecture Notes in Computer Science*, pages 1–15. Springer, Berlin/Heidelberg, 2007.

[157] N. Radde and L. Kaderali. Inference of an oscillatory model for the yeast cell cycle. to appear in Discrete Applied Mathematics, Special Issue *Networks in Computational Biology*, 2007.

[158] L. Rand, J. Hinds, B. Springer, P. Sander, R.S. Buxton, and E.O. Davis. The majority of inducible DNA repair genes in *Mycobacterium tuberculosis* are induced independently of RecA. *Mol. Microbiol.*, 50(3):1031–1042, 2003.

[159] I. Roeder and I. Glauche. Towards an understanding of lineage specification in hematopoietic stem cells: A mathematical model for the interaction of transcription factors GATA-1 and PU.1. *J. Theor. Biol.*, 241:852–865, 2006.

[160] S. Rogers and M. Girolami. A Bayesian regression approach to the inference of regulatory networks from gene expression data. *Bioinformatics*, 21(14):3131–3137, 2005.

[161] P.-C. Romond, M. Rustici, D. Gonze, and A. Goldpeter. Alternating oscillations and chaos in a model of two coupled biochemical oscillators driving successive phases of the cell cycle. *Ann. N-Y Acad. Sci.*, 879:180–193, 1999.

[162] C. Sabatti and G.M. James. Bayesian sparse hidden components analysis for transcription regulation networks. *Bioinformatics*, 22(6):739–746, 2006.

[163] K. Sachs, O. Perez, D. Pe'er, D.A. Lauffenburger, and G.P. Nolan. Causal protein-signaling networks derived from multiparameter single-cell data. *Science*, 308:523–529, 2005.

[164] G. Sanguinetti, N.D. Lawrence, and M. Rattray. Probabilistic inference of transcription factor concentrations and gene-specific regulatory activities. *Bioinformatics*, 22(22):2775–2781, 2006.

[165] M. Santillán and M.C. Mackey. Dynamic regulation of the tryptophan operon: A modeling study and comparison with experimental data. *Proc. Natl. Acad. Sci.*, 98(4):1364–1369, 2001.

[166] S. Schaefler and W.K. Maas. Inducible system for the utilization of $\beta$-Glucosides in *Escherichia coli* II. Description of mutant types and genetic analysis. *J. Bacteriol.*, 93:264–272, 1967.

[167] T. Scheper, D. Klinkenberg, C. Pennartz, and J. van Pelt. A mathematical model for the intracellular circadian rhythm generator. *Journal of Neuroscience*, 19(1):40–47, 1999.

[168] M.J. Schilstra and H. Bolouri. Modelling the regulation of gene expression in genetic regulatory networks. Technical report, Science & Technology Research Centre, University of Hertfordshire, 2002.

[169] H. Schmidt and E.W. Jacobsen. Linear systems approach to analysis of complex dynamic behaviours in biochemical networks. *J. Syst. Biol.*, 1(1):149–158, 2004.

[170] K. Schnetz. Silencing of *Escherichia coli bgl* promoter by flanking sequence elements. *EMBO J.*, 14:2545–2550, 1995.

[171] K. Schnetz. Silencing of the *Escherichia coli bgl* operon by RpoS requires Crl. *J. Microbiol.*, 148:2573–2578, 2002.

[172] K. Schnetz and B. Rak. Regulation of the *bgl* operon of *Escherichia coli* by transcriptional antitermination. *EMBO J.*, 7:3271–3277, 1988.

[173] K. Schnetz and B. Rak. $\beta$-glukoside permease represses the *bgl* operon of *Escherichia coli* by phosphorylation of the antiterminator protein and also interacts with glucose-specific enzyme III, the key element in catabolite control. *Proc. Natl. Acad. Sci.*, 87:5074–5078, 1990.

[174] I. Shmulevich, E. Dougherty, S. Kim, and W. Zhang. Probabilistic Boolean networks: a rule-based uncertainty model for gene regulatory networks. *Bioinformatics*, 18(2):261–274, 2002.

[175] I. Shmulevich, E.R. Dougherty, and W. Zhang. From Boolean to probabilistic Boolean networks as models of genetic regulatory networks. *Proceedings of the IEEE*, 90(11):1778–1792, 2002.

[176] I. Shmulevich, A. Saarinen, O. Yli-Harja, and J. Astola. *Inference of genetic regulatory networks via best-fit extension*. Springer, US, 2003.

[177] E.D. Siggia, J. Lippincott-Schwartz, and S. Bekiranov. Diffusion in inhomogeneous media: Theory and simulations applied to whole cell photobleach recovery. *J. Biophys.*, 79:1761–1770, 2000.

[178] M. Slutsky and L.A. Mirny. Kinetics of protein-DNA interaction: facilitated target location in sequence-dependent potential. *J. Biophys.*, 87:4021–4035, 2004.

[179] H.L. Smith. Systems of ordinary differential equations which generate an order preserving flow: A survey of results. *SIAM Review*, 30:87–113, 1988.

[180] H.L. Smith. *Monotone dynamical systems: An introduction to the theory of competitive and cooperative systems*. Mathematical Surveys and Monographs. American Mathematical Society, 1995.

[181] P. Smolen, D.A. Baxter, and J.H. Byrne. Modeling transcriptional control in gene networks - methods, recent results, and future directions. *Bull. Math. Biol.*, 62:247–292, 2000.

[182] E.H. Snoussi. Necessary conditions for multistationarity and stable periodicity. *J. Biol. Syst.*, 6:3–9, 1998.

[183] P.T. Spellman, G. Sherlock, M.Q. Zhang, and *et al.* Comprehensive identification of cell cycle-regulated genes of the yeast *Saccharomyces cerevisiae* by microarray hybridization. *Mol. Biol. Cell*, 9:3273–3297, 1998.

[184] D. Spiegelhalter, A. Dawid, S. Lauritzen, and R. Cowell. Bayesian analysis in expert systems. *Statistical Science*, 8:219–282, 1993.

[185] G. Stoll, J. Rougemont, and F. Naef. Few crucial links assure checkpoint efficiency in the yeast cell-cycle network. *Bioinformatics*, 22(20):2539–2546, 2006.

[186] J. Strösser, A. Lüdke, S. Schaffer, R. Krämer, and A. Burkovski. Regulation of GlnK activity: modification, membrane sequestration and proteolysis as regulatory principles in the network of nitrogen control in *Corynebacterium glutamicum*. *Mol. Microbiol.*, 54(1):132–148, 2004.

[187] N. Sun, R.J. Carroll, and H. Zhao. Bayesian error analysis model for reconstructing transcriptional regulatory networks. *Proc. Natl. Acad. Sci.*, 103(21):7988–7993, 2006.

[188] M. Swat, A. Kel, and H. Herzel. Bifurcation analysis of the regulatory modules of the mammalian $G_1$/S transition. *Bioinformatics*, 20(10):1506–1511, 2004.

[189] D. Thieffry and R. Thomas. Qualitative analysis of gene networks. *Pac. Symp. Biocomp.*, 3:77–88, 1998.

[190] R. Thomas. On the relation between the logical structure of systems and their ability to generate multiple steady states or sustained oscillations. In J. Della-Dora, J. Demongeot, and B. Lacolle, editors, *Numerical methods in the study of critical phenomena*, volume 9 of *Springer Series in Synergetics*, pages 180–193. Springer Verlag, 1981.

[191] R. Thomas. Laws for the dynamics of regulatory networks. *J. Dev. Biol.*, 42:479–485, 1998.

[192] R. Thomas and R. D'Ari. *Biological Feedback*. CRC Press, Boca Raton, FL, USA, 1990.

[193] R. Thomas, D. Thieffry, and M. Kauffman. Dynamical behaviour of biological regulatory networks – I. biological role of feedback loops and practical use of the concept of the loop-characteristic state. *Bull. Math. Biol.*, 57:247–276, 1995.

[194] J.J. Tyson. Biochemical oscillations. In C.P. Fall, E.S. Marland, J.M. Wagner, and J.J. Tyson, editors, *Computational Cell Biology*, volume 20 of *Interdisciplinary Applied Mathematics*, chapter 9, pages 230–260. Springer series, 2005.

[195] J.J. Tyson, A. Csikasz-Nagy, and B. Novak. The dynamics of cell cycle regulation. *BioEssays*, 24:1095–1109, 2002.

[196] J.J. Tyson and H.G. Othmer. The dynamics of feedback control circuits in biochemical pathways. *Progr. Theor. Biol.*, 5:1–62, 1978.

[197] P. Uetz and E. Pohl. Protein-Protein- und Protein-DNA-Interaktionen. In Wink.M., editor, *Molekulare Biotechnologie - Konzepte und Methoden*, chapter 23, pages 385–408. Wiley-VCH, 2004.

[198] R.R. Vallabhajosyula, V. Chickarmane, and H.M. Sauro. Conservation analysis of large biochemical networks. *Bioinformatics*, 22(3):346–353, 2006.

[199] J.H. van Lint and R.M. Wilson. *A course in combinatorics*. Cambridge University Press, 1998.

[200] E.P. van Someren, B.L.T. Vaes, W.T. Steegenga, A.M. Sijbers, K.J. Dechering, and M.J.T. Reinders. Least absolute regression network analysis of the murine osteoblast differentiation network. *Bioinformatics*, 22(4):477–484, 2006.

[201] E.P. van Someren, L.F.A. Wessels, and M.J.T. Reinders. Linear modeling of genetic networks from experimental data. In *Proceedings of the 8th International Conference on Intelligent Systems for Molecular Biology (ISMB2000)*, pages 355–366, La Jolla, California, USA, 2000.

[202] J.C. Venter and *et al.* The sequence of the human genome. *Science*, 291(5507):1304–1351, 2001.

[203] J.M.G. Vilar, H.Y. Kueh, N. Barkai, and S. Leibler. Mechanisms of noise-resistance in genetic oscillators. *Proc. Natl. Acad. Sci.*, 99(9):5988–5992, 2002.

[204] E.O. Voit. *Computational Analysis of Biochemical Systems*. Cambridge University Press, 2000.

[205] E.O. Voit and J. Almeida. Decoupling dynamical systems for pathway identification from metabolic profiles. *Bioinformatics*, 20(11):1670–1681, 2004.

[206] P.H. von Hippel and O.G. Berg. On the specificity of DNA-protein interactions. *Proc. Natl. Acad. Sci.*, 83:1608–1612, 1986.

[207] G.C. Walker. *The SOS response of Escherichia coli*, pages 1400–1416. ASM Press, Washington, 1996.

[208] J. Wang, E.D. Gilles, J.W. Lengeler, and K. Jahreis. Modeling of inducer exclusion and catabolite repression based on a PTS-dependent sucrose and non-PTS-dependent glycerol transport systems in *Escherichia coli* K-12 and its experimental verification. *J. Biotechnol.*, 92(2):133–158, 2001.

[209] A. Werhli, M. Grzegorczyk, and D. Husmeier. Comparative evaluation of reverse engineering gene regulatory networks with relevance networks, graphical gaussian models and Bayesian networks. *Bioinformatics*, 22(20):2523–2531, 2006.

[210] L.F.A. Wessels, E.P. van Someren, and M.J.T. Reinders. A comparison of genetic network models. *Pac. Symp. Biocomp.*, 6:508–519, 2001.

[211] F.X. Wu, W.J. Zhang, and A.J. Kusalik. Modeling gene expression from microarray expression data with state-space equations. *Pac. Symp. Biocomp.*, 9:581–592, 2004.

[212] B. Xing and M.J. van der Laan. A causal inference approach for constructing transcriptional regulatory networks. *Bioinformatics*, 21(21):4007–4013, 2005.

[213] G. Yagil and E. Yagil. On the relation between effector concentration and the rate of induced enzyme synthesis. *J. Biophys.*, 11(1):11–27, 1971.

[214] K. Yamamoto, S. Muniruzzaman, M. Rajagopalan, and M.V.V.S. Madiraju. Modulation of *Mycobacterium tuberculosis* DnaA protein-adenine-nucleotide interactions by acidic phospholipids. *J. Biochem.*, 363:305–311, 2002.

[215] T. Yu and K.-C. Li. Inference of transcriptional regulatory network by two-stage constrained space factor analysis. *Bioinformatics*, 21(21):4033–4038, 2005.

[216] M. Zou and S.D. Conzen. A new dynamic Bayesian network (DBN) approach for identifying gene regulatory networks from time course microarray data. *Bioinformatics*, 21(1):71–79, 2005.

# Index

cone, 114
cooperative binding, 43
cooperative system, 114
core
     mechanism, 50, 63, 109, 188, 190
     model, 5, 50, 60, 63, 64, 109, 110, 120,
          121, 125, 126, 128, 131, 132, 190
     network, 5, 52, 53, 57, 58, 62, 63, 109,
          121, 127, 188, 190
     system, 49, 50
cumulative distribution function, 87

d-separation, 15
density function, 87
     joint, 88
     marginal, 88, 95
     mean, 87
     support, 87
     variance, 88
differential equation
     attractor, 37
          basin of attraction, 37, 129, 143, 149,
               161, 177, 178
     delay, 17, 169, 185
     equilibrium point, 19, 26
          asymptotically stable, 27, 178
          hyperbolic, 26
          stable, 26, 142, 178
     fixed point, 26
          stability, 142
     flow, 21
          monotonous, 114
          order preserving, 115
     invariant set, 33, 37, 45
     limit set, 36, 128, 136
          $\alpha$-limit point, 36
          $\omega$-limit point, 36
          $\omega$-limit set, 143
     linearization, 26
     nullcline, 128, 164
     ordinary, 16
     partial, 17
     periodic orbit, 37, 110, 114, 126, 142

     stability, 37
     phase portrait, 29, 142
     piecewise linear, 44
     planar, 110
     positive half-trajectory, 21
     positive system, 45, 128
     steady state, 26, 67
     stiff, 46, 167
     trajectory, 21, 126
     trapping region, 44, 47, 111
     vector field, 20
dimer, 95, 122, 125
     -hetero, 9
     -homo, 9
directed acyclic graph, 15
distribution
     gamma, 88, 94, 95
          rate parameter, 88
          shape parameter, 88
     Gaussian, 88
     hierarchical, 95
     Normal, 88
downstream silencer, 70
dynamical system, 19, 20

edge
     weight, 112, 176
empirical Bayesian method, 106
enhancer, 9
ensemble, 200
epigenetic effect, 117
equilibrium constant, 41
error function, 11
eukaryote, 8
Euler integration, 92
evidence, 91
expression pattern, 8

feedback, 5
feedback loop, 67, 111
free enthalpy, 199
function
     expected value, 87

# Erklärung

Ich versichere, daß ich die von mir vorgelegte Dissertation selbständig angefertigt, die benutzten Quellen und Hilfsmittel vollständig angegeben und die Stellen der Arbeit - einschließlich Tabellen, Karten und Abbildungen -, die anderen Werken im Wortlaut oder dem Sinn nach entnommen sind, in jedem Einzelfall als Entlehnung kenntlich gemacht habe; dass diese Dissertation noch keiner anderen Fakultät oder Universität zur Prüfung vorgelegen hat; dass sie - abgesehen von unten angegebenen Teilpublikationen - noch nicht veröffentlicht worden ist, und dass ich eine solche Veröffentlichung vor Abschluss des Promotionsverfahrens nicht vornehmen werde. Die Bestimmungen dieser Promotionsordnung sind mir bekannt. Die von mir vorgelegte Dissertation ist von Professor Dr. U. Faigle betreut worden.

Teilpublikation:

1. Gebert, J., Lätsch, M., Pickl, S.W., Radde, N., Weber, G.-W., Wünschiers, R., 2004. *Genetic networks and anticipation of gene expression patterns.* AIP Conference Proceedings of Computing Anticipatory Systems (CASYS'03), 718, 474-485.

2. Gebert, J., Öktem, H., Pickl, S.W., Radde, N., Weber, G.-W., Yilmaz, F.B., 2004. *Inference of gene expression patterns by using a hybrid system formulation - an algorithmic approach to local state transition matrices.* Anticipative & Predictive Models in Systems Science 1, G.E. Lasker, D.M. Dubois (eds.), Canada, 63-66.

3. Ergenc, T., Pickl, S.W., Radde, N., Weber, G.-W., 2005. *Generalized semi-infinite optimization and anticipatory systems.* International Journal of Computing Anticipatory Systems 15, CHAOS, 3-30.

4. Gebert, J., Radde, N., 2006. *A new approach for modeling prokaryotic biochemical networks with differential equations.* Conference Proceedings of 7th International Conference on Computing Anticipatory Systems (CASYS'05), Liege, Belgium, 526-533.

5. Radde, N., Gebert, J., Forst, C.V., 2006. *Systematic component selection for gene-network refinement.* Bioinformatics 22(21), 2674-2680.

6. Gebert, J., Radde, N., Weber, G.-W., 2007. *Modelling gene regulatory networks with piecewise linear differential equations.* Special issue 'Challenges of Continuous Op-

timization in Theory and Applications', European Journal of Operational Research 18(3).

7. Gebert, J., Radde, N., Faigle, U., Strösser, J., Burkovski, A., 2007. *Modelling and simulation of nitrogen regulation in Corynebacterium glutamicum.* to appear in Discrete Applied Mathematics, special issue 'Networks in Computational Biology'.

8. Radde, N., Kaderali, L., 2007. *Inference of an oscillating model for the yeast cell cycle.* to appear in Discrete Applied Mathematics, special issue 'Networks in Computational Biology'.

9. Radde, N., Kaderali, L., 2007. *Bayesian inference of gene regulatory networks using gene expression time series data.* Lecture Notes in Bioinformatics (LNBI) 4414, Bird07, Springer Verlag, 1-15.

10. Kaderali, L., Radde, N., 2007. *Inferring Gene Regulatory Networks from Gene Expression Data.* In "Computational Intelligence in Bioinformatics", Chapter 2, Studies in Computational Intelligence (SCI) series, Springer-Verlag, Berlin.

11. Radde, N., Gebert, J., Faigle, U., Schrader, R., Schnetz, K., 2007. *Modeling feedback loops in the H-NS-mediated regulation of the Escherichia coli bgl operon.* Journal of Theoretical Biology 250(2), 298-304.

12. Radde, N. 2007. *The effect of time scale differences and time-delays on the structural stability of oscillations*, submitted.

13. Radde, N., Kaderali, L., 2007. *A Bayes Regularized ODE Model for the Inference of Gene Regulatory Networks*, in preparation.